Stratospheric Transport and Chemical Parameterisations in ECMWF Analyses: Evaluation and Improvements using a 3D CTM

Beatriz Marina Monge-Sanz

Submitted in accordance with the requirements for the degree of
Doctor of Philosophy

University of Leeds
School of Earth and Environment

August 2008

The candidate confirms that the work submitted is her own and that appropriate credit has been given where reference has been made to the work of others.

Publication Statement

Chapter 3 of this thesis has been partly published in the AGU journal *Geophysical Research Letters*, details of the published article are outlined below. The author of this thesis is also the lead author of the jointly-authored publication. This page states that the ideas contained within the publication are those of the lead author and all work, both practical and written, has been carried out solely by her. The contribution of the secondary authors has been in the role of supervising and giving helpful advice and guidance.

Part of the discussion included in Chapter 2 regarding problems and experiences found with CTMs using existing (re)analyses was published in the *Proceedings of the ECMWF/GEO Workshop on Atmospheric Reanalysis* (2006). Details of this publication are included below. This extended abstract was written solely by the first author, with the helpful advice of the second author. Ideas contained therein derive from work carried out for this thesis, but also from work and experiences of other CTM modellers. Proper acknowledgement of external contributions is given in the publication itself.

B. M. Monge-Sanz, M. P. Chipperfield, A. J. Simmons, S. M. Uppala, "Mean age of air and transport in a CTM: Comparison of different ECMWF analyses", *Geophys. Res. Lett.*, Vol. 34, L04801, doi:10.1029/2006GL028515, 2007.

B. M. Monge-Sanz, M. P. Chipperfield, "Chemical Transport Modelling", Proceedings of the ECMWF/GEO Workshop on Atmospheric Reanalyses, UK, 19-22 June 2006, *ECMWF*, pp. 39-44, November 2006.

Acknowledgements

I sincerely thank my supervisor, Martyn Chipperfield, for his continuous guidance, support, encouragement and advice during these years and, above all, for the pleasure of learning from him.

I am also extremely grateful to Adrian Simmons and Sakari Uppala, for giving me the nice opportunity of working with them at ECMWF in the challenging world of reanalysis.

Agathe Untch and Jean-Jacques Morcrette are specially thanked for all their work and help with the methane scheme tests at ECMWF.

I thank Paul Berrisford and Wuhu Feng for helping with the ECMWF data, and John Methven and Steve Arnold for help with trajectory calculations and code. I am equally grateful to Daniel Cariolle for helpful discussions on the ozone scheme, and to John McCormack for providing the CHEM2D coefficients. Thanks to Piers Forster for useful conversations on the methane-radiation interaction and to Elias Hólm for many communications on the ECMWF system. I also thank Alan Gadian, and Doug Parker for following my work as part of my RSG, and Computer Support in Leeds and the ECMWF for valuable assistance.

Paco, Manuel and Magdalena are thanked for priceless help with logistics during my visits to ECMWF (and for that first 'mus' game). I would like to extend my gratitude to all ECMWF staff for really making me feel home every time I have been to Reading.

I will always be grateful to Prof. Sabino Palmieri for introducing me to the stratospheric world with his wisdom and enthusiasm, and the rest of the GMET in Rome, where it all began. I also express my gratitude to Prof. Amalio Fdez-Pacheco, for his encouragement to start this PhD.

Many others have also contributed throughout this adventure with their friendship and company. My many office mates: Alex, Steve, Justin P., Dom, M. Grazia, John, Lara, Clare, Nigel, Gerry, everyone in 2.30 ... too long a list but I thank you all. Mireia and Beatriz L., sharing much more than a nationality with me. Senai, with all those talks and laughs that have so much helped to preserve my sanity during the last year of my thesis. All my friends in Italy and Spain, including the 'barbeque squad', and especially Yolanda, Roberta and Giampiero, for the very good memories we build every time we meet.

Very special thanks go to my parents and sister for everything they have always done and for being always close to me, no matter the distance, and to Carlos for his endless love and support.

Finally, I would like to dedicate this thesis to the women in my family, to their strength, intelligence, determination and passion. Thanks.

Abstract

This thesis tackles two main problems in stratospheric modelling. First, the accuracy of the stratospheric transport provided by meteorological analyses, which is crucial for off-line chemistry transport models (CTMs) to produce accurate distributions of tracers. Second, the description of stratospheric radiatively active gases included in numerical weather prediction (NWP) general circulation models (GCMs), which in many cases is too simple for current stratospheric purposes.

Stratospheric CTMs driven by existing (re)analyses are known to produce too young age-of-air distributions, *i.e.* they overestimate the stratospheric circulation, and produce excessive subtropical mixing. In this thesis the TOMCAT/SLIMCAT CTM has been used to evaluate different stratospheric (re)analyses from the European Centre for Medium-Range Weather Forecasts (ECMWF), including experimental datasets from the ERA-Interim preparatory phase, to assess how the newer analyses compare with previous ones, such as ERA-40 or U.K. Met Office. Various transport diagnostics have been calculated to assess the Brewer-Dobson circulation and mixing processes in the different datasets. Problems detected in the past for ERA-40 have been greatly overcome in the recent ECMWF reanalysis tests, which provide realistic age-of-air in the lower stratosphere, and better overall agreement with observations. Causes for the improvements are also explored, revealing the roles that the assimilation technique or the analysis frequency play in the description of stratospheric transport. Information derived from these investigations fed into the final set-up for the ERA-Interim reanalysis production.

The detail and accuracy of the stratospheric chemistry provided by the CTM encouraged the development of two stratospheric chemical parameterisations, one for O_3 (COPCAT) and one for CH_4 and water vapour (CoMeCAT). In the current ECMWF O_3 scheme the heterogeneous chemistry is treated inaccurately, while CH_4 is considered as a well-mixed gas with a tropospheric value all throughout the atmosphere. An advance of the COPCAT O_3 parameterisation, based on the Cariolle and Déqué (CD) approach, is the implicit inclusion of heterogeneous chemistry. The new O_3 scheme has been evaluated within the same CTM used to calculate it, providing

information on the validity of the CD approach. The new scheme is comparable to full-chemistry in many regions and successfully includes heterogenous processes, simulating a realistic Antarctic O_3 hole. Improvements to the current ECMWF scheme are identified.

The CoMeCAT CH_4/H_2O scheme, suitable for any global model, has been implemented in 3D CTM runs and in the ECMWF GCM providing realistic profiles. Results are compared against the CTM full-chemistry, and GCM runs using the default ECMWF options for CH_4 and water vapour. CoMeCAT coupled to the GCM radiation changes the temperature field, warming the upper stratosphere by up to 2 K in zonal mean distributions. Stratospheric profiles from the new scheme agree well with Halogen Occultation Experiment (HALOE) CH_4 and H_2O observations.

Contents

List of Figures

List of Tables

List of Acronyms

2D	Two-Dimensional
3D	Three-Dimensional
3D-Var	Three-Dimensional Variational Data Assimilation
4D-Var	Four-Dimensional Variational Data Assimilation
AC	Analysis Correction
ACATS	Airborne Chromatograph for Atmospheric Trace Species
ACE-FTS	Atmospheric Chemistry Experiment Fourier Transform Spectrometer
AGU	American Geophysical Union
ALPHA	Advanced Level Physics High Altitude
ASHOE	Airborne Southern Hemisphere Ozone Experiment
BDC	Brewer-Dobson Circulation
CCM	Chemistry Climate Model
CCMVal	Chemistry Climate Model Validation
CD	Cariolle and Déqué
CDAS	Climate data assimilation system
CFC	Chlorofluorocarbon
CHEM2D	The NRL 2D photochemical transport model
CHEM2D-OPP	CHEM2D Ozone Photochemistry Parameterization
CIRA	COSPAR International Reference Atmosphere
CLAES	Cryogenic Limb Array Etalon Spectrometer
CoMeCAT	Coefficients for Methane from a Chemistry And Transport Model
COPCAT	Coefficients O_3 Parameterisation from a Chemistry And Transport Model
COSPAR	Committee On Space Research

CRIEPI	Central Research Institute of Electric Power Industry
CTM	Chemical Transport Model (also Chemistry and Transport Model)
DA	Data Assimilation
DAO	Data Assimilation Office
DAS	Data Assimilation System
DU	Dobson Unit
ECHAM	European Centre Hamburg Model
ECMWF	European Centre for Medium-Range Weather Forecasts
EP	Earth Probe
ERA	ECMWF Re-Analysis
ERA-15	ECMWF 15-year Re-Analysis
ERA-40	ECMWF 40-year Re-Analysis
ESA	European Space Agency
EUMETSAT	European Organisation for Exploitation of Meteorological Satellites
FGAT	First Guess at Appropriate Time
FUB	Free University of Berlin
FVDAS	Finite Volume Data Assimilation System
FVGCM	Finite Volume General Circulation Model
GCM	General Circulation Model
GEMS	Global & regional Earth-system Monitoring using Satellite & in-situ data
GEO	Group on Earth Observations
GEOS	Goddard Earth Observing System
GFDL	Geophysical Fluid Dynamics Laboratory
GHG	Greenhouse Gas
GOME	Global Ozone Monitoring Experiment
GSFC	Goddard Space Flight Center
GWD	Gravity Wave Drag
HALOE	Halogen Occultation Experiment
IFS	Integrated Forecast System
IMATCH	Isentropic Model of Atmospheric Transport and Chemistry

JFM	January-February-March
JJA	June-July-August
JMA	Japan Meteorological Agency
JPL	Jet Propulsion Laboratory
JRA-25	Japanese 25-year Re-Analysis
KNMI	Royal Netherlands Meteorological Institute
KNMI TM	KNMI Tracer Model
LIDAR	Light Detection And Ranging
LINOZ	Linear Ozone scheme from McLinden *et al.* (2000)
LS	Lower Stratosphere
LW	Longwave
MACCM3	Middle Atmosphere Community Climate Model 3
MAESA	Measurements for Assessing the Effects of Stratospheric Aircraft
MIDRAD	Middle atmosphere Radiation
MIPAS	Michelson Interferometer for Passive Atmospheric Sounding
MLS	Microwave Limb Sounder
MMII	Models and Measurements II
MOBIDIC	Model of Bidimensional Chemistry
MPV	Modified Potential Vorticity
NASA	National Aeronautics and Space Administration
NAT	Nitric Acid Trihydrate
NCAR	National Center for Atmospheric Research
NCEP	National Centers for Environmental Prediction
NH	Northern Hemisphere
NOAA	National Oceanic and Atmospheric Administration
NOGAPS	Navy Operational Global Atmospheric Prediction System
NRL	Naval Research Laboratory
NWP	Numerical Weather Prediction
OI	Optimum Interpolation
OMI	Ozone Monitoring Instrument

OMS	Observations of the Middle Stratosphere
POAM	Polar Ozone and Aerosol Monitoring
POLARIS	Photochemistry of Ozone Loss in the Arctic Regions in Summer
ppbv	part per billion by volume
ppmv	part per million by volume
pptv	part per trillion by volume
PSC	Polar Stratospheric Cloud
PV	Potential Vorticity
PVU	Potential Vorticity Unit
REPROBUS	Reactive Processes Ruling the O_3 Budget in the Stratosphere
RSS	Remote Sensing Systems
SA-IPSL	Aeronomy Service - Pierre-Simon Laplace Institute
SAGE	Stratospheric Aerosol and Gas Experiment
SAT	Sulfuric Acid Trihydrate
SBUV	Solar Backscatter Ultra Violet instrument
SCOUT-O3	Stratospheric-Climate Links on the UTLS
SH	Southern Hemisphere
SLT	Semi Lagrangian Transport
SPADE	Stratospheric Photochemistry Aerosol and Dynamics Experiment
SPARC	Stratospheric Processes and their Role in Climate
SSM/I	Special Sensor Microwave/Imager
SST	Sea-Surface Temperature
STE	Stratosphere-to-Troposphere Exchange
STRAT	Stratospheric Tracers of Atmospheric Transport
SW	Shortwave
SWV	Stratospheric Water Vapour
SYNOZ	Synthetic Ozone scheme from McLinden *et al.* (2000)
TIROS	Television and Infrared Observation Satellite
TO	Total Ozone
TOMS	Total Ozone Mapping Spectrometer

TOPOZ	Towards the Prediction of Stratospheric Ozone
TOVS	TIROS Operational Vertical Sounder
TTL	Tropical Tropopause Layer
UARS	Upper Atmosphere Research Satellite
UKMO	United Kingdom Meteorological Office
US	Upper Stratosphere
UTC	Coordinated Universal Time
UTLS	Upper Troposphere and Lower Stratosphere
UV	Ultra Violet
VarBC	Variational Bias Correction
vmr	volume mixing ratio
VSLS	Very Short-Lived Species
WMO	World Meteorological Organization

Abbreviations for some journal articles

CD86	Cariolle and Déqué (1986)
S2003	Schoeberl *et al.* (2003)
MC2006	McCormack *et al.* (2006)
ML2000	McLinden *et al.* (2000)
EL2000	Eluszkiewicz *et al.* (2000)

Chapter 1

General Introduction

1.1 Motivation

Nowadays, chemical transport models (CTMs) are routinely used to investigate the distribution and evolution of chemical species in the atmosphere. Important research topics carried out with CTMs include stratospheric ozone evolution and trends, polar chemistry and its link with dynamics, stratosphere-to-troposphere exchange (STE) processes and air quality assessments. Most CTMs use an 'off-line' approach, which means that winds and temperatures are not calculated by the CTM but taken from general circulation models (GCMs) or from meteorological analyses.

The off-line approach allows CTMs to integrate highly detailed chemistry descriptions while keeping computational cost within reason. In addition, when using meteorological analyses, the CTM simulation is linked to the real atmospheric conditions and results can be compared against observations on a particular date. However, this makes CTMs rely on the accuracy of the external meteorological data used to drive the simulations. This apparent disadvantage can be turned into a useful research topic, as CTMs can therefore be used to evaluate the quality of different (re)analysis data.

Recently, problems in the stratospheric representation provided by different

(re)analyses such as U.K. Met Office Upper Atmosphere Research Satellite (UARS) or the ECMWF 40-year reanalysis (ERA-40) have been detected (*e.g.* Manney *et al.* 2003; Meijer *et al.* 2004; Chipperfield 2006). To what extent these problems are also present in more recent datasets, as well as whether such problems can be ultimately corrected in future (re)analyses, needs to be evaluated. The first part of this thesis uses a CTM to scientifically assess the accuracy of several meteorological datasets from the European Centre for Medium-Range Weather Forecasts (ECMWF) and explores reasons for the different descriptions they provide.

Currently, GCMs used by numerical weather prediction (NWP) centres include very simple descriptions for just a few stratospheric compounds. Only ozone and water vapour schemes have been developed with any level of complexity, though these still need improvement. In most GCMs (*e.g.* ECMWF) other radiative gases like CH_4, CO, CO_2 and clorofluorocarbons (CFCs) are included only as global mean values. Including more complex representations for, at least, the main radiative gases would help to provide more realistic stratospheric analyses.

NWP models cannot yet afford full-chemistry descriptions; however, the detail of the chemistry included in CTMs, and their long experience in stratospheric studies, makes these models the ideal tool for producing simple chemistry parameterisations to be included in a NWP GCM. This thesis develops parameterisation schemes based on a CTM for stratospheric ozone, methane and water vapour and evaluates their performance against full-chemistry and current ECMWF options (when available).

1.2 Stratospheric transport and CTMs

Inaccurate transport processes jeopardise the ability of a CTM to reproduce realistic chemical distributions. Recent studies have revealed problems in meteorological analyses from several data assimilation systems (DAS) such as ECMWF, U.K. Met Office (UKMO) and Goddard Earth Observing System (GEOS) (Schoeberl *et al.*,

2003; Meijer *et al.*, 2004; Chipperfield, 2006).

For multiannual stratospheric studies, an accurate representation of the Brewer-Dobson circulation (BDC) is essential for CTMs to achieve realistic tracer distributions. However, ERA-40 (Uppala *et al.*, 2005) and ECMWF operational winds have been reported to produce a much too young age-of-air (*e.g.* van Noije *et al.* 2004; Meijer *et al.* 2004; Scheele *et al.* 2005; Chipperfield 2006). U.K. Met Office winds (Swinbank and O'Neill, 1994) have produced ages even younger than ERA-40 (Chipperfield, 2006). The underestimation of the age of air implies that the models overestimate the BDC, which clearly affects their ability to reproduce observed tracer distributions.

Meteorological analyses have also been found to produce too much subtropical exchange of air compared to analogous fields from GCMs (*e.g.* Schoeberl *et al.* 2003). Based on these results, a strong debate currently exists on whether DAS winds are good enough for long stratospheric studies and whether DAS fields are susceptible to improvement beyond their present state (Stohl *et al.*, 2004; Rood, 2005).

This thesis evaluates the accuracy of several meteorological datasets from the ECMWF and the U.K. Met Office, including experimental ECMWF runs produced with their most recent NWP/DAS model, and explores reasons for the different descriptions these datasets provide. ECMWF GCM winds are also compared against their data assimilation equivalent fields.

1.3 Stratospheric Ozone in Global Models

Understanding the distribution of, and changes to, stratospheric ozone is one of the most challenging topics in atmospheric science. This is due to both the number of feedbacks that exist between ozone and other atmospheric issues (radiation, trans-

port, climate...) and the impact such feedbacks have on human life and biodiversity. Because ozone absorbs solar radiation it is the main player in shaping the atmospheric temperature profile above the tropopause (and also below as a greenhouse gas). Therefore, stratospheric ozone and ultra violet (UV) radiation interact affecting atmospheric circulation and chemistry.

Full-chemistry CTMs like the one used in this thesis produce ozone distributions in very good agreement with observations. More simple descriptions like those used in NWP GCMs do not perform equally well. For instance, without the assimilation of ozone observations, the current ECMWF scheme is not able to reproduce realistic polar ozone values (*e.g.* Dethof and Hólm 2004). A realistic background ozone field is essential for the correct assimilation of radiances into a NWP data assimilation (DA) system. Therefore, the more accurate the ozone distribution the higher the quality of the (re)analyses produced by the NWP/DA system. A realistic enough ozone field also allows for radiation coupling, making the release of surface UV warnings possible. So far, the ECMWF ozone field has not been operationally interactive with radiation (A. Simmons, personal communication, 2005). Furthermore, as forecast skill depends on the accuracy of the initial conditions (analysis), the improvement of the ozone representation will also have a positive effect on weather forecasts, allowing more reliable long-term forecasts. The impact stratospheric O_3 has on tropospheric pressure and winds has already been shown by *e.g.* Thompson and Solomon (2002) or Shindell and Schmidt (2004).

This thesis explores an ozone parameterisation which is an improvement of the current ECMWF ozone approach (Cariolle and Déqué, 1986). The parameterisation proposed implicitly includes all known heterogeneous ozone chemistry processes. Additionally, in this work the Cariolle and Déqué (1986) approach can be assessed within the same CTM used to obtain the parameterisation coefficients and accurately compared against the full-chemistry version of the model.

1.4 Stratospheric Water in Global Models

Stratospheric humidity in the ECMWF model is linked to the radiation code and, therefore, has an impact on the (re)analyses produced through data assimilation. ECWMF stratospheric water vapour has been reported to be too dry in the stratosphere (Simmons *et al.*, 1999). Discrepancies with observations are also found in the ERA-40 stratospheric humidity field (*e.g.* Uppala *et al.* 2005; Oikonomou and O'Neill 2006).

Methane oxidation is the main source of stratospheric water (*e.g.* Le Texier *et al.* 1988). The ECMWF water scheme is based on this assumption but does not take into account any changes in tropospheric CH_4 trends and completely relies on the accuracy of stratospheric transport to get the correct latitudinal variability of H_2O.

In this thesis a new stratospheric methane linear scheme is developed, based on full-chemistry, for use in global models. The scheme is also used to derive a stratospheric source for water vapour. The scheme is tested in the SLIMCAT CTM and also implemented in the ECMWF GCM, where it is used both interactively and non-interactively with their radiation scheme. The CH_4/H_2O parameterisation is validated against full-chemistry and HALOE observations.

1.5 Thesis objectives

The motivations for this thesis have been presented above; here a list of the main objectives is summarised:

i) Evaluate how well different (re)analyses perform in terms of stratospheric transport for multiannual CTM simulations. Understand reasons for the differences in their performance.

ii) Provide information for the production of the next ECMWF reanalysis series (ERA-Interim).

iii) Develop a linear parameterisation of stratospheric ozone including complete heterogeneous chemistry effects based on a full-chemistry 3D CTM. Implement the new scheme in the CTM and compare against current ECMWF ozone scheme and the full-chemistry CTM.

iv) Develop a new methane linear parameterisation for the stratosphere that can also be used to derive stratospheric water vapour. Compare against the CTM full-chemistry.

v) Implement the new methane and water vapour schemes in the ECMWF general circulation model and evaluate their performance.

1.6 Thesis structure

This thesis is divided into two main parts, the first one deals with the stratospheric transport representation achieved in the CTM with different (re)analyses. The second part explores ways to improve the description of the main radiatively active gases in a global model. A chapter-by-chapter outline is given below.

Chapter 2 discusses the existing problems in the performance of stratospheric (re)analyses and their effect on transport in CTM simulations. Techniques currently applied to overcome such problems are also considered, as well as their limitations and issues that still need to be solved. Chapter 2 also includes the description of the CTM used in this work.

Chapter 3 presents results obtained from the CTM simulations using different (re)analysis datasets, including ERA-40 and a new experimental ECMWF test (EXP471). Calculated diagnostics are explained and results analysed to provide an extensive comparison between the stratospheric datasets employed. Some results from this chapter have already been published, the corresponding *Geophys. Res. Lett.* article is included in Appendix A.

Chapter 4 explores the reasons for the differences observed in Chapter 3. For this, different datasets are used to drive the CTM which allow the evaluation of the impact of different aspects of the data assimilation process. Also, a set of ECMWF GCM winds is compared with the analysis data.

Chapter 5 is the equivalent to Chapter 2 but for the stratospheric parameterisations part of this thesis. It presents the current situation with ozone and water vapour schemes, discussing more in detail the current ECMWF schemes. Problems in the performance of such schemes are identified and improvements needed are proposed.

Chapter 6 develops an alternative ozone parameterisation, based on the Cariolle and Déqué (1986) scheme, obtained from the full-chemistry CTM. The new scheme includes heterogeneous chemistry implicitly. The new parameterisation is tested within the same CTM used to calculate it, and compared against the current ECMWF scheme.

In Chapter 7 a new methane parameterisation is calculated for the stratosphere, which can also be used to compute a stratospheric source for water vapour. The scheme is suitable for any global model and has been tested in the CTM and the ECMWF GCM. Distributions obtained with this scheme are compared against the full chemistry CTM and the current operational ECMWF options.

Chapter 8 summarises the main results and contributions derived from this thesis, and discusses potential research lines that originate from the work presented here. This thesis has already opened different research lines and active collaborations with NWP/DAS centres have already started.

Chapter 2

Stratospheric Meteorological Analyses and Chemical Transport Models

2.1 Introduction

Off-line chemistry transport models (CTMs) are a key tool for investigating numerous important aspects of atmospheric science. Stratospheric ozone evolution and trends, tracer distributions and air quality assessments are among the topics that benefit from the application and development of CTMs. These models use external wind and temperature fields to advect tracers that, at the same time, follow a series of chemical integrations to provide the global distributions of the chemical species included in the model. As a result, for a CTM to provide accurate tracer distributions and concentrations, two requirements must be fulfilled: Accurate chemical descriptions and accurate transport representation.

Given the detail of the chemistry included in CTMs, and their long experience in stratospheric studies, the accuracy of the full chemistry description is ensured to a major extent, which makes these models the ideal tool for producing simple chemistry parameterisations to be included in general circulation models (GCMs).

However, the off-line approach makes CTMs very sensitive to the quality of the driving fields, the accuracy of the stratospheric transport representation might therefore limit the precision of the results that can be obtained with these chemistry transport models. An evaluation of the meteorological analysis quality must then be performed prior to the utilisation of the CTM for the improvement of stratospheric tracer parameterisations.

This chapter evaluates, based on published results, the performance of existing stratospheric (re)analyses, their effects on tracer transport in CTMs, and the techniques CTMs apply to ameliorate such effects. The CTM used in this thesis is also described in this chapter. Section 2.2 summarises stratospheric transport aspects that are essential for long CTMs simulations, while the main datasets used to drive such simulations are described in Section 2.3. A discussion of CTM studies using these data, the problems highlighted in such works and the solutions currently applied are included in Sections 2.4 and 2.5, respectively. A description of the TOMCAT/SLIMCAT CTM used throughout this thesis can be found in Section 2.6. Section 2.7 summarises the main results from the discussions included in this chapter.

2.2 Stratospheric transport

2.2.1 Stratospheric circulation

A schematic representation of the stratospheric circulation is shown in Figure 2.1. The tropical tropopause is the main entrance region for air masses into the stratosphere. The air ascends over the tropics and, once in the upper stratosphere, it flows from the summer hemisphere to the winter hemisphere to descend over the winter pole. The air masses eventually come back to the troposphere, not only down through the polar vortex, but also by stratosphere-to-troposphere exchange (STE) processes at mid latitudes. The large-scale tropical ascent and winter pole descent, the so-called Brewer-Dobson circulation (BDC), are wave-drag driven and,

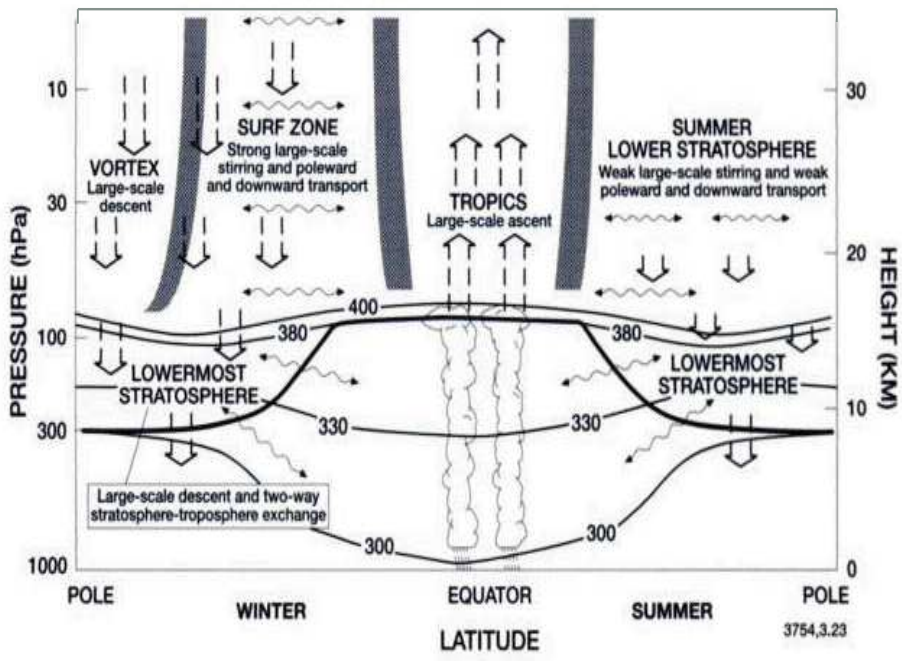

Figure 2.1: *Main stratospheric circulation processes. The different arrows illustrate different kinds of air mass transport. Transport barriers are indicated by the wide grey bands. From WMO Ozone Assessment 1998 (WMO, 1999).*

together with quasi-horizontal mixing processes, are the main features of the circulation in this region. The BDC was first identified by Brewer (1949) and Dobson (1956) through measurements of water vapour and ozone respectively. The downwelling is much weaker in the summer hemisphere and the circulation is stronger during the northern hemisphere winter than during the southern hemisphere winter, due to the different surface orography and generation of planetary waves between both hemispheres.

If only the upwelling and downwelling branches of the BDC were present in the stratosphere, the shape of the isopleths of long-lived tracers would present a much more abrupt subtropical gradient than shown in Figure 2.2 for CH_4. The transport of masses on isentropic quasi-horizontal surfaces acts to flatten the contours through horizontal mixing processes. These mixing processes, also known as eddy horizontal

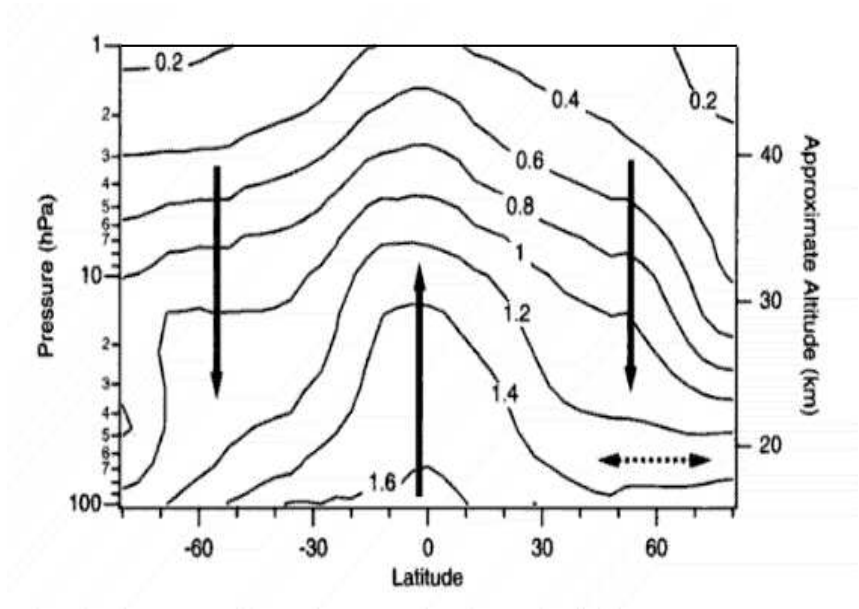

Figure 2.2: *Zonal mean distribution of CH_4 (ppmv) in the stratosphere for December 1992 measured from UARS satellite. The Brewer-Dobson circulation lifts the isopleths up over the tropics and pushes them down over high latitudes. At the same time, the eddy mixing processes act to flatten the contours on isentropic surfaces. Adapted from Dessler (2000).*

transport, are due to wave breaking on isentropic surfaces. Eddy horizontal transport is not equally intense for all latitudes, the regions where the horizontal mixing is slower are known as "transport barriers". These tropical barriers are found at 20°N and 20°S, and the winter polar barrier at 65°N or 65°S (see Figure 2.1). Such barriers are responsible for the pronounced gradients that long-lived tracers exhibit in their concentrations between tropical, midlatitude and polar regions. Further evidence for the existence of these barriers is the fact that the tape recorder signal for water vapour detected over the tropics is still discernable at 10 hPa (Mote et al., 1996; 1998), which indicates the presence of strong constraints to meridional mixing between tropics and subtropics (Figure 2.3). Transport barriers do not provide complete isolation between adjacent regions, but make mixing processes through barriers much slower compared to time scales for meridional mixing within one latitudinal

region, which led Plumb and Ko (1992) to propose their "tropical pipe" model. In the case of the winter polar barrier, filamentation and stirring processes cause mixing of air from the vortex with lower latitude masses (Juckes and McIntyre, 1987; Haynes, 2005).

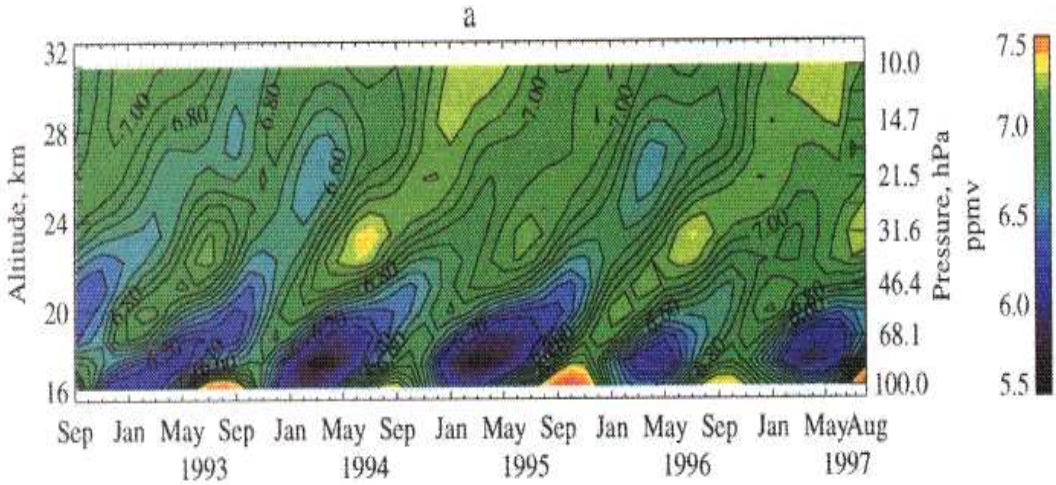

Figure 2.3: *Time series of the tape recorder signal in 2[CH_4]+[H_2O] (ppmv) from the Halogen Occultation Experiment (HALOE). From Mote et al. (1998).*

As represented in Figure 2.1, air masses in the stratosphere eventually return to the troposphere via the descent in the polar vortex and also via stratosphere to troposphere exchange (STE) processes at mid and high latitudes. That these stratospheric circulation processes are accurately represented in the fields driving CTM simulations is thus essential not only for stratospheric studies, but also for tropospheric investigations.

2.2.2 Stratospheric transport in CTMs

CTM predictions of chemical distributions depend critically on the accuracy of the description of transport in the model. Even when a CTM has the potential to correctly simulate the distributions of chemical species, if the quality of the fields used to drive the CTM is not sufficient the accuracy of the distributions will be degraded,

no matter how complex the chemistry (and radiation) codes in the CTM.

This is a particularly important problem in the stratosphere, where CTMs include a complex stratospheric description but the quality of analyses still needs to be evaluated carefully in that region. Nowadays most NWP and data assimilation (DA) systems have had their vertical domains increased to also include the stratosphere. The analyses produced by these systems are essential for stratospheric CTM studies, but their quality needs to be assessed to identify limitations and required improvements.

To evaluate transport in the stratosphere, the mean age-of-air (Hall *et al.*, 1999) and the age spectrum (Kida, 1983; Hall and Plumb, 1994) have become standard model tests (Waugh and Hall, 2002). These transport diagnostics are independent of chemistry, which makes them particularly appealing for CTM intercomparisons. An additional advantage of the mean age-of-air is that it can be derived from observations of conserved linearly increasing tracers like CO_2 and SF_6 (Andrews *et al.*, 2001; Boering *et al.*, 1996).

From 1996 to 1999 the National Aeronautics and Space Administration (NASA) coordinated a series of transport experiments to compare the stratospheric performance of almost 30 different atmospheric models (Park *et al.*, 1999). Most of the models included in this Models and Measurements II assessment (MMII) were found to underestimate the mean age-of-air compared to the existing observational values (Waugh and Hall, 2002). Two-dimensional (2D) and three-dimensional (3D) models using GCM and DAS winds were evaluated in the assessment, revealing that the strength of the stratospheric transport was being overestimated in most models. The use of such winds for CTMs studies would result in too fast transport of tracers and unrealistic chemical distributions. That is why, prior to any tracer simulation, modellers should be aware of the limitations of the datasets used and how to minimise their deficiencies. Moreover, modellers should analyse what dataset is most

appropriate to force their CTMs.

2.2.3 Winds for off-line simulations: DAS v. GCMs

Off-line CTMs can be forced by meteorological fields from a data assimilation system (DAS) or from a general circulation model (GCM). The major advantage of using assimilated (or analysed) fields is that in such a case the results from the CTM are directly comparable with observations on a particular day. However, the data assimilation process itself introduces discontinuities in the physical state of the NWP model that can affect the assimilated winds and therefore the modelled tracer transport. On the other hand, GCMs winds are physically self-consistent; no physical imbalances are introduced by inserting observations into the free-running model. However, GCM winds suffer from problems related to the lack of observational constraints. Too cold temperatures in the poles, especially in the southern hemisphere (SH); dispersion in the amplitude and mean value of the annual cycle of tropical tropopause temperatures and biases in the total ozone amount are some of the main problems exhibited by GCMs (*e.g.* Eyring *et al.*, 2006). General cold biases existed in many of the GCM models evaluated in Austin *et al.* (2003), biases that partly came from insufficient wave propagation from the troposphere (Newman *et al.*, 2001). These biases affect, among other things, the occurrence of polar stratospheric clouds (PSCs) and the ozone distribution. The inclusion of non-orographic gravity wave drag (GWD) schemes has reduced the stratospheric temperature biases in those models able to include such schemes. However, the source spectrum for these GWD schemes is prescribed externally and does not allow for temporal changes to be considered (Eyring *et al.*, 2006). The need of long series of observations to provide a statistical comparison with model results is also an issue for this kind of model in the stratosphere, where very limited observations exist prior to the satellite era.

In DAS, the physical imbalances created by the observation insertions generate spurious gravity waves that propagate into the stratosphere, where they artificially

enhance the circulation. These undesired effects introduced by data assimilation are of particular relevance for multiannual simulations, where transport of long-lived tracers is most affected and where inaccurate STE processes quantification can also affect tropospheric chemistry and dynamics.

Most existing analyses exhibit problems with the representation of the stratospheric circulation, *i.e.* the combined effects of the Brewer-Dobson circulation (BDC) and the meridional mixing processes. They produce a too strong BDC and not enough tropical isolation, resulting in a much too strong exchange of tracers between the tropics and higher latitudes. It is, therefore, a major question under debate whether analysed fields provided by DAS are good enough for long CTM simulations or not (*e.g.* Schoeberl *et al.* 2003; Douglass *et al.* 2003). Recently some authors have even suggested that a point might have been reached where the intrinsic elements of data assimilation prevent certain transport applications from further improvement (Stohl *et al.*, 2004; Rood, 2005).

Schoeberl *et al.* (2003) (hereafter referred to as S2003) compared winds from two DAS (UKMO and GEOS-4) with winds from the Finite Volume General Circulation Model (FVGCM). Their comparison highlighted the limitations of the DAS winds, and showed that GEOS-4 winds produced too strong vertical and horizontal tropical ventilation compared to the FVGCM winds. As the FVGCM was the core model used to produce the GEOS-4 set, these results were used in S2003 to argue that DAS winds were probably unsuitable for long-term stratospheric transport studies and preference should be given to GCM winds over DAS winds. This statement dates from 2002 using old UKMO analyses (Swinbank and O'Neill, 1994) and a preliminary version of GEOS-4 winds (S. Pawson, personal communication 2005). Nevertheless, data assimilation centres have continuously improved their systems, and increasing feedback from analyses users now provides useful information to them.

In S2003 the results obtained with the GCM winds are presented as the refer-

ence to compare with, when the results obtained with the FVGCM winds actually seem to be artificially too quiet (Figure 2.4). As Bregman *et al.* (2006) indicate, tropical air parcel dispersion should be interpreted with care because results are very sensitive to the starting level of the trajectories. Parcel distributions obtained from simulations with different starting levels are shown in Bregman *et al.* (2006) and, based on volcanic aerosol observations by Grant *et al.* (1994), they suggest that perhaps the results shown in S2003 with the GCM winds should not be taken as an ideal reference.

Further investigation is needed in this field to evaluate the quality of the newest available stratospheric analyses in terms of their performance in multiannual tracer transport simulations. And also to discern what aspects of the recent improvements introduced by DAS have played a main role in the stratospheric representation, as well as to identify areas where more development should still be done.

2.3 DAS products

2.3.1 Analysed winds

One could define analysed products to be a very useful result of combining imperfect models and biased observations. An analysis is the result of combining some background information, typically coming from a short forecast run of an NWP model, with observations taken during the same period of time comprised by the background. This data assimilation technique is widely used by operational centres to improve the quality of their forecasts, and to produce time series of analysis for long (multidecadal) periods of time, the so-called reanalysis datasets.

By using the analysis corresponding to the previous time step to initialise the forecast, the NWP model is constrained by more realistic initial conditions than by just letting the model evolve freely; in a free run inaccuracies in the initial conditions could result in a forecast state very much divergent from reality. By assimilating

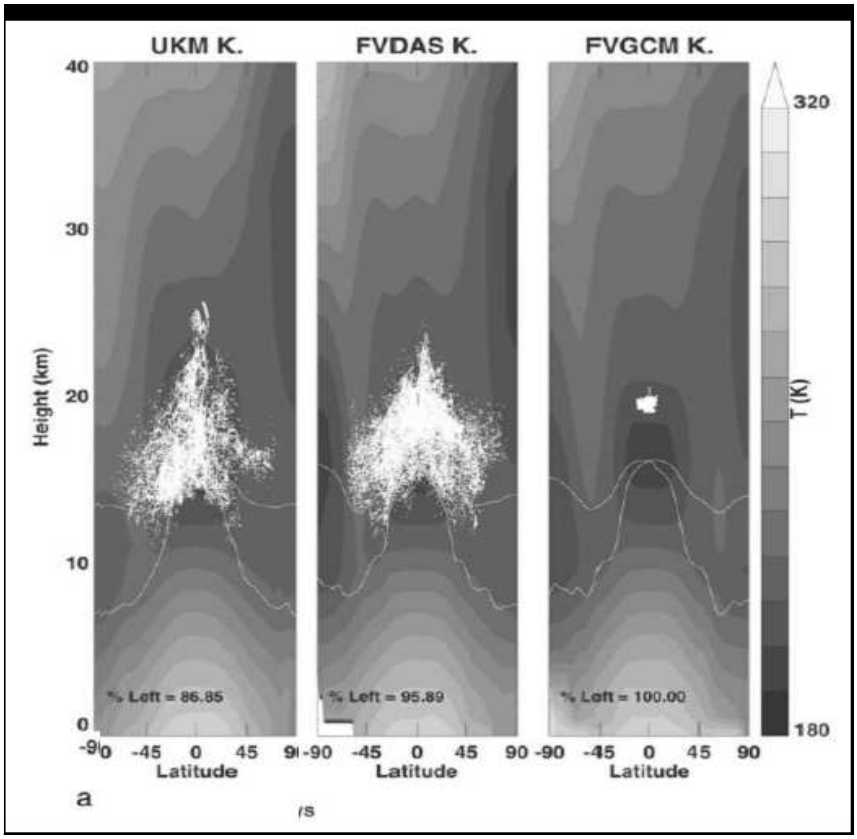

Figure 2.4: *Kinematic trajectories obtained after a 50-day backwards simulation using two assimilated winds datasets: UKMO winds (left panel) and FVDAS winds (middle panel), and one set of GCM winds (right panel). The initial position of particles is located at 20 km over the equator. The thin white lines show the tropopause and the 380 K isentrope. The percent of parcels remaining in the stratosphere at the time are indicated in each panel. Taken from Schoeberl* et al. *(2003).*

data the model is continuously adapted to match the observed atmospheric features. The disadvantage associated with data assimilation is, however, that the continuous adjustments create artificial discontinuities in the model physics which produce undesired effects (*e.g.* spurious gravity waves). This needs to be taken into account when using data assimilation products for seasonal to multiannual studies.

The primary concern of DAS/NWP centres, such as ECMWF or U. K. Met Office, is the production of high quality weather forecasts for short and medium-

range. This produces a long archive of operational analysis that can also be used for other research purposes, including CTMs simulations. However, operational analyses are subject to the changes introduced by the continuous improvements incorporated to the NWP/DAS models and the changes in the observations used in time. These changes can sometimes lead to wrong conclusions when using these operational datasets for multiannual studies and, most of the times, changes in the DAS system introduce biases that are larger than the climatic trends some studies aim to detect. To solve this, following the proposals by Bengtsson and Shukla (1988) and Trenberth and Olson (1988), some DAS centres have produced reanalysis data series. Reanalyses are backwards series of analyses produced with one up-to-date version of the data assimilation and forecast system, so that the reanalysis can take advantage of the latest improvements introduced in the system without suffering from inhomogeneities. In practice there will always be some inhomogeneities due to changes in the observations assimilated within the complete reanalysis period. Some of the main existing analyses and reanalysis products are described next.

2.3.2 Reanalyses datasets

ERA-15

ERA-15 was the first reanalysis series produced by the ECMWF. It covers the period 1979-1993 and it was based on an Integrated Forecast System (IFS) version with 31 vertical hybrid levels and a T106 horizontal resolution. An optimal interpolation (OI) assimilation method was used. This first generation dataset was widely used, but deficiencies were soon reported. Problems with ERA-15 in the troposphere included a cold bias in surface temperatures and too coarse orography (Kållberg, 1997). In terms of the stratosphere, the IFS model used only reached 10 hPa and had just five model levels above 100 hPa, which was a strong limitation for stratospheric studies and multiannual tropospheric research that needed to consider stratospheric influences. In addition, the period covered by ERA-15 was too short for climatic studies. Larger reanalysis periods were already a necessity, but depended on the

availability of larger computational power and storing capacity.

NCEP/NCAR

This reanalysis was carried out by the U.S. National Centers for Environmental Prediction (NCEP) in collaboration with the National Center for Atmospheric Research NCAR (Kalnay *et al.*, 1996). Like ERA-15, it was produced in the mid 1990s and belongs to the first generation of reanalysis. The reanalysis period starts in 1948 and it has been continued in near real-time as a climate data assimilation system, or CDAS (Kistler *et al.*, 2001). The system uses a three-dimensional variational (3D-Var) assimilation algorithm. Reanalyses data are provided in 17 constant pressure vertical levels. This dataset was not created for stratospheric studies and data are only available up to 10 hPa. A second version of this reanalysis was performed (Kanamitsu *et al.*, 2002) that corrected some human errors detected in the first release that could not be corrected in time. This second reanalysis is, however, based on the same system as the first one.

ERA-40

Almost ten years after the completion of ERA-15 computational developments would allow for the production of a 45-year reanalysis series by the ECMWF: ERA-40 (Uppala *et al.*, 2005). This series, completed in 2003, belongs to a second generation of reanalysis that benefit from all the experience gained with the production of the previous series. The computer resources available allowed the use of a more recent IFS version and increased resolution. The stratosphere was this time included up to 0.1 hPa with 24 model levels, out of 60, above 100 hPa. More, and more complex, parameterisations were incorporated, including one simple ozone parameterisation (Dethof and Hólm, 2004) that allowed O_3 analysis. Thanks to the inclusion of ozone a better use of satellite radiances was possible, and a better representation of the stratosphere was also achieved.

ERA-40 was produced with a system based on the IFS cycle 23r4 (operational

in 2001-2002), although it was necessary to adapt the system to cope with the requirements of a reanalysis rather than operational analyses. Other adjustments, like the reduction of the horizontal resolution or the use of 3D-Var instead of four-dimensional variational (4D-Var) data assimilation method (already operational in 2002), were made to reduce computational cost. The model resolution adopted for ERA-40 was T159L60, instead of the T511L60 in the operational model at that time.

Since its completion, ERA-40 data have been used in numerous studies and projects, not only on climate and chemistry, but also on health, energy, biodiversity and natural hazards, among others. Hollingsworth and Pfrang (2005) report on the variety and quantity of ERA-40 existing applications. Additional information on some projects involving ERA-40 can be found on the following ERA-40 website: http://www.ecmwf.int/research/era/era40survey/. Health applications include studies to predict malaria outbreaks (Thomson *et al.*, 2006), or to evaluate the predictability of extreme events such as the 2003 summer heat wave (Schär *et al.*, 2004). The impact of climate variability on crop yields has been also studied using ERA-40 data (*e.g.* Challinor *et al.* 2005) and some studies have used this reanalysis dataset for energy demand and production estimations (*e.g.* Benito Garcia-Morales and Dubus 2007).

JRA-25

The Japanese 25-year Re-Analysis (JRA-25) is a joint research project between the Japanese Meteorological Agency (JMA) and the Central Research Institute of Electric Power Industry (CRIEPI). The reanalysis period is January 1979 to December 2004. The global model resolution is T106L40 (with the model top at 0.4hPa). The assimilation algorithm used is 3D-Var, as in the JMA's operational system of April 2004, but with some additional data assimilated from the Special Sensor Microwave/Imager (SSM/I) and the TIROS Operational Vertical Sounder (TOVS). The completion of this reanalysis dataset was accomplished in mid 2006. Recent detailed information on this dataset can be found in Onogi *et al.* (2007).

2.3.3 Operational analyses

UKMO analyses

U.K. Met Office produced the first analyses including the whole stratosphere (Swinbank and O'Neill, 1994). Such analyses were initially produced in support of the UARS mission, and later production continued with a similar data assimilation system. These analyses are interpolated onto the UARS satellite levels and are archived every 24h (12 UTC). These data were made widely available and have been used in numerous model studies (*e.g.* Chipperfield 1999; Rogers *et al.* 1999). There are, however, other assimilated products that have become more successful for CTM studies given the quality of the stratospheric representation they provide (*e.g.* Chipperfield 2006). The most recent UKMO model versions include changes that provide a better quality of winds and temperatures in the stratosphere than previous UKMO model configurations. Two of the changes in the model, switching to a semi-Lagrangian method and implementing a 4D-Var assimilation algorithm, are expected to have increased the quality of the UKMO stratospheric analysis making them closer to ECMWF's (re)analyses (M. Kiel, personal communication, 2006). Nevertheless, these new analyses have not been tested yet in stratospheric studies with CTMs.

ECMWF operational

All the analyses produced to initialise ECMWF forecasts are archived daily (00, 06, 12 and 18 UTC), and can then be used to drive CTMs. The advantage of using operational winds is that they are produced with the latest model version and existing deficiencies are frequently revised and corrected. The disadvantage comes from the same fact, the corrections (improvements) introduced in the system cause biases with respect to the previous version that affect the results obtained from off-line models. Even so, reanalyses have not always been available and they do not cover the most recent years (ERA-40 stops in August 2002). In other cases, CTM simulations are short enough to take advantage of the corresponding archived

operational analyses without suffering from any discontinuity in the system. An additional use for these analyses is the evaluation of the effects caused by those system upgrades[1]. Significant changes that are thought to have played a major role for stratospheric transport have been the implementation of the 4D-Var assimilation method (November 1997), improved error statistics treatment (June 2005) and continuous developments in parameterisations of convection, ozone and humidity. More detailed information on recent changes in the IFS model is included in Chapter 4.

ECMWF analyses have been very widely used for stratospheric CTM studies, which is why the completion of ERA-40 in 2003 was eagerly anticipated by the CTM community: It would allow the use of a long series of data produced with the same system, and would exhibit the highest quality the ECMWF system could afford for such an ambitious project at that time. ECMWF operational data and ERA-40 data have been extensively used by chemistry-transport modellers for different stratospheric and tropospheric studies. Among the stratospheric topics investigated with ERA-40 are those on polar ozone loss (*e.g.* Chipperfield *et al.* 2005), mid-latitude ozone trends (*e.g.* Feng *et al.* 2007), ozone recovery detection (*e.g.* Hadjinicolaou *et al.* 2005), STE process trends (*e.g.* van Noije *et al.* 2004; van Noije *et al.* 2006) or tropical tropopause layer (TTL) variability (*e.g.* Krüger *et al.* 2008).

This wide range of studies has permitted the identification of features needing to be solved for an accurate stratospheric representation. The main problems for upper atmosphere studies detected in ERA-40, and in other existing DAS products, are discussed in Section 2.4. This thesis evaluates the effects that recent developments included in the ECMWF system have on stratospheric transport. Results from such evaluation are presented in Chapters 3 and 4.

[1]Detailed information on the changes introduced in each new version of the ECMWF model can be found here: http://www.ecmwf.int/products/data/operational_system/evolution

GEOS analyses

This dataset is produced by the Data Assimilation Office (DAO) of the NASA by assimilating observations into the Goddard Earth Observation System (GEOS) model. The first version was produced in the 1990s, recently GEOS-4 version has been produced (Bloom *et al.*, 2005). From version GEOS-2 these analyses have included the whole stratsophere. The GEOS-4 data have been used in relevant studies comparing the performance of analysed winds versus GCM winds (*e.g.* Douglass *et al.* 2003; Schoeberl *et al.* 2003) that, as mentioned earlier, have provoked an active scientific debate on the suitability of DAS products for long term stratospheric studies (Stohl *et al.*, 2004; Rood, 2005).

FUB analyses

The Free University of Berlin (FUB) was pioneer at the production of a data series following a very different approach to all the other existing reanalyses described here. The FUB reanalysis are not based on an automatic assimilation of archived observations but it is a subjective analysis based on radiosonde data. These data are available since 1957 (geopotential only) with temperature data added from 1964 ownwards, ending in 2001. The entire dataset can be found in CD format (Labitzke and Coauthors, 2002). However, given the characteristics of their "by-hand" production, these data are available only on 3 levels, and the horizontal resolution is limited to 5°x5°. Besides, these data are restricted to the Northern Hemisphere. Nowadays these dataset cannot overall compete against second generation reanalyses like ERA-40 or JRA-25, however, very good agreement was found between the FUB temperature field and independent radiosondes measurements (B. Knudsen, personal communication, 2006), see also Section 2.4.2.

All the (re)analyses described here have been used in relevant CTM studies whose main results for the stratosphere are discussed in Section 2.4.

2.4 Stratospheric analyses to force CTMs

This section presents the problems that currently exist on using analyses for stratospheric off-line chemistry-transport runs, together with some important effects such problems cause in tracers modelling. Monge-Sanz and Chipperfield (2006) summarised problems experienced by CTM modellers with different existing (re)analyses and requirements for future datasets; these aspects are analysed here in more detail. A discussion of the correction methods applied at the moment by CTMs is also found in this section. Inaccuracies in the stratospheric winds and temperature fields have been reported for most existing analyses and reanalyses (Randel *et al.*, 2004a; Manney *et al.*, 2005).

2.4.1 Stratospheric circulation

CTM studies using DAS products have reported two major problems concerning stratospheric transport:

- Too strong Brewer-Dobson circulation (*e.g.* Meijer *et al.* 2004; Chipperfield 2006.)
- Excessive horizontal mixing in the tropical region (*e.g.* Schoeberl *et al.* 2003; Tan *et al.* 2004.)

Tape recorder

The seasonally varying signal of the water vapour in the tropical stratosphere, the so-called "tape recorder" signal (Mote *et al.* 1996; 1998), reflects how rapidly air masses are transported upwards from the tropical tropopause into the stratosphere. The tape recorder is thus a good measure for the strength of the BDC over the tropics. Compared to the Halogen Occultation Experiment (HALOE) satellite measurements of the quantity $2[CH_4]+[H_2O]$, the specific humidity field time series over the tropics for ERA-40 exhibits a too fast and strong tape recorder signal (see *e.g.* Chipperfield, 2006). This indicates that the tropical ascent in ERA-40 is too strong, which affects

not only the humidity field but the transport of any tracer into and within the stratosphere. Age-of-air computations have shown that the inaccuracies are not restricted to the equatorial region only, and are not exclusive to ERA-40 but a general issue in analysed datasets (Waugh and Hall, 2002; Schoeberl *et al.*, 2003; Meijer *et al.*, 2004; Scheele *et al.*, 2005; Chipperfield, 2006).

Age-of-air

An example of the excessively strong stratospheric transport in CTMs is illustrated in Figure 2.5. This figure shows the mean age-of-air at 20 km altitude obtained with two different CTMs: TOMCAT/SLIMCAT on the left (from Chipperfield 2006), and the Royal Netherlands Meteorological Institute tracer model (KNMI TM) on the right (from Meijer *et al.* 2004). Both models strongly underestimate the age-of-air with ERA-40 and UKMO winds. Not only are values too young compared to observations but also the latitudinal gradient is far too weak. These features indicate too rapid vertical transport on the one hand (too strong BDC), but also too much mixing between tropics and subtropics. The rest of the lines in this figure are obtained by applying some kind of correction technique to the model or analyses, and are discussed in Section 2.5.

Transport barriers

As shown in Figure 2.5, too much subtropical mixing leads to weak meridional gradients of tracers. Different meteorological analyses exhibit very different transport barrier strengths. The NCEP analyses used in the intercomparison study by Manney *et al.* (2005) showed a too weak transport barrier in the equatorial lower stratosphere (LS). The same study revealed weaker barriers in that region for GEOS-4 and NCEP/NCAR than for the ECMWF and UKMO analyses. Tracer distributions can therefore depend strongly on the specific analyses used. Apart from the variability among analyses, mixing across the tropical barrier has been reported to be too strong in DAS products, compared to GCM fields. For the Finite Volume DAS (FVDAS) Tan *et al.* (2004) found that excessive mixing was correlated to a

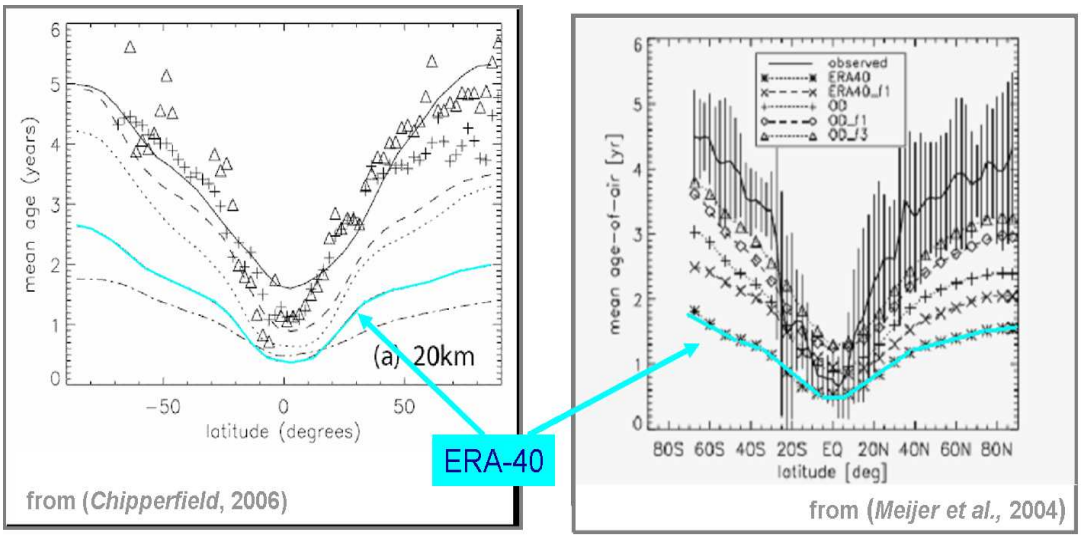

Figure 2.5: *Mean age-of-air at 20 km obtained with TOMCAT/SLIMCAT (left) and the KNMI TM model (right). Both models strongly underestimate the age-of-air with ERA-40 winds for 2000. Lines corresponding to older distributions in this figure are obtained using newer analyses (ECMWF operational) or by applying some kind of correction technique, as discussed in Section 2.5. Adapted from Chipperfield (2006) and Meijer* et al. *(2004).*

higher number of eddy structures in the tropical region, and that the impact of data insertion was larger in the tropics.

2.4.2 Stratospheric temperatures

Temperatures in ERA-40 have been reported to present a cold bias in the upper stratosphere, as well as unrealistic oscillations in the vertical, especially large over the South Pole (Randel *et al.*, 2004a; Simmons *et al.*, 2005). Also studies comparing temperatures from different reanalyses against temperatures from radiosondes (*e.g.* Knudsen 1996; 2003) reveal the existence of an important cold bias over the Arctic for ERA-40, while NCEP/NCAR is found to be too warm compared to radiosondes in this region (B. Knudsen, personal communication, 2006). On the other hand, NCEP/NCAR reanalyses were designed for tropospheric studies and are not recom-

mended for polar investigations due to temperature biases in the LS (Manney *et al.*, 2005).

FUB reanalyses provide more realistic polar temperatures than NCEP/NCAR reanalysis Manney *et al.* (2005) and, for most of the period covered by ERA-40, also more realistic than ERA-40 (B. Knudsen, personal communication, 2006). These data help to show that some deficiencies in the polar temperature field could be corrected in reanalyses like ERA-40 by assimilating more radiosonde data. There is now ongoing research on the homogenisation of data from radiosonde for this purpose (Haimberger, 2006). It might be surprising that also for the satellite era the FUB data are better than the automatised analyses (ERA-40 and NCAR). However, one feasible explanation is that when radiosonde data are sparse, the analysis relies on modelled temperatures and satellite derived temperatures. If this goes on for a long time, radiosonde temperatures could be flagged as erroneous and not used in the assimilation (B. Knudsen, personal communication, 2006). Also the weighting functions for the assimilated satellite data can lead to erroneous vertical distribution of temperatures. It is therefore desirable that future (re)analyses include as much radiosonde data as possible to get a more realistic temperature structure over the poles, which will result in more realistic PSC area calculations. More radiosonde data would help to further constrain analysed polar temperatures, and reduce the discrepancies between different (re)analyses.

Manney *et al.* (2003) found that minimum temperatures over the Arctic could vary up to 5 K between different analyses, and areas of low temperatures may differ by an average of 25%. For variable winter conditions (like in 1995/1996) the accurate representation of local features, such as temperature minima on the Arctic vortex edge, depends on technical characteristics of the analyses such as resolution or data assimilation algorithm used to produce the analyses (Manney *et al.*, 2003). It seems reasonable then to expect improvements in the polar stratosphere description by improving technical aspects of the DAS.

2.4.3 Effects on CTM simulations

Ozone distributions

Figure 2.6 shows total ozone (TO) column distributions obtained with ERA-40 winds in the REPROBUS CTM (Lefèvre *et al.*, 1994). It can be seen how, compared to Total Ozone Mapping Spectrometer (TOMS) observations, the model simulates too high values over high latitudes and too low values over low latitudes. These biases correspond to the too rapid BDC that acts to remove too much ozone from the tropics (or not giving air masses the time for the formation of ozone) and accumulating ozone over the poles (too strong BDC descent branches). The problem is common to other CTMs, TOMCAT/SLIMCAT included (WMO, 2007).

Distributions of long-lived tracers

Multiannual simulations with accurate stratospheric transport are needed to study the evolution of long-lived tracers. However, the too strong BDC and mixing reported for DAS products prevent CTMs from obtaining realistic distributions. As shown in Figure 2.6, the accumulation of excessively high O_3 concentrations is a problem for CTMs, as well as the too weak latitudinal gradients (too flat shape of isentropes) of other tracers like CH_4 (*e.g.* Strahan and Polansky 2006) or N_2O (*e.g.* Berthet *et al.* 2006) due to the excess horizontal mixing. Also, the simulation of Cl_y concentrations is highly dependent on transport (Waugh *et al.*, 2007). Inaccuracies in modelled Cl_y affect the ability to detect polar ozone recovery trends, which is currently an active research field (WMO, 2007).

PSC occurrence

One of the key roles in the destruction of O_3 over polar regions is played by the heterogeneous chemistry that takes place on polar stratospheric clouds (PSCs). This kind of cloud can form only at the low temperatures found inside the polar vortex in winter and spring. To correctly simulate the polar ozone loss, CTMs need accurate polar temperatures to calculate the areas covered by PSCs. However, the prob-

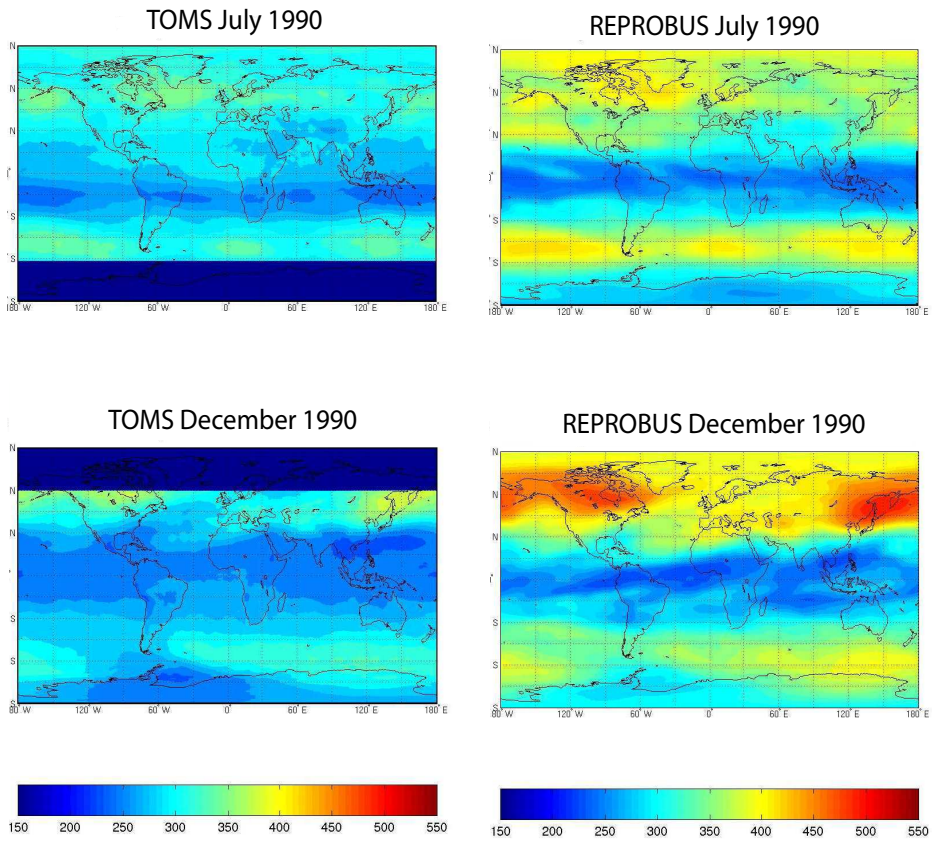

Figure 2.6: *Total ozone (TO) distribution in Dobson units (DU) for July (top row) and December (bottom row) 1990 as simulated by the REPROBUS CTM using ERA-40 6h forecasts (right) and from TOMS observations (left). Courtesy of F. Lefèvre and T. Song (SA, IPSL, Paris, France).*

lems that current (re)analyses exhibit in the temperature field make the calculation of realistic PSC areas impossible, seriously affecting polar ozone loss studies (*e.g.* Knudsen 2003; Manney *et al.* 2005).

In Manney *et al.* (2005), several analysis datasets are compared to assess how well they reproduce the 2002 Antarctic stratospheric warming. Among the datasets considered were ERA-40 reanalyses, operational analyses from the ECMWF, several GEOS-4 analysis versions, NCEP analyses and reanalyses and UKMO analy-

ses. ECMWF and GEOS-4 analyses reproduce better the polar vortex structure and evolution, and also the filamentation and lamination results are better for these datasets, which are the higher resolution analyses. Reanalyses from NCEP produce particularly short PSC lifetimes, and ERA-40 presents unrealistic oscillations of temperature over the South Polar region in 2002.

More recent ECMWF systems seem to have solved the oscillation problems found in ERA-40. However, the improvement is apparently due to a more efficient data assimilation and not to improvements in the IFS model itself, as the new ECMWF model Cycle version T799L91 again presents some T oscillations over the South Pole (much less significant than in ERA-40 though). This presumably occurs because now the mesosphere is also included in the model, and the amount of data assimilated for this region is much smaller than for the rest of the atmosphere, which makes oscillations generated in the mesosphere propagate downwards (E. Hólm, personal communication, 2006).

Polar temperature inaccuracies cause particular trouble over the Arctic since the vortex structure is more unstable there than in the Antarctic. Occasional errors in the analyses can give a completely different amount of PSCs and, therefore, of Arctic ozone loss, water vapour, chlorine and nitrogen compound concentrations. Intercomparison between different studies is also particularly difficult, as the use of a different meteorological dataset can lead to very different conclusions in polar air processing investigations (Manney *et al.*, 2003).

STE flux

Stratospheric transport also affects the budgets of tracers in the troposphere as it controls the exchange between stratosphere and troposphere (STE). Calculations made by CTMs with ERA-40 data reveal that the flux of stratospheric ozone reaching the troposphere presents important discontinuities and is higher than the flux obtained using ECMWF operational analyses (van Noije *et al.* 2004; 2006).

In van Noije *et al.* (2004) the excessive flux obtained with ERA-40 winds for the year 1997 is reported but no clear reason for this is given, pointing instead to the need for further investigation and for better dynamical parameterisations over the tropics. van Noije *et al.* (2006) complemented their previous studies by using the whole series of ERA-40 winds, and comparing the final ERA-40 years with operational analyses. They found that when using forecasts the STE fluxes are reduced for both ERA-40 and operational data. Also in van Noije *et al.* (2006) an interesting comparison is performed between ERA-40 and a short (Jan-Mar 1973) experimental run of ERA-40 in which no satellite radiances were assimilated. For this experimental run the STE of ozone is lower over the Northern Hemisphere than for the normal ERA-40 run. From the Van Noije et al. studies it appears that with ERA-40 STE fluxes show sensitivity to both forecast range and satellite observations, and also that improvements in the data assimilation system (4D-Var operational analysis v. ERA-40) improve STE calculations.

In van Noije et al. (2004; 2006) the ozone fluxes are calculated with the linearised ozone model LINOZ (McLinden *et al.*, 2000) implemented in the KNMI chemical transport model. One problem for this kind of ozone flux computations is the scarce observational datasets to compare with. So far the best existing data record is still the one provided by Gettelman *et al.* (1997) from UARS data (T. van Noije, personal communication, 2008). This dataset is, however, restricted to one level (100 hPa) and dates from the mid 1990s. More recent, and global, observations would be needed in order to detect any possible changes in the BDC.

Processes in the TTL

The tropical tropopause layer (TTL) has been identified as the main entrance region from the troposphere into the stratosphere (*e.g.* Fueglistaler *et al.* 2004). The TTL is therefore of particular interest as processes in this region play a key role in the dehydration of air entering the stratosphere, and are then responsible for the

water vapour budgets in the atmosphere. Understanding circulation processes and temperature structure within the TTL will help to understand key issues such as stratospheric water vapour (SWV) distribution and variability or the role of very short-lived species (VSLS) in ozone depletion (WMO, 2007).

However, there is not enough constraint for DAS products in the TTL region. Studies using ERA-40 data (*e.g.* Krüger *et al.* 2008) warn about the possibility that inhomogeneities in the ERA-40 series and differences between ERA-40 and operational ECMWF might affect results, introducing a bias larger than the searched trend in the tropopause cold point distribution. In addition, residence times in the TTL are critical to evaluate changes in the air composition when travelling from the troposphere to the stratosphere; nevertheless, significantly different values are found in different studies, ranging from 20 days (Fueglistaler *et al.*, 2004) to 80 days in Folkins and Martin (2005). Also the vertical motion field in the analyses is too noisy for this type of study (Tegtmeier, 2007; Krüger *et al.*, 2008). Therefore, the representations of both temperature and vertical motion need to be improved in DAS models to achieve a realistic TTL description. For instance, one of the main problems in ERA-40 is the excessively dry lower and middle stratosphere (Uppala *et al.*, 2005). For future (re)analyses, improving the vertical advection (reduction of noise in vertical winds) and improving the temperature structure (reduction of biases) would improve the representation of the water vapour transport across the tropical tropopause.

As discussed above, there are a number of issues concerning analysed datasets that affect CTM simulations in different important aspects. CTMs cannot ignore the effects caused by the inaccurate stratospheric representation in the analyses, and research has been done towards the correction, or minimisation, of these effects within the CTMs themselves. The next section discusses the main fixes currently applied by CTM modellers in stratospheric simulations.

2.5 Correction strategies within CTMs

Analyses and reanalyses are already a final product when CTMs use them, thus the only possibility is to apply some correction techniques, within the CTMs themselves, to deal with the problems described above and improve the stratospheric transport. To overcome the too rapid stratospheric vertical transport and the excessive mixing, chemistry-transport modellers have implemented various techniques that can be grouped in two different categories:

- Modifications to the model configuration.
- Modifications to the analysis dataset or its use.

2.5.1 Model configuration

Use of $\sigma - \theta$ coordinates

Instead of using $\sigma - p$ levels in the stratosphere, the use of isentropic coordinates helps to separate horizontal and vertical motion. And since stratospheric transport on θ coordinates is quasi-horizontal, numerical errors due to vertical advection are reduced, and planetary waves are better handled. Figure 2.5 illustrates the difference in the zonal mean age-of-air at 20 km obtained with the same ERA-40 data using the TOMCAT configuration ($\sigma - p$ levels) of our CTM and using the SLIMCAT configuration ($\sigma - \theta$ levels)[2]. The dotted line in the left panel of Figure 2.5 is obtained with ERA-40 winds using a $\sigma - \theta$ vertical coordinate and, as in the TOMCAT configuration, computing vertical motion from the horizontal divergence. The underestimation obtained with the TOMCAT simulation (blue line in same figure) is clearly overcome with the use of $\sigma - \theta$ levels, with this second configuration the CTM results are very close to the observational ones. This option has been used in different studies (*e.g.* Chipperfield 1999; Chipperfield 2003) and several models

[2]See Section 2.6 for the definition of these two different configurations of the TOMCAT/SLIMCAT CTM.

(Mahowald *et al.*, 2002; Thuburn, 2003).

However, even if the use of isentropic coordinates improves this aspect of the simulations, there are a number of reasons why pressure coordinates could still be preferable:

- CTMs should ideally mimic the transport in the NWP model used to produce the analyses, and NWP models use p coordinates.
- Isentropic coordinates are useful in the stratosphere to separate horizontal and vertical transport, but generally do not allow for mass conservation.
- Isentropic coordinates cannot be used for the troposphere anyway, and now there is increasing interest in models with no borders separating troposphere and stratosphere.

Increasing resolution

Changes in the resolution of a CTM affect the age-of-air obtained with that model (*e.g.* Eluszkiewicz *et al.* 2000; Chipperfield 2006; Strahan and Polansky 2006). However, the extent of the effect depends on the vertical advection scheme the CTM uses. In TOMCAT/SLIMCAT very small differences were seen when using the non diffusive Prather (1986) second-order moments scheme with different resolutions, larger differences appeared when switching to the semi-Lagrangian transport (SLT) scheme (Chipperfield, 2006). The effects caused by resolution changes depend also on the specific CTM used. Chipperfield (2006) found that increasing horizontal resolution in TOMCAT/SLIMCAT decreased the age-of-air in the upper stratosphere (US), while Strahan and Polansky (2006) observed the opposite effect on age-of-air, ozone and methane distributions with the Goddard Space Flight Center (GSFC) CTM (Douglass *et al.*, 2003), both models using a SLT advection scheme. These two studies also showed how changes in the vertical resolution have a much smaller effect than changes in the horizontal resolution.

Changing the resolution can thus change the distribution of tracers, but knowing how much the distribution will change or whether the changes will be for better or worse depends on the particular CTM. And in any case, the effects on the modelled age-of-air due to resolution changes are found to be much smaller than those due to other modifications, such as changing the vertical coordinate or the set of analyses used (Chipperfield, 2006; Strahan and Polansky, 2006).

Advection scheme

Different advection schemes were tested in Eluszkiewicz *et al.* (2000) (hereafter EL2000) within the Geophysical Fluid Dynamics Laboratory (GFDL) SKYHI GCM (Hamilton *et al.*, 1995). They found large differences in the age of air obtained with this GCM using a SLT scheme or a non-diffusive (centred-difference) scheme; ages obtained with the SLT were around 7 years younger. Four versions of the same SLT algorithm were tested in the NCAR Middle Atmosphere Community Climate Model 3 (MACCM3) and, on average, age values were 3 years older than those obtained with the SKYHI simulations. Chipperfield (2006) also found that the use of a SLT scheme, while keeping all the other model options unchanged, resulted in younger age values than the use of the non-diffusive Prather (1986) scheme, although the differences were significantly smaller than those produced in the model used by EL2000. These results indicate that stratospheric transport is sensitive to model numerics, but again the exact effects of one choice or another depend on the model used.

The study by EL2000 also showed that the choice of the advection scheme does not affect the age-of-air results obtained with 2D models. In this kind of model the stratospheric circulation is prescribed by the residual circulation and a certain parameterisation for the horizontal diffusion. By inspecting a wide range of diffusion coefficients EL2000 pointed that it is the smoothly varying circulation and not the diffusion that makes 2D models almost insensitive to the advection scheme. It is then the existence of spurious vertical features that make 3D models so sensitive

to the advection scheme. However, 2D models do also exhibit a young bias in the age-of-air, thus the spurious vertical features in the vertical transport cannot be the only reason why models reproduce a too strong stratospheric circulation.

Vertical transport

CTMs can take the vertical wind field directly from the analyses or diagnose it from horizontal fields (i.e. divergence of the horizontal winds). The first option would involve additional processing (interpolation or averaging of vertical winds onto the model grid) and in any case it might produce vertical transport inconsistent with the separately processed horizontal winds. The second option, which uses horizontal winds already processed on the model grid, helps to ensure the vertical and horizontal mass transport are consistent. This issue of consistency, and how crude interpolation of wind fields can cause problems in CTM tracer transport, is discussed in Bregman *et al.* (2003). Besides, the vertical velocity field has been found to be too noisy in the ECMWF analyses (*e.g.* Fueglistaler *et al.* 2004; Tegtmeier 2007; Krüger *et al.* 2008), even if in Fueglistaler *et al.* (2004) they decided to use the instantaneous vertical velocity in the ECMWF analyses for other advantages such as resolution.

To avoid these problems with the vertical field, off-line CTMs can adopt two options. First they can calculate the vertical motion from the divergence of the horizontal winds; ECMWF, for instance, archive the divergence field. As a second option, CTMs can also compute the vertical motion from the radiative heating rates by converting the diabatic heating rate Q into vertical mass flux w_m, as it is for example done in the NCAR Isentropic Model of Atmospheric Transport and Chemistry (IMATCH) (Mahowald *et al.*, 2002) or in TOMCAT/SLIMCAT (Chipperfield, 2006):

$$w_m = -Q(\frac{p}{p_0})^{\frac{R}{C_p}} \frac{1}{g} \frac{dp}{d\theta} \tag{2.1}$$

where p_0 is a reference pressure (Pa), R is the gas constant (J/kg), C_p the dry air

heat capacity (J/kg), and g the gravitational acceleration (m/s^2).

One of the radiation schemes included in TOMCAT/SLIMCAT, the CCMRAD scheme (Briegleb, 1992) is similar in complexity to the scheme used by the ECMWF. However, for the method to be as consistent as possible with the analyses, the radiation scheme used to obtain the heating rates should be identical to the one used by the GCM that produces the analyses. A similar option is the calculation of the heating rates by independent methods/models to provide a new modified series of analyses in which the vertical velocity has been substituted by the field calculated from heating rates (*e.g.* Wohltmann and Rex 2008), and then use this modified series to run the CTMs.

The use of heating rates improves the age-of-air results obtained (Chipperfield, 2006) and also the transport representation in the TTL (Krüger *et al.*, 2008). The main disadvantage of using heating rates is that differences in the radiation schemes used may cause inconsistencies between vertical and horizontal winds, although some procedures have been proposed to make vertical motion from the radiation scheme consistent with the horizontal winds (Weaver *et al.*, 2000). In any case, a better option would be the use of archived heating rates from the analyses, however, these are not always available.

2.5.2 Analyses datasets

Use of forecasts

The discontinuities created in the NWP/DA system due to the assimilation of observations generates spurious eddies and waves that artificially enhance the stratospheric circulation. These physical imbalances introduced by DA can be reduced using forecasts longer than 6 hours instead of analyses. In this way the physical model will run freely (without observation insertion) for a longer time and the imbalances will be less pronounced.

CTMs using ECMWF forecasts obtain more realistic results than with the corresponding analyses. In Meijer *et al.* (2004) and Scheele *et al.* (2005), the use of ERA-40 forecasts resulted in older (more realistic) mean age-of-air values than ERA-40 analyses. However, results improved further if instead of using ERA-40 forecasts, the model switched to operational ECMWF data produced with the more complex 4D-Var assimilation method. In Meijer *et al.* (2004) the operational forecasts again gave older ages than the operational analyses. However it is worth noting that the use of long forecasts (72h), while resulting in older ages than shorter forecasts, did not necessarily result in more realistic values. From Figure 2 in Meijer *et al.* (2004) (included here as right panel in Figure 2.5) one can see that 72h data are too old over the tropics compared to observations, as if everything had been shifted upwards, suggesting that the vertical motion is now too slow. The main problem with the use of forecasts is that then the frequency of the fields read in by the CTM would always be longer than 6h and there are already works suggesting that 3h winds should be used (see next point).

Increasing read-in frequency

Typically the winds and temperatures are read in by the CTM every 6 hours, the frequency with which the NWP centres like ECMWF archive their analyses. Winds can then be assumed constant by the CTM until the next read-in step, however this introduces discontinuities between read-in steps that will add artificial variability. To avoid this problem winds can be interpolated in time within the CTM between two consecutive updates, this is the approach adopted by TOMCAT/SLIMCAT. Another option is the use of averaged winds (Pawson *et al.*, 2007), but this might cause excessive dynamical smoothing.

Recently, some CTM studies have reported on the benefits of using 3-hourly meteorological data instead of the widely used 6-hourly ones (*e.g.* Legras *et al.* 2005; Berthet *et al.* 2006; Bregman *et al.* 2006). These studies have compared the

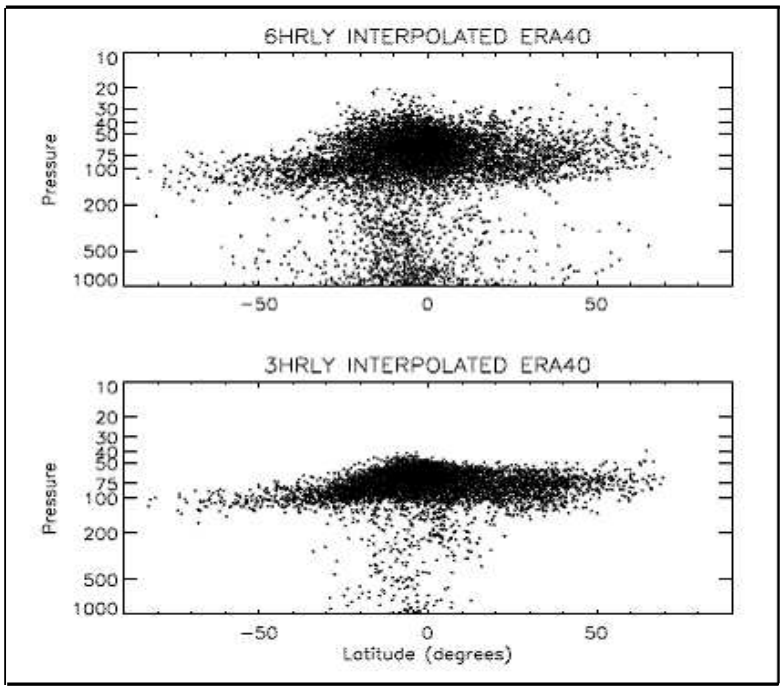

Figure 2.7: *Trajectory distributions after 50-day backwards simulation of the KNMI TM using ERA-40 6h winds (above) and ERA-40 3h winds. Taken from Bregman* et al. *(2006).*

performance of ERA-40, or ECMWF operational, 6-hourly analyses against the performance of 3-hourly analyses. The CTM with 3-hourly winds results in older mean age-of-air values and less particle dispersion over the tropics compared to the same CTM with 6-hourly winds (Figure 2.7). However, one problem comes from the way in which the 3-hourly data for these studies are constructed. Since meteorological analyses are archived every 6 hours, to get 3 hourly analyses it is necessary to interleave analyses and forecasts, and this means that two different levels of noise are being mixed. It is then not possible to discern how much improvement is due to the increased frequency (3h v 6h winds) and how much to the less noisy forecasts. Bregman *et al.* (2006) avoided this inconsistency by using ERA-40 forecasts (instead of analyses) which are archived every 3h (B. Bregman, personal communication, 2008).

As discussed above, all these correction techniques have implicit shortcomings

that make the direct use of high quality analyses much more desirable. Not only are better (re)analyses needed to improve the quality of the CTM stratospheric simulations, but also more complete and recent observations that allow for more global comparisons. This is a particularly important issue for age-of-air distributions, for which up until now only balloon and aircraft measurements taken in the 1990s are available. Newer observations would permit the detection of any changes in the Brewer-Dobson circulation; if the BDC has strengthened in the last decade, missing these changes would mean that we are somewhat underestimating the quality of recent analyses. More global satellite based measurements would enlarge the regions where the simulations can be compared, which would be of importance in order to validate and employ the analyses provided by DAS that are rapidly increasing their vertical domains.

There is also need for research that evaluates why the representation of the stratosphere in the analyses is not yet good enough. NWP/DAS models require better stratospheric parameterisations of radiatively active gases (O_3, H_2O, CH_4). This would have a direct positive impact in the radiative representation and the dynamics of the NWP model and would allow for a more effective assimilation of satellite radiances.

2.6 The TOMCAT/SLIMCAT CTM

The 3D off-line CTM TOMCAT/SLIMCAT (Chipperfield, 2006) has been used throughout this thesis. This CTM is the combination into one single model library of the CTMs TOMCAT (*e.g.* Chipperfield *et al.* 1993) and SLIMCAT (Chipperfield, 1999). TOMCAT was initially written for stratospheric studies and later developed for tropospheric applications by adding detailed tropospheric parameterisations, at the same time that SLIMCAT was developed for stratospheric uses. TOMCAT used to make use of the ECMWF analyses, which up to 1999 extended only up to 10 hPa, while SLIMCAT was written to make use of the UKMO stratospheric analyses avail-

able already in the 1990s. However, after ECMWF model extended its vertical range up to 0.1 hPa and completed the ERA-40 reanalyses TOMCAT and SLIMCAT were combined into one model that extends from the surface to the top of the atmosphere without any boundaries at the tropopause. The new TOMCAT/SLIMCAT permits the use of different vertical coordinates, vertical motion and advection schemes, as well as different analyses and reanalyses. TOMCAT/SLIMCAT includes also a module for the calculation of particle trajectories, which allows for a Lagrangian as well as the default Eulerian approach.

2.6.1 General configuration

The horizontal grid is completely variable in resolution and in latitudinal regularity. Also the number of vertical levels is flexible, and the vertical coordinate can be either $\sigma - p$ (TOMCAT mode) or $\sigma - \theta$ (SLIMCAT mode). As described in Chipperfield (2006), the TOMCAT mode uses terrain-following levels up to a certain level (typically 100 hPa) and from there upwards it changes to pure pressure levels. Therefore pressure values at model half-levels are given by

$$p_{k+\frac{1}{2}} = Ap_0 + Bp_s \tag{2.2}$$

where p_0 is the reference pressure (*e.g.* 100 hPa) and p_s is the surface pressure taken from the analyses. When using the CTM in SLIMCAT mode the vertical coordinate responds to a hybrid $\sigma - \theta$ system. In this case model levels above the reference potential temperature, θ_0, are identified by the potential temperature at the interface (half model levels)

$$\theta_{k+\frac{1}{2}} = C\theta_0 \quad (C \geq 1) \tag{2.3}$$

while levels below θ_0 are identified by the corresponding pressure values:

$$p_{k+\frac{1}{2}} = Cp_{\theta_0} + (1 - C)p_s \quad (C < 1) \tag{2.4}$$

The vertical motion can be calculated from the divergence of the horizontal winds or, when using the SLIMCAT mode, from heating rates calculated with one of the two radiation schemes included in the CTM: MIDRAD (Shine, 1987) and CCMRAD (Briegleb, 1992). The runs used in this thesis have used CCMRAD, as it is more similar to the ECMWF radiation scheme.

Different options can be used for the advection of tracers in TOMCAT/SLIMCAT. The Prather (1986) scheme with zero, first and second-order moments, or a semi-Lagrangian scheme. The conservation of second-order moments (Prather, 1986) has been chosen for most of the runs performed for this thesis, the reasons for this choice are the lower diffusivity and the mass conservation exhibited by this scheme.

TOMCAT/SLIMCAT also parameterises subgrid processes in the troposphere such as convection (Stockwell and Chipperfield, 1999) and mixing in the boundary layer (Louis, 1979; Holtslag and Boville, 1993). Since the scope of this work focuses on the stratospheric region, the effects of the different choices for these parameterisations have not been considered, even if their influence will always be present, in particular in the upper troposphere/lower stratosphere (UTLS) region. The runs included in this thesis do not use any scheme for moist convection, and simple complete mixing throughout the troposphere has been chosen.

2.6.2 Lagrangian module

In the off-line Lagrangian scheme used in this thesis, the trajectory position is computed from the same meteorological data used to force the Eulerian simulations (Chapter 3). Horizontal and vertical motion are calculated at the centre of the Eulerian grid and then interpolated to the trajectory position in that particular grid cell. Also the same general configuration options (vertical coordinate, vertical motion) are available for the Lagrangian runs.

The time evolution of an air parcel trajectory is

$$\frac{d\vec{x}}{dt} = \vec{v}(t, \vec{x}) \tag{2.5}$$

where $\vec{v}(t, \vec{x})$ is the 3D wind velocity from the meteorological analysis for the location $\vec{x}$ and the time t. An explicit 4th-order Runge-Kutta method (Fisher *et al.*, 1993) is used to advance the trajectory position forward (or backward) in time. With this Runge-Kutta scheme the trajectory position in $t + \Delta t$ is approximated by

$$\vec{x}(t + \Delta t) = \vec{x}(t) + \vec{k}_1/6 + \vec{k}_2/3 + \vec{k}_3/3 + \vec{k}_4/6 \tag{2.6}$$

where the $\vec{k_i}$ terms are given by

$$\begin{aligned}
\vec{k}_1 &= \Delta t \cdot \vec{v}(t, \vec{x}) \\
\vec{k}_2 &= \Delta t \cdot \vec{v}(t + \Delta t/2, \vec{x}(t) + \vec{k}_1/2) \\
\vec{k}_3 &= \Delta t \cdot \vec{v}(t + \Delta t/2, \vec{x}(t) + \vec{k}_2/2) \\
\vec{k}_4 &= \Delta t \cdot \vec{v}(t + \Delta t, \vec{x}(t) + \vec{k}_3)
\end{aligned} \tag{2.7}$$

2.6.3 Winds in TOMCAT/SLIMCAT

Winds and temperatures are taken off-line by TOMCAT/SLIMCAT. As already noted, TOMCAT/SLIMCAT is flexible in terms of the winds datasets it can use. The ECMWF datasets have, however, been the most extensively used since 1999, when they extended into the stratosphere up to 0.1 hPa, and even more after the completion of ERA-40 for multiannual runs for long-term trends investigations (*e.g.* Chipperfield *et al.* 2005). Forcing winds and temperatures are typically read in by TOMCAT/SLIMCAT every 6 hours (frequency with which the assimilated fields are archived) and then interpolated in time until the next read in step. The read-in frequency can be modified to adapt to different archived analyses (*e.g.* forecasts longer than 6h). The necessary forcing files are derived from ECMWF spectral and gridpoint data. Spectral files contain temperature, vorticity, *ln* of surface pressure and divergence. While the specific humidity is retrieved in gridpoint representation.

Data from ECMWF model levels are then averaged onto the CTM grid.

All the CTM aspects so far described (winds, advection scheme, vertical coordinate, resolution and vertical motion) influence the 3D transport in the CTM as shown in different studies (*e.g.* Eluszkiewicz et al., 2000; Chipperfield, 2006; Strahan and Polansky, 2006). In order to isolate the effect of using one set of stratospheric analyses or another, the same advection scheme, coordinate, resolution and vertical motion have been kept unchanged for different winds. Nevertheless, several runs have also been performed to assess the effects caused by changing other model characteristics, like vertical motion and coordinate (see Chapter 4). TOMCAT/SLIMCAT can also be run with winds from a free-running GCM model. This option has also been exploited in this thesis to compare the ECMWF analyses performance against one free run of the ECMWF IFS.

TOMCAT/SLIMCAT, like all CTMs, suffers from excessive stratospheric transport when using analysed winds and has implemented some of the correction techniques described earlier in this chapter (Chipperfield, 2006). For stratospheric simulations, the use of isentropic coordinates in the stratosphere and heating rates for the vertical motion has produced results in good agreement with available observations when using ECMWF data (*e.g.* Feng *et al.* 2007). However as discussed above, better use of the analyses would be done if no correction techniques had to be applied and the CTM coordinate system resembled the one in the model providing the analyses (the ECMWF model in this case).

2.6.4 Chemistry in TOMCAT/SLIMCAT

Obviously, the reliability of the tracer concentrations in a CTM depends not only on the analyses used, but also on the accuracy and completeness of the chemistry description used by the CTM. A full-chemistry run of TOMCAT/SLIMCAT involves around 50 chemical species in more than 100 gas-phase reactions (Chipperfield, 1999). TOMCAT/SLIMCAT includes both short and long-lived chemical species.

For consistency reasons and to reduce computation times, short-lived species are grouped together into chemical families. The model also includes a complete description of the stratospheric heterogenous chemistry, taking into account reactions on liquid aerosols, nitric acid trihydrate (NAT), sulfuric acid trihydrate (SAT) and ice particles. Different options exist so that the user can choose which ones, among all the possible heterogeneous reactions, are used.

The model reads the photochemical reaction rates from 4-dimensional look-up tables (function of pressure, latitude, O_3 column and zenith angle) and interpolates them to any considered atmospheric location and time. The photochemical data are taken from the Jet Propulsion Laboratory (JPL) publication JPL2003 (Sander *et al.*, 2003). To allow for an accurate representation of the diurnal cycle, chemical timesteps no longer than 15 minutes are recommended, otherwise the day-to-night variability might be unrealistically smoothed, and also negative concentrations would be more likely to appear. The runs performed in this thesis use a 15-minute chemical step to allow for reasonable simulation times while avoiding the two mentioned problems.

In addition to the default chemical tracers included in the model, the user can include supplementary tracers to calculate different transport or chemistry diagnostics. Examples of such tracers are idealised tracers used for age-of-air calculations (Chipperfield, 2006) or the passive O_3 tracer used to compute chemical O_3 loss amounts (*e.g.* Feng *et al.* 2005; Chipperfield *et al.* 2005).

2.6.5 TOMCAT/SLIMCAT in this thesis

If the only variation between different runs of the same CTM is in the winds used to drive the simulations, then such CTM turns into a very useful tool to evaluate the quality of the wind fields. This characteristic has been exploited in this thesis for the TOMCAT/SLIMCAT model to assess the quality of different ECMWF stratospheric datasets, as will be presented in Chapters 3 and 4.

To improve the quality of the stratospheric analyses, NWP/DAS models need to pay increasing attention to the chemistry schemes they employ. Also here CTMs can be extremely helpful given their longer experience in stratospheric chemistry. The current ECMWF ozone parameterisation (Cariolle and Déqué, 1986) will be compared against TOMCAT/SLIMCAT full-chemistry 3D runs in Chapter 6. The same linear approach used by Cariolle and Déqué (1986) will be applied to develop an alternative O_3 scheme and a new CH_4 stratospheric scheme based on the CTM runs as described in Chapters 6 and 7, respectively.

2.7 Summary and open issues

The scope of this chapter was the review of the main existing published results on stratospheric transport issues related to CTM simulations. The current situation on the use of stratospheric meteorological analyses by CTMs has been presented. CTM results are very sensitive to the forcing meteorological analyses, nevertheless this apparent disadvantage has actually revealed a key tool for the evaluation of different winds and temperatures datasets.

Modellers need to be aware that, due to the large variability between the representations provided by different analyses, important differences in stratospheric studies may derive from the choice of the meteorological data used, *e.g.* as pointed by Manney *et al.* (2003) for Arctic stratospheric studies.

Main transport characteristics in the stratosphere are well known, however, other important details such as the quantification of the exchange of air masses across mixing barriers, or the exact mechanisms of exchange between troposphere and stratosphere, are still unclear (*e.g.* Fueglistaler *et al.* 2004; Folkins 2005; Fueglistaler and Fu 2006). Good quality analyses, together with more observations, are essential to quantify and clarify these transport features.

The data assimilation technique has been presented in different studies to be responsible for the artificial enhancement of the BDC and the subtropical mixing. The correction techniques applied by the CTMs to overcome the deficiencies detected in the winds and temperatures have intrinsic problems, making the existence of a high quality meteorological dataset that could be used directly by CTMs more desirable. Comparisons of analyses produced with, for instance, different horizontal and vertical resolution, or with a different assimilation technique (3D-Var or 4D-Var) have already suggested that developing the DAS systems improves the products obtained (Manney et al., 2003; 2005; Meijer et al., 2004; Scheele et al., 2005; Chipperfield 2006).

To evaluate the quality of the analyses, more recent and global observations are needed. In particular, satellite-based estimations of the age-of-air would be of great help to detect any changes in the BDC that could have taken place during the last decade, leading therefore to a more realistic assessment of the recent analyses quality.

Research should focus not only on the data assimilation method itself, but also on improving the stratospheric chemistry in NWP/DAS models. Better stratospheric parameterisations of radiatively active gases (O_3, H_2O, CH_4) would result in improved radiative representation and dynamics of the NWP model, which would allow for a more effective satellite radiances assimilation.

Chapters 3 and 4 present the results obtained for this thesis from a detailed comparison of several ECMWF stratospheric analyses produced with different versions of their DAS, helping to show how advances in data assimilation have direct implications for tracer transport modelling with CTMs. Chapters 6 and 7 deal with the improvement of chemical parameterisations in the NWP model used to produce the ECMWF analyses.

Chapter 3

Evaluation of Different Stratospheric Meteorological Analyses in TOMCAT/SLIMCAT Simulations

3.1 Introduction

In this chapter the TOMCAT/SLIMCAT CTM is used to evaluate the quality of different stratospheric (re)analyses from the ECMWF. One set of U.K. Met Office data is also used to compare results from our simulations with those in Schoeberl *et al.* (2003). This evaluation will show to what extent the problems discussed in Chapter 2 for ERA-40 are present in datasets produced with newer data assimilation systems (DAS) and, therefore, whether recent advances in data assimilation techniques have had a positive influence on the representation of the stratospheric transport.

To compare the different sets of winds, multiannual simulations with TOMCAT/SLIMCAT have been carried out in which several tracers have been added to compute various transport diagnostics. Age-of-air calculations have been used to

obtain a global picture of the stratospheric transport, trajectory calculations used to investigate the vertical and horizontal dispersion in the tropical LS region, and "tape recorder" simulations with an idealised sinusoidal tracer to explore the vertical advection and horizontal mixing of air masses over the tropics. Calculations of the eddy modified potential vorticity (MPV) flux (Lait, 1994; Schoeberl *et al.*, 2003) are also provided as a further diagnostic for horizontal processes in the tropical and subtropical stratosphere. In addition, different CTM configurations (vertical coordinate and vertical motion) have been used to test the influence that some of the correction techniques described in Chapter 2 have on the different winds tested here.

The stratospheric (re)analyses used for the simulations are described in Section 3.2. The subsequent sections deal with the different diagnostics used to evaluate the winds' performance. A direct comparison of wind velocities and temperature distributions for the four datasets compared is shown in Section 3.3. Then, age-of-air results are presented in Section 3.4, Lagrangian trajectory distributions in Section 3.5, "tape recorder" simulations in Section 3.6, and MPV fluxes in Section 3.7. Each of these sections includes a description of the experimental set-up used for the calculation of the corresponding diagnostic, as well as information about the observational datasets used for validating the CTM results. Section 3.8 summarises what has been deduced from all the simulations included in this chapter. The contents of this chapter have been partly published in Monge-Sanz *et al.* (2007), and a copy of this article can be found in Appendix A.

3.2 Stratospheric analysis data used

The main (re)analysis products currently available have been presented in Chapter 2. Here, an additional new experimental dataset from ECMWF is also described, and detailed information is given on the exact periods used for all datasets.

3.2.1 ECMWF reanalyses experimental tests

In preparation for their next reanalysis run, ECMWF produced short experimental datasets with a new DAS. In this thesis several of these experiments have been tested. This work exploits the potential of a CTM to evaluate the quality of analysis datasets, and results shown here provide feedback to the assimilation centres (in this case ECMWF) to inform decisions on the final set-up of the complete reanalysis.

In particular, an ECMWF experimental run called EXP471 has been tested in this chapter, to see how well it describes stratospheric transport. EXP471 starts on September 1999 and runs until December 2000. As a complete year of data is required to capture the seasonal signal of the BDC, only the year 2000 data have been used for the TOMCAT/SLIMCAT simulations. The EXP471 dataset has been produced with an updated 4D-Var assimilation method with a 12h window, using two minimisation loops. The IFS cycle used to produce this run was Cy29r1 (this version was used for ECMWF operations from April to June 2005). More detailed information on the system used to produce this dataset, and its developments with respect to the system used to generate ERA-40, can be found in Chapter 4.

3.2.2 ERA-40 reanalyses

Year 2000 ERA-40 data have been employed to compare against the interim reanalysis tests. These data were produced with a 3D-Var assimilation algorithm, and the IFS cycle version Cy23r4 (operational from June 2001-January 2002). The resolution was T159 (lower than for operations in that time). More information on this dataset can be found in Chapter 2 and Chapter 4, the latter in comparison with the other datasets used in the present work. The wide use CTMs have made of ERA-40 makes stratospheric deficiencies of these winds well documented (see Chapter 2) and therefore simulations with ERA-40, despite known problems, provide a useful reference to confront results obtained with newer analysis datasets.

3.2.3 ECMWF operational analyses

The ECMWF operational analyses for 2000 were produced with a 4D-Var assimilation method; in this year ECMWF operations switched from 6h assimilation window to a 12h window on the 9th September. Several IFS cycle versions were set in operations along year 2000: Cy21r4 until April, Cy22r1 from April to June and Cy22r3 from June onwards. All these versions have 60 vertical levels, 29 of them above 200 hPa, the same as ERA-40. In addition, in November 2000, the horizontal resolution was upgraded from T319 to T511. These operational analysis data were then produced with an earlier version of the IFS model than ERA-40, but a more sophisticated assimilation method and higher resolution. As for the ERA-40 dataset described above, these analyses are archived every 6 hours (00h, 06h, 12h, 18h). In this thesis, these winds will be denoted 'OPER' winds (or OPER 2000 where ambiguity in the year exists).

3.2.4 UKMO 'UARS' analyses 2000

The U.K. Met Office analyses (Swinbank and O'Neill, 1994) for the year 2000 have also been used. These data were produced with an optimum interpolation (OI) assimilation scheme called 'analysis correction' (AC) (Lorenc *et al.*, 1991). Data are stored on a global grid of 2.5° latitude x 3.75° longitude, on 22 presure levels from the surface up 0.32 hPa, interpolated from the UKMO model to the Upper Atmossphere Research Satellite (UARS) observation levels. These analyses are archived every 24 hours. These were the first analysed winds comprising the whole of the stratosphere, and were easily available and widely used by the modelleing community (*e.g.* Knudsen 1996; Chipperfield 1999; Rogers *et al.* 1999; Schoeberl *et al.* 2003). In this thesis, these winds will be denoted 'UKMO' winds. This UKMO dataset enables a comparison of our results with the results in Schoeberl *et al.* (2003), as the same UKMO winds were used in that work.

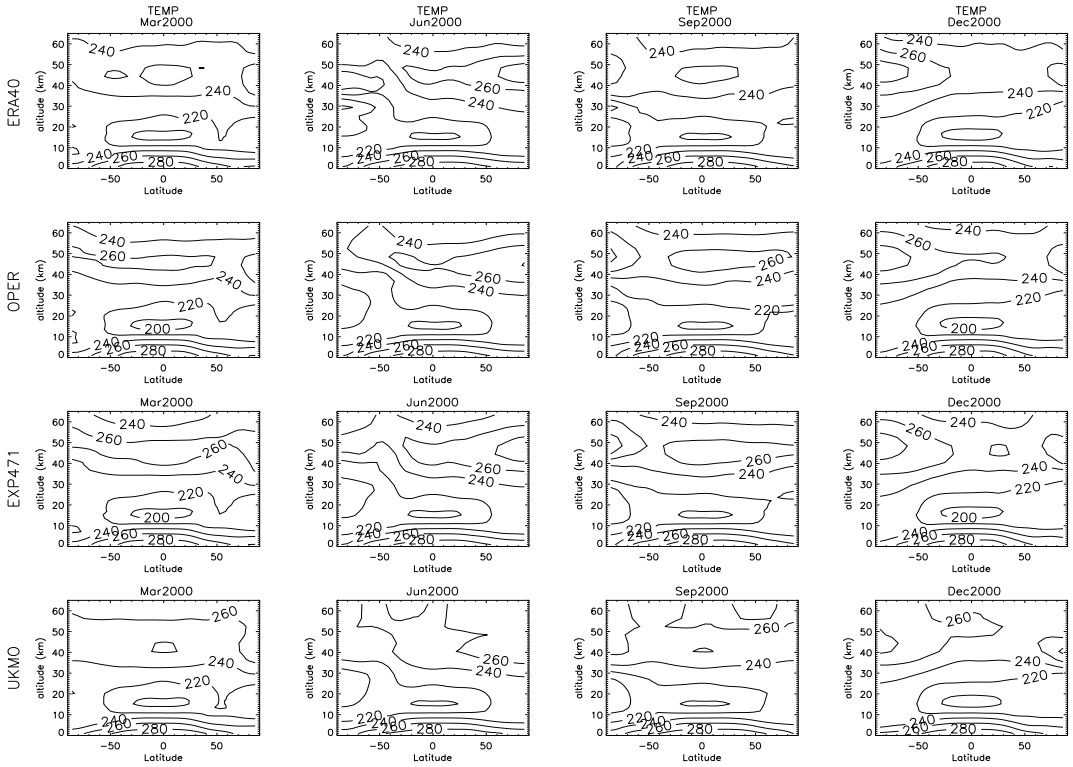

Figure 3.1: *Monthly means of zonally averaged temperature (K) in March, June, September and December 2000, for ERA-40 (top row), OPER (second row), EXP471 (third row) and UKMO (bottom row) analyses.*

3.3 Wind velocities and temperatures

As an initial intercomparison between datasets, the corresponding temperature and wind velocity distributions have been analysed.

3.3.1 Temperatures

Figure 3.1 shows the zonal mean temperatures in March, June, September and December 2000 for the four sets of (re)analyses used. Oscillations in temperature present in ERA-40 (June, top row in Figure 3.1) were corrected in later ECMWF system versions and do not appear in OPER and EXP471 datasets. All datasets agree on the overall structure. However, the two more recent datasets (OPER and EXP471) agree better with each other than with the other two. ERA-40 presents a

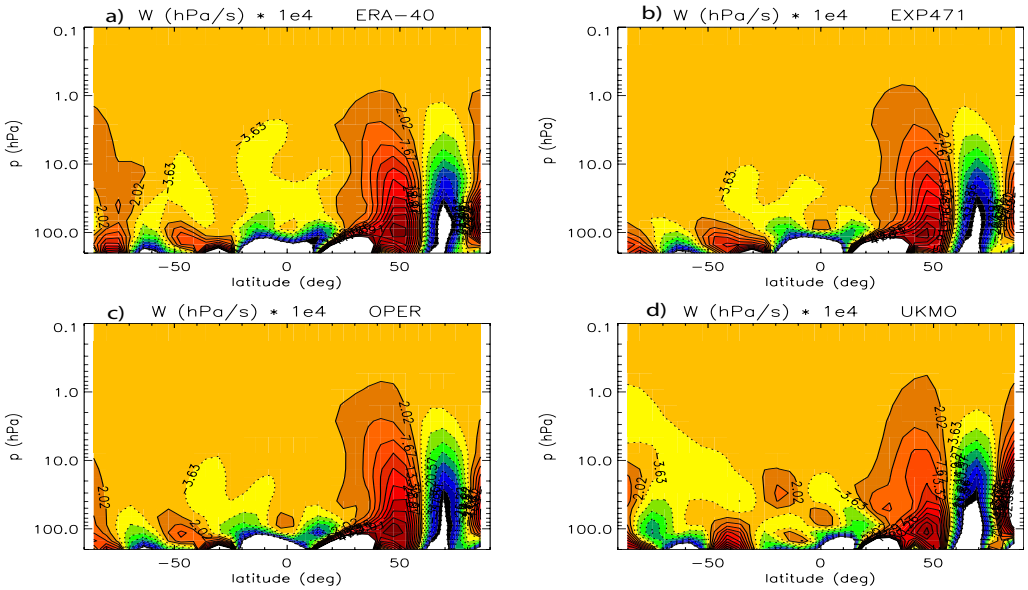

Figure 3.2: *Zonal mean of vertical wind velocity (hPa/s) averaged over January 2000, in the region 200-0.1 hPa. Panels show (a) ERA-40, (b) EXP471, (c) OPER and (d) UKMO datasets. Negative values (dashed contour lines) represent ascending winds and positive values (solid contour lines) descending winds.*

too cold upper stratosphere (Randel *et al.*, 2004a), while this region for UKMO is warmer than for the rest.

3.3.2 Wind velocities

The vertical winds w in the stratosphere for the four datasets are given in Figure 3.2, which shows the zonal mean averaged over January 2000. All winds present the same overall structure. However, in ERA-40 the tropical ascent reaches higher than in the other winds, and the same happens with the ascent region over southern mid-latitudes in UKMO. Both ERA-40 and UKMO velocities are larger over the summer hemisphere than in EXP471 and OPER, while the two newer datasets agree well with each other. The standard deviation (std) for the winds shown in Figure 3.2 are in Figure 3.3. Here, it can be seen that ERA-40 exhibits larger std of w winds than the rest, followed by OPER, and that EXP471 and UKMO winds are those with more restricted std.

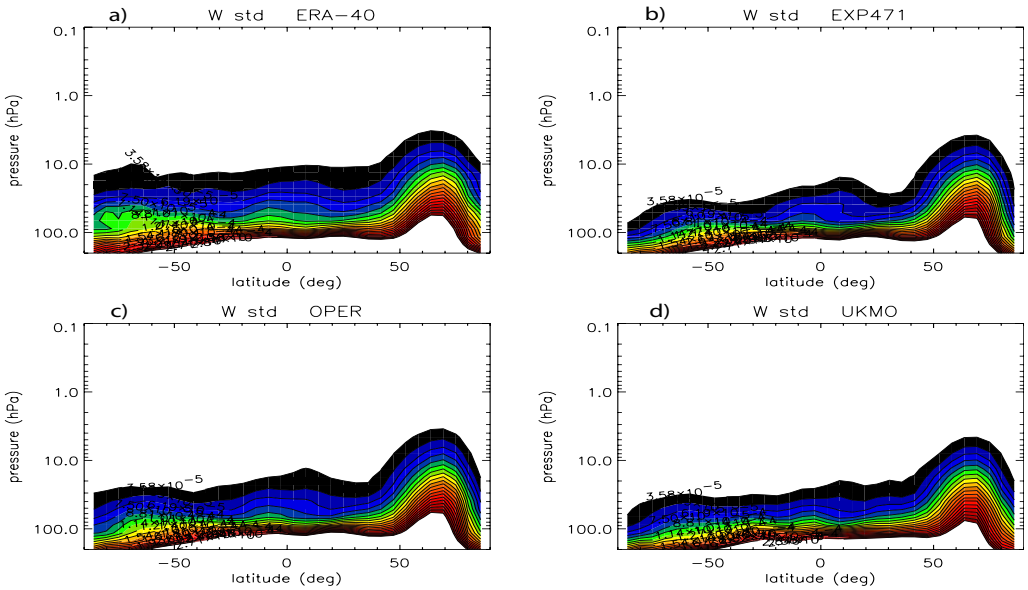

Figure 3.3: *Standard deviations (Pa/s) for the winds shown in Figure 3.2.*

The zonal wind velocities, u, averaged for January 2000 are shown in Figure 3.4. Here all winds agree very well, except for the region with maximum westerly winds over northern mid-high latitudes, where ERA-40, and UKMO, show a lower maximum than the two newer ECMWF datasets. Also differences in the region with maximum easterly winds (above 1 hPa over SH midlatitudes) can be observed, values there are larger for the new EXP471 winds.

Figure 3.5 shows the corresponding meridional wind, v, velocities. In this case the differences between datasets in the stratosphere are more obvious. Above 1 hPa, both ERA-40 and OPER exhibit two maxima over the tropics, while EXP471 and UKMO show only one maximum. The maximum velocities in these upper region are larger for UKMO and OPER (>3.0 m/s), around 0.5 m/s slower for ERA-40 and more than 1.0 m/s slower for the new EXP471. The largest positive values around the tropical tropopause are shown by ERA-40 and OPER; EXP471 and especially UKMO show smaller tropical maxima.

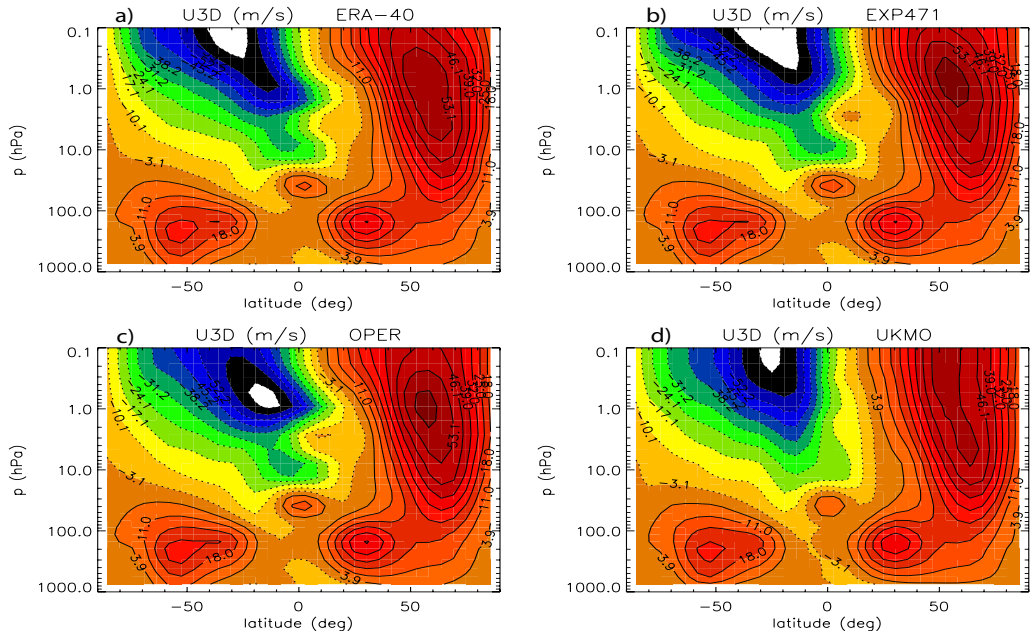

Figure 3.4: *Zonal mean of zonal wind velocity (m/s) averaged over January 2000, for (a) ERA-40, (b) EXP471, (c) OPER and (d) UKMO datasets. Negative values (dashed contour lines) represent easterly winds and positive values (solid contour lines), westerly winds.*

3.4 Age-of-air

3.4.1 Age-of-air as a transport diagnostic

Age-of-air calculations have become a standard test for models to quantify stratospheric transport (*e.g.* Hall *et al.* 1999; Waugh and Hall 2002; Meijer *et al.* 2004). Properties of air parcels need to be described by statistical functions that take into account the characteristics acquired by the parcels on passing times and locations. The age spectrum is the statistical distribution of air parcels as a function of time since they last left the troposphere (Kida, 1983). This concept was mathematically developed by Hall and Plumb (1994), who defined the age spectrum as a Green function $G(x, x_0, t)$ that, for a tracer mixing ratio, propagates a boundary condition from a source region x_0 (typically the tropical tropopause) into the stratosphere. The mean age $\Gamma(x, x_0)$ at a certain stratospheric location is then the average over

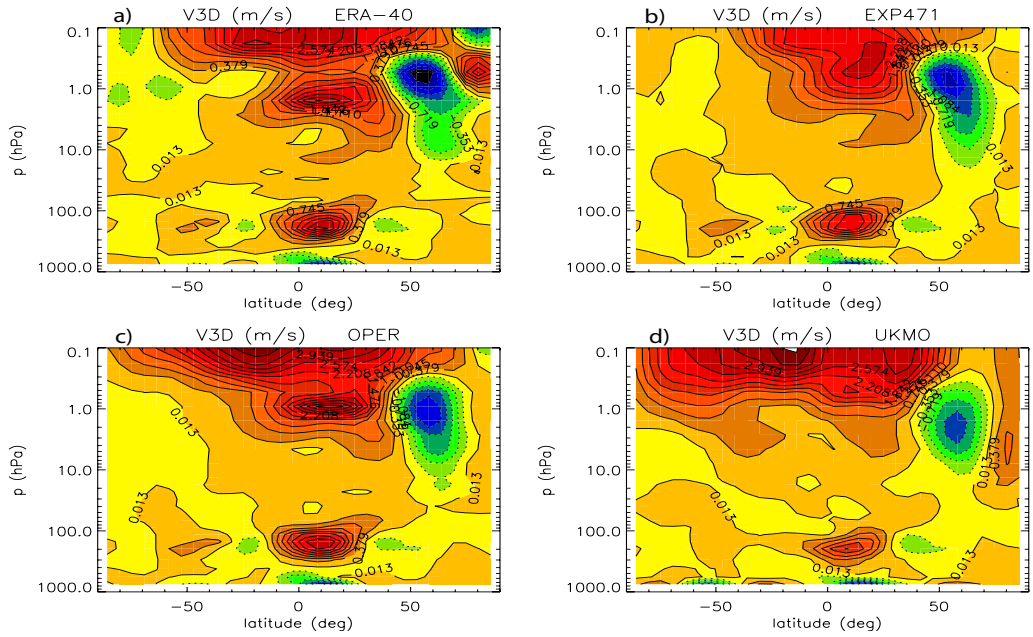

Figure 3.5: *Zonal mean of meridional wind velocity (m/s) averaged over January 2000, for (a) ERA-40, (b) EXP471, (c) OPER and (d) UKMO datasets. Negative values (dashed contour lines) represent southwards winds and positive values (solid contour lines), northwards winds.*

the age spectrum at that location:

$$\Gamma(x, x_0) = \int_0^\infty t\, G(x, x_0, t)\, dt \tag{3.1}$$

In the particular case of a conserved tracer, *i.e.* linearly increasing tropospheric mixing ratio and no stratospheric sources or sinks, the mean age can be computed from concentration measurements (Figure 3.6). If $\gamma(x, t)$ is the mixing ratio of the considered tracer at time t and location x, then

$$\Gamma(x, x_0) = t - \frac{\gamma(x, t)}{\alpha} \tag{3.2}$$

where α is the tropospheric trend of the tracer mixing ratio.

CO_2 and SF_6 are two long-lived constituents that approximately fulfil the linearly conserved conditions and can therefore be used to derive the stratospheric mean

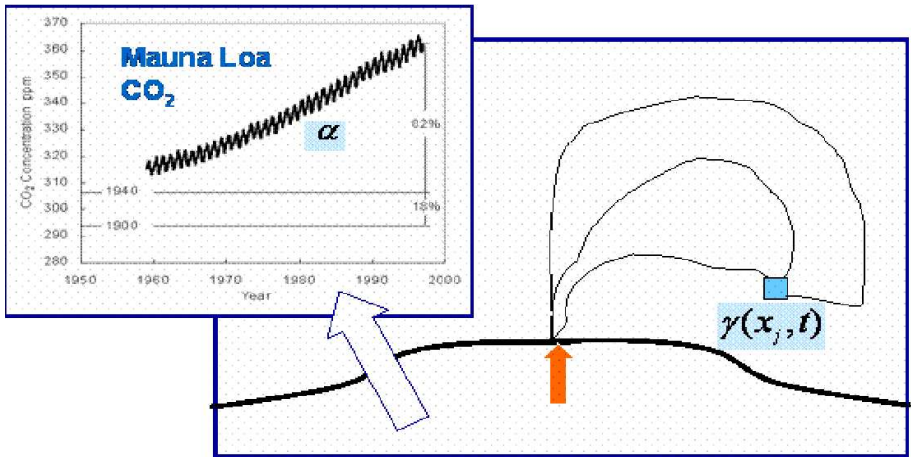

Figure 3.6: *Schematic for the computation of the mean age-of-air from mixing ratio measurements of a conserved linearly increasing tracer like CO_2. The mean age at a stratospheric location $\vec{x}$, $\Gamma(\vec{x}, t)$, can be inferred from the tracer concentration at that location ($\gamma(\vec{x}, t)$) and the tropospheric linear trend of the same tracer (α).*

age-of-air. These two gases are complementary as the tropospheric annual cycle of CO_2 prevents it from being used to calculate age values in the lower stratosphere, while SF_6 concentrations in the upper stratosphere are affected by mesospheric loss (Reddman *et al.*, 2001).

3.4.2 Observational data

Mean age observations

Mean age can thus be calculated from observations of CO_2 and SF_6. In this work observation-based mean age values have been obtained from Andrews *et al.* (2001) and Ray *et al.* (1999). Between 1992 and 1998 NASA ER-2 aircraft and high-altitude balloons measured concentrations of CO_2 and SF_6. The ER-2 measurements were part of the campaigns Stratospheric Photochemistry Aerosol and Dynamics Experiment (SPADE), Airborne Southern Hemisphere Ozone Experiment/Measurements for Assessing the Effects of Stratospheric Aircraft (ASHOE/MAESA), Stratospheric Tracers of Atmospheric Transport (STRAT) and Photochemistry of Ozone Loss in

the Arctic Regions in Summer (POLARIS). Balloon flights were part of the Observations of the Middle Stratosphere (OMS) experiments. The balloons reached maximum altitudes of 31 km, while the aircraft missions did not go above 21 km. This limits the range covered to the LS and middle atmosphere and does not give a complete picture of the latitudinal gradient above 21 km as the OMS flights covered only three latitude values (65°N, 35°N and 7°S).

Waugh and Hall (2002), using the age values calculated from the existing observations between 18-32 km, inferred a global distribution for the annually averaged mean age-of-air (Figure 3.7). This schematic distribution is symmetric between hemispheres as most of the observations have been taken in the northern hemisphere (NH); in practice the strength of the BDC is hemisphere-dependent, and slightly older age values should be found for the SH.

There are some measurements of HF, HCl and CF_4 concentrations from spaceborne platforms that reach higher altitudes (55-60 km), see Table 1 in Waugh and Hall (2002). These measurements and the inferred age-of-air values have been performed by Anderson *et al.* (2000), Gunson *et al.* (1996) and Harnisch *et al.* (1998). However, these gases do not have steady linearly increasing tropospheric trends; restrictions in the emissions of halogen source gases have caused a turnover in the tendency of tropospheric concentrations. This would cause problems for evaluating stratospheric age values, as air masses with different ages would correspond to the same concentration value, invalidating the calculation method which is based on the one-to-one correspondence between concentration values and mean age values.

Age spectrum observations

Unlike the mean age, the age spectrum cannot be directly estimated from observations. Long, reliable datasets of inert tracers would be required that do not exist at present. The use of active chemical tracers for age spectrum computations has been explored by Schoeberl *et al.* (2005). They used four different tracers (CH_4, N_2O,

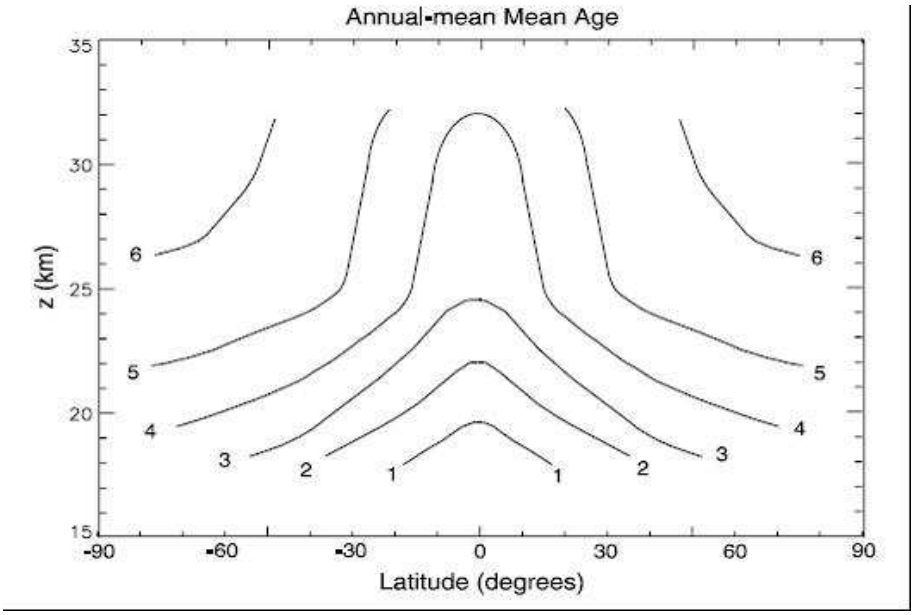

Figure 3.7: *Schematic for mean age zonal mean distribution (years), inferred from existing observations (see text for details). Taken from Waugh and Hall (2002).*

F11 and F12) from three different campaigns and instruments (OMS data for 7°S on 14th February 1997; 1 month of ACE-FTS observations and data from UARS for January 1993) to reproduce different parts of the spectrum which together provided a complete spectrum distribution. However, Schoeberl *et al.* (2005) found several problems in their study. First, the existence of a limitation in altitude as F11 and F12 measurements were too noisy above 30 km, which made spectra above this altitude not reliable. Second, the increase in tropospheric concentrations that occurred between the campaigns considered was not negligible, which produced a young bias in the obtained ages. Also the different instrumental biases must be taken into account. Schoeberl *et al.* (2005) also acknowledged that the use of only four tracers might not be robust enough. With more comprehensive satellite observations this kind of technique will likely be able to provide very useful information in the future. No observational data have been used to compare against the TOMCAT/SLIMCAT age spectrum calculations, yet the mean age values obtained from the spectra have been validated against the datasets described above.

3.4.3 Experiment set-up

In this thesis two different approaches have been adopted for the calculation of the mean age-of-air. The first one mimics the behaviour of an ideal, linearly increasing tracer, and the second one reproduces a Green function evolution that allows the calculation of the complete age spectrum and, from the spectrum, the mean age.

A series of 20-year CTM runs have been performed with a horizontal resolution of 5.6° latitude × 7.5° longitude. The CTM has used 24 vertical levels between the surface and ∼60 km. The winds used to drive the model runs are those described in Section 3.2: ERA-40, OPER, UKMO and EXP471. All runs have used repeating meteorological fields for 2000, as this is the only complete year for the interim reanalysis EXP471. The model tracers included for this work were:

i) an ideal inert tracer with linearly increasing tropospheric concentration (described later in this section)

ii) a pulse tracer released at the tropical troposphere (described later in this section)

iii) a sinusoidal tracer to simulate the 'tape recorder' signal (described in Section 3.6)

Ideal linear tracer for mean age

In this case an ideal inert tracer has been included in TOMCAT/SLIMCAT whose tropospheric value increases linearly with time. The tropospheric mixing ratio of this tracer is incremented at every time step and overwritten at the surface, the tracer is assumed well-mixed through the troposphere. This kind of tracer is also known as 'clock-type' tracer. The mean age-of-air is then diagnosed considering the tropical tropopause as reference. The stratospheric concentrations of this tracer are compared to its value at the boundary location, since the troposphere is well-mixed, the value at the tropopause is equal to the value overwritten at the surface (see

Figure 3.6).

For each set of winds a TOMCAT simulation was performed, i.e. with $\sigma - p$ levels and vertical motion calculated from the divergence of the horizontal winds. For EXP471 and ERA-40 winds a SLIMCAT simulation was also run, *i.e.* using isentropic vertical levels in the stratosphere (an hybrid $\sigma - \theta$ system) and vertical transport in the stratosphere calculated from heating rates diagnosed by the CCMRAD radiation scheme embedded in SLIMCAT (Chipperfield, 2006; Briegleb, 1992).

Pulse tracer for age spectrum

The main advantage of using the mean age as transport diagnostic is the possibility of comparison against observational values. However, the mean age does not provide a complete picture of the stratospheric transport. The age spectrum gives additional information on the temporal evolution of the concentration of tracers at different locations. Therefore, even if it is not comparable to any observation, it gives valuable information on transport processes within the CTM. The mean-age can also be calculated from this approach as the first moment of the spectrum.

To calculate the age spectrum we have included a pulse tracer in our model. The volume mixing ratio (vmr) of this tracer was set equal to 1 in the tropical lower troposphere (5.6°S - 5.6°N, 0-3 km) for the first month of the simulation. Subsequently the vmr in this region was reset to zero. The experiment is therefore equivalent to considering a delta function boundary condition that is propagated in time and space. The time evolution of the vmr of this tracer for a certain location in the stratosphere will give the age spectrum distribution for that location. A schematic representation of this methodology can be seen in Figure 3.8.

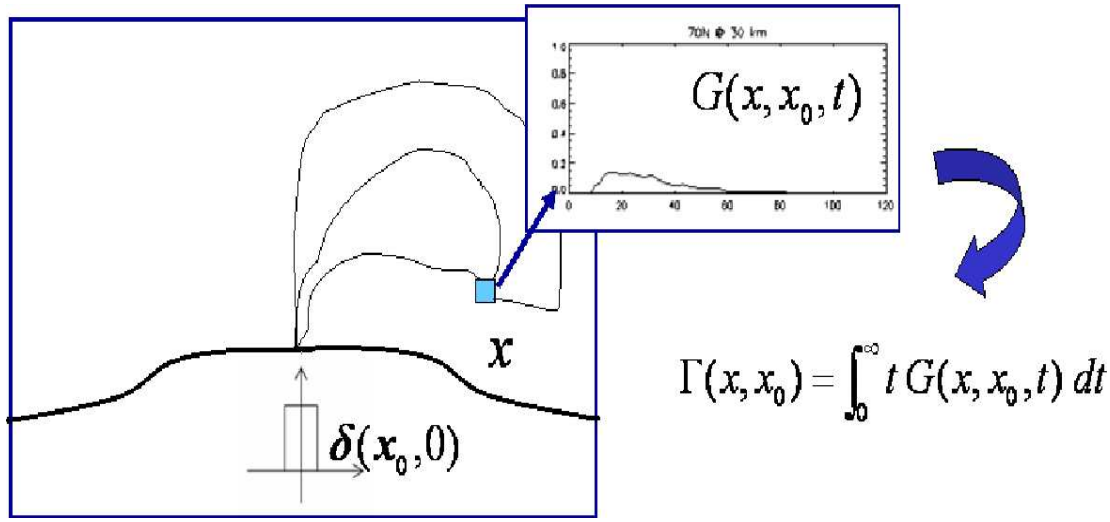

Figure 3.8: *The mixing ratio boundary condition δ at the reference location x_0 is propagated by the Green function $G(x, x_0, t)$ in time and space. The Green function at a certain stratospheric location x (blue square in the left panel) is the age spectrum for that location (small panel on the right). Then, by integrating the age spectrum in time, the first momentum of the spectrum, the mean age value $\Gamma(x, x_0)$ is obtained for the considered point x.*

3.4.4 Results from linear tracer approach

Global zonal distributions

In Figure 3.9 the annual mean zonal mean age-of-air is shown as a function of altitude for the four different forcing analyses datasets. These distributions have been obtained with TOMCAT ($\sigma - p$) simulations. By comparing against Figure 3.7 it can be seen that the simulated age distributions are younger and that the latitudinal gradient should be stronger, especially between tropics and subtropics. However, the extent of the disagreement with observations depends strongly on the winds used to drive the CTM simulation. ERA-40 produces unrealistic contours both in shape and magnitude; note the depression in the contours between 25-35 km over the tropics. The run with UKMO winds results in abnormally young ages at all altitudes, even younger than ERA-40-based values. This is mainly due to the

model recalculating the vertical motion from the divergence of the archived u and v fields on interpolated pressure levels rather than using any directly archived vertical velocities. This method is also used for ECMWF analyses but here the CTM has the divergence field saved directly on the original model levels. The 4D-Var OPER and EXP471 winds both show contour distributions in reasonable agreement with those expected from the stratospheric circulation pattern, and in more agreement with Figure 3.7 than the other two analyses. The interim reanalysis EXP471 produces older (more realistic) ages than OPER winds, and also more realistic distributions compared to balloon profile measurements (see below in this section).

Age at 20 km

For a more critical comparison with observations results in the LS region are analysed in more detail. Figure 3.10a shows the annual mean zonal mean age-of-air obtained with TOMCAT/SLIMCAT at 20 km altitude, together with the mean age values derived from the ER-2 aircraft observations. In the tropics all the simulations lie within the 2σ error range. However, in mid and high latitudes there are large differences between model runs. ERA-40 winds give age values 2-3 years younger than observed and clearly produce a too weak latitudinal gradient. This is even more evident for UKMO winds, indicating excessive transport between tropics and subtropics. The use of the 4D-Var OPER winds significantly improve the results, in agreement with what previous studies have found (*e.g.* Meijer *et al.*, 2004; Chipperfield, 2006). OPER winds show older ages and improved latitudinal gradients, but values are still about 2 years too young for latitudes poleward of 40°. The new ECMWF reanalysis winds (EXP471) are the ones that produce the oldest and most realistic ages compared to observations. For these new winds both TOMCAT ($\sigma - p$) and SLIMCAT ($\sigma - \theta$) simulations differ from the observations by less than one year (red lines in Figure 3.10a). Furthermore, with the new EXP471 winds, the $\sigma - \theta$ model produces only slightly older ages than the $\sigma - p$ model, while with ERA-40 the differences between the two models were over 2 years at 20 km (Figure 3.15), and up to 3 years at higher altitudes (Figure 3.14). This indicates that the noise

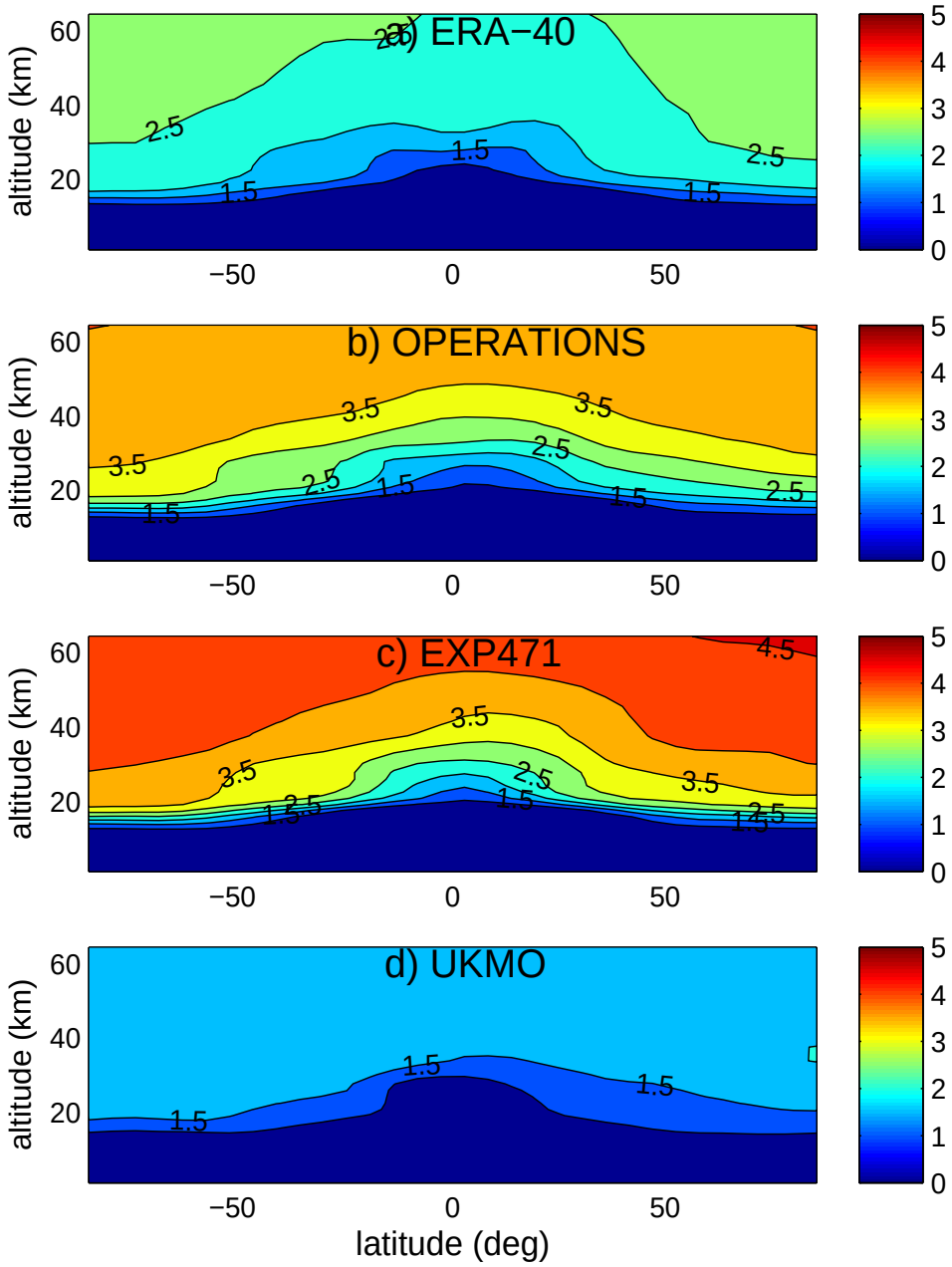

Figure 3.9: *Cross sections of the annual mean age-of-air (years) from TOMCAT $\sigma - p$ simulations with different data assimilation winds for year 2000 as indicated in the panel labels. Mean age values have been computed from a linearly increasing ideal tracer.*

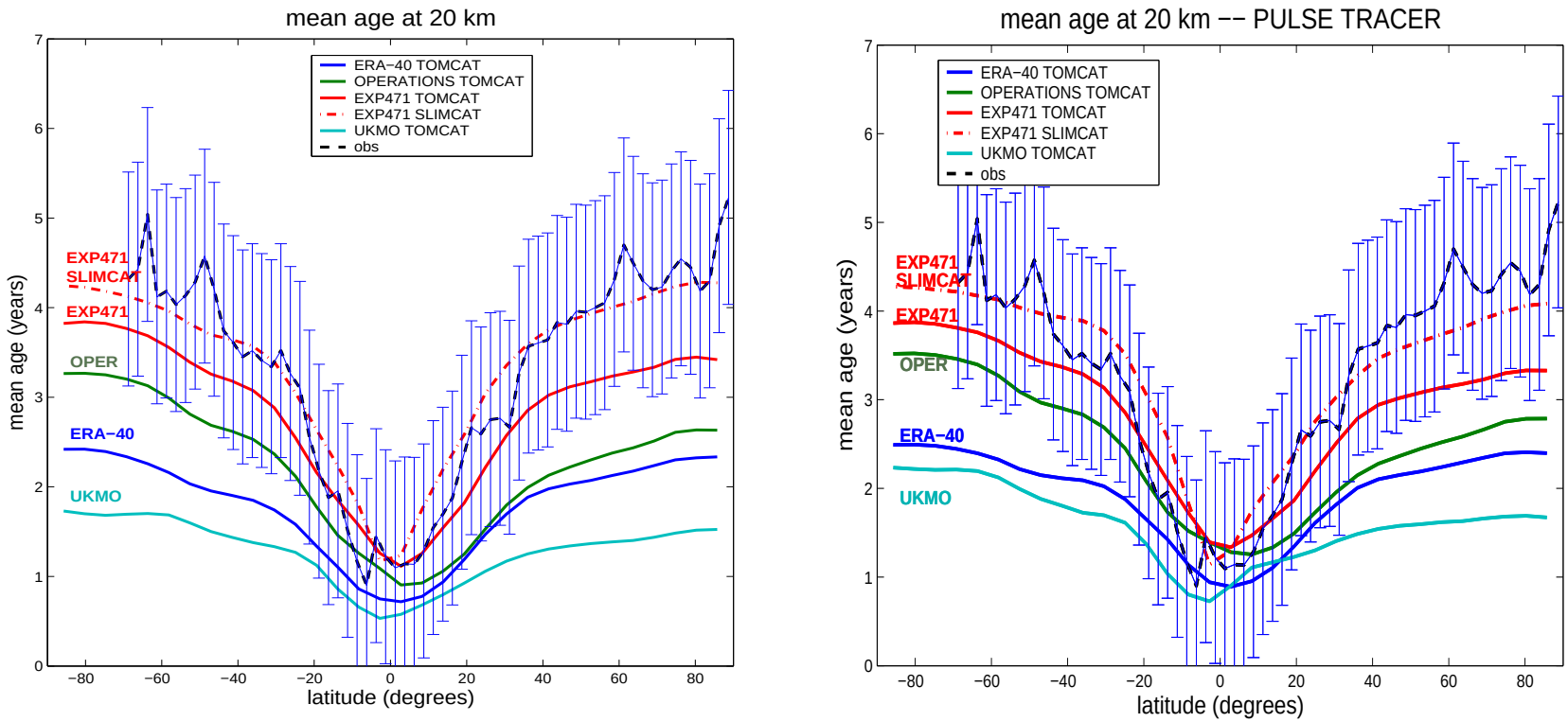

Figure 3.10: *Mean age-of-air at 20 km altitude from TOMCAT/SLIMCAT simulations (coloured lines) using different ECMWF and UKMO analyses for year 2000, compared with the mean age-of-air derived from in-situ ER-2 aircraft observations of* CO_2 *(Andrews* et al.*, 2001) and* SF_6 *(Ray* et al.*, 1999) (black dashed line).* 2σ *error bars have been included for the observations. Results correspond to ERA-40 (dark blue), ECMWF operational (green), EXP471 (red), and UKMO (light blue) winds, using a linear tracer (left panel) and a pulse tracer (right panel).*

in the vertical advection (which is reduced by the use of isentropic levels) has been very much reduced in EXP471 with respect to ERA-40; the remaining noise is still responsible for the younger ages TOMCAT obtains with EXP471 with respect to SLIMCAT. Further discussion on the differences between TOMCAT and SLIMCAT runs is included in Section 3.4.6.

Vertical profiles

Vertical distributions of mean age-of-air are shown in Figure 3.11 for three different latitudes (5°S, 40°N and 65°N), where results from the TOMCAT simulations are plotted along with in-situ SF_6 (Elkins *et al.*, 1996; Ray *et al.*, 1999) and CO_2 (Boering *et al.*, 1996; Andrews *et al.*, 2001) observations, as well as SF_6 whole air samples (Harnisch *et al.*, 1996). All winds underestimate the mean age above 20 km. As for the zonal distributions, OPER winds present better agreement with observations than ERA-40, and EXP471 winds produce the results closest to the observation profiles at the three latitudes studied.

3.4.5 Results from age-spectrum

The mean age values obtained from the age spectra at 20 km altitude are shown in Figure 3.10b to illustrate that both methods, ideal linear tracer and age spectrum, are equivalent for the calculation of the mean age.

The zonal mean spectra for the three latitudes considered in Schoeberl *et al.* (2003) (0°, 40°N and 70°N) have been examined at 5 different altitudes, to see how the pulse tracer is advected through the stratosphere in the model. Figure 3.12 shows the normalised spectra for ERA-40 and EXP471 winds at these locations. The results confirm that TOMCAT simulations with ERA-40 winds produce too fast vertical advection, which is reflected in only a small offset in time for the peak in the spectrum on going to higher altitudes (Figure 3.12). This changes when EXP471 winds are used; in this case the propagation of the pulse is slower both in the vertical and in the horizontal, resulting in age spectrum shapes in much

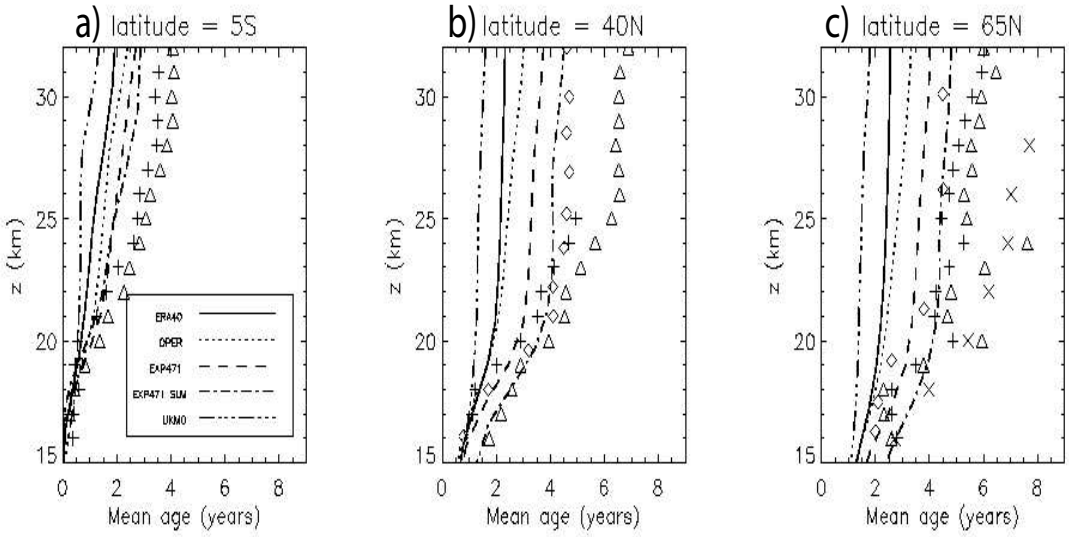

Figure 3.11: *Vertical distribution of mean age-of-air at (a) 5°S, (b) 40°N and (c) 65°N. TOMCAT (σ-p) simulations have been driven by ERA-40 (solid line), OPER (dotted line), EXP471 (dashed line) and UKMO (dot-dot-dot-dashed line); one SLIMCAT ($\sigma - \theta$) simulation with EXP471 winds(dot-dashed line) is also included. Symbols are for mean age values based on in situ observations of SF_6($\triangle$) and CO_2 (+) in all panels (Elkins* et al.*, 1996; Ray* et al.*, 1999; Boering* et al.*, 1996; Andrews* et al.*, 2001); (b) additional whole air samples of SF_6 ($\diamond$) and (c) whole air samples of SF_6 inside the vortex* ($\diamond$) *and outside the vortex* ($\times$) *(Harnisch* et al.*, 1996).*

better agreement with the Brewer-Dobson circulation. These panels thus confirm what was first deduced from the ideal tracer calculations: The excess vertical and horizontal transport in the LS has been much reduced in the new EXP471 winds with respect to ERA-40. The spectra help to show that also for higher altitudes the new winds produce a slower (more realistic) transport towards high latitudes from the tropics. This fact is also reflected in zonal mean age distributions which still show a latitudinal gradient at altitudes above 20 km, in contrast with ERA-40 winds (Figure 3.13). This figure shows that for altitudes around 40 km OPER

winds also exhibit latitudinal variation, however at 60 km only the new EXP471 winds maintain some latitudinal variation.

3.4.6 Results SLIMCAT v. TOMCAT

The use of isentropic coordinates has been presented in Chapter 2 (Section 2.5.1) as one of the techniques used by some CTMs to correct for excessive vertical and horizontal transport in the winds. As already seen in Figure 3.10 the difference between the use of a TOMCAT and a SLIMCAT run with the new EXP471 winds is <1 year, which means it is smaller than the variation in the mean age caused by the use of a different set of winds, for instance. In the tropics, between 10°N-10°S, the TOMCAT and SLIMCAT simulations of the mean age with EXP471 winds differ by less than 0.4 years for the NH and less than 0.2 years for the SH (Figure 3.10). This is in contrast with what the trajectory model results in Schoeberl *et al.* (2003) predicted for a CTM using diabatic heating rates. Those results predicted much older tropical ages for the diabatic heating rates due to the exchange of air between tropics and subtropics. This section analyses in more detail in which regions the two CTM configurations (TOMCAT/SLIMCAT) still differ.

The cross-sections in Figure 3.14 give information on the zonal differences between a SLIMCAT and a TOMCAT simulation with ERA-40 winds (left panels) and with EXP471 winds (right panels). In the case of ERA-40 the use of SLIMCAT leads to a realistic distribution; the use of θ levels and heating rates have in this case corrected the excessive tropical-subtropical mixing and the too fast vertical transport. Differences reach values larger than 3 years in the upper stratosphere for all latitudes. On the other hand, for the EXP471 winds the two configurations give distributions very similar in shape (although the TOMCAT one results in slightly flatter contours over the tropics). The differences for EXP471 are less than 0.5 years in the mid-upper stratosphere but slightly larger (up to 1.2 years) at lower altitudes and high latitudes. With EXP471 SLIMCAT gives older age values than TOMCAT everywhere except for the equatorial region at around 35 km, where the age values

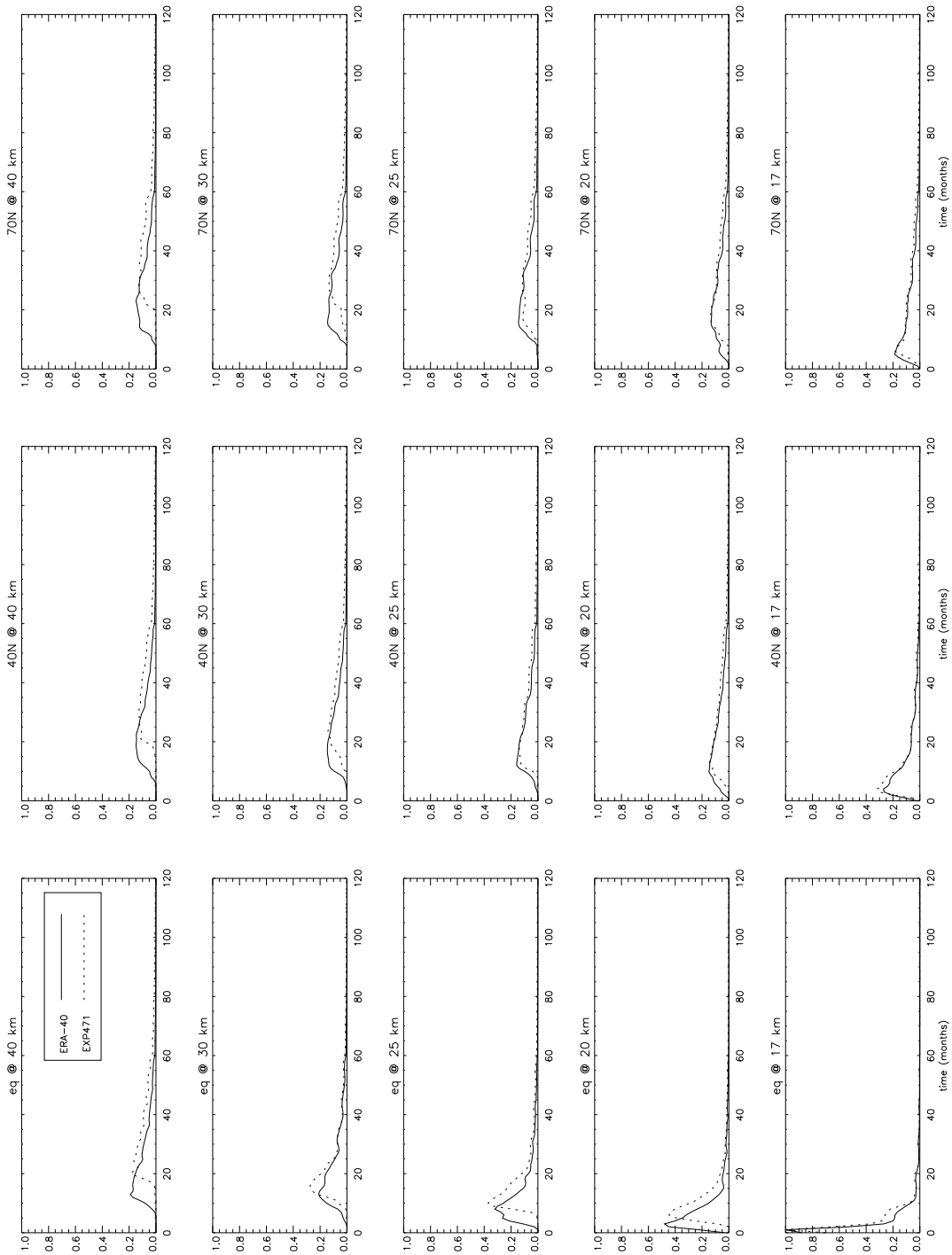

Figure 3.12: *Normalised age spectra for 5 altitudes (17, 20, 25, 30 and 40 km) and 3 latitudes (equator, 40°N and 70°N) obtained from TOMCAT simulations with ERA-40 winds (solid line) and with EXP471 winds (dashed line).*

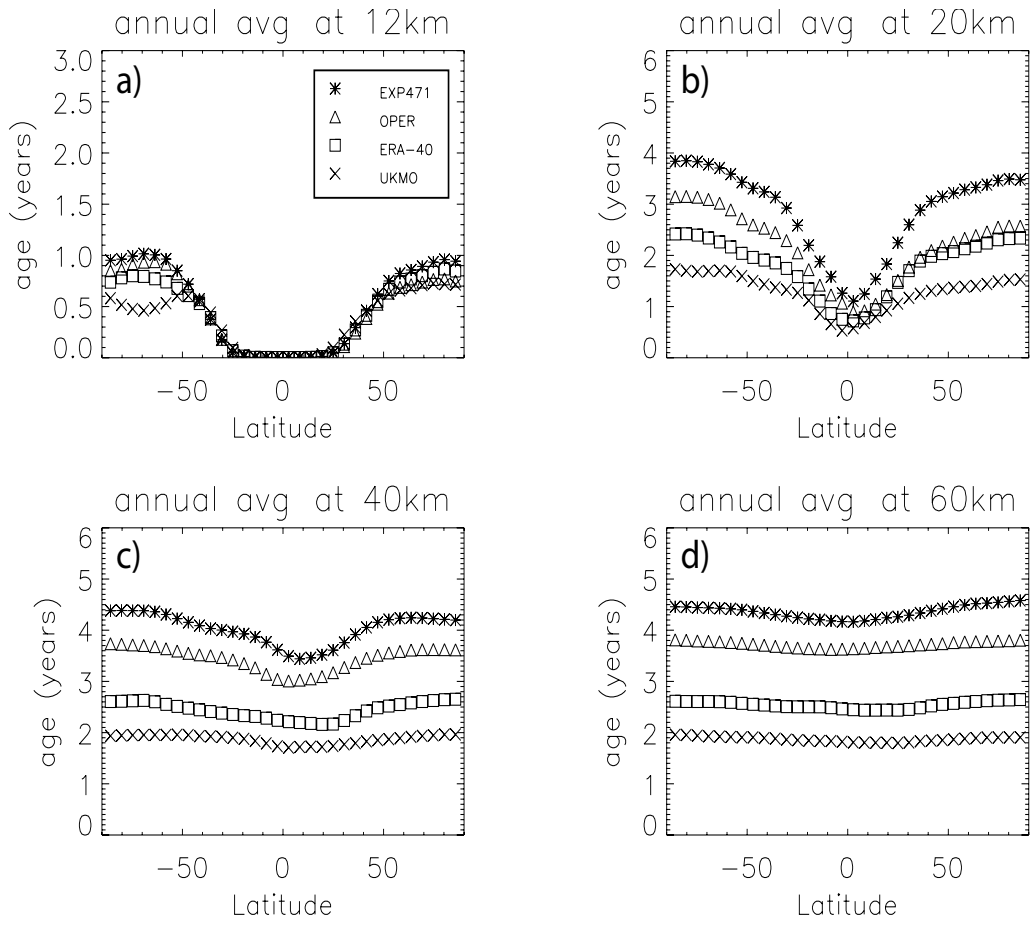

Figure 3.13: *Zonal mean annual mean age-of-air (years) at different altitudes obtained with TOMCAT when forced with the four different datasets, all runs used perpetual 2000 meteorology.*

are slightly younger for SLIMCAT. This indicates that the tropics are still somewhat more isolated when isentropic coordinates are used in the stratosphere. However, the differences are clearly much smaller with EXP471 winds than in the case of the equivalent TOMCAT and SLIMCAT simulations for ERA-40 winds.

Figure 3.15 shows the zonal mean age at 20 km obtained from SLIMCAT runs with the three ECMWF wind sets. Differences between winds are now much smaller than they were with TOMCAT (compare with Figure 3.10), the maximum difference is found between OPER and ERA-40 at NH high latitudes. For ERA-40 and OPER

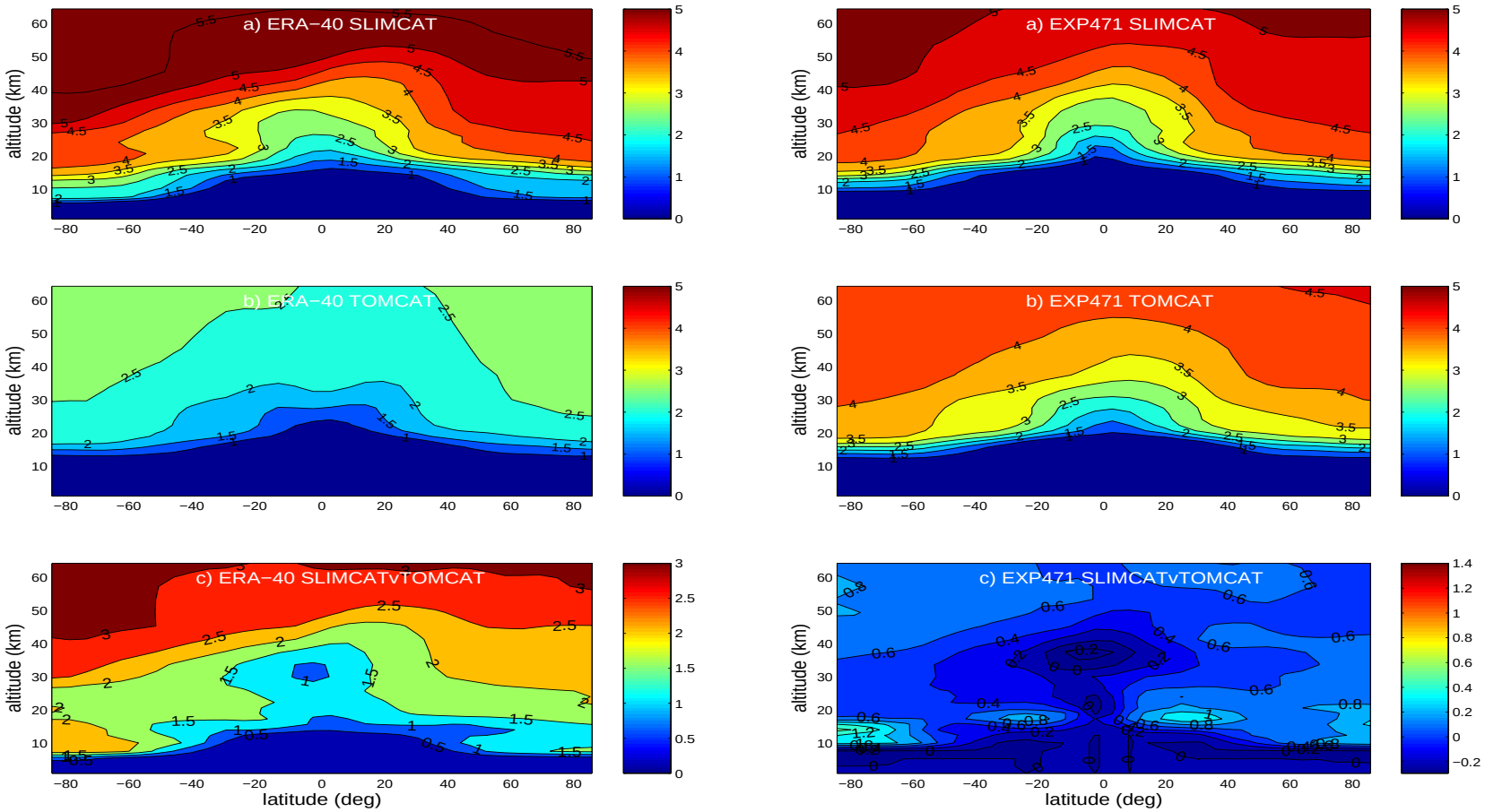

Figure 3.14: *Mean age-of-air zonal mean distributions with ERA-40 winds (left panels) for (a) SLIMCAT and (b) TOMCAT simulations. Panel (c) represents the differences between the simulations. Note the different colour scale for panel (c). Panels on the right are the same but for EXP471 winds.*

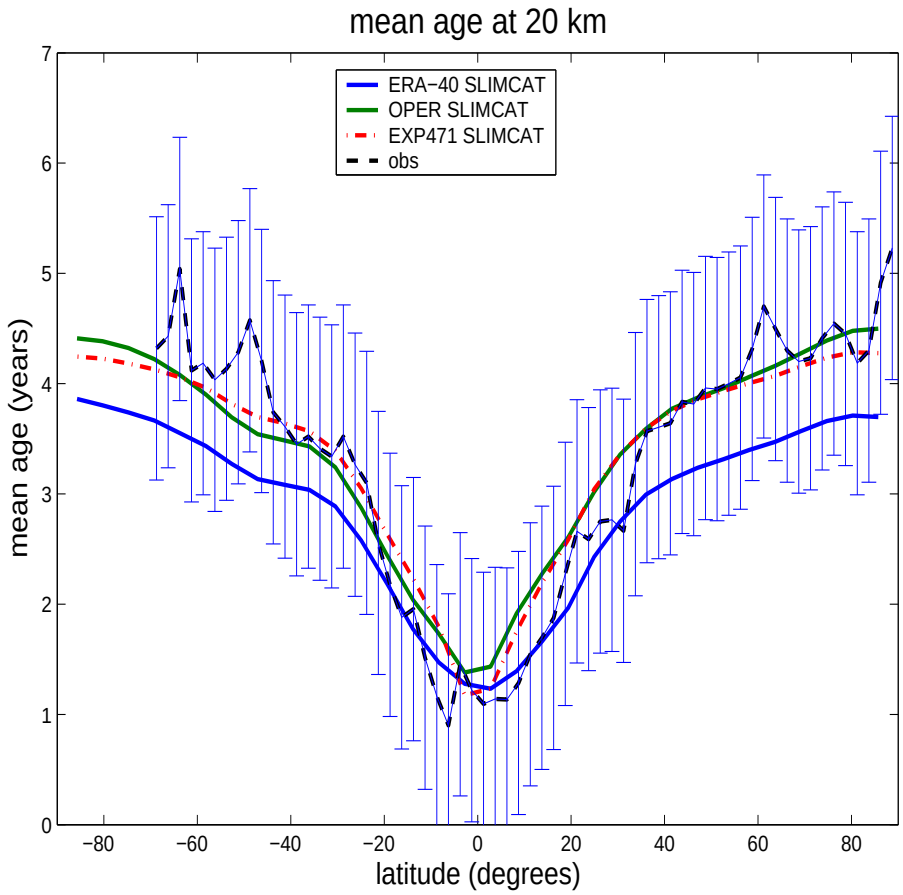

Figure 3.15: *As Figure 3.10 but for SLIMCAT ($\sigma - \theta$) runs. Differences between the runs are significantly smaller than for the TOMCAT simulations with the same winds.*

the SLIMCAT runs are much closer to the observational values than the TOMCAT runs (Figure 3.10).

The SLIMCAT and TOMCAT simulations with EXP471 winds have also been compared using age spectrum calculations. This comparison is shown in Figure 3.16, where spectra for the two CTM configurations using EXP471 winds have been overlaid for the same locations as in Figure 3.12. Both simulations are almost identical at the tropical tropopause (consistent with the same tropical LS mean-age values in Figure 3.10b). Above 20 km at the equator, the timing of the peak of the spec-

trum is similar for both SLIMCAT and TOMCAT, although the SLIMCAT peaks tend to be sharper, which agrees with the stronger latitudinal gradient exhibited by SLIMCAT zonal mean age.

This comparison between SLIMCAT and TOMCAT simulations indicates that, as the assimilation products develop (*e.g.* move to 4D-Var, correct observational biases *etc.*), the difference using θ or pressure levels becomes smaller, as proved by the small differences EXP471 winds exhibit with respect to the large differences found for ERA-40 winds with the two configurations. Small differences still exist for the two EXP471 simulations which show that there is some remaining noise, presumably introduced by data assimilation, that causes the weaker tropical isolation achieved by TOMCAT.

The LS, and in particular the tropical tropopause, is the key region for the correct simulation of stratospheric transport. Since the main entrance into the stratosphere is the tropical tropopause, problems in this region would propagate into the whole stratosphere. Moreover, seeing the differences in the latitudinal gradients for all the winds used (Figure 3.10), one of the main differences between the analyses sets tested in this work seems to be the excessive exchange of air between tropics and subtropics. To examine in more detail how the different winds represent transport in the tropical LS region several Lagrangian simulations described in Section 3.5 were performed.

3.5 Trajectory calculations in the LS

The lack of wind observations in the tropics makes this region more sensitive to the effects of data assimilation. Tan *et al.* (2004) found that the forcing by the analysis increments was one of the causes for the excessive subtropical transport in the FV-DAS. In our case, to examine in more detail how the different assimilation methods compared affect the exchange of air between the tropics and higher latitudes, we

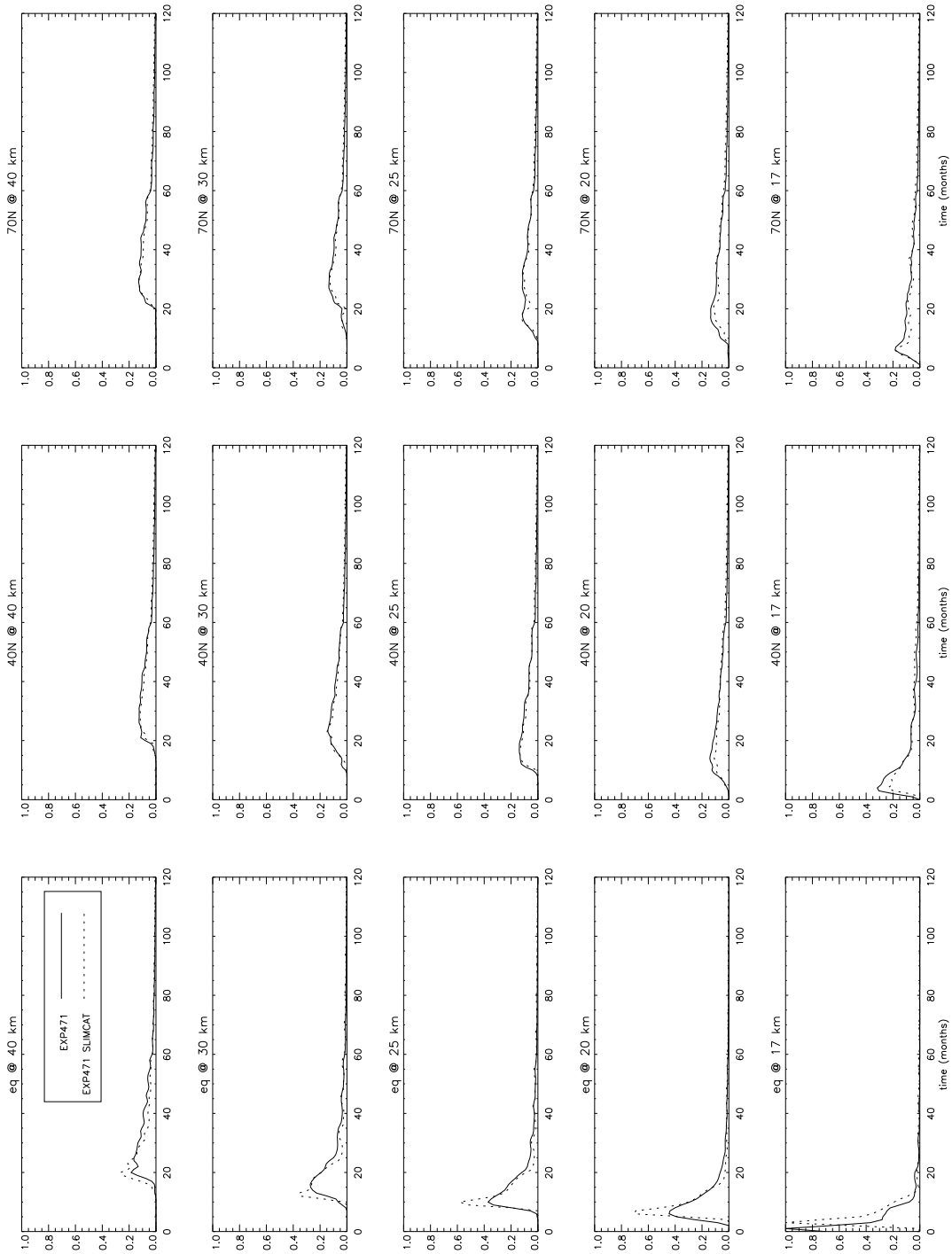

Figure 3.16: *Normalised age spectra for same altitudes and latitudes as in Figure 3.12, obtained from a TOMCAT (solid line) and a SLIMCAT (dashed line) simulation, both with EXP471 winds.*

have performed trajectory experiments using the off-line Lagrangian scheme embedded in TOMCAT/SLIMCAT (see Section 2.6).

Unlike an Eulerian model, a Lagrangian model follows the evolution of each air parcel individually in time and space. Thus, a Lagrangian perspective adds valuable information in terms of the source region of the air masses and the path they follow from/towards a considered location. That is why Lagrangian calculations of parcel distributions in the LS can help to quantify the exchange of air between tropics and subtropics for the different analyses used.

3.5.1 Experiments set-up

To investigate the different analyses in the tropical lower stratosphere (LS), we have carried out backward trajectory calculations with TOMCAT/SLIMCAT for the 4 different analyses. Even if both forward and backward trajectories approaches lead to almost identical results for time scales of weeks (Methven, 1997), backwards trajectories are statistically much more robust. In a forward simulation the number of particles will decrease with altitude, according to the decrease in air density one finds when moving upwards in the atmosphere. Therefore, to achieve the same statistical robustness, a forward simulation would require a larger number of initial particles than a backward simulation.

Kinematic trajectories are those in which air parcels are advected by vertical wind fields; diabatic, or isentropic, trajectories use heating rates to obtain the vertical motion. With the CTM used in this thesis both kinematic and diabatic trajectories can be carried out just by choosing the appropriate model configuration (TOMCAT or SLIMCAT mode). In the kinematic (or TOMCAT) trajectories the vertical motion is computed from the omega equation from the divergence of the horizontal winds. While for the isentropic (or SLIMCAT) trajectories the vertical motion comes from the calculated heating rates. The vertical motion and vertical coordinate options for TOMCAT and SLIMCAT modes are set as described in Section 3.4.3.

In the simulations shown here particles are initialised in a tropical location in the LS and then integrated backwards in time to see the origin of the air masses that reach the LS location where the simulation starts. These experiments give information on the amount of vertical diffusion and horizontal mixing in the tropical LS region. The same model configuration has been used for all the winds sets, so that different results are due to differences in the assimilated winds, as discussed in Section 3.4.6 and Chapter 4.

The experiments included here released 36,000 particles, uniformly distributed along a 2° latitudinal band centred at the equator at 40 hPa (TOMCAT) or 460 K (SLIMCAT). For the trajectory studies the model was run backwards for 50 days from January 1, 2001 (December 30, 2000 for EXP471). At every time step, horizontal position of each particle is given by its latitude and longitude coordinates, and the pressure value gives the particle vertical location. Additional attributes for each particle are: Temperature (K), potential temperature (K) and potential vorticity (PVU)[1]. The time step used for the experiments performed here is 30 minutes, although output values are evaluated only every 10 days. Every particle is also provided with a tropospheric flag that identifies when particles have re-entered the troposphere. The criterion used in the runs to give this flag the tropospheric value is two conditions being simultaneously fulfilled: The absolute value of the potential vorticity being less than 1 PVU and the potential temperature being below 380 K. In this way the number of particles that remain in the stratosphere at the end of the simulation is known, giving additional information on the accuracy of the winds in terms of dispersion. After a 50-day run, for the initial position considered here, all particles should still be in the stratosphere, thus the larger the percentage of particles in the stratosphere the more realistic the winds.

[1]PVU stands for *potential vorticity unit* and its value is: 1PVU= 10^{-6} m^2 s^{-1} K kg^{-1}.

3.5.2 Results from TOMCAT trajectories

Figure 3.17 shows the distribution of particles after a 50-day TOMCAT run with the winds indicated for each panel. It can be seen that the vertical transport of particles in TOMCAT simulations is significantly stronger for UKMO and ERA-40 winds than it is for ECMWF operational or EXP471 winds. Note that the presence of particles above the starting level (which is completely unrealistic for a backwards run) has been drastically reduced when using the OPER winds set, and almost eliminated with the new EXP471 winds. Also the horizontal dispersion of particles in the LS region is reduced when the newer ECMWF winds are used. The percentage of particles that remain in the stratosphere after 50 days is indicated for each panel in Figure 3.17. The anomalously low number of particles for UKMO winds is due to the method in which vertical motion is calculated for these winds in our CTM (see Section 3.4.4). A significant contribution to the large number of particles that have crossed the tropopause is very likely to come from the fact that the divergence field is not stored in the analysis grid, but also the fact that the UKMO analyses used are daily analysis instead of 6-hourly analysis is partly causing the difference between UKMO and ERA-40 results (see Chapter 4).

On the other hand, if we compare the parcel distributions in Figure 3.17 with Figure 1a in Schoeberl *et al.* (2003) (included here as Figure 3.18), it can be seen that results for the UKMO winds are very similar, indicating that using one set of winds or another is playing a far more important role than the use of a different CTM, or the fact that the initial vertical location for the particles release differ between our experiments and those in Schoeberl *et al.* (2003). Moreover, the off-line Lagrangian model developed by John Methven at the University of Reading (Methven, 1997) has also been used to validate the results obtained by TOMCAT with ERA-40 winds. Methven's model, which is widely used by the U.K. tropospheric modelling community, was run backwards for 50 days to evaluate the dispersion of trajectories in the LS region using 2001 ERA-40 winds (J. Methven, personal communication, 2005). Results from Methven's simulations agreed very well with our TOMCAT results.

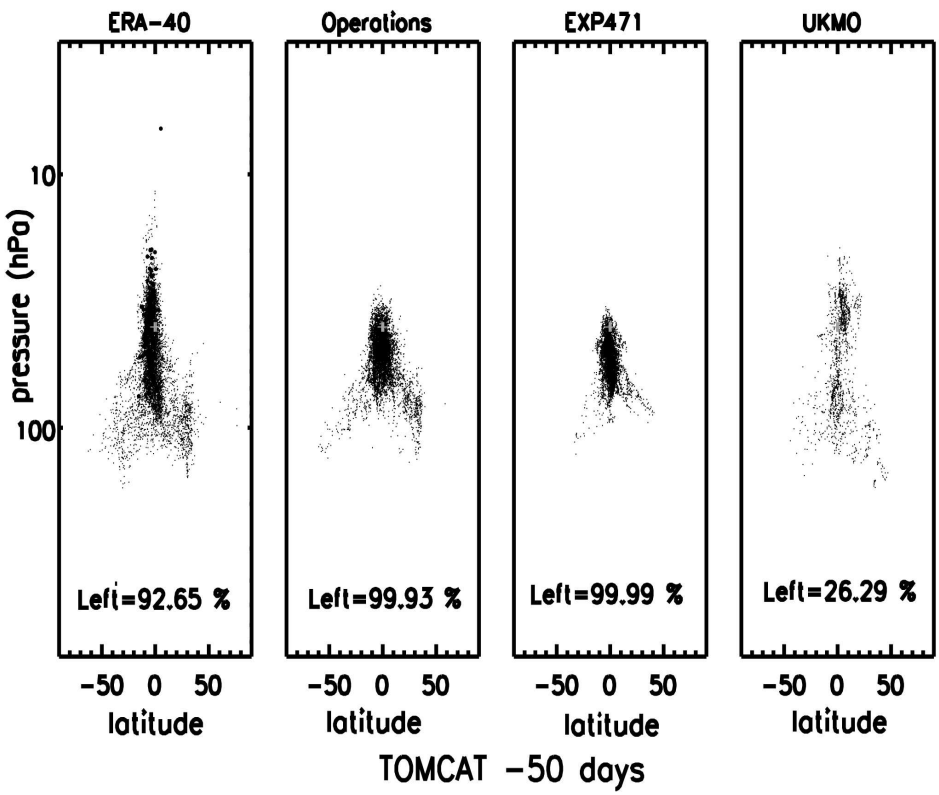

Figure 3.17: *Distribution of particles (black dots) after 50 days of backward kinematic trajectories with σ-p CTM forced by 4 different analyses. For each panel the percentage of particles left in the stratosphere after 50 days is indicated. Initial position of particles is 40 hPa over the equator (indicated by a cross).*

Differences in the distribution of particles in Figure 3.17 are consistent with the differences observed in the mean age. The winds producing the younger mean age (ERA-40 and UKMO) are also the winds that show a larger vertical mean transport and vertical dispersion of particles. This explains the excessively young mean age found over the tropics for the simulations using these winds. For ERA-40 versus EXP471 the differences in Figure 3.17 are mainly due to vertical dispersion of the particles, including unrealistic ascent, rather than differences in the mean vertical

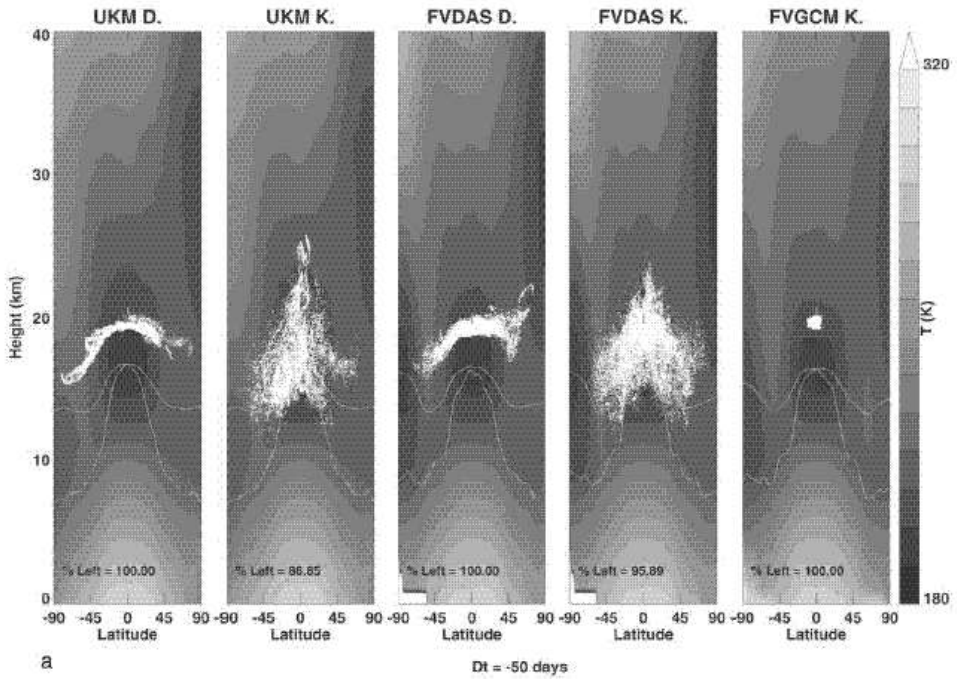

Figure 3.18: *The distribution of parcels 50 days after the beginning of the back trajectory calculation performed in (Schoeberl* et al.*, 2003). The lower thin white lines show the tropopause and the upper thin white line the 380K isentrope. The initial position of particles is over the equator at 20km of altitude. Grayscale indicates zonal mean temperature. The winds used are as indicated by the panel lables. Letter D is for diabatic trajectories, K is for kinematic trajectories. The percentage of particles remaining in the stratosphere after 50 days are indicated in each panel. Taken from Schoeberl* et al. *(2003).*

velocity. The reduction of latitudinal dispersion in the new winds can be seen from the stronger confinement of particles in Figure 3.17 and is confirmed by the longitude/latitude plots shown in Figure 3.19. This reduction in dispersion contributes to the improvement of the latitudinal gradient when operational, and more significantly, when EXP471 winds are used. Figure 3.19 shows how the excessive horizontal dispersion in ERA-40 is reduced when using OPER winds, especially in the southern hemisphere. However, the plume of particles at 40°N between 100-200°E only disappears when switching to the new EXP471 winds.

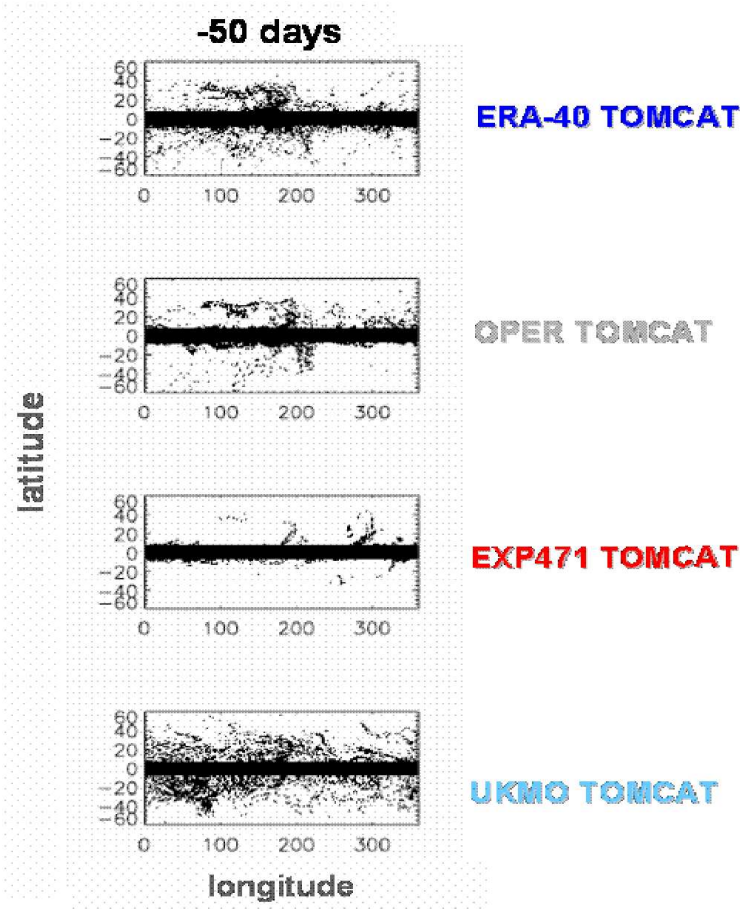

Figure 3.19: *Horizontal distribution of particles (composite of all stratospheric vertical levels) after a 50-day run of TOMCAT (σ-p). Winds as indicated by panel labels.*

3.5.3 Results from SLIMCAT trajectories

Figure 3.20 shows the distribution of parcels after a 50-day backward run of SLIMCAT. Seeing the reduction in the dispersion of particles with the 4D-Var winds in Figure 3.17, one would also expect a significant reduction in the horizontal spread for the isentropic trajectories. However, in this case there are not large differences between winds sets for SLIMCAT trajectories. This seems to be consistent with the mean age results shown in Section 3.4, where it has been shown that mean age values with the SLIMCAT configuration show much smaller differences between winds than the TOMCAT runs (Figures 3.14 and 3.15).

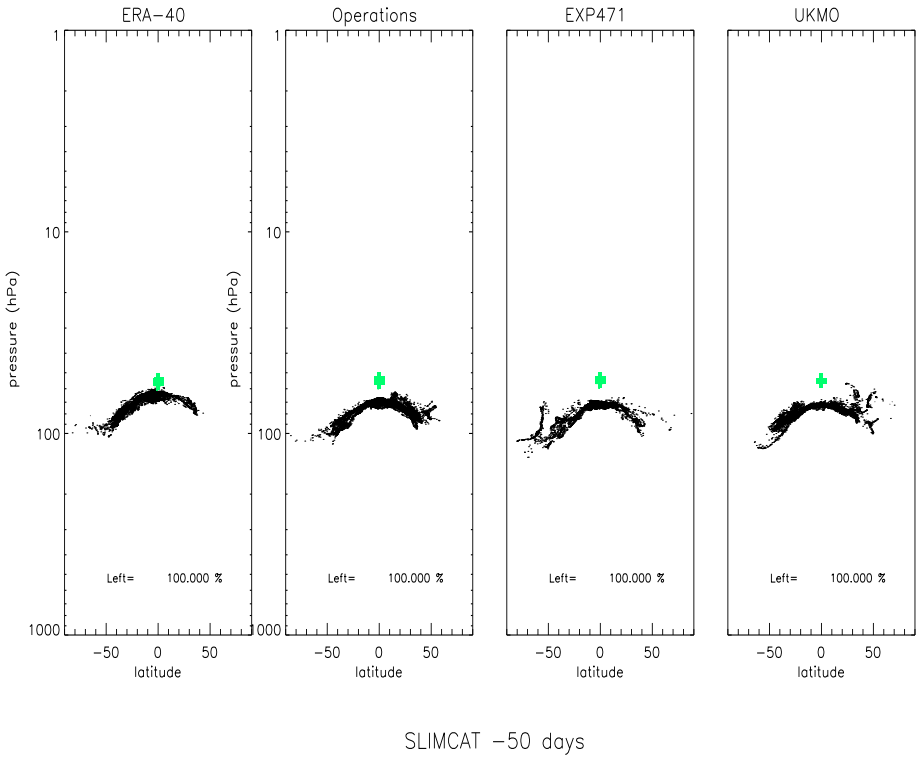

Figure 3.20: *Distribution of particles (black dots) after 50 days of backward kinematic trajectories with $\sigma - \theta$ CTM forced by same winds as in Figure 3.17. For each panel the percentage of particles left in the stratosphere after 50 days is indicated. Initial position of particles over the equator is indicated by a cross.*

Parcel distributions are very difficult to compare against observations. Sporadic aerosol emissions from volcanic eruptions can provide information on horizontal dispersion, but altitude coverage is limited. Aircraft Light Detection and Ranging (LIDAR) observations show that in the tropical stratosphere there are horizontal layers in which the tropical air masses are more isolated; these layers are interleaved with layers in which the horizontal mixing is stronger (Grant *et al.*, 1994). For this reason, the fact that the horizontal dispersion is not reduced for the newer winds is not necessarily unrealistic. Bregman *et al.* (2006) carried out trajectory simulations releasing particles from two different levels, and noted that the horizontal dispersion of particles depended on the vertical level used to initialise them. Nevertheless, as

Chapter 4 shows, a large part of the horizontal dispersion in the LS can be attributed to the data assimilation process.

3.6 Tape recorder signal

The amount of tropospheric water vapour that gets into the stratosphere critically depends on the temperature of the tropical tropopause (the cold point trap). Tropical tropopause temperatures exhibit a strong seasonal dependency, with coldest temperatures during the NH winter. The coldest temperatures produce the strongest dehydration of the air entering the stratosphere. This large annual cycle for water vapour in the LS was shown by Mote *et al.* (1996), who labelled it the 'tape recorder' signal as temperature at the tropopause is marking the air in a way similar to how a magnetic tape is marked when it is recorded. Mote *et al.* (1996) observed this signal from different instruments' observations of the quantity $2CH_4+H_2O$. Halogen Occultation Experiment (HALOE), Stratospheric Aerosol and Gas Experiment II (SAGE II), Microwave Limb Sounder (MLS) and Cryogenic Limb Array Etalon Spectrometer (CLAES) observations were used in Mote *et al.* (1996), as well as in-situ measurements from one NASA ER-2 aircraft campaign (ASHOE/MAESA). The 'tape recorder' diagnostic is therefore easily comparable against satellite observations (see Section 3.6.2 for more information on the observations used for validating TOMCAT results). Recently the stratospheric 'tape recorder' has also been detected in the distribution of CO from Aura MLS observations (Schoeberl *et al.*, 2006) however, simulations in this thesis focus only on the water vapour tape recorder.

This diagnostic is one of the standard tests now applied to stratospheric models to evaluate the representation of the subtropical mixing barrier. In the past, many models have not reproduced this feature well (*e.g.* Hall *et al.* 1999; Eyring *et al.* 2005). The vertical propagation of the tape recorder signal allows the estimation of the vertical ascent over the tropics to be 0.2-0.4 mm/s, stronger in northern winter, weaker in northern summer (Mote *et al.*, 1996). Thus, modelling the tape

recorder signal with TOMCAT/SLIMCAT will provide quantitative information on the vertical propagation of air masses over the tropics in the model simulations. The more realistic results shown with EXP471 winds in the previous sections also suggest that these winds will produce a more realistic tape recorder signal than ERA-40, UKMO and OPER winds. The experiments performed in this section will be able to check whether the improvements seen with EXP471 winds in the LS region reach higher altitudes.

3.6.1 Experiment set-up

The seasonally varying signal of the water vapour in the tropical stratosphere, can be modelled by simply including a tracer with a sinusoidally varying mixing ratio at the tropical tropopause (period 1 year, amplitude ± 1) within the CTM. The same TOMCAT simulations used in the rest of this study also contain such a tracer and have been therefore used for the tape recorder analysis.

3.6.2 Observations

The TOMCAT modelled tape recorder has been compared against observationally based values of the signal derived from the UARS HALOE instrument (Mote *et al.*, 1998). The time series of $2CH_4+H_2O$ measured by HALOE from 1992-1997 were analysed by Mote *et al.* (1998) with an empirical orthogonal function method. The amplitude and phase of the tape recorder signal derived from this method, together with estimations from in-situ CO_2 observations (Boering *et al.*, 1996), have been used to validate TOMCAT results. These observations have already been used in published work, *e.g.* in Mote *et al.* (1998) or the NASA Models and Measurements II (MMII) study (Hall *et al.*, 1999), to evaluate the tape recorder signal reproduced by different models.

3.6.3 Tape recorder results

To obtain information on the temporal evolution of the tropical tape recorder signal, the complete time series from the TOMCAT simulations have been plotted. Figure 3.21 shows the time series of the 'sin' tracer, averaged over the tropics (between 11.1°S - 11.1°N), using ERA-40 and EXP471 winds. Switching to the new EXP471 winds provides a more realistic tape recorder, the amplitude of the signal has been reduced, and the phase increased with respect to ERA-40, indicating a reduction in the strength of transport processes over the tropics. These results constitute a further proof of the more realistic vertical and horizontal transport achieved by the new EXP471 winds.

Figure 3.22 shows the vertical profiles averaged over the tropics (11.1°S-11.1°N) for the amplitude and phase of the tape recorder obtained by TOMCAT with the four sets of winds used here, along with values derived from observations. EXP471 results are the closest to the observations; in particular, the signal phase is very well reproduced with these winds. ECMWF OPER and ERA-40 winds produce less realistic tape recorder, while the UKMO winds used here appear particularly poor. These differences in the tape recorder are consistent with the improvements that EXP471 exhibits in the trajectory calculations in terms of both vertical and horizontal mixing. Some model studies (Mote *et al.*, 1998) have shown that vertical diffusion plays a key role in the dilution of the tape recorder. The fact that EXP471 maintains the tape recorder signal up to higher altitudes than previous analyses is then further evidence of the reduction in the vertical dispersion of the winds produced with the recent ECMWF system.

Results in this section show that the improvements exhibited by OPER winds, and moreover by EXP471 winds, come not only from a reduction in the horizontal mixing in the tropical region (tropics are more isolated in the more recent winds), but also from a more realistic vertical motion. Therefore, the results obtained here constitute a further proof of vertical motion and mixing processes being significantly

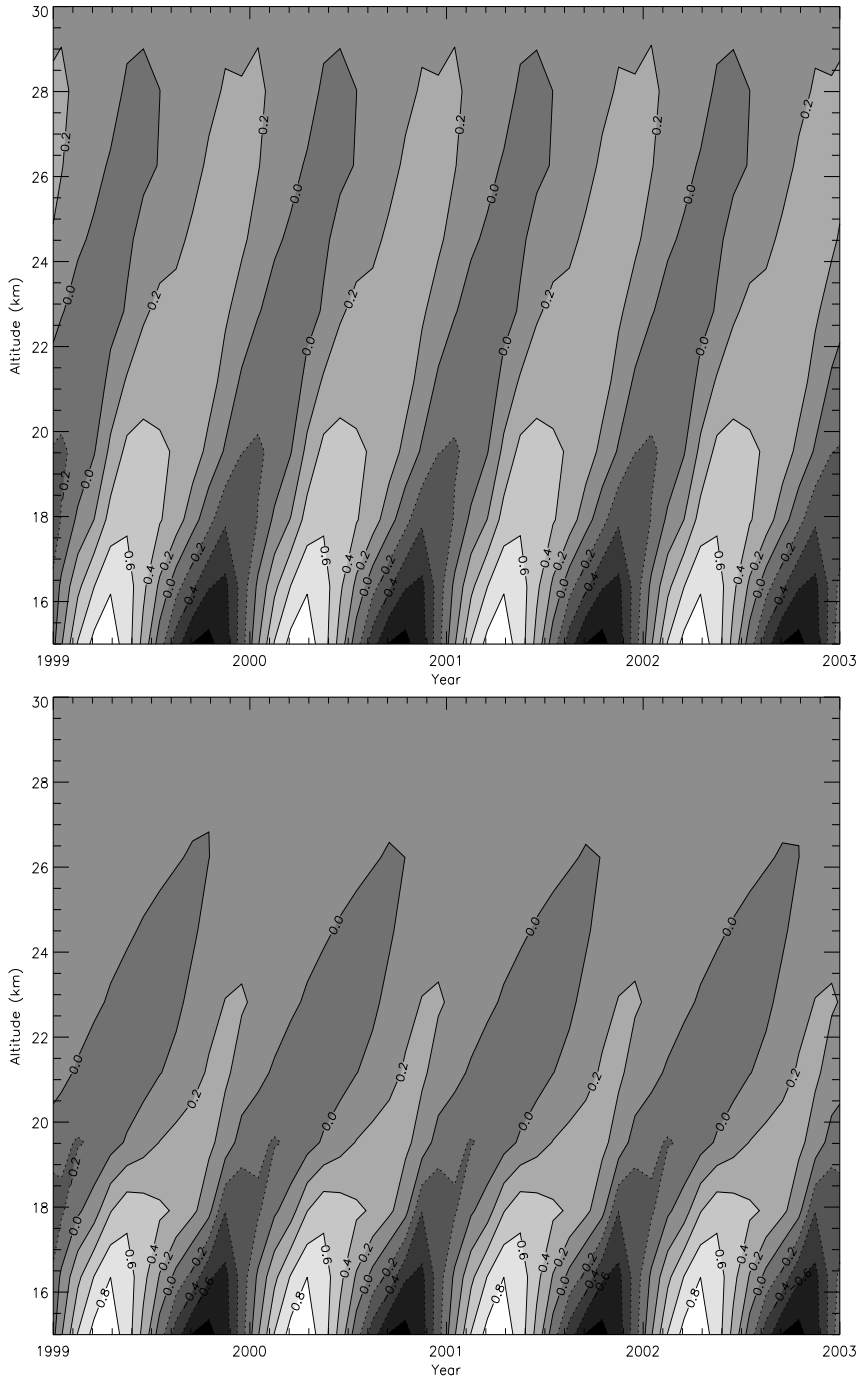

Figure 3.21: *Temporal evolution of the simulated tape recorder (tracer vmr) in TOMCAT from a 'sin' tracer using ERA-40 winds (above) and EXP471 winds (below) for model years 1999-2003 (note that years are arbitrary as the model used perpetual meteorology for 2000). Contour intervals are 0.2, dashed contours are for negative values.*

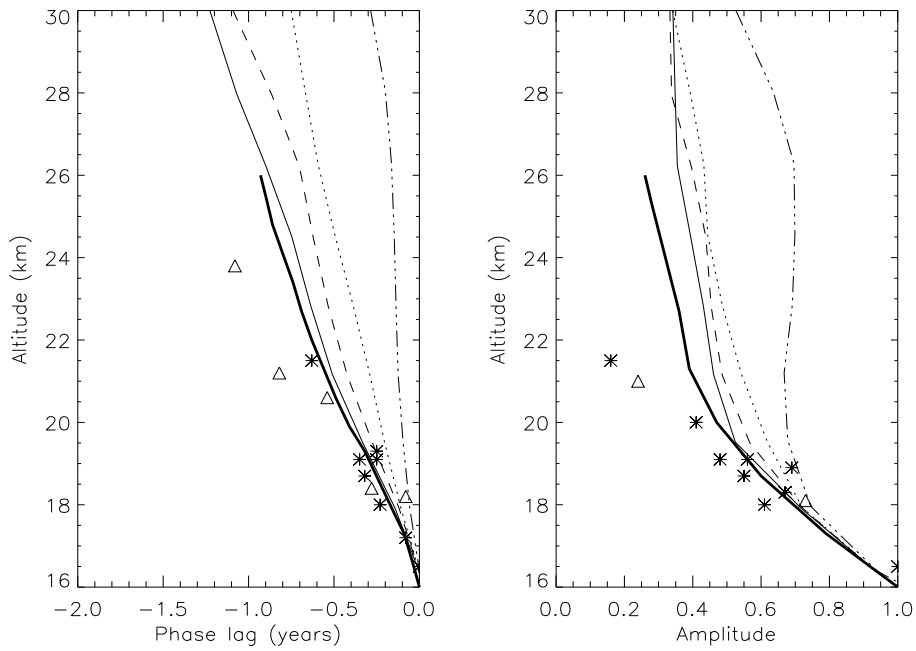

Figure 3.22: *Vertical tropical profiles of the phase (left panel) and the amplitude (right panel) of the tape recorder obtained by TOMCAT with ERA-40 (dotted line), OPER (dashed line), EXP471 (solid thin line) and UKMO (dot-dot-dot-dashed line) winds. The thick solid line shows estimate from HALOE observations (Mote* et al.*, 1998) and the symbols estimates from OMS in situ measurements of CO_2 (stars) and H_2O+2CH_4 (triangles). Observations data from Hall* et al. *(1999).*

better represented for the more recently produced ECMWF winds.

3.7 Eddy MPV flux

The definition of the Ertel potential vorticity, or simply potential vorticity (PV), is

$$PV = \rho^{-1}\vec{\xi_a} \cdot \nabla\theta \tag{3.3}$$

where $\vec{\xi_a}$ is the absolute vorticity vector:

$$\vec{\xi_a} = 2\vec{\Omega} + \nabla \times \vec{u} \tag{3.4}$$

$\vec{\Omega}$ is the rotational vector of the Earth, and $\vec{u}$ the 3D wind field. PV is often used on isobaric surfaces (Butchart and Remsberg, 1986), which simplifies equation (3.3) to

$$PV = -g(\xi_a)\frac{\partial\theta}{\partial p} \tag{3.5}$$

where g is the gravitational acceleration and $\xi_a = \xi + f$ is the vertical component of the absolute vorticity $\nabla \times \vec{u}$, where f is the Coriolis parameter and $\xi = \partial v/\partial x - \partial u/\partial y$.

PV as defined in (3.5) gives important information on the horizontal wind flow. However, its strong dependence on altitude (the term $\partial\theta/\partial p$ varies exponentially with z) makes it difficult to use PV to intercompare different θ levels or have a cross-section view of an atmospheric region. To overcome this drawback, Lait (1994) suggested an alternative definition for PV, the modified potential vorticity (MPV). As defined by Ertel (1942) the function θ in (3.3) can be substituted by any other monotonic differentiable function of θ. Lait (1994) chose the function $S(\theta) = -(2/11)\theta^{-11/2}$ to eliminate the strong dependence with altitude. The new MPV field will then be equal to the Ertel PV in (3.5) multiplied by $dS/d\theta$, which leads to

$$MPV = PV\left(\frac{\theta}{\theta_0}\right)^{-9/2} \tag{3.6}$$

where the factor θ_0 is included to make the scaling factor $dS/d\theta$ dimensionless. The eddy MPV flux is then defined by

$$flux = v' \cdot MPV' \tag{3.7}$$

where the primes indicate deviations from the zonal mean of the corresponding individual field, and v is the meridional wind component. The eddy MPV flux is a diagnostic for the transport of air masses from the tropics to midlatitudes and polar regions via eddy mixing processes. This diagnostic has been used in this thesis to further compare and quantify differences in the subtropical mixing processes for the

winds tested here. This diagnostic also provides an additional comparison with the winds used in Schoeberl *et al.* (2003), hereafter S2003.

3.7.1 Experimental set-up

From the TOMCAT/SLIMCAT potential temperature field MPV has been obtained from (3.6). Then, the eddy MPV flux defined in (3.7) has been calculated for the four wind datasets used in the previous sections. The field has been obtained from a 1-month (January 2000) simulation in which the output was stored every 6 hours. Unless otherwise stated, in all the runs shown here the factor θ_0 =380K has been used.

3.7.2 Results

The zonal mean of the MPV eddy flux for January 2000 is shown in Figure 3.23 for the tropical and subtropical middle atmosphere (200-0.1 hPa and 40°S-40°N). Features in good agreement with that expected for the northern hemisphere winter have been obtained. The maximum values for the eddy flux in the region of interest are located at northern stratospheric midlatitudes where, according to the stratospheric transport patterns, most horizontal air flux takes place in NH winter. The four panels in Figure 3.23 show a similar overall structure; the gradient for the isolines peaks towards the tropics, between 1-3 hPa, although it is weaker for EXP471 winds than for the other two ECMWF products. A strong vertical gradient exists however for EXP471 winds in subtropical winter latitudes between 3-6 hPa.

Figure 3.23 is analogous to Figure 10 in S2003, which has been reproduced here as Figure 3.24. In their MPV figure, S2003 compare the eddy flux obtained with the FVDAS winds (preliminary test for GEOS-4 winds) and the eddy flux obtained with the corresponding GCM winds. In the stratosphere the fluxes are weaker for the GCM than for the DAS winds they used; S2003 argue the excessive fluxes come from the data assimilation process and result in a weak tropical barrier combined

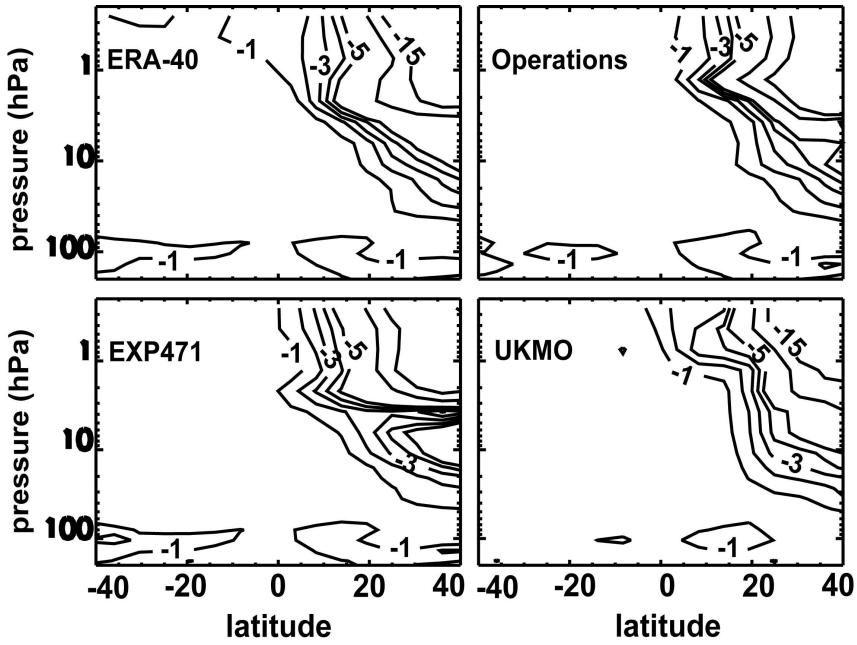

Figure 3.23: *Zonal mean monthly mean eddy MPV flux obtained with σ-p (TOMCAT) CTM for different analyses for January 2000, for the region 40°S-40°N, and above 200 hPa. Isolines are ±15, ±10, ±5, ±4, ±3, ±2, ±1 ($\times 10^{-6}$ $Km^3s^{-2}kg^{-1}$).*

with too strong overturning circulation. S2003 did not comment on the spurious features they obtained with the FVDAS winds in the summer hemisphere stratosphere. None of the DAS winds tested in this thesis present such spurious fluxes for January in the SH (see Figure 3.23). On the other hand, in S2003, the corresponding FVGCM panel appears to show an extremely weak MPV eddy flux above the tropopause; for the month of January a more complex structure in the winter-hemisphere stratosphere would be expected. Such an excessive horizontal 'quietness' is also reflected in the panel corresponding to FVGCM kinematic trajectories (Fig. 1a in S2003, Figure 3.18 in this chapter), where too weak horizontal dynamics seem to have occurred during a 50-day run. The fact that at least part of the horizontal dispersion presented by the DAS winds trajectories corresponds to real transport features has been also pointed out by Bregman *et al.* (2006) and is in agreement with volcanic aerosol observations (Grant *et al.*, 1994).

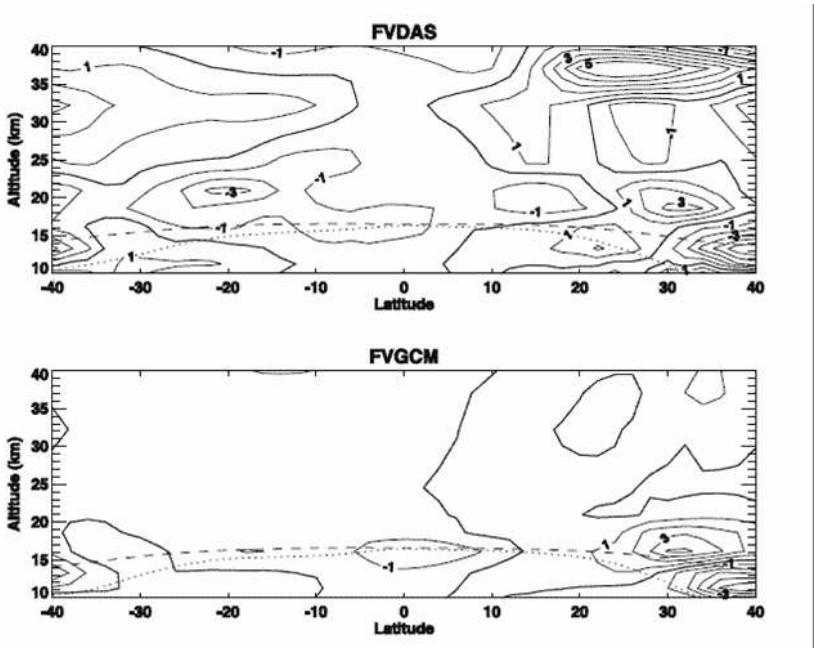

Figure 3.24: *Comparison of MPV eddy flux (in PVU × m/s) obtained for the tropical stratosphere with the Goddard Center CTM using preliminary version of GEOS-4 winds (top panel) and FVGCM winds (bottom panel) for January 2000. PVU stands for potential vorticity units, i.e. (*$\mathrm{K\,m^2\,s^{-1}\,kg^{-1}}$*). Taken from Schoeberl* et al. *(2003).*

Gabriel and Schmitz (2002) used a 2D model to compute the Eliassen-Palm flux divergence to evaluate the time variability of the zonal mean eddy flux. Their 2D model was based on the 3D GCM ECHAM3 and their computations were done with ERA-15 winds. Results in Gabriel and Schmitz (2002) do not show any spurious features for the summer hemisphere stratosphere. The fact that these unrealistic features are not shown by fields from ERA-15 (Gabriel and Schmitz, 2002), nor from ERA-40, UKMO, OPER 2000 or EXP471 (this work) indicates that the problem shown in S2003 is not characteristic for all DAS, but most probably due to a particular problem in the GEOS analysis version they used. Note that S2003 used an early test version of GEOS-4 that was not used for later studies (Pawson *et al.*, 2007).

None of the four panels in Figure 3.23 shows such excessive MPV flux in the subtropical region as the FVDAS runs in S2003. Therefore, differences in horizontal

advection, as shown by the MPV fluxes are probably not having such a large effect on mean age-of-air as differences in the vertical motion in this study. Thus, for this work, differences in the structure of the vertical velocities (Section 3.3) of the analyses tested as well as important differences in horizontal and vertical dispersion in the LS region (Section 3.5) appear to play the main roles in the different stratospheric transport.

3.8 Conclusions

The scope of this chapter was evaluating the reliability of different stratospheric (re)analyses to reproduce accurate transport processes in a stratospheric CTM. The evaluation was intended to show to what extent transport problems detected in ERA-40 have been overcome in more recent ECMWF datasets, with particular emphasis on the experimental test of ERA-Interim data (EXP471).

The age-of-air distributions obtained with operational and new EXP471 winds are more accurate than with ERA-40 winds, indicating that the recent ECMWF products solve to a large extent the overestimation of the BDC when used for multiannual simulations with TOMCAT/SLIMCAT. Also, trajectory experiments and tape recorder simulations have shown that the tropical isolation is much better represented by the ECMWF operational and interim reanalysis than by UKMO, ERA-40 winds, or the GEOS-4 winds used in Schoeberl *et al.* (2003). The MPV results included in this chapter have shown that horizontal advection is not the main difference between the four datasets tested. However, vertical advection and mixing in the tropical LS region are playing major roles in the different stratospheric representation achieved with these datasets.

Findings in this chapter contrast with some literature statements suggesting that intrinsic limitations in the data assimilation technique would prevent stratospheric analyses from further improvement (Schoeberl *et al.*, 2003; Stohl *et al.*, 2004; Rood,

2005). As this work has shown, the recent ECMWF DAS provides significantly higher quality stratospheric products than previous DAS. This demonstrates that more investigation was needed in this field at the start of this project, and that this thesis has opened new research lines and collaborations between operational weather centres and the CTM modelling community.

This chapter provides evidence that all the recent advances made in the ECMWF assimilation system have significantly improved the quality of the stratospheric (re)analysis, and that these improvements can be directly translated into an enhanced representation of the stratospheric circulation for CTM simulations. The use of a CTM to evaluate experimental reanalysis tests is a novelty introduced by this thesis that has proved to give excellent results. The information provided by the TOMCAT/SLIMCAT simulations shown here has been used by ECMWF to decide the final system implementation to produce their new ERA-Interim reanalysis (Monge-Sanz *et al.*, 2007; Simmons *et al.*, 2007).

The next question to answer is why the vertical advection and the mixing in the LS region are presenting differences between the datasets used here. What has changed in the production of the winds that is affecting the stratospheric transport in such a significant way? The use of the more sophisticated 4D-Var assimilation method is no doubt having a big impact in the description of the BDC, as the use of improved error statistics, better model physics and more accurate observations. But can these influences be quantified? Many have been the changes introduced in the system used for the three ECMWF products tested here. Such changes concern not only the data assimilation method but also developments in the IFS model and the amount and quality of the assimilated observations. Once the changes in the system are identified, is it possible to quantify the influence each change has on the stratosphere? The main difficulty is to have long experimental datasets that permit the evaluation of each separate change in stratospheric transport time scales. Chapter 4 deals with these issues and poses some challenges for future research lines

in order to answer these questions.

Chapter 4

Causes for Different Stratospheric Transport using Several ECMWF Analysis Datasets

4.1 Introduction

This chapter seeks the answers to the questions raised at the end of Chapter 3. The differences observed in the performance of the ECMWF winds tested in Chapter 3 are here linked to developments introduced in the DAS systems used to produce the winds. The aim of this chapter is discern what changes in the ECMWF system have most contributed, and quantify to the possible extent how much each change has contributed to a better description of the stratosphere. To achieve this, TOMCAT/SLIMCAT has been driven with additional wind sets from interim reanalysis experiments provided by the ECMWF. Such additional data have been produced with different DAS that allow the exploration of the effect of only one system change at a time. In addition, the effect of using ECMWF DAS or GCM winds will be contrasted. For this the CTM has been run with a set of ECMWF GCM winds and results are compared against those presented in Chapter 3. The GCM winds were archived every 12 hours, which also allows an evaluation of the CTM analysis read-in frequency effects on stratospheric transport.

The new ECMWF system used to produce the interim reanalyses tested in Chapter 3 is described in Section 4.2. The main developments incorporated by the system are also compared to their equivalents in previous systems (those used to produce ERA-40 and OPER winds). Section 4.3 then uses winds from ECMWF DAS experiments to evaluate the effect some of those system changes have on transport in the LS region. Section 4.4 is a comparative study between one set of ECMWF GCM winds and the DAS winds used in Chapter 3. Update frequency issues derived from the GCM versus DAS results are analysed in Section 4.5. Conclusions are presented in Section 4.6.

Out of the scope of this thesis is a detailed evaluation of every single change introduced in the ECMWF DAS/IFS systems. For this thesis ECMWF allowed access to all their existing interim experiments, but in no case was it possible for us to decide what experiments would be produced to test the impact of any particular system development. The fact that stratospheric studies need long sets of winds (e.g. 1-year data are necessary to capture the seasonal signal in the age-of-air) limits the experiments that could be used and the diagnostics that could be performed.

4.2 New ECMWF system

The large differences in the results obtained for each of the winds datasets (Chapter 3) lead to the unavoidable question of what is the cause for the improvements; first the improvements in OPER over ERA-40, but above all the improvements in the new EXP471. The only possible completely accurate answer is that there have been many variations in the systems used to produce the different winds. The ERA-Interim tests are based on a system that includes all the accumulated improvements done in the IFS model Cycle over the past 5 years, as well as a more sophisticated 4D-Var assimilation method. Thus, the production of the different ECMWF datasets used in this thesis vary in the assimilation scheme (3D- or 4D-Var, 6- or 12-

hourly cycling), the horizontal resolution and the version of the forecasting system employed. Forecasting system changes since ERA-40 have included changes in the amount, type, bias-correction and quality control of the data assimilated, changes in the parameterization of radiation and convection, and changes in the analysis of humidity and the dynamical background-error constraint, among others. It is not straightforward to identify which of the many changes are mainly responsible for improving the stratosphere, especially as the changes were implemented gradually over time and were not tested individually over periods of assimilation long enough to identify significant changes in the stratospheric circulation.

The main system changes are detailed next grouped into changes in the ECMWF assimilation method, in the observational data assimilated and in the IFS model. A deeper insight is provided for those changes more likely to influence stratospheric transport in CTM simulations.

4.2.1 Changes in the assimilation method

The ECMWF assimilation system used for the ERA-Interim tests includes many advances compared to the one used for ERA-40 reanalysis. The main ones are the use of a 12h 4D-Var assimilation technique (Rabier *et al.*, 2000) instead of a 3D-Var, the use of the VarBC variational bias correction for satellite radiances (Auligné *et al.*, 2007) and improvement in the statistical treatment of errors (Fisher, 2003). The following list gives the most relevant changes in the assimilation method.

- 12h 4D-Var instead of 3D-Var FGAT
- T255 horizontal resolution instead of T159
- Adaptive bias correction for satellite radiances (VarBC)
- Correction of biases in SHIP/SYNOP surface pressures
- New humidity analysis

- Improved background errors treatment
- Improved data quality controls

Developments in the IFS model and incorporation of new observational datasets need to be added to the list of improvements, as discussed in Sections 4.2.2 and 4.2.3. Some of these changes are already present in the system used to produce the OPER winds, while others are unique to EXP471 (and most recent ECMWF operational winds - not tested here). Table 4.2.1 details main changes introduced in the production of every set of winds used in this thesis.

4D-Var assimilation method

One important factor in the improvement exhibited by EXP471 over ERA-40 and UKMO winds comes from the use of the more sophisticated 4D-Var assimilation method (Rabier *et al.*, 2000). The 4D-Var assimilation technique is a development of the 3D-Var method that includes also the time dimension. In the 3D-Var assimilation method all the observations within the assimilation window are assumed to be valid at the analysis time (Figure 4.1), while the 4D-Var method is designed to make the best possible use of the observations, assimilating them at the actual time they have been taken, grouped in 30 minute slots (Figure 4.2a). The more consistent treatment given to the data insertion in the 4D-var procedure significantly reduces the dynamical imbalances with respect to the 3D-Var method (*e.g.* Gauthier and Thepaut 2001).

In the 3D-Var method implemented for ERA-40 the observations were compared with the first guess (i.e. background field on the background trajectory from the previous 6h analysis) at the appropriate time, which is called the 3D-Var FGAT method. This is a better option than comparing observations against the background trajectory at the analysis time directly (3D-Var). The 4D-Var technique is more complex to implement as it requires the additional model operator to evolve forward in time, the tangent linear model and the adjoint model to propagate information

Table 4.1: *System developments introduced in the production of the different ECMWF wind datasets used in this thesis.*

System development	***Analysis Dataset***						
	ERA-40	**OPER**	**EXP471**	**EXP444**	**EXP445**	**EXP446**	**EXP451**
IFS Cycle version	23r4	21r4/22r1/22r3	29r1	28r4	28r4	28r4	28r4
3D-Var	✓	-	-	✓	-	-	-
4D-Var	-	✓	✓	-	✓	✓	✓
6h assimil. window	✓	✓	-	✓	-	✓	-
12h assimil. window	-	-[a]	✓	-	✓	-	✓
2nd minimisation	-	✓	✓	-	-	-	✓
Wavelet J_b	-	-	✓	-	-	-	-
J_b statistics 3D-Var ensemble	✓	✓	-	-	-	-	-
J_b statistics 4D-Var ensemble	-	-	✓	✓	✓	✓	✓
ω-equation balance operator	-	-	✓	✓	✓	✓	✓

[a] Operational winds used a 6h window length for most of year 2000, switching to a 12h window on the 9th September.

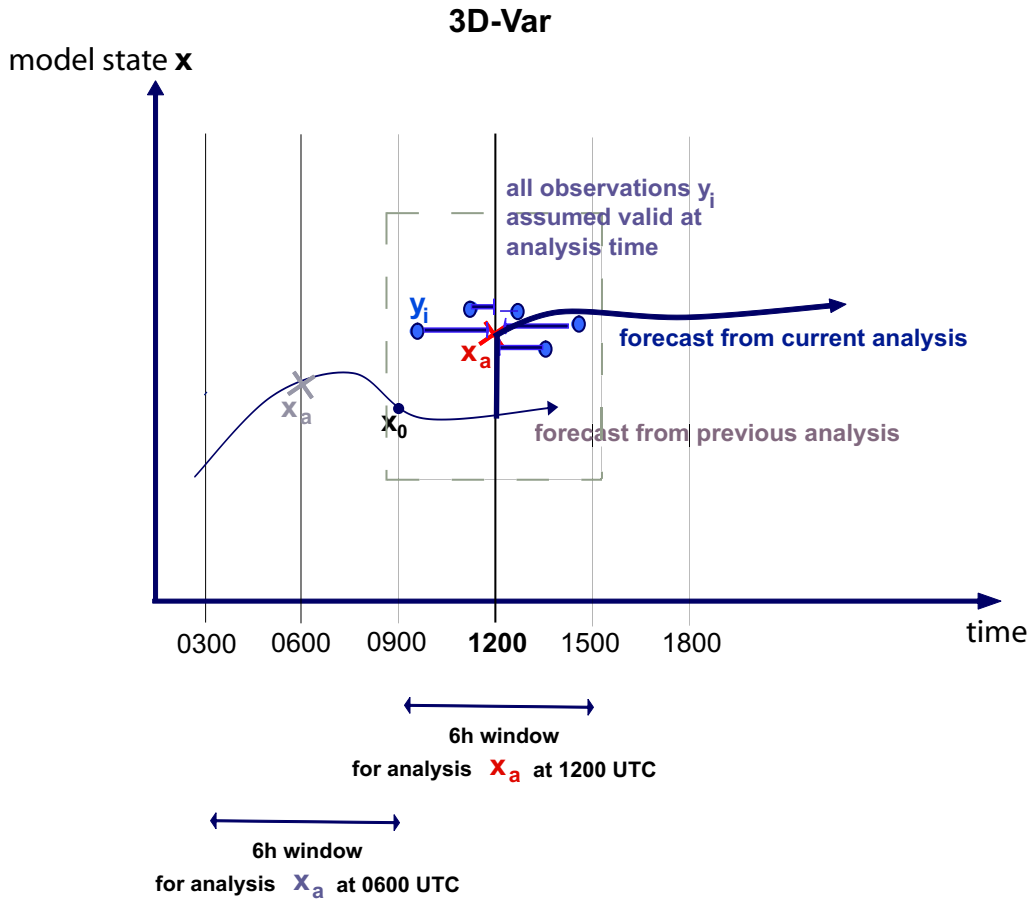

Figure 4.1: *Schematic showing the 3D-Var assimilation procedure with a 6h assimilation window.*

within the assimilation window. Due to its additional complexity with respect to 3D-Var, 4D-Var could not be implemented in the production of ERA-40, even if the technique was already operational at that time, as the computational resources allocated for the reanalysis were not able to deal with it. At ECMWF 4D-Var became operational in November 1997, and both OPER and EXP471 winds use it.

Length of the assimilation window

Even if both the operational and the new reanalysis winds come from 4D-Var assimilation, the length of the assimilation window used in operations was 6h for much of the year 2000 (it changed to 12h in September 2000) rather than the 12h window

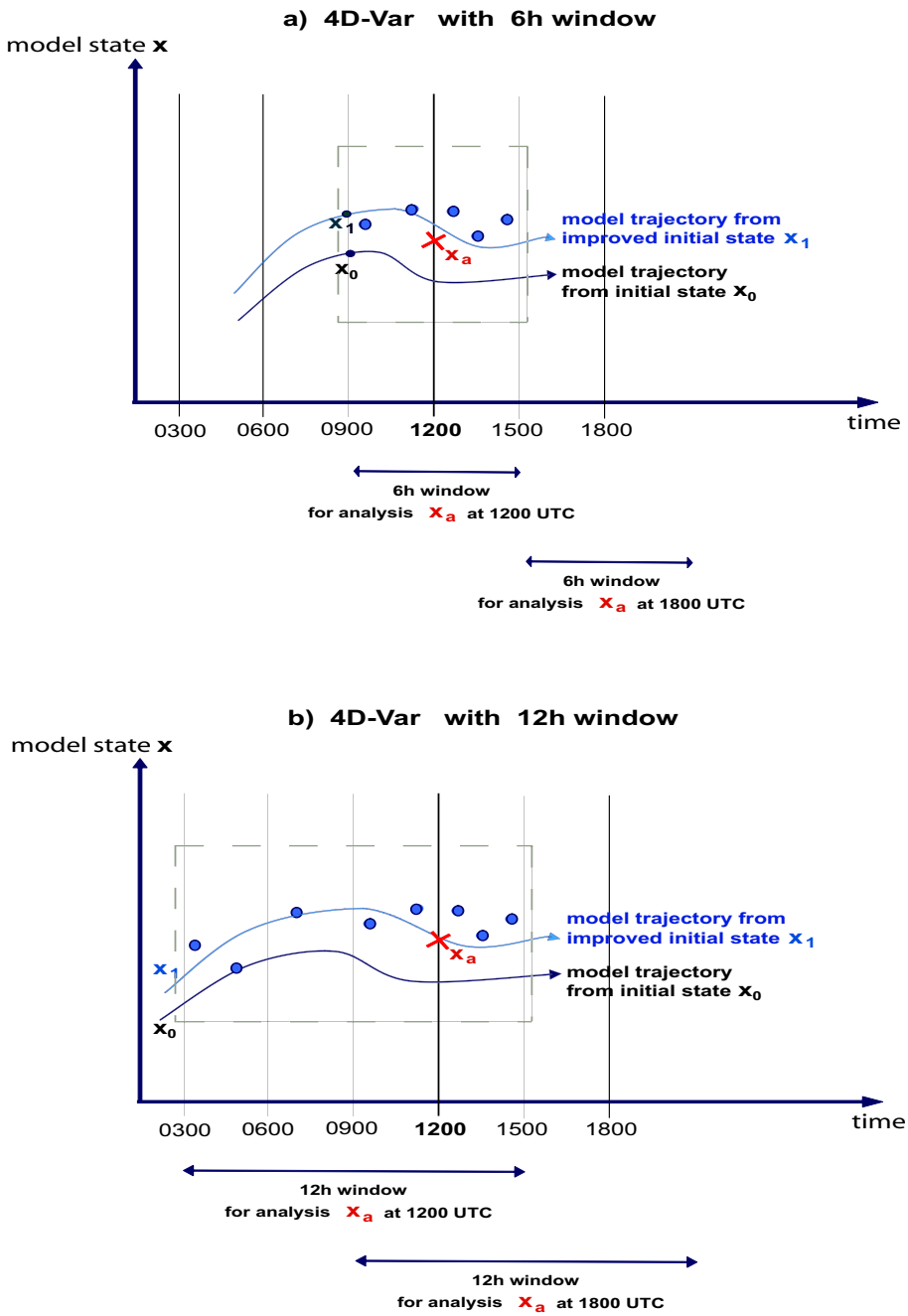

Figure 4.2: *Schematic showing the 4D-Var assimilation procedure (a) with a 6h assimilation window and (b) with a 12h assimilation window.*

used throughout EXP471. This means that more information from observations is used to constrain the analysis in EXP471 than in operations 2000, and that the background trajectory in EXP471 comes from a 12h forecast instead of a 6h forecast as in OPER.

The 4D-Var assimilation procedure with a 6h assimilation window is illustrated in Figure 4.2a. This method uses all the observations in a 6h window centred at the time of the analysis (*e.g.* 1200UTC). First, the full resolution model is run from the previous analysis (0600UTC) and observed-model departures are calculated. Then several inner and outer loops are implemented. In the inner loops the model state at the start of the assimilation window (0900UTC for the 1200UTC analysis) is adjusted so that the 6-hour forecast trajectory minimises the cost function J (*i.e.* the forecast trajectory better fits the observations). Several runs of a low resolution linearised model are carried out for this stage. The high resolution model is rerun from the adjusted (improved) initial state and observation departures are calculated again (this is the outer loop). The whole process is repeated twice (two minimisations) to produce the analysis $\vec{x_a}$ at the corresponding time (1200UTC in this example).

In the new 4D-Var procedure all data within a 12h window (e.g. 0300-1500 for the 1200UTC (re)analysis), are grouped into 30 minutes time intervals to compute the observation-model differences (Figure 4.2b). Therefore, the forecast trajectory is now 12-hour long, and not 6-hour, which reduces the discontinuities (imbalances) introduced in the model physics. However, this also means that the model is assumed to be perfect over a 12h period. This can cause problems if large model biases exist. The longer the assimilation window the more problems in the inner loop, as the trajectory will not fit the observations at the end of the window as well as it would for a shorter window length.

Statistical treatment of background errors

Approximately 85% of the information contained in an analysis comes from the background state, and the remaining 15% from the observations assimilated in the last analysis cycle (Cardinali *et al.*, 2004). The background state propagates the observational information assimilated in previous cycles, therefore the statistical description of the background errors is key for the correct propagation of that information. The background term of the cost function is represented by the matrix J_b, and is used to penalise the departures model-background that are less likely to be true. The statistical probability of departures is represented by the covariance matrix; this matrix encodes how information from observations in previous analysis cycles is propagated to neighbouring grid points and levels.

ERA-40 and ECMWF operations from 1997 to 2005 used the Derber-Bouttier J_b (Derber and Bouttier, 1999), which had only limited spatial variability, i.e. the information is propagated to nearby grid points in the same way independently of where those grid points are located. EXP471 however, makes use of a new method that became operational in 2005 that efficiently adds spatial structure to the background error covariances. This new covariance model is known as "Wavelet" J_b (Fisher, 2003), as it resembles the mathematical wavelets functions' ability of resolving both frequency and space. EXP471 is the only interim test among those used in this thesis produced with this new wavelet J_b formulation; it was first introduced in IFS Cy29r1 and the experimental runs EXP444-445-446 were produced with earlier IFS cycle versions (see Table 4.1).

The better treatment of background errors in the more recent ECMWF DAS winds is likely to have reduced spurious propagation of eddy motion associated with analysis increments, which was linked by Tan *et al.* (2004) to an excessive subtropical horizontal transport in the Goddard FVDAS, especially in the LS. Nevertheless, to quantify the influence of the new background error model, appropriate runs of the ECMWF system should be carried out in which that was the only change in

the system compared to a reference run (e.g. EXP471), to be later analysed by the CTM model. Such experimental runs do not exist at present.

Also, as noted by Fisher (2006), future increases in the length of the assimilation window would be expected to produce further improvements in the (re)analysis than developing the covariance models. With a longer assimilation cycle the information that needs to be incorporated from observations in previous cycles decreases, the ideal situation would be that in which all observations could be considered in one go for the complete forecast period (e.g. 5 days), in such case the propagation of information would be unnecessary.

4.2.2 Changes in the assimilated observations

The ERA-Interim runs use most of the observational datasets included in ERA-40 plus the observations operationally archived in the last years. Besides, experience gained with ERA-40 results in better quality control of data, in an improved treatment of radiosonde data (bias corrections and homogeneisation), and in the correction of important biases in satellite radiances that were partly responsible for the too strong BDC in ERA-40 (Uppala *et al.*, 2005). Other observation datasets that have been added to ERA-Interim tests and will be used in the next ECMWF reanalysis are (Simmons *et al.*, 2007):

- Direct assimilation of SSM/I radiances calibrated by RSS
- Inclusion of reprocessed ozone GOME profiles
- Improved bias correction of TOVS radiances
- New ESA altimeter wave-heights from 1991 onwards.
- Reprocessed Meteosat winds from EUMETSAT.

4.2.3 Main changes in the IFS system

It would be too long to list all the changes the IFS model versions have incorporated from the production of ERA-40 until the production of the interim tests. On average between 2-3 different IFS Cycle model versions are implemented by ECMWF each year, with all the individual improvements each version puts in place[1]. ERA-40 was produced with the IFS 23r4, after which 10 different Cycle model versions were implemented by ECMWF until the production of EXP471. The following list only intends to point towards the main changes that will have influenced the stratospheric transport in a more direct way.

- Improved radiation scheme
- Physical parameterisations
- Improved ozone parameterisation
- Improved convection parameterisations
- Improvements in numerics
- Revised cloud physics
- Improved moist boundary layer scheme
- Aerosol climatology included

After listing these main changes most likely to have caused differences in the stratospheric transport, a cautionary note should be added here. To quantify the influence each of the listed changes has on the final stratospheric improvement, ideally (re)analysis data produced with one single change at a time should be used. However, it needs to be considered that it is all the mentioned changes, and feedbacks between them, acting together that results in the final improvement. Evaluation of

[1]Detailed information on the ECMWF system changes and when they became operational can be found at http://www.ecmwf.int/products/data/operational_system/evolution/index.html

each separate change might not be straightforwardly related to the improved stratospheric transport in TOMCAT/SLIMCAT seen when using the final (re)analysis product.

Using additional ERA-Interim experiments, Section 4.3 evaluates how some of the system advances described in the current section affect transport in the stratosphere. The changes that have been possible to analyse are, however, restricted to changes in the assimilation method only, due to the availability of ERA-Interim experiments.

4.3 Sensitivity runs

As described in Section 4.2, there have been too many recent developments in the ECMWF system to be able to evaluate each one of them separately. However, focusing on the impact the new assimilation method has, a set of four additional ERA-Interim experiments allows us to explore how some of the more important changes in the assimilation technique have affected vertical advection and horizontal mixing in the UTLS.

4.3.1 Datasets used

The ERA-Interim experiments used in this chapter are: EXP444, EXP445, EXP446 and EXP451. All of them were produced with the same IFS Cycle version (28r4), the only differences between them are in the assimilation system used:

- EXP444: 3D-Var FGAT
- EXP445: 4D-Var, 12h window
- EXP446: 4D-Var, 6h window
- EXP451: 4D-Var, 12h window, two minimisation loops

Comparing the first experiment with the following two allows the evaluation of the effect caused by the introduction of the 4D-Var assimilation, while comparison between the 4D-Var runs EXP445 and EXP446 has provided information on the use of a longer or shorter assimilation window. EXP451, has been used to analyse the effects of a second minimisation loop in the data assimilation process. EXP451 is equivalent to EXP445 but included two minimisation loops, unlike EXP445 and EXP446, which included only one. For all these datasets the same trajectory calculations as for the other winds have been performed, and the equivalent latitude/altitude and latitude/longitude particle distributions plotted after a 50-day run of TOMCAT (see Chapter 3 for information on the calculation of diagnostics).

4.3.2 Assimilation method: 4D-Var v. 3D-Var

From Figure 4.3 it can be seen that changing from a 3D-Var to a 4D-Var system is one determining factor in the reduction of the excessively large vertical dispersion. The first and second panels (ERA-40 and EXP444 respectively) have been produced with the same 3D-Var assimilation method but different IFS versions, and both exhibit vertical dispersion twice as large as the other two panels, which have been produced with a 4D-Var method. Somewhat surprisingly, in terms of the horizontal dispersion, the 3D-Var dataset EXP444 is no worse than the 4D-Var EXP445. However, the logical explanation for this might well be that, having the vertical velocities reduced for the 4D-Var data, the particles are now exposed for a longer time to the horizontal mixing in the UTLS, resulting in more particles being horizontally dispersed.

The differences in the horizontal dispersion can be more clearly seen in the latitude/longitude (Figure 4.4), where EXP445 (4D-Var 12h) turns out to be the case with the largest horizontal dispersion of particles, especially in the northern hemisphere. The use of a 6h assimilation window (EXP446) reduces the density of horizontally advected particles. If this 4D-Var run EXP445 is now compared with the EXP471, which is also a 12h 4D-Var run but using a more advanced IFS

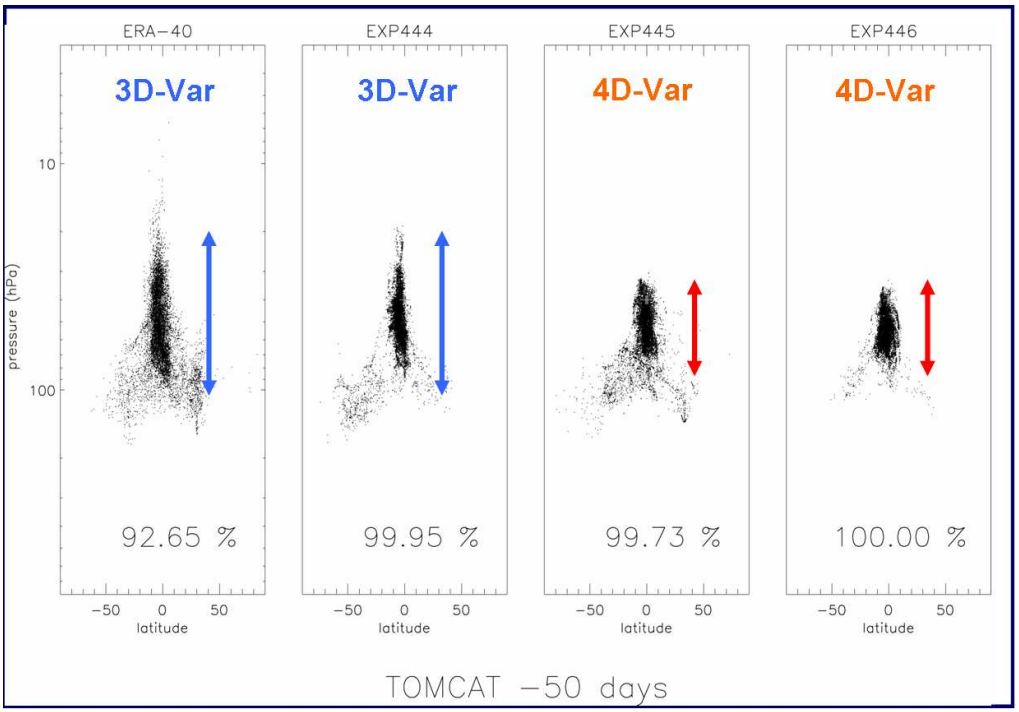

Figure 4.3: *Distribution of particles (black dots) after 50 days of backward kinematic trajectories with σ-p CTM (TOMCAT) forced by 4 different analyses. The leftmost panel is for ERA-40 winds, while the other three are for three ERA-Interim experiments produced with the same version of the model, but with differences in the assimilation method employed. The vertical dispersion in the 3D-Var runs is twice as large as in the 4D-Var ones. For each panel the percentage of particles left in the stratosphere after 50 days is indicated. Initial position of particles is indicated by a cross.*

model version, the horizontal dispersion is much reduced for EXP471 (lower panel in Figure 4.4). EXP471 has been produced with a more recent IFS version (Cy29r1) but it also uses a second minimisation, as is usually done in 4D-Var analyses, while the three additional experimental runs EXP444-445-446 used only one minimisation (see Section 4.3.4).

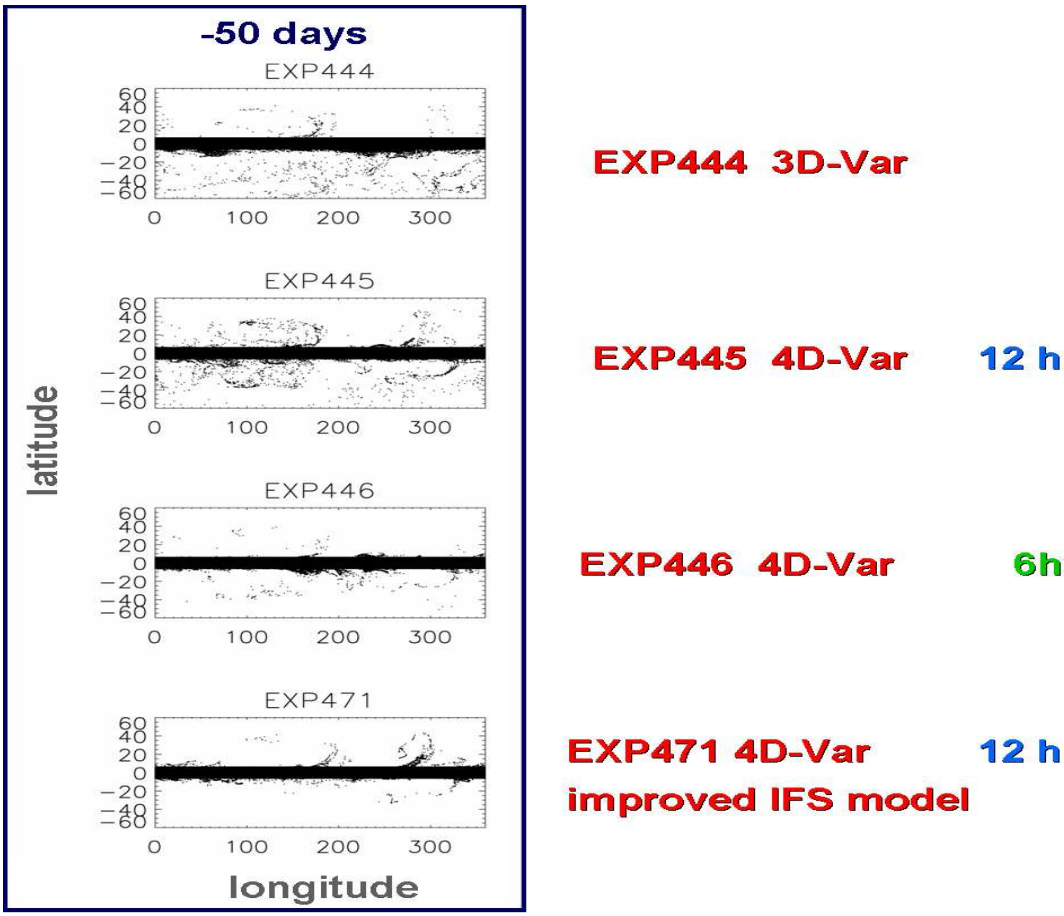

Figure 4.4: *Horizontal distribution of particles (composite of all levels) after 50 days of TOMCAT (σ-p) trajectories. The top three panels are for the three ERA-Interim experiments shown in Figure 4.3. The bottom panel is for EXP471 winds, produced with a more recent IFS model version. The improvements included in EXP471 have a positive impact in the reduction of the horizontal dispersion when a 12h assimilation window is used.*

4.3.3 Assimilation window: 12h v. 6h

Returning to the set EXP444-445-446, it might seem counter-intuitive that results worsened when using a longer assimilation window (EXP445 v. EXP446 in Figure 4.4), *i.e.* when more observations are going into the analysis. Results obtained here indicate that some deficiency in this version of the forecast model (Cy28r4) might also be causing departures to be too large with a 12h window; the longer the assimi-

lation window, the more obvious the imperfections in the model. If we compare this 4D-Var run EXP445 with our EXP471, which is also a 12h 4D-Var run but using a more developed IFS model version, the horizontal dispersion is much reduced for EXP471 (last panel in Figure 4.4). Therefore, the recent changes included in the IFS model seem to have had a positive impact on the use of a longer assimilation window; although for an accurate comparison we should compare also against one dataset produced with the same system as EXP471 but using a 6h window (this dataset does not exist).

Again, to find out which changes in the IFS are responsible for the improvement with a 12h window between EXP445 and EXP471, experimental runs for every single change would be needed, and such experiments do not exist at present. Nevertheless, improvements in the IFS radiation model (*e.g.* Fueglistaler *et al.* 2008) and IFS convection schemes (*e.g.* Tompkins *et al.* 2004; Tompkins *et al.* 2007) are believed to play an important role in the UTLS transport processes. Also the better statistical treatment of the background errors in EXP471 (Section 4.2.1) will have significantly reduced the horizontal mixing, and these aspects should be investigated in the future.

4.3.4 Second minimisation

In the ECMWF 4D-Var two minimisation cycles (two outer loops) are run for higher accuracy in the analysis increments. The first minimisation is responsible for most of the increments, while the second minimisation usually adds only corrections to the departures previously obtained. However, one of the aspects that is clearly affected by the number of minimisations used is the hydrological cycle, which is in much better balance after two minimisations (A. Simmons, personal communication, 2005). To see how the number of minimisations affects transport in the UTLS, trajectory results from EXP451 and EXP445 winds have been compared. Figures 4.5 and 4.6 show that the horizontal dispersion in the LS is reduced when a second minimisation is included (EXP451); while vertical dispersion remains practically unchanged (Figure 4.5).

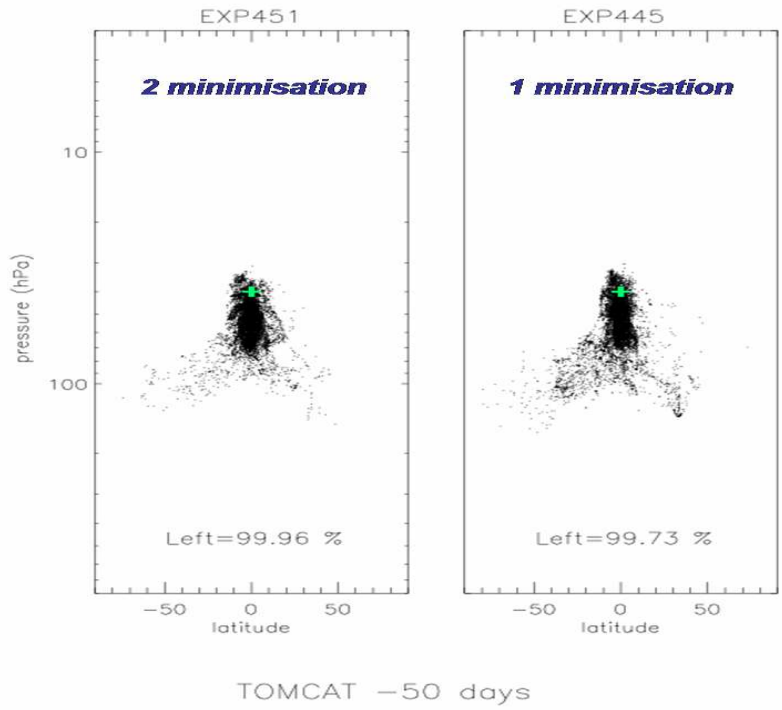

Figure 4.5: *Distribution of particles (black dots) after 50 days of backward kinematic trajectories with σ-p CTM (TOMCAT) forced by EXP451 (two minimisation cycles) and EXP445 (one minimisation cycle). Both sets of winds come from IFS Cy28r4, therefore differences between both runs give information on the effect of the 2nd minimisation in the analysis production. The vertical distribution remains practically unchanged however, differences in the horizontal dispersion can be noted (see also Figure 4.6). The percentage of particles left in the stratosphere after 50 days is indicated. Initial position of particles is represented by a cross.*

4.4 GCM winds v. DAS winds

As discussed in Chapter 2, great debate existed at the start of this PhD project on the suitability of DAS winds for stratospheric transport simulations, and on the possibility of improving DAS winds beyond their status at the time. Results presented in Chapter 3 show the improvements achieved by recent DAS systems on the representation of the stratospheric transport. These results show that EXP471 winds are

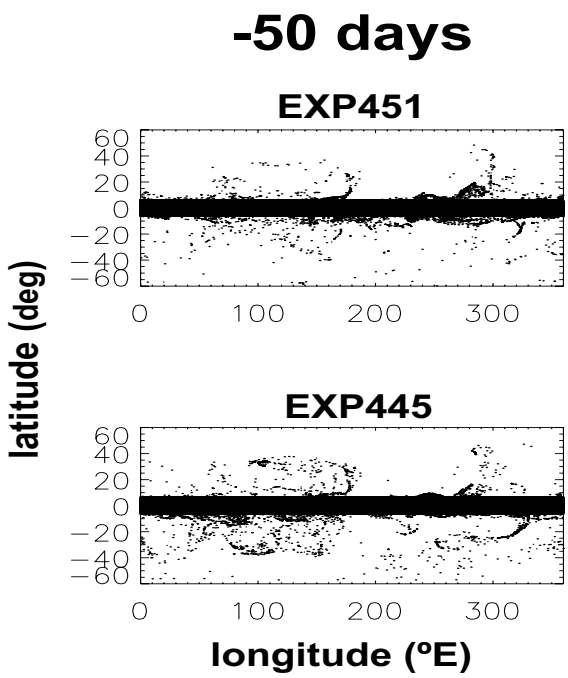

Figure 4.6: *Horizontal distribution of particles (composite of all stratospheric levels) after 50 days of TOMCAT (σ-p) trajectories. Same winds as in Figure 4.5 have been used. The horizontal dispersion of particles has been reduced by using winds produced with two minimisation cycles (EXP451, upper panel).*

much more accurate for stratospheric CTM runs than any previous (re)analysis data, and therefore show that DAS winds were indeed likely to improve and that, similarly, data assimilation methods and systems will most probably continue improving.

To answer the question on whether DAS winds are more realistic than GCM winds for CTM stratospheric simulations, one set of winds from the ECMWF GCM has been used here to run TOMCAT/SLIMCAT. The same transport diagnostics performed in Chapter 3 have been carried out for the GCM winds and results have been compared against those obtained with the DAS winds datasets.

4.4.1 GCM winds dataset

Data from one free-running version of the assimilation model used for ERA-40 were used. This GCM winds dataset, here called EXP364, was produced by ECMWF to compare against the ERA-40 series (Uppala *et al.*, 2005) for validation and internal tests. The free-running model was forced only by daily sea-surface temperatures (SSTs), with no other observations affecting the run. These instantaneous GCM winds were archived every 12h (00 and 12UT) and comprise the whole ERA-40 period (1958-2002). Here, winds for a 1-year period starting on Jan 1st 2000 have been used.

4.4.2 GCM v. DAS: Age of air

Age-of-air calculations have been carried out as described in Chapter 3, using the GCM winds and the ECMWF DAS datasets ERA-40, OPER and EXP471. The DAS winds have been updated every 12h in the CTM for consistency with the GCM winds frequency.

Global zonal distributions

Annual mean altitude/latitude cross-sections of the mean age-of air (Figure 4.7) show that results with GCM EXP364 winds are 0.5 years older than ERA-40 12h winds everywhere, except over the SH pole where GCM winds produce age values ∼1 year older. The vertical gradient is also weaker for ERA-40 than for the GCM winds. In this case changing to OPER 2000 and EXP471 improves results over both ERA-40 and GCM winds; age values are 0.5-1.0 years older than GCM winds with OPER winds, and between 1.0-1.5 years older with EXP471. In terms of the contour shapes, however, all panels in Figure 4.7 show unrealistic distributions, with the young tropical peak shifted towards subtropical latitudes. It is strange that this shift takes place towards the south for ERA-40 and towards the north for the GCM winds. Comparing with Figure 3.9, the changes in the distributions for the DAS winds in Figure 4.7 have to be related to the different update frequency. Section 4.5

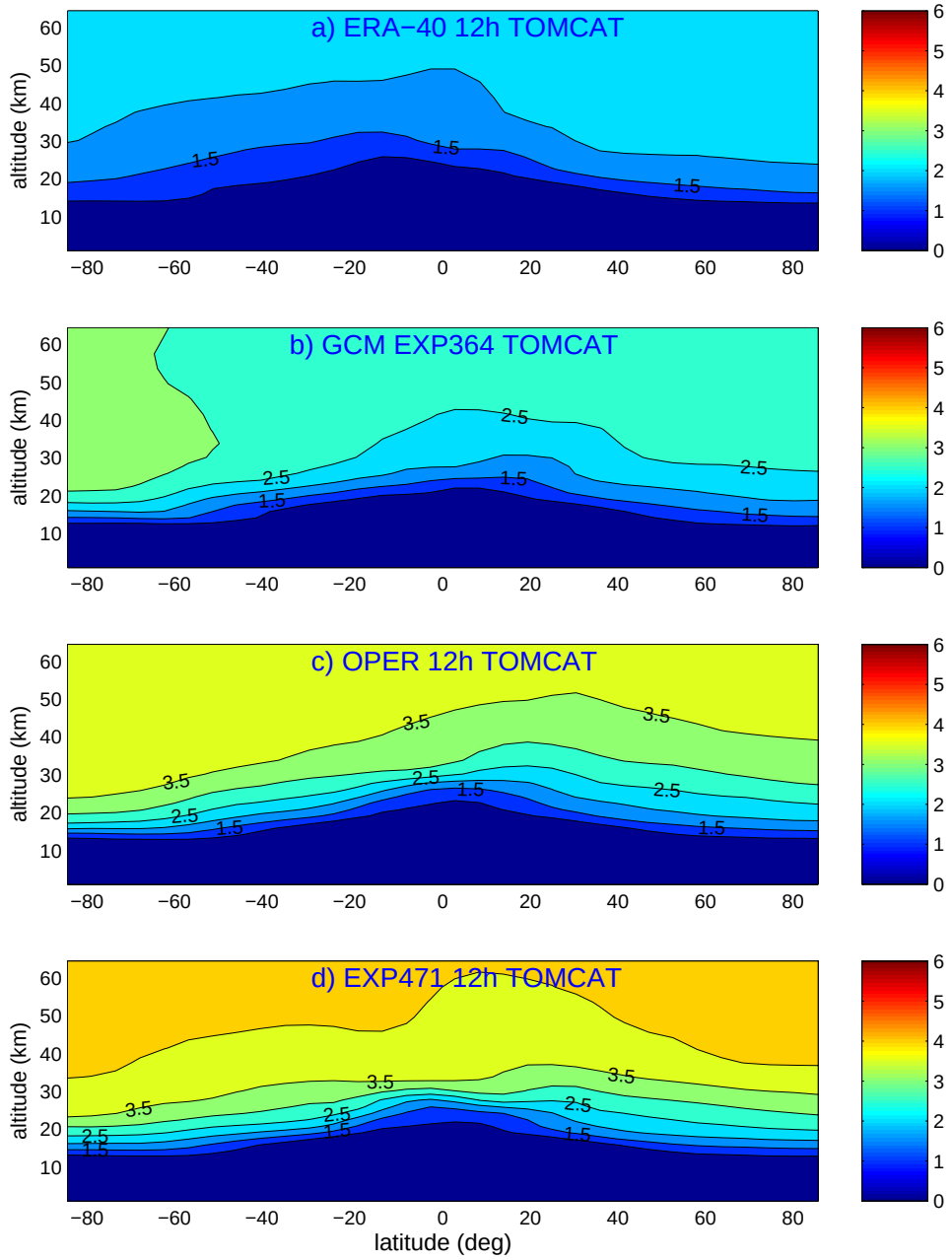

Figure 4.7: *Cross sections of the annual mean age of air (years) from TOMCAT ($\sigma - p$) simulations. The CTM has been driven by (a) ERA-40, (b) GCM EXP364, (c) OPER and (d) EXP471 winds. All winds are updated every 12h and correspond to perpetual year 2000.*

deals with differences due to the analyses update frequency.

Age at 20 km

Figure 4.8 shows mean age values at 20km obtained with the 12-hourly winds and the GCM winds. Except for the tropical region, all winds produce too young values compared to observations. Differences between winds are more marked in the SH, where results with GCM, OPER and EXP471 winds are very close to one another,

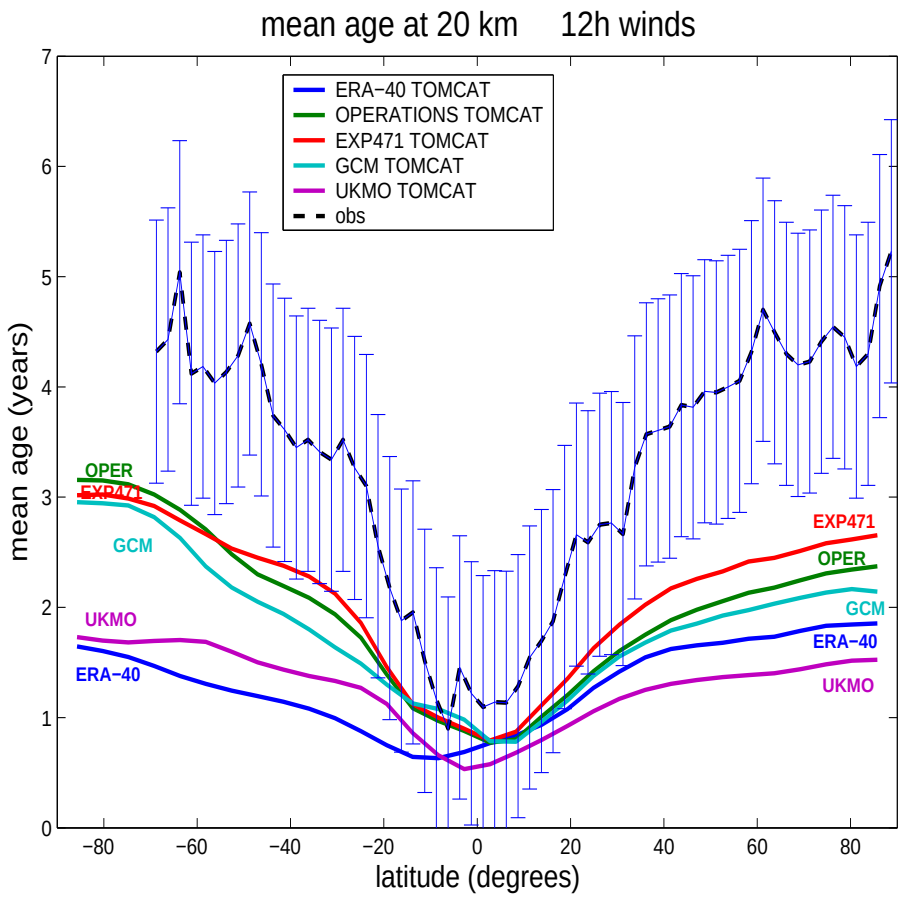

Figure 4.8: *Mean age of air at 20 km altitude from TOMCAT simulations (coloured lines) using ECMWF and UKMO DAS winds for year 2000, as well as ECMWF GCM winds (light blue). Observational values (black dashed line) as in Figure 3.10. DAS winds used are ERA-40 (dark blue), ECMWF operational (green), EXP471 (red), and UKMO (magenta).*

giving values more than one year older than ERA-40. In the NH age values are even younger than in the SH for all winds but ERA-40. GCM, OPER and EXP471 differ more among them than in the SH; the oldest values are obtained with EXP471, followed by OPER, GCM and ERA-40. Also, the UKMO winds curve has been added to show that 12-hourly ERA-40 is closer to the 24-hourly UKMO winds than the 6-hourly ERA-40 was. In the SH UKMO winds produce older results than ERA-40 (up to 0.3 years older) but for northern latitudes UKMO winds are younger than ERA-40. The latitudinal gradient is much too weak for both UKMO and ERA-40.

Results with the 12-hourly winds have been compared for different altitudes, Figure 4.9 shows zonal mean age distributions with the 12-hourly winds at 12, 20, 40 and 60 km. At all levels, except 12km, the oldest values correspond to EXP471 winds, then OPER winds followed by the GCM, and the youngest ones are obtained with ERA-40. At 12km all winds are very close, but ERA-40 is slightly younger than the rest, indicating more subtropical exchange of air than in the rest of winds already at this level.

Vertical profiles

Figure 4.10 shows vertical profiles (15-32 km) for the tropics (5°S), midlatitudes (40°N) and 65°N. TOMCAT profiles have been compared against the same set of observations used in Chapter 3 (Section 3.4.4). Up to 20 km all winds are very close; EXP471 the oldest one, ERA-40 the youngest one, and GCM younger than OPER. Above 20 km differences increase with altitude but differences between winds are smaller than for the 6-hourly wind age profiles (Figure 3.11). At all levels ERA-40 produces the youngest results and EXP471 the oldest, except in the tropics. Over the tropics OPER and EXP471 exhibit the same features, being younger than GCM between 20-28 km and becoming the oldest ones above 28 km; more than 1 year older than GCM and 2 years older than ERA-40 at the highest tropical levels. For the midlatitude and high latitude profiles the mean age steadily increases with altitude but with too low a slope compared with observations, and model values remain up

to 4 years younger than observations at 32 km.

4.4.3 GCM v. DAS: Trajectories

The altitude/latitude parcel distributions shown in Figure 4.11 are for the GCM EXP364 winds, ERA-40, OPER and EXP471 winds. DAS winds have been read-in by the CTM every 12h. From Figure 4.11 it can be seen that the horizontal dispersion in the LS is greatly reduced when using the GCM winds. The vertical distribution is very similar to that with ERA-40, with unrealistic spurious dispersion

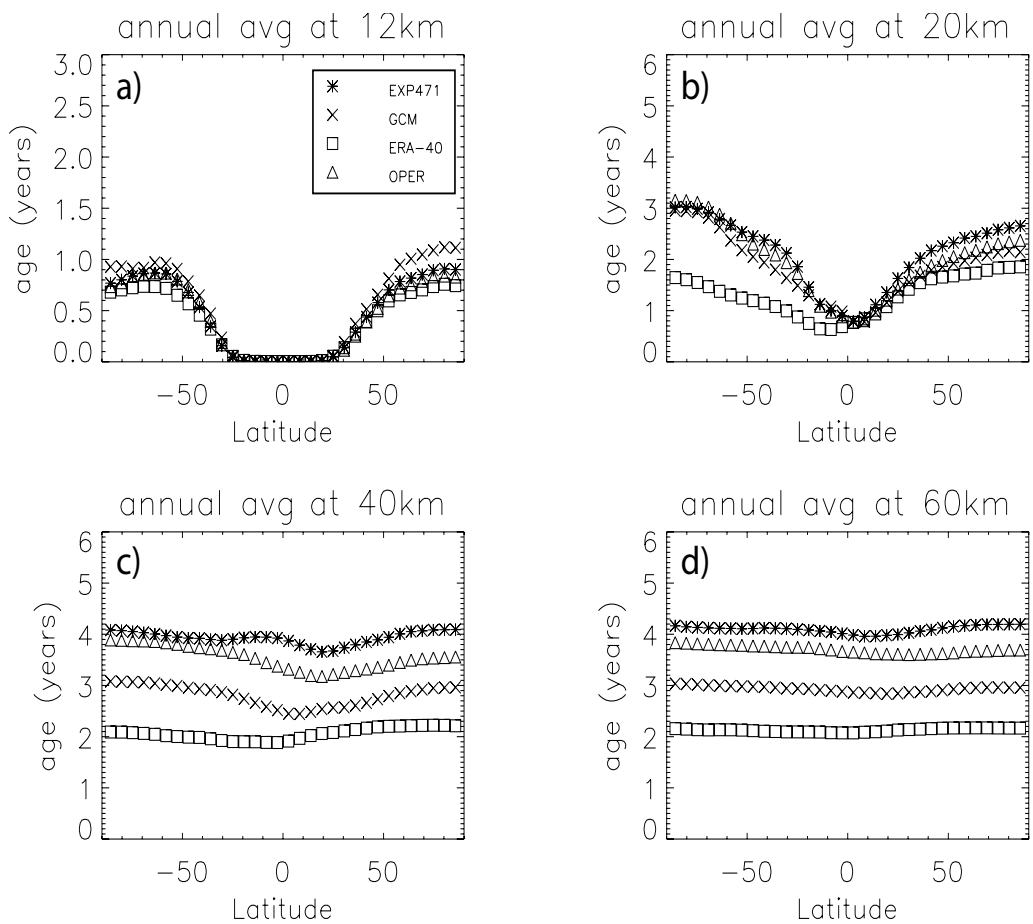

Figure 4.9: *Mean age of air (years) at (a) 12 km, (b) 20 km, (c) 40 km and (d) 60 km from TOMCAT simulations. Winds used to drive the CTM are ERA-40 (squares), GCM (crosses), OPER (triangles) and GCM364 (stars), all of them with a 12-hour update frequency. The analogous results using 6-hourly winds are in Figure 3.13.*

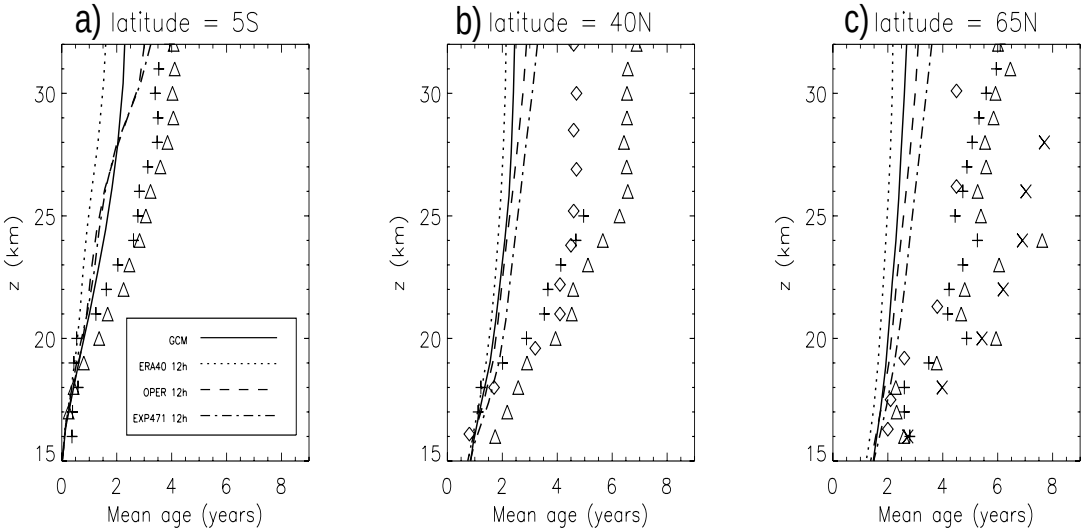

Figure 4.10: *Vertical distribution of mean age-of-air at (a) 5°S, (b) 40°N and (c) 65°N. TOMCAT simulations have been driven by GCM (solid line), ERA-40 (dotted line), OPER (dashed line) and EXP471 winds(dot-dashed line), all of them with a 12-hour update frequency. Observations as in Figure 3.11.*

reaching up to the highest model levels. As this vertical dispersion is present in both the GCM winds and the reanalysis winds produced with the same model version, the problem cannot be mainly due to imbalances generated by data insertion, although the vertical dispersion is slightly larger for ERA-40 than for GCM. It could be related to the fact that 12h data are being used. However, the fact that neither OPER nor EXP471 show spurious dispersion above 20 hPa rules out this hypothesis, pointing towards some deficiency in the IFS model version that would have been corrected in subsequent model versions. Specific humidity and tape recorder studies have detected the excessive vertical tropical transfer for the ECMWF model used in GCM 364 and ERA-40 (*e.g.* Simmons *et al.* 1999; Uppala *et al.* 2005; Oikonomou and O'Neill 2006).

The vertical dispersion in the stratosphere is significantly reduced with OPER winds. However, the number of particles that have re-enterd the troposphere after 50 days is notably larger for OPER than for ERA-40. This contrasts with what

happened with 6h winds (see Figure 3.17 in Chapter 3). In the 12h case, with the reduction in the vertical motion (OPER v. ERA-40) particles stay longer in the LS which makes them more likely to re-enter into the tropospheric circulation. Unexpectedly, for EXP471 the vertical dispersion is slightly larger than for OPER winds. This fact might be related to the different length of the assimilation window in OPER and EXP471, for update frequencies longer than the assimilation cycle length (as it happens here for OPER: 12-hourly frequency update but 6h window) might help to compensate imbalances. However, this would need further investigation.

Figure 4.12 presents a composite of the longitude/latitude distribution of particles in all vertical levels. This figure shows that the horizontal mixing in the LS is larger for OPER than for ERA-40 (consistent with particles remaining longer in the LS tropical region for OPER). EXP471 exhibits a more reduced horizontal dispersion than the other two DAS winds. The GCM winds, as seen in Figure 4.12 are the ones that present less longitude/latitude dispersion; and the only ones that do not exhibit spurious unrealistic dispersion after 30 days (left panels in Figure 4.12). The region where more horizontal mixing occurs for all DAS winds is found between 100°-200°E longitude. This region coincides with the western Pacific warm pool, which has been identified to be the main entrance region for air into the TTL and stratosphere (*e.g.* Fueglistaler *et al.* 2004).

4.4.4 GCM v. DAS: Tape recorder

The TOMCAT tape recorder time series obtained with GCM winds and ERA-40 12-hourly winds are shown in Figure 4.13. The periodic signal is somewhat smoother for the GCM winds, especially between 18-24 km. The decay in the signal is slightly faster for ERA-40, for which the signal reaches only ∼22km compared to almost 24 km for GCM winds. This is consistent with the TOMCAT trajectories, the larger horizontal dispersion exhibited by ERA-40 12-hourly winds over the tropics (Figure

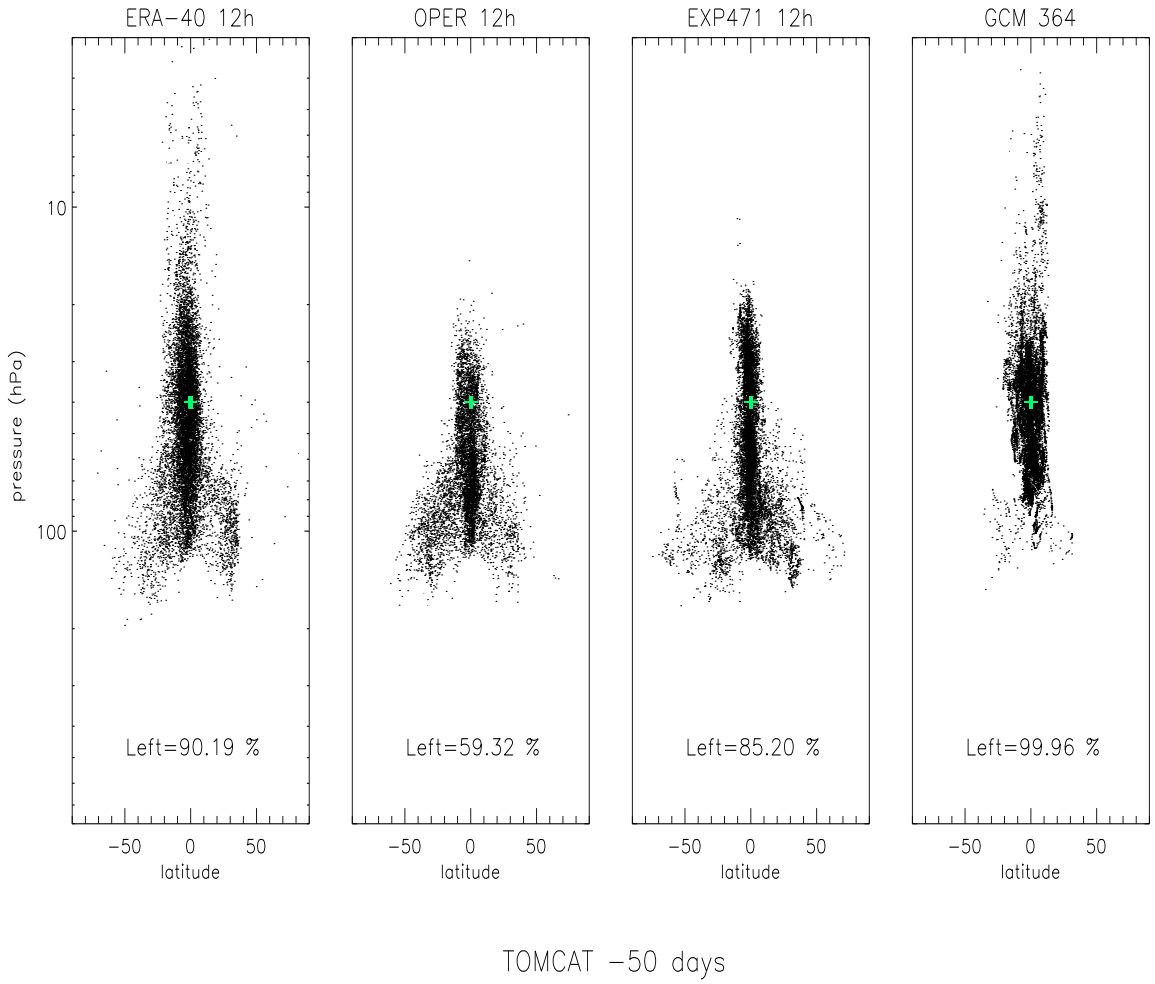

Figure 4.11: *As Figure 3.17 but ECMWF DAS winds have been read-in every 12 h by TOMCAT and the rightmost panel corresponds to GCM EXP364 winds.*

4.11) is responsible for the faster decay in the tape recorder in the LS region. Figure 4.13 also shows that for the GCM winds the phase of the signal is slightly longer than for ERA-40 winds, in agreement with GCM winds being less dispersive.

Phase and amplitude features can be more clearly seen in Figure 4.14, where the phase for the GCM and 12-hourly winds are shown, along with those from CO_2 and H_2O+2CH_4 observations described in Chapter 3 (Section 3.6). As in the case of the mean age profiles, the 12-hourly wind runs are closer between them (Figure 4.14) than the 6-hourly runs for the tape recorder profiles (Figure 3.22). For the phase

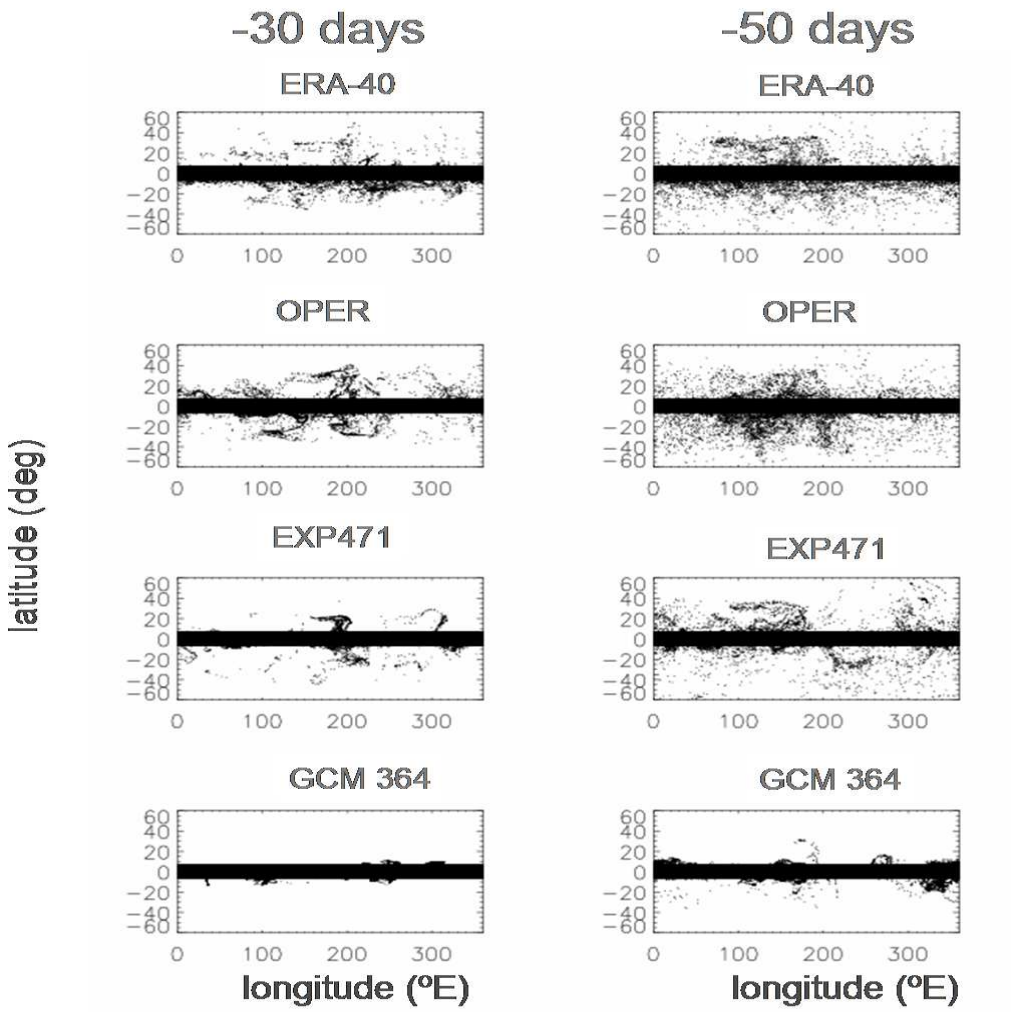

Figure 4.12: *Horizontal parcel distribution (composite of all levels) from GCM and 12-hourly DAS winds. Distributions after 30-day TOMCAT simulations (left column panels) and after 50-day simulations (right column panels) are shown. Winds as indicated by labels.*

profile very small differences occur between winds below 20 km (< 0.2 months). Above 20 km, GCM is the closest one to observations, followed by OPER, EXP471 and ERA-40.

Regarding the signal amplitude (right panel in Figure 4.14), up to 20-22 km ERA-40 is the closest to observational values, followed by GCM, OPER and EXP471

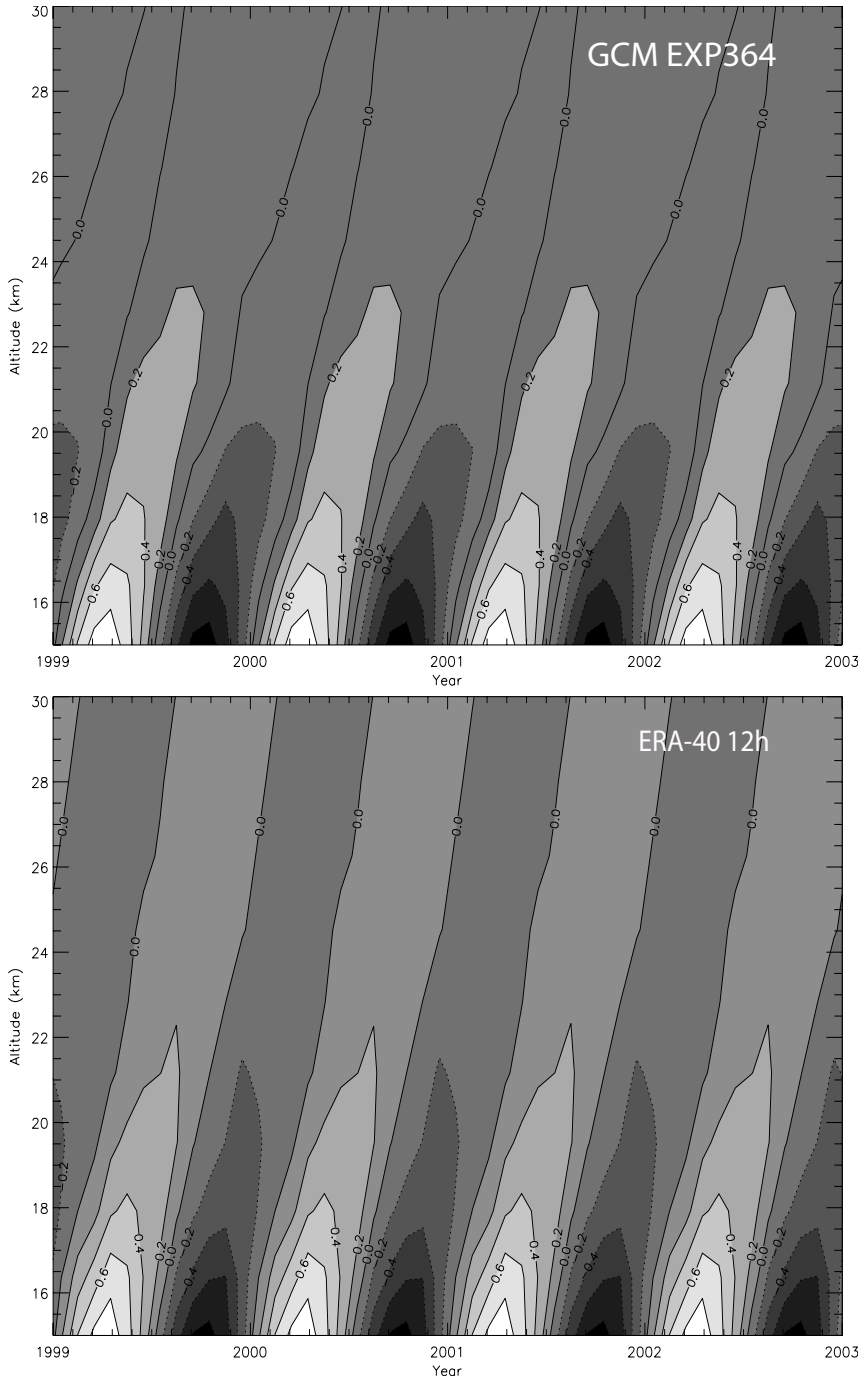

Figure 4.13: *Temporal evolution of the tape recorder in TOMCAT from a 'sin' tracer for model years 1999-2003 (vmr of the 'sin' tracer is shown) for a simulation using GCM winds (upper panel) and using 12-hourly ERA-40 (bottom panel). Years are arbitrary as perpetual meteorology for 2000 has been used. Contour intervals are 0.2, dashed contours indicate negative values.*

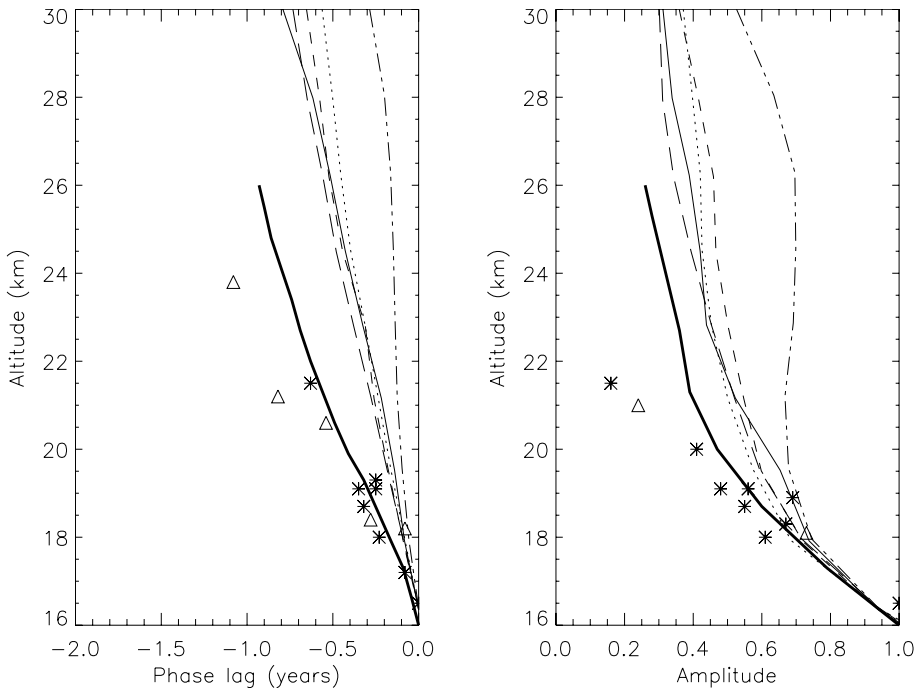

Figure 4.14: *Vertical tropical profiles of the phase (left panel) and the amplitude (right panel) of the tape recorder obtained by TOMCAT with ERA-40 12-hourly (dotted line), OPER 12-hourly (dashed line), EXP471 12-hourly (solid thin line), UKMO (dot-dot-dashed line) and GCM (long-dashed line) winds. The thick solid line shows estimate from HALOE observations (Mote* et al.*, 1998) and the symbols estimates from OMS in situ measurements of CO_2 (stars) and H_2O+2CH_4 (triangles). Observations data from Hall* et al. *(1999).*

winds respectively. Somewhat surprisingly the "best winds" produce results further from observations. Above 22 km GCM is the best option, EXP471 gives slightly larger amplitudes (< 0.1 larger), and ERA-40 and OPER follow in proximity to the observational amplitude profile. UKMO run lies further from observations than the rest, both for amplitude and phase, but it needs to be noted that these UKMO winds are not 12-hourly but 24-hourly.

The ECMWF model used for EXP364 GCM winds, and earlier model versions, were found to produce too fast upward transfer over the tropics (Simmons *et al.*,

1999), vertical transport being faster in ERA-40 DAS than in GCM (Oikonomou and O'Neill, 2006). Also, the vertical decay in the annual cycle of specific humidity was faster in ERA-40 than in EXP364 (Uppala *et al.*, 2005). This is in agreement with differences found here in the tape recorder simulations, and those in the trajectory results shown in Section 4.4.3.

4.5 12h v. 6h analysis frequency

The results and discussion presented above have provided not only a comparison between DAS and GCM winds, but also an interesting comparison between the performance of 12-hourly and 6-hourly DAS winds. The fact that the winds of the GCM EXP364 were archived only every 12 hours made necessary to run the TOMCAT/SLIMCAT CTM with 12-hourly DAS winds for an accurate comparison, revealing the strong influence that diurnal and semidiurnal tides have on stratospheric transport modelling.

4.5.1 Age-of-air

Comparing Figure 4.7 and Figure 3.9 it can be seen that a 12h update frequency results in younger age values for ERA-40 ($\sim$0.5 year younger) than the 6h update. For OPER and EXP471 reducing the update frequency to 12h does not have a major effect on the age values but notably affects the shape of the contours. The young tropical peak has been displaced towards higher latitudes in all cases, to south for ERA-40 and to north for OPER and EXP471 winds. In addition, EXP471 presents unrealistic contour depression over the tropics (Figure 4.7d), in a similar way to ERA-40 with 6h update (Figure 3.9a). The winds least affected by the change in the update frequency are OPER. As seen in Figure 4.10, 12-hourly winds do not capture the vertical structure of the mean age-of-air for any of the latitudes shown, not only in terms of the age value itself, but also in terms of the profile shape. Profiles with 12-hourly winds exhibit a continuous, although too weak, vertical increase with no inflexion above 20 km as observations show.

4.5.2 Trajectories

The increase of the horizontal dispersion in the LS region for the 12-h winds (Figure 4.11) with respect to the 6-hourly ones (Figure 3.17) is significantly smaller than increases in the vertical dispersion. EXP471 are the winds where horizontal mixing is most affected by the frequency update. For ERA-40 and OPER the horizontal dispersion reaches the same latitude range for both update frequencies, and the lon/lat distribution for ERA-40 12h and ERA-40 6h are remarkably similar. This indicates that frequency update is not the main determining factor in the reduction of excessive horizontal dispersion in the LS as has been suggested by *e.g.* Bregman *et al.* (2006). The fact that the GCM winds exhibit such a reduced horizontal mixing compared to any of the DAS winds points to the data assimilation process as principal responsible for the mixing excess in the LS. This is not the case for the vertical dispersion, for which the read-in frequency of the analyses seems to play a main role. All the runs with 12-hourly DAS winds present more spurious, unrealistic vertical dispersion above the initialisation level of 50hPa than their counterparts with 6-hourly winds. Also, the number of particles remaining in the stratosphere after a 50-day run is significantly smaller for the 12-hourly winds (up to 40% smaller for OPER winds), indicating that the spurious vertical transport has been unrealistically increased.

4.5.3 Tape recorder

Tape recorder time series with 12-hourly ERA-40 winds (Figure 4.14) exhibit a significant smaller phase lag compared to 6-hourly ERA-40 winds (Figure 3.22). 12-hourly ERA-40 results in slightly higher amplitudes above 24 km and slightly lower below that level. Overall, using 12-hourly winds affects the amplitude of the tape recorder signal less than its phase. Phase values for 6-hourly ERA-40 (Figure 3.22) are very similar to those obtained with GCM winds. While in terms of amplitude, GCM results are between ERA-40 and OPER 6-hourly winds. Differences in tape recorder amplitude and phase are much smaller between 12-hourly runs than they

re between 6-hourly runs. This is due to the vertical dispersion being more similar between the four 12-hourly wind sets than it was between the 6-hourly sets.

4.5.4 TOMCAT v. SLIMCAT

Using GCM winds appears to be equivalent for transport in the LS to the use of an increased frequency (6h v. 12h) in the DAS analyses. Nevertheless, frequencies larger than 6h seem to affect vertical dispersion too severely to make such frequencies suitable for CTM simulations in the stratosphere, at least for $\sigma - p$ CTMs that use vertical velocities from divergence, as is the case for TOMCAT. The absence of diurnal cycle when using frequency updates over 12 hours overestimates the tropical ascent. On the other hand, by default, SLIMCAT ($\sigma - \theta$) calculates day-averaged heating rates, which could make results obtained with 12h fequency more similar to the 6h frequency results than in the case of TOMCAT. Figure 4.15 shows age-of-air cross-sections from TOMCAT and SLIMCAT runs using ERA-40 winds, both 12-hourly and 6-hourly, and the absolute differences between the runs. For these winds, differences values are smaller for TOMCAT than for SLIMCAT, however, the age distribution with 12h winds is more realistic with SLIMCAT.

4.6 Conclusions

This chapter has examined aspects of one data assimilation system (DAS), as well as CTM frequency update and kind of winds used (GCM or DAS) to see how, and by how much, such issues affect stratospheric transport in TOMCAT. It has been shown that using a 4D-Var assimilation method reduces the vertical dispersion of TOMCAT trajectories in the stratosphere by a factor of 2, compared to the use of 3D-Var winds. For the same DAS, using a longer assimilation window (12h v. 6h) affects the horizontal distribution of trajectories, increasing or decreasing it depending on the IFS model version. Here aspects related to statistical error treatment and physical parameterisations seem to be determining.

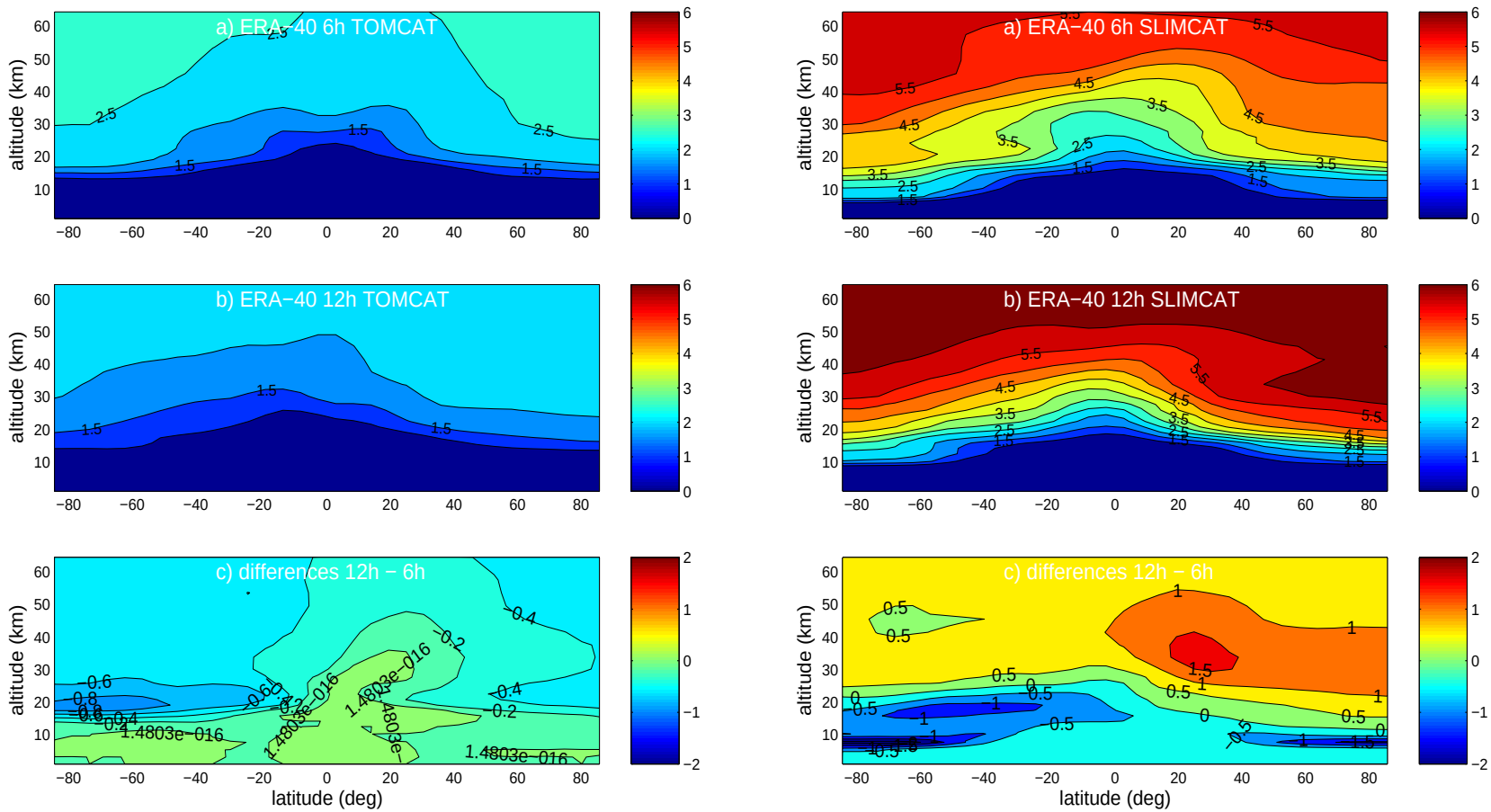

Figure 4.15: *Annual mean zonal mean age-of-air distributions (in years) with ERA-40 winds for TOMCAT (left column) and SLIMCAT (right column). Runs have been obtained with 6h winds (top) and 12h winds (middle); differences between 12h and 6h winds are also represented (bottom). All runs use perpetual 2000 meteorology.*

One set of GCM winds (EXP364) has been compared with the corresponding DAS winds (ERA-40), indicating that data assimilation affects the horizontal dispersion in the UTLS by increasing horizontal mixing with respect to a free running GCM. However, spurious vertical mixing is mainly related to the read-in frequency of the winds in the CTM. 12-hourly DAS winds present too enhanced vertical mixing compared to the 6-hourly DAS winds, while the GCM EXP364 winds (12-hourly winds) present very similar vertical mixing to the corresponding DAS winds (ERA-40 12-hourly). GCM winds produce age-of-air results in better agreement with observations than ERA-40, due to the reduction of horizontal dispersion in the GCM winds. However, the differences in the tape recorder diagnostic are very small due to the fact that vertical dispersion is almost identical for both sets.

Results in this chapter show that CTMs should use update frequencies of 6 hours or less in order to correctly model vertical air transfer, otherwise the absence of information on diurnal variations negatively affect the calculation of vertical transport. Problems due to the 12h frequency make it difficult to decide whether GCM winds are better than DAS. While age values are older with GCM than with the corresponding DAS (ERA-40), the shape of the zonal distribution is not realistic, and the tape recorder signal is not significantly improved compared to ERA-40. The same study should be performed with 6-hourly GCM winds. ECMWF plans to produce a simulation equivalent to EXP364 for their new reanalysis, it would be extremely useful if winds from such simulation were archived every 6 hours, or less.

Using read-in frequencies below the length of the assimilation window used to produce the winds (*e.g.* using 6-hourly winds produced with a 12-hour assimilation window) might reduce both vertical and horizontal diffusion, as results with 12-hourly EXP471 winds seem to indicate (Figure 4.11). Nevertheless, to confirm this point more investigation would be needed with (re)analysis sets designed for this purpose. As it has been shown in this chapter, the diurnal cycle is another cause for the poor performance of the UKMO winds in results presented in Chapter

3. The UKMO winds used were archived daily and therefore no information on the diurnal cycle of the vertical velocities was provided to the CTM.

Results in Chapter 3 and Chapter 4 have shown that ECMWF DAS winds have been recently improved. These chapters have evaluated DAS aspects that have caused the improvement and pointed towards aspects that deserve attention in order to achieve future improvements. Nevertheless, one important question still remains: the quality of the current ECMWF stratospheric analyses, is it only related to the data assimilation process? Or is it also related to the level of complexity with which the stratosphere is described in the IFS model? Nowadays most NWP models, ECMWF included, do not contain detailed enough parameterisations of radiatively active chemical species in the stratosphere. The accuracy of the concentrations and distribution of such species clearly affect the representation of the stratosphere (*e.g.* Curry *et al.* 2006).

Chapters 3 and 4 have shown CTMs are very effective tools to evaluate the quality of the (re)analyses produced by meteorological centres such as ECMWF. However, the stratospheric experience of CTMs could also be used 'a priori' to improve chemical descriptions in the NWP core model. Chapter 5 examines the schemes currently used by ECMWF to parameterise main radiatively active gases, while Chapters 6 and 7 propose, and quantify the performance of improvements and/or new ways to parameterise ozone, methane and water vapour in the stratosphere in the ECMWF IFS model.

Chapter 5

Parameterisations of Stratospheric O_3 and H_2O for Global Models

5.1 Introduction

High resolution numerical weather prediction (NWP) models cannot yet afford an operational description of atmospheric chemistry. NWP systems must therefore make use of simplified parameterisations of the species most relevant to them, *i.e.* radiatively active gases such as O_3, H_2O, CH_4 or CFCs, as these constituents are essential for the correct assimilation of radiances. While the description of some of these gases is still merely a global mean constant value, more detailed descriptions of ozone and water vapour have been implemented.

It was when the ECMWF model extended its vertical range up to the stratopause that including a stratospheric ozone scheme became necessary (Dethof and Hólm, 2004). Without an ozone description the radiation scheme in the stratosphere is far from complete and therefore assimilation of satellite radiances in this region would not be correct. Also, a new water vapour scheme was implemented in the ECMWF model coinciding with the production of ERA-40 to make better use of all the satellite observations entering the reanalyses.

This chapter examines how the schemes representing stratospheric ozone and water vapour have developed in the last few decades, and provides a summary of the current schemes used by the ECMWF IFS model. The main aims of this chapter are to identify deficiencies in the current ECMWF O_3 and H_2O schemes and to propose improvements. Section 5.2 describes how ozone parameterisations have progressed over the last three decades, giving information on their performance and the problems they still exhibit. A more detailed discussion of the current ECMWF O_3 scheme is provided in Section 5.3, which also identifies weaknesses that need to be addressed. Similarly, a description of the existing H_2O schemes is found in Section 5.4, and a discussion of the current ECMWF scheme for water vapour is in Section 5.5. A summary of the chapter as well as proposed improvements for the schemes are given in Section 5.6. Chapters 6 and 7 analyse the implementation of such improvements.

5.2 Ozone parameterisations: Historical evolution

In the lower stratosphere (LS) ozone is a relatively long lived-tracer and therefore its distribution is dominated by transport. However, in the upper stratosphere O_3 photochemistry terms are much larger than the transport term, therefore, the continuity equation for this compound can be approximated by the difference between production and loss rates:

$$\frac{\partial f}{\partial t} = (P - L) \tag{5.1}$$

where f is the local O_3 mixing ratio, and P and L are the chemical production and loss rates respectively. On the other hand, O_3 chemistry is highly nonlinear, involving reactions and processes on a wide range of time scales, making it difficult to implement in any model. For this reason efforts have been made towards a linear scheme for the O_3 time tendency $\partial f/\partial t$. This section describes how O_3 schemes have evolved in time, since the pioneering attempts to parameterise equation (5.1) in the 1960s and 1970s to the most recent schemes including heterogeneous polar

loss terms.

5.2.1 First O_3 schemes

The first works on linear O_3 schemes expressed ozone (or odd oxygen) production and loss in terms of the major known reactions. Given the dependency of such reactions on O_3 mixing ratio and temperature, it was possible to use a linear approximation for equation (5.1) in the form

$$\frac{\partial f}{\partial t} = (P - L)[f, T] = -Af' - BT' \tag{5.2}$$

where f' and T' are perturbations over the steady state values of O_3 and temperature. In these early studies, values for the coefficients A and B where analytically derived resolving the necessary continuity equations (*e.g.* Lindzen and Goody 1965; Blake and Lindzen 1973; Stolarski and Douglass 1985). The O_3 reactions considered were first simply the Chapman reactions (Chapman, 1930), then additional reactions with nitrogen and hydrogen compounds were added (Blake and Lindzen, 1973; Cunnold *et al.*, 1975), and later also with chlorine species (Cariolle, 1983; Stolarski and Douglass, 1985).

As the chemistry of O_3 became better understood, more and more reactions needed to be incorporated. While this was possible for 1D column models or 2D-models, resolving all the continuity equations was unfeasible for three-dimensional GCMs. Also, the incorporation of long-lived species (NO_y, Cl_y, Br_y) required long integrations of the models. Besides, for the resolution of the continuity equations, the total concentrations have to be specified. In the 1980s, the global coverage of measurements for many species involved in O_3 reactions was not good enough for such a purpose. These problems made it more convenient to switch to a different kind of approach for ozone modelling based on numerical, instead of analytical, solutions. Cariolle and Déqué (1986), hereafter CD86, described the first numerically obtained O_3 parameterisation and validated the scheme in a 3D GCM.

5.2.2 The Cariolle and Déqué (CD) ozone scheme

The Cariolle and Déqué scheme (CD scheme) is based on equation (5.2), *i.e.* it considers $(P-L)$ to be a function of O_3 mixing ratio and temperature, and includes an additional term to take into account the dependency of the chemical reaction rates on the local UV flux (the so-called 'self-healing' term); this UV flux depends on the ozone column density above the considered level. The expression for the O_3 rate of change in the CD approach is therefore

$$\frac{\partial f}{\partial t} = (P-L)[f, T, c_{O_3}] = -Af' - BT' - Cc_{O3} \tag{5.3}$$

where c_{O_3} is the ozone column above the considered local point. In their case, the coefficients A, B and C were numerically calculated from perturbation experiments using the 2D photochemical model MOBIDIC (Cariolle and Brard, 1984). The expression in equation (5.3) is expanded in a first-order Taylor series:

$$\frac{\partial f}{\partial t} = c_0 + c_1(f - \bar{f}) + c_2(T - \bar{T}) + c_3(c_{O_3} - \bar{c}_{O_3}) \tag{5.4}$$

where the coefficients c_i, $i = 0, 1, 2, 3$, are computed with the 2D model for every latitude, pressure and month of the year. The terms $\overline{f}$, $\overline{T}$ and $\overline{c}_{O3}$ are photochemical equilibrium values (function of latitude, pressure and month) that are obtained from a reference state of the model used to compute the coefficients or from a climatology. T, f and c_{O_3} are the GCM prognostic values of temperaure, ozone mixing ratio and partial ozone column.

The first two terms on the right-hand side of equation (5.4) correspond to the linearization of production and loss rates; the third term in equation (5.4) takes into account the temperature dependence of many chemical reaction rates. The fourth term treats the effect due to variations in the ozone column, since O_3 variations imply UV flux differences and thus changes in the O_3 production and loss rates.

The coefficients

The coefficients c_i in equation (5.4) are given by the partial derivatives of the corresponding variable

$$\begin{aligned} c_0 &= (P-L)_0 \\ c_1 &= \left.\frac{\partial(P-L)}{\partial f}\right|_0 \\ c_2 &= \left.\frac{\partial(P-L)}{\partial T}\right|_0 \\ c_3 &= \left.\frac{\partial(P-L)}{\partial c_{O3}}\right|_0 \end{aligned} \tag{5.5}$$

where the subscript 0 indicates that the values are calculated for the reference state established by $\overline{f}$, $\overline{T}$ and $\overline{c}_{O3}$.

CD86 calculated the coefficients in (5.5) from runs of the 2D model in which all variables except the one corresponding to the partial derivative under calculation were kept constant. Concentrations of long-lived species were also kept constant. The version of the MOBIDIC model used to calculate this first version of coefficients resolved continuity equations for only 12 chemical species (Cariolle and Brard, 1984).

The photochemical relaxation time, τ_{O_3}, can be directly computed from the second coefficient c_1:

$$\tau_{O_3} = -\left(\left.\frac{\partial(P-L)}{\partial f}\right|_0\right)^{-1} \tag{5.6}$$

τ_{O_3} indicates how long it takes for the O_3 tracer to relax back to the reference (or climatology) $\overline{f}$ for each latitude and level.

Implementation in a 3D model

If no dynamical processes are considered, then the steady state for the O_3 mixing ratio based on the CD parameterisation has the form

$$f^{ss} = \bar{f} + \left[(P-L)_0 + \left.\frac{\partial(P-L)}{\partial T}\right|_0 (T-\bar{T}) + \left.\frac{\partial(P-L)}{\partial c_{O_3}}\right|_0 (c_{O_3} - \bar{c}_{O_3}) \right] \tau_{O_3} \quad (5.7)$$

By inserting the expression of τ_{O_3} and f^{ss} in equation (5.4), the ozone tendency can be rewritten as

$$\frac{\partial f}{\partial t} = -\frac{f - f^{ss}}{\tau_{O_3}} \quad (5.8)$$

This expression can be integrated in time and solved by the 3D model to obtain $f(t + \Delta t)$ as a function of $f(t)$, where Δt is the 3D model time step.

The CD86 scheme has been widely used in 3D models as it has proved to produce good results while having the advantage of simplicity. The scheme, or an updated version of it, has been adopted by many NWP/DAS systems like ECMWF, U. K. Met Office, Météo France and U.S. Naval Research Laboratory (NRL). Nevertheless, even if overall the method has proved to be successful, some shortcomings have also become apparent.

Problems in the CD86 scheme

Ozone relaxation times τ_{O_3} in the lower stratosphere have been found to be too short in the CD scheme, not only in the original CD86 scheme but also in later versions (v1.0, v2.1 and v2.3) obtained with the MOBIDIC 2D CTM (McCormack *et al.*, 2004; Geer *et al.*, 2007). This results in the scheme not capturing as much zonal variation as exhibited by satellite measurements such as SAGE III or Polar Ozone and Aerosol Monitoring (POAM III) (McCormack *et al.*, 2004). However, in the upper stratosphere, the problem is the opposite: CD coefficients produce relaxation times significantly longer than other recent sets of coefficients obtained with different models, see Section 5.2.3 and Geer *et al.* (2007). In addition, the radiation term ($c_3 = \partial(P-L)/\partial c_{O3}$) is too large in the CD86 scheme, one of the consequences is too much production in the Antarctic spring, where O_3 column values are low.

However, the main problem is that O_3 heterogeneous chemistry is not part of the original scheme, the ozone hole chemistry was not known at the time of the original development, and the scheme does not provide any treatment of the heterogeneous polar ozone loss or mid-latitudes heterogeneous chemistry. Even if later versions of the scheme (*e.g.* Dethof and Hólm 2002; Dethof and Hólm 2004) include an extra heterogeneous term for the polar regions, active only where temperatures are below 195 K, the complete scheme does not produce realistic enough results (see Section 5.3). The heterogenous effects on mid-latitudes are simply missed by the current ECMWF scheme, despite the fact that heterogeneous reactions on sulfate aerosols significantly change the partitioning NO_x/HO_x, making NO_x or HO_x cycles to be the main one for O_3 loss in the mid-latitudes LS region (Rodriguez *et al.*, 1991; King *et al.*, 1991). This kind of effect should be taken into account in an improved scheme.

The quality of the results obtained with the CD scheme depends not only on the method itself, but also on the coefficients used. A more sophisticated calculation of the coefficients c_i in equation (5.4) would add to the performance of the CD scheme. The use of a photochemical model with up-to-date, comprehensive chemistry, higher resolution, preferably a 3-dimensional CTM, with more realistic O_3 background field than the 2D model used in CD86, would result in more realistic coefficients and a more effective parameterisation. That is why, based on the original CD86 scheme approach, several research groups have developed different versions of the parameterisation, as it is described in Section 5.2.3.

5.2.3 Recent O_3 schemes

Since Cariolle and Déqué (1986), subsequent O_3 parameterisations have been updates of the CD86 scheme aimed at improving some aspects of the original scheme by obtaining better coefficients using more complete photochemical models than used in CD86 (*e.g.* McLinden *et al.* 2000; McCormack *et al.* 2004; McCormack *et al.* 2006). Here, the main improvements included by these updated schemes are described, along with the problems such schemes still do not solve.

LINOZ

McLinden *et al.* (2000) (hereafter ML2000) used the Prather photochemical box model (Prather, 1992) to obtain one set of coefficients c_i with updated chemistry, the LINOZ scheme. The chemistry included in the box model involved 43 species, and 137 reactions (101 kinetic reactions and 36 photolysis reactions). Besides this general chemistry, seven heterogenous reactions on binary sulphate aerosols were added for the calculations in ML2000. Another development with respect to CD86 was the adoption of more recent absorption cross-sections and rate coefficients. LINOZ coefficients were provided for 18 latitude values (85°S-85°N) with a 2-km resolution on 25 pressure altitudes from 10-58 km. Like the rest of schemes discussed in this chapter, coefficients are provided for each month of the year, with no variation from one year to another.

In ML2000 τ_{O_3} and f^{ss} were considered constant along the model time step Δt, therefore equation (5.8) could be solved analytically

$$f(t+\Delta t) = f(t) + [f^{ss} - f(t)]\left[1 - exp\left(\frac{-\Delta t}{\tau_{O_3}}\right)\right] \tag{5.9}$$

By adopting this solution ML2000 allow for stability for time steps Δt larger than the relaxation time τ_{O_3}. Otherwise, instabilities could occur for upper stratospheric levels, where relaxation times can be only a few minutes.

LINOZ relaxation time values, τ_{O_3}, have been found to be more realistic in the LS than the original CD86 scheme (*e.g.* McLinden *et al.* 2000; McCormack *et al.* 2004; Geer *et al.* 2006), and, overall, 3D models with the LINOZ scheme capture the seasonal variation of O_3 and main zonal and vertical features in the lower and middle stratosphere (McLinden *et al.*, 2000). However, this scheme produces too much O_3 loss above 10 hPa and is therefore unsuitable for upper stratospheric studies (McCormack *et al.*, 2004; Geer *et al.*, 2007). McCormack *et al.* (2004) argued that the problem was related to too large background ozone concentrations that cause the term $(P - L)_0$ to be too large.

The validity of the linear approximation was tested for different ranges of T and O_3 conditions and shown to be valid for the usual ozone mixing ratio values seen within a NWP model. However, ML2000 found discrepancies for variations of temperature and ozone column of ±20 K and ±30 % respectively. Even if they claim such conditions can be found only in the LS, where the ozone chemistry is relatively slow, the situation should be re-evaluated for more recent atmospheric conditions (and if possible for future ozone and temperature scenarios).

Another shortcoming of this scheme is that the chemical model used to calculate the LINOZ coefficients did not include any treatment for polar stratospheric clouds (PSCs) and ternary aerosols. LINOZ fails therefore to simulate the heterogeneous chemistry that takes place inside the polar vortex, and does not achieve a realistic representation of O_3 in high latitudes. However, this scheme, unlike the CD scheme, includes seven heterogeneous reactions involving sulfate aerosols relevant for mid-latitude heterogeneous chemistry.

ECMWF

The current parameterisation in the ECMWF model follows the CD86 scheme but includes also one additional term to represent the heterogeneous chemistry taking place in polar regions (Dethof and Hólm, 2004), and uses an updated version of the c_i coefficients provided by Météo France. The scheme is fully described in Section 5.3.

CHEM2D-OPP

CHEM2D-OPP is the prognostic ozone photochemistry parameterisation implemented in the Navy Operational Global Atmospheric Prediction System-Advanced Level Physics High Altitude (NOGAPS-ALPHA) NWP model (Eckermann *et al.*, 2004). The NRL CHEM2D model was used to calculate the coefficients c_i. The reason for including prognostic ozone in this model was, as with the ECMWF and

U.K. Met Office models, the use of the scheme for the operational assimilation of satellite radiances.

An initial version of this CHEM2D-OPP parameterisation (McCormack *et al.*, 2004) included only the first two terms of equation (5.4). Such version has not been used in this thesis, as a newer, revised and more complete one became available in 2006. The version of CHEM2D-OPP used for comparison in Chapter 6 is CHEM2D-OPP v2.5 from McCormack *et al.* (2006)[1], hereafter referred to as MC2006.

CHEM2D-OPP coefficients were calculated for 35 latitudes (85°N-85°S) and 24 levels (1000-0.001 hPa), for every month of the year. The four coefficients c_i are provided by the 2D model, while the reference state values ($\bar{f}$, $\bar{T}$ and $\bar{c}_{O_3}$) are taken from external climatologies. The COSPAR International Reference Atmosphere, CIRA86, (Fleming *et al.*, 1990) climatology or the Stratospheric Processes and their Role in Climate (SPARC) climatology (Randel *et al.*, 2002) are used for T; the climatology used for ozone is a combination of the Fortuin and Kelder (1998) climatology (from surface to 0.3 hPa) and output from the CHEM2D model (above 0.3 hPa).

In MC2006, for the implementation of the CHEM2D-OPP scheme, a backward-Euler solution was adopted

$$f(t + \Delta t) = f(t) + [f^{ss} - f(t)] \left[\frac{t_c}{1 + t_c} \right] \tag{5.10}$$

where $t_c = \Delta t / \tau_{O_3}$. Another difference in the calculation of the CHEM2D-OPP coefficients is that τ_{O_x} values are calculated with the photochemical model for the odd oxygen family O_x, then scaled to τ_{O_3} values and then converted into coefficient c_2 values; instead of calculating c_2 for O_3 directly as in the other schemes discussed in this chapter. This is due to the net tendency term $(P - L)$ being calculated for

[1]The NRL has an official web page for CHEM2D-OPP for news, updates and users lists: http://uap-www.nrl.navy.mil/dynamics/html/chem2dopp/chem2d_opp.html

O_x and then scaled to obtain the corresponding value for O_3.

The scheme takes into account loss reactions with HO_x, NO_x, ClO_x and Br_x, which is a development over the CD86 scheme. Also the fact that coefficients are provided up to very high altitudes (0.001 hPa) is a major advantage of this scheme over previous versions, especially now that most NWP/DAS systems are extending their vertical range into the mesosphere, where a realistic O_3 distribution is necessary to achieve realistic CH_4 and H_2O budgets. However, the vertical resolution of the CHEM2D-OPP coefficients has not been increased with respect to previous schemes. The need for an additional term/tracer to simulate the polar loss is also an issue for this scheme.

Problems with these recent O_3 schemes

Some of the problems these recent schemes present have already been discussed when describing each particular scheme. Here the main shortcomings of all them are summarised.

All of the schemes described need an extra term for modelling polar heterogeneous chemistry effects, such as a cold-tracer (*e.g.* Chipperfield *et al.* 1994), or a local term based on temperature threshold (*e.g.* Dethof and Hólm 2002); these two aproaches have problems. A cold tracer need to be carefully tuned to provide realistic results, while a local term fails to parameterise polar heterogeneous processes.

All schemes presented so far, except LINOZ, come from a 2D model, which decreases the capacity of the calculated coefficients to adapt to real meteorological or chemical features that will be present in a 3D global model. The use of a more realistic photochemical model, such as a 3D CTM, would help to provide a more efficient parameterisation.

No sensitivity to annual variability is included in the linear coefficients in any of

the schemes described. The meteorological and chemical conditions in the 2D model used to obtain the coefficients are representative of an average climatological year. This causes the schemes to be less sensitive to conditions differing from those used in the 2D calculations.

Only the additional heterogeneous term included (see Section 5.3) can provide an annual dependency on the chlorine total content of the atmosphere in the particular year. Nevertheless, variations in the amounts of Cl alter O_3 concentrations and distributions not only over polar regions, but also over lower latitudes, as such variations alter reactions that have been implicitly parameterised in the first four terms of equation (5.4). That is why including heterogeneous chemistry reactions in the calculation of all the linear coefficients would provide a more realistic parameterisation at all latitudes and levels. This new approach is undertaken in this thesis (see Chapter 6).

Other O_3 schemes

The CD scheme is the most widely used O_3 parameterisation, however it is not the only one. Here other successful O_3 schemes are briefly described.

The ozone scheme adopted by the GEOS DAS (Riishojgaard *et al.*, 2000) resolves the following equation for the ozone mixing ratio f

$$\frac{\partial f}{\partial t} + \vec{u} \cdot \nabla f = P - f \cdot L \tag{5.11}$$

here $\vec{u}$ is the wind velocity vector, and P and L the ozone production and loss rates respectively. In the GEOS system such production and loss rates are calculated by a 2D photochemical model and tabulated for every latitude and level. Riishojgaard *et al.* (2000) reported differences of 20-25% between their O_3 analyses and observations from TOMS, SBUV and World Meteorological Organization (WMO) ozone sondes. Analysed O_3 was too low over the tropics and too high in the extratropics. These biases, although still exist, have been reduced in more recent versions (*e.g.*

Bloom *et al.* 2005). In GEOS-4 the parameterised P and L rates come from a 2D CTM (Fleming *et al.*, 2001), and P is adjusted so that P/L correspond to the Langematz (2000) O_3 climatology (Bloom *et al.*, 2005).

Also, more simple approaches than those based on the CD scheme have been used for simpler applications. The 'synthetic ozone', SYNOZ, (McLinden *et al.*, 2000) was designed to model stratosphere-to-troposphere O_3 flux for tropospheric models. It described stratospheric O_3 as a passive tracer released at the tropics (30°N and 30°S) between 10-70 hPa at the tropopause at the rate of the prescribed O_3 cross tropopause flux. This scheme was proposed as an alternative to LINOZ for tropospheric CTMs with a poor description of the stratosphere and/or unrealistic cross-tropopause O_3 flux.

There have also been some attempts into the use of more complex nonlinear schemes for ozone parameterisation (*e.g.* Taylor and Bourqui 2005). Ozone chemistry is extremely non-linear, and O_3 distribution is also shaped by non-linear transport processes; for these reasons, non-linear approaches to parameterise ozone into NWP and DAS systems will most probably play a significant role in a near future. For the time being, however, computational resources and NWP models structure make it easier to implement linear schemes.

5.3 Current ECMWF O_3 scheme

5.3.1 The scheme

In the ECMWF model O_3 has been a prognostic variable since 1999, when it was included as part of the European Centre plans to extend their model to cover the whole stratosphere (Untch *et al.*, 1999). The current O_3 treatment in the ECMWF IFS model consists of an updated version of the linear parameterisation of Cariolle and Déqué (1986). The ECMWF version uses an additional term in equation (5.4) for simple representation of the heterogeneous chemistry in PSCs (Dethof and Hólm,

2004). The scheme used now by ECMWF is based on the expression

$$\frac{\partial f}{\partial t} = c_0 + c_1(f - \bar{f}) + c_2(T - \bar{T}) + c_3(c_{O_3} - c_{\bar{O}_3}) + c_4(Cl_{EQ})^2 f \tag{5.12}$$

where Cl_{EQ} is the equivalent chlorine content of the stratosphere, and is the only parameter that varies from year to year. The fifth term is only active when temperature falls below 195 K, for daytime latitudes poleward of 45°. In the current scheme version (v2.3) $[\mathrm{Cl}_{EQ}]^2$ must be scaled to $[\mathrm{Cl}_{EQ}/3.8]^2$ to take into account that the heterogeneous term coefficient is representative for the year 2000. Actually, the dependence polar ozone loss exhibit with total chlorine is not quadratic (*e.g.* Searle *et al.* 1998), thus this formulation of the heterogenous term is not realistic. Problems related to the heterogenous term in equation (5.12) are discussed in Section 5.3.2, and the inaccuracy of the quadratic dependence on $\mathrm{Cl}_E Q$ is further discussed in Section 5.3.3.

The updated parameterisation coefficients (v2.3) were produced by Pascal Simon (Météo-France) using an updated version of MOBIDIC (Cariolle and Brard, 1984). For this version the 2D model used reaction rates from JPL2003 (Sander *et al.*, 2003), and took the residual circulation from a scenario of the ARPEGE-Climat GCM (Déqué et al., 1994) that considers the dynamical effects of radiatively active gases such as CO_2, N_2O, CH_4, CFCs and Br_x (Cariolle and Teyssèdre, 2007). However, the 2D model did not include any heterogeneous chemistry, as in its predecessor versions.

In the ECMWF scheme, equilibrium values are not taken from the default values provided by the 2D CTM, as they were found to produce significant biases in the ECMWF O_3 analysis. These biases came from the differences existing between the O_3 observations assimilated by ECMWF and the default $\bar{f}$ climatology (Dethof and Hólm, 2004). Instead, the ECMWF scheme takes the ozone equilibrium values (mixing ratio and column) from the Fortuin and Langematz (1995) climatology.

5.3.2 ECMWF O_3 scheme performance

Ozone analyses produced with the current version of the ECMWF scheme (updated coefficients v2.3) produce results in better agreement with observations than those obtained with previous versions of the CD scheme in the ECMWF model, (see Geer *et al.* 2006, and Chapter 6 in this thesis). However, the parameterisation in equation (5.12) still presents biases compared to observations. The main problems are still the overestimation of polar ozone column and the scheme not producing a realistic simulation of the ozone hole in absence of ozone data assimilation. The overestimation of polar columns, also present in the previous set of CD coefficients used by ECMWF (v2.1), has been improved in v2.3 but not solved (see Chapter 6). Dethof and Hólm (2004) highlighted some deficiencies in the ECMWF O_3 model that, although to a lesser extent than in ERA-40, are also apparent in current ECMWF O_3 analyses (*e.g.* Geer *et al.* 2006).

The pre-satellite period of ERA-40 (1957-1972), the satellite period without O_3 observations (1973-1978) and the satellite period with O_3 observations (1979-2002) were compared in Dethof and Hólm (2004). They showed the overestimation in the ERA-40 ozone column when no O_3 data were assimilated, especially in the northern hemisphere (NH) winter. Over mid-latitudes the agreement was better for pre-satellite years than in the 1973-1978 period, indicating that radiance assimilation is affecting O_3 transport, causing the excessive accumulation over the pole. In pre-satellite years, discrepancies in the southern high latitudes are mainly due to temperature biases in ERA-40 erroneously activating the heterogeneous term in equation (5.12) and causing too much O_3 destruction (Dethof and Hólm, 2004). In contrast, the last period of ERA-40 (as well as more recent ECMWF analyses) shows too weak destruction over the SH polar spring. For these ERA-40 years, the Antarctic ozone hole is not reproduced unless O_3 observations are assimilated. Figure 5.1, reproduced from Dethof and Hólm (2002), compares the total ozone (TO) column from one ECMWF model run in which no O_3 data are assimilated, and from ERA-40, against TOMS column for 10th February 1992. The run without assimila-

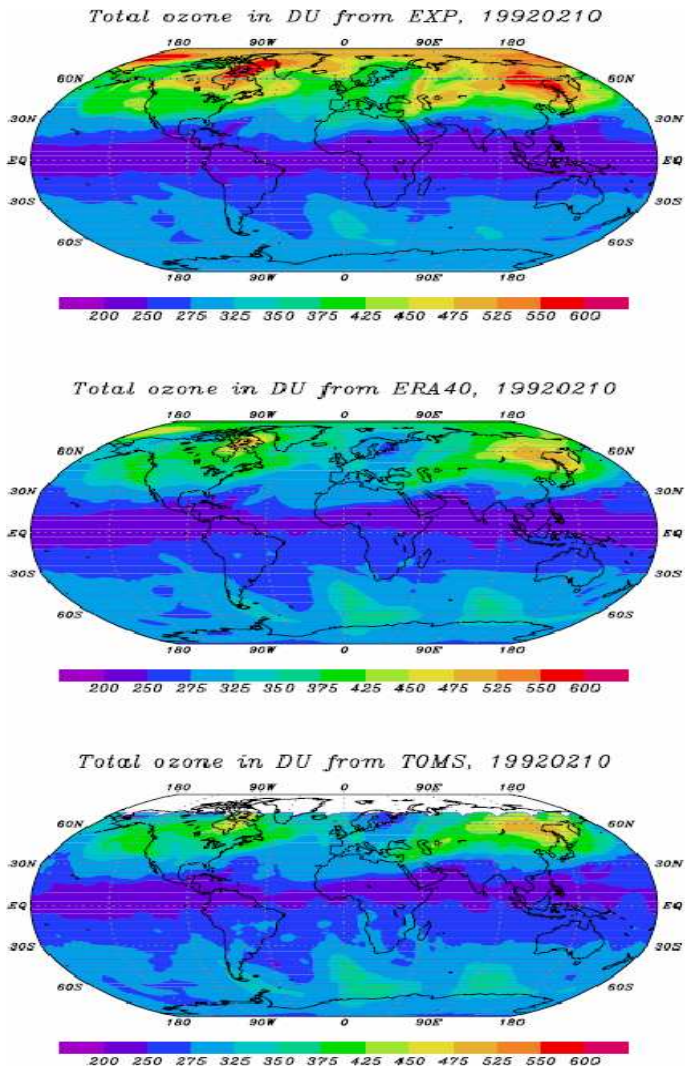

Figure 5.1: *Total ozone column (DU) on 10th February 1992 from an ECMWF model run in which no ozone observations are assimilated (top), from ERA-40 (middle), and from TOMS observations (bottom). Taken from Dethof and Hólm (2002).*

tion clearly overestimates column values over NH high latitudes; ERA-40 agrees well with TOMS, although values are still higher than observed, especially over northern Canada. Therefore, without O_3 assimilation the ECMWF local heterogeneous term in equation (5.12) is not able to produce realistic ozone loss for the Arctic vortex conditions. Also in the SH, the lack of a realistic ozone hole in absence of O_3 assimilation (Figure 5.2) clearly indicates the inaccuracy of the current ECMWF heterogeneous term to reproduce the real ozone destruction.

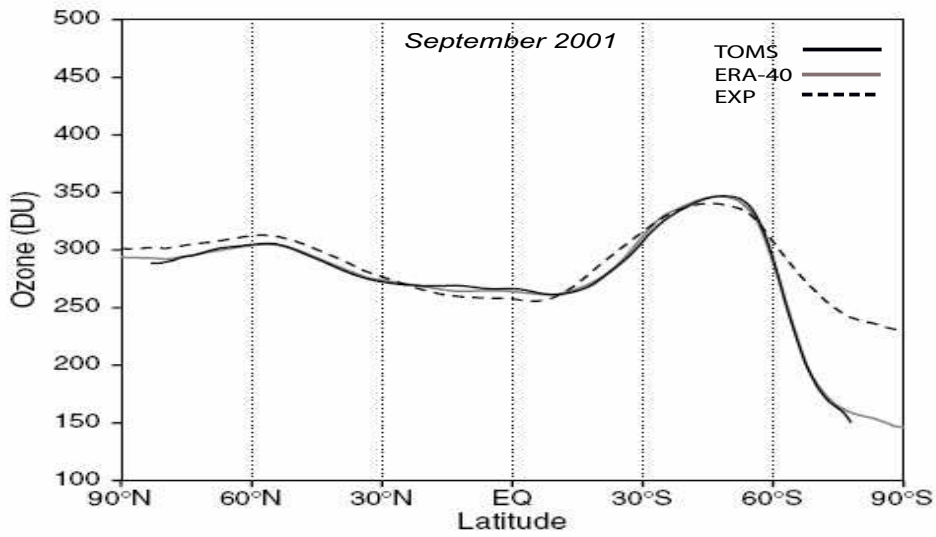

Figure 5.2: *Zonal average TO column (DU), averaged for September 2001, from ERA-40 (grey solid line), an experimental run with no data assimilation (dashed line) and from TOMS observations (black solid line). Adapted from Dethof and Hólm (2004).*

Figure 5.3 is an example of how the current (2007) ECMWF model reproduces stratospheric O_3 column. Ozone distributions in this figure are for the 4th September 2006, when the Antarctic ozone hole is present. The overall agreement is very good, but there is a general model overestimation at mid and high latitudes, and a small underestimation over tropical and subtropical latitudes compared to the Ozone Monitoring Instrument (OMI) satellite.

Dethof and Hólm (2004) also highlighted the necessity for better vertical ozone distributions in the ECMWF model. Figure 5.4 shows vertical profiles at Hohenpeissenberg (47.8°N, 11°E) for the period 1967-1971 (pre-satellite period). ERA-40 summer profiles agree well with ozonesondes. However, in winter ERA-40 ozone maxima are localised at too low altitudes and concentrations are overestimated in the LS. In the vertical distribution biases come not only from the O_3 model but also

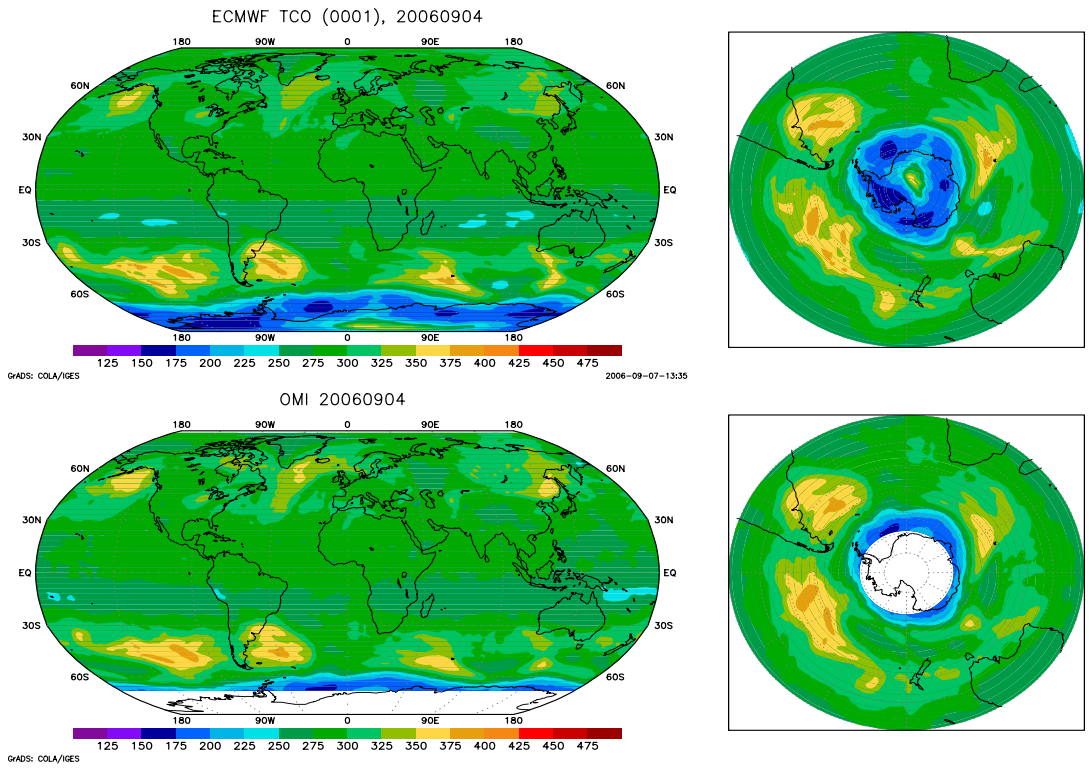

Figure 5.3: *Total ozone column from ECMWF analysis for the 4th September 2006 (upper panels) and as observed by OMI satellite (lower panels). Courtesy of Rossana Dragani (ECMWF).*

from the Solar Backscatter Ultra Violet instrument (SBUV) profiles assimilated. Dethof and Hólm (2004) showed how assimilating O_3 profiles previously bias-corrected improved the agreement between model profiles and independent measurements.

5.3.3 Improvements needed in the ECMWF O_3 scheme

So far the ECMWF O_3 scheme has not been implemented interactively in the ECMWF forecast model. The calculation of heating rates using the prognostic O_3 from equation (5.12) has only been experimentally tested and found to produce too large temperature biases to be used operationally (Morcrette, 2003). A more realistic O_3 scheme would be suitable for coupling with the radiation scheme, allowing for UV warnings to be provided with the operational ECMWF forecasts.

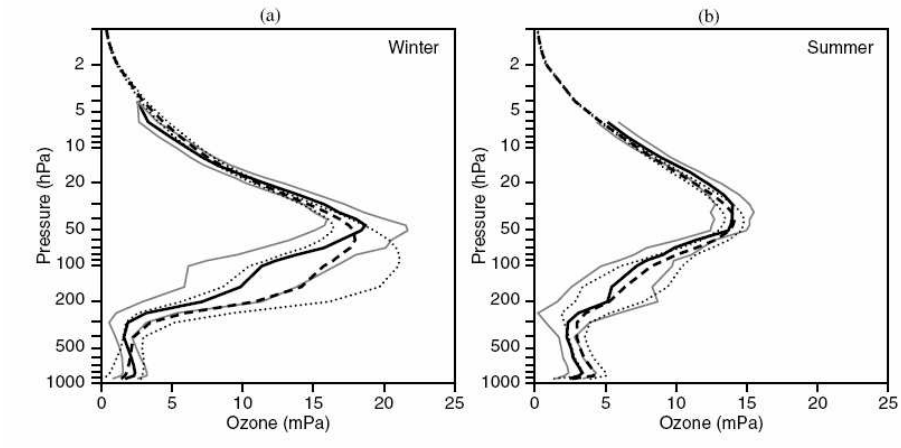

Figure 5.4: *Mean ozone profiles (1967-71) at Hohenpeissenberg for (a) winter (62 sondes JFM) and (b) summer (43 sondes JJA). Sonde data (thick solid) are shown with $\pm 1\sigma$ (thin solid), ERA-40 profiles (thick dashed) are also shown with $\pm 1\sigma$ standard deviation (dotted). From* Dethof and Hólm *(2004).*

Interannual variability has not been included in the coefficients c_i, however, trends in meteorological conditions and chemical composition can significantly alter chemistry, not only for the polar regions. For this reason, in the same way as the 5th term in equation (5.12) includes some annual variability in Cl_{EQ}, it would also be necessary that c_1, c_2 and c_3 were tuned according to different atmospheric conditions. In particular for reanalysis applications it would be recommended to re-evaluate the coefficients for every decade (or less).

The previous point is linked with the fact that the coefficients described in this chapter have not been calculated including heterogeneous chemistry reactions, this makes the calculation scenario unrealistic and affects also latitudes outside the polar regions. The unrealistic situation over the poles is later compensated for by the inclusion of a cold tracer or an heterogeneous local term as in the ECMWF scheme. However, the unrealistic effect over mid and low latitudes is not compensated in any way in the current schemes. The assimilation of O_3 observations is probably mitigating this effect in the ECMWF model. The inclusion of heterogeneous chemistry

in the computation of the parameterisation coefficients could provide a more realistic O_3 field and therefore a more effective assimilation of radiances in the ECMWF system.

The heterogeneous term

Using a localised heterogeneous term like the 5th term in equation (5.12) produces unrealistic results and too weak polar ozone loss. Conceptually, this kind of term is too restrictive with respect to our understanding of heterogeneous processes. First of all, the heterogeneous chemistry loss is not proportional to the square of the chlorine content (Cl^2_{EQ}); as shown by Searle *et al.* (1998), an exponent value of 1.5 is much more representative of the typical conditions encountered in an activated polar vortex. In addition, not only chlorine cycles play a role in destroying polar ozone, the ClO+BrO cycle can account for up to 50% of the polar depletion, and for this one the Cl dependency is linear. So, by considering the ozone loss to be quadratic in Cl^2_{EQ}, the ECMWF scheme would be overestimating the rate of polar ozone loss. The amount of O_3 destruction simulated by ECMWF is, however, insufficient (Dethof and Hólm, 2004), and the Antarctic hole tends to last shorter than observed.

The temperature threshold for the formation of PSCs actually depends on altitude and trace gas concentrations. The adopted threshold temperature of 195 K in equation (5.12) is representative of an altitude of ∼20km and 5 ppbv HNO_3 (*e.g.* Hanson and Mauersberger 1988; Carslaw *et al.* 1994). For a more realistic scheme, the temperature threshold in the heterogeneous term should include altitude dependency, and whenever possible be linked to the concentrations of H_2O, HNO_3 and H_2SO_4 aerosol.

The more fundamental shortcoming of the heterogeneous approach in equation (5.12) is that it assumes air masses activation and O_3 destruction (under sunlight exposure) to take place at the same time. In reality, the activation of air masses

takes place during the polar night inside the polar vortex, when temperature is low enough. With the return of spring sunlight to polar latitudes, the processed air is able to destroy ozone. However, the destruction can also happen during winter if activated air masses can reach lower latitudes (for instance by filamentation or vortex break-up) and there be exposed to sunlight, triggering O_3 destruction. This latter kind of process is completely missed by a localised temperature term. A more realistic approach would be the use of a cold-tracer (*e.g.* Chipperfield *et al.* 1994). With this kind of approach, the model keeps memory of the quantity of air processed by PSCs and of the amount of time that this air has been subsequently exposed to sunlight. The cold-tracer approach is therefore able to propagate the O_3 destruction to areas outside the region where PSCs are formed, i.e. outside the restricted ($T < 195K$) region. This kind of approach requires two tracers, one for O_3 and the additional cold-tracer. The cold-tracer approach implies the adoption of certain values for the activation and deactivation parameters, values that depend on the meteorological conditions and concentration of species; it is thus difficult to make a choice of values appropriate for the wide range of atmospheric conditions required in the production of a reanalysis series for instance. The effect of using a cold-tracer added to the gas-phase part of the CD scheme has been tested in our CTM (see Chapter 6).

Another option that represents a good compromise between a realistic heterogeneous chemistry and a simple one-tracer scheme is the use of a scheme of the form described in equation (5.4), the one without the additional 5th term, using instead one set of coefficients c_i that implicitly include the heterogeneous chemistry effects. This not only is expected to improve the representation of polar ozone, but has also the advantage of including mid-latitudes heterogeneous processes that have been so far ignored by most O_3 schemes. This approach has been explored in this thesis, and a set of coefficients with implicit heterogeneous chemistry has been calculated and tested with SLIMCAT CTM runs in Chapter 6.

5.4 H_2O schemes

Water is a radiatively active atmospheric constituent and is also key for many physical and chemical processes. However, until now stratospheric water vapour simulations within 3D global models have been problematical due to the variety of processes involved. The distribution of water vapour in the stratosphere is the result of a combination of factors: Humidity entry rate through the TTL, oxidation of CH_4 in the stratosphere, mesospheric photolysis, transport and mixing within the stratosphere and exchange processes through the tropopause. These processes also depend on others, like tropospheric entry rate depending mainly on convection and tropopause temperatures. In addition, feedbacks exist between all the above factors, *e.g.* radiation, stratospheric circulation and tropical tropopause temperatures. An accurate simulation of stratospheric water vapour is therefore a complicated task that requires different aspects of the DAS/NWP model to interact with a similar accuracy so that larger biases in one factor are not detrimental for the others. In turn, an accurate H_2O distribution in the stratosphere is crucial for realistic radiative calculations, and thus for satellite radiance assimilation.

5.4.1 Methane oxidation

Methane oxidation has been identified as a major source for stratospheric H_2O (*e.g.* Bates and Nicolet 1950; Jones and Pyle 1984; Remsberg *et al.* 1984; Le Texier *et al.* 1988). Le Texier *et al.* (1988) provided a detailed study of methane oxidation and water yield, recognising also the role played by molecular hydrogen H_2 in the CH_4 /H_2O relationship. Loss of CH_4 in the stratosphere takes place mainly through the following reactions

$$CH_4 + OH \rightarrow CH_3 + H_2O \tag{5.13a}$$

$$CH_4 + O(^1D) \rightarrow CH_3 + OH \tag{5.13b}$$

$$CH_4 + Cl \rightarrow CH_3 + HCl \tag{5.13c}$$

These main reactions initiate a sequence of further reactions that result in the production of $2H_2O$ and CO, which eventually will end up as CO_2. In the whole process H_2 is also formed, which causes the yield CH_4 /H_2O to be slightly less than 2. Nevertheless, this is compensated by the fact that molecular hydrogen itself is oxidised to H_2O at a rate that almost completely balances the H_2 formation from CH_4 (*e.g.* Dessler 2000). Hurst *et al.* (1999) used in-situ measurements of H_2 and CH_4 in the lower stratosphere to constrain the ratio between H_2O production and CH_4 loss (P_{H_2O}/L_{CH_4}). They used National Oceanic and Atmospheric Administration (NOAA) measurements from the Airborne Chromatograph for Atmospheric Trace Species (ACATS) (Elkins *et al.*, 1996), taken during the Stratospheric Tracers of Atmospheric Transport (STRAT) campaign (1995-1996) and the Photochemistry of Ozone Loss in the Arctic Region in Summer (POLARIS) campaign (1997). The correlation degree between P_{H_2O}/L_{CH_4} was found to depend on the age of the air masses, with a strong linear anticorrelation existing only for air parcels older than 3.8 years. For these air masses their measurement-based results agreed with their kinetics calculations reaching the conclusion that the quantity $H_2O + 2CH_4$ is conserved as air masses in the extratropical stratosphere get old. Hurst *et al.* (1999) found that younger air masses were influenced by the H_2O annual cycle in the tropical tropopause, but uncertainties in the age of air estimation of ∼0.4 years made an accurate examination of the annual cycle impossible.

In a global model the total hydrogen amount $\mathcal{H}$ must be conserved under mixing and transport

$$\mathcal{H} = H_2O + 2 \cdot CH_4 + H_2CO + H_2 \tag{5.14}$$

Recent studies have shown that the quantity $\mathcal{H}$ is also uniformly distributed in the stratosphere when the last two terms are neglected (*e.g.* Randel *et al.* 2004b), identifying CH_4 oxidation as the main source of water vapour within an accuracy of 0.05 ppmv (Austin *et al.*, 2007). Methane has no sources in the stratosphere, apart from the entry through the tropopause, which makes it possible to use CH_4

oxidation to parameterise water vapour increases in the stratosphere.

5.4.2 H_2O and CH_4 parameterisations

Some simple parameterisations for water vapour and methane have been implemented in GCMs (*e.g.* Le Texier *et al.* 1988; MacKenzie and Harwood 2004; Austin *et al.* 2007). MacKenzie and Harwood (2004) used the Thin Air 2D photochemical model (Kinnersley and Harwood, 1993) to obtain the rate coefficient k for the pseudo-reaction that groups the whole CH_4 oxidation process described by Le Texier *et al.* (1988)

$$CH_4 \xrightarrow{k} 2H_2O \tag{5.15}$$

the rate k was obtained as a function of latitude, altitude and season using the expression

$$k = \frac{1}{2}\frac{d[H_2O]}{dt} \cdot [CH_4] \tag{5.16}$$

Austin *et al.* (2007) studied the evolution of stratospheric H_2O concentrations in a chemistry climate model (CCM) ensemble run from 1960-2005. They examined the H_2O concentrations coming from the CCM photochemistry scheme (via CH_4 oxidation), and concentrations obtained from a parameterisation involving entry rates, CH_4 oxidation and also mean age of the air, as the amount of CH_4 oxidised depends on the time air masses have spent in the stratosphere. They formulated the water concentration at a stratospheric location $\vec{x}$ and time t to be

$$H_2O(\vec{x}, t) = A + B \tag{5.17}$$

where A, the entry term, and B, the methane oxidation term, can be expressed as

$$A = H_2O|_e(t - \gamma) \tag{5.18a}$$

$$B = 2 \cdot [CH_4|_0(t - \gamma) - CH_4(\vec{x}, t)] \tag{5.18b}$$

with $\gamma = \gamma(\vec{x}, t)$ the mean age-of-air for that particular location, and $H_2O|_e$ the water vapour amount remaining from the H_2O entry. At present, the kind of parameterisation used in Austin *et al.* (2007) could not be implemented by ECMWF due to the lack of age-of-air and CH_4 tracers in the IFS model.

In Austin *et al.* (2007) CH_4 oxidation (term B in equation (5.17)) was found to present a positive tendency from 1980-1997. This means that any model not taking into account such an increase would have underestimated stratospheric H_2O amounts in that period. The analytical treatment used by ECMWF to parameterise the methane source for H_2O (Section 5.5) does not account for any variation in CH_4 amounts or oxidation rates, and in fact the dry bias presented by ERA-40 is more pronounced in the later years, from 1989-2002 (*e.g.* Uppala *et al.* 2005). Section 5.5 describes in detail the current operational ECMWF scheme used for water vapour.

5.5 Current ECMWF H_2O scheme

5.5.1 The H_2O scheme

The ECMWF model includes a simple parameterisation of stratospheric water vapour based on the oxidation of CH_4. The current scheme also includes a sink term representing the photolysis of H_2O in the mesosphere. The ECMWF CH_4 scheme is a simplification of the approach originally adopted at the Department of Meteorology of the University of Edinburgh (A. Simmons, personal communication, 2007). ECMWF does not assimilate stratospheric humidity data, but uses directly the background humidity field in the analysis (A. Simmons and E. Hólm, personal communication, 2008). Therefore, it is the model dynamics and physics which shapes the stratospheric humidity, ultimately constrained to observations by the winds and temperature fields (Simmons *et al.*, 1999).

Observations give evidence that the following quantity is fairly uniformly distributed in the stratosphere with a value of ~ 6.8 ppmv (Randel *et al.*, 2004b)

$$2[CH_4] + [H_2O] \tag{5.19}$$

where here [ ] stands for volume mixing ratio (vmr). For the ERA-40 reanalysis and previous ECMWF systems, the value used was 6 ppmv, but this value was later shown to be too dry compared to climatologies, such as the UARS climatology analysed by Randel *et al.* (1998). The ECMWF model assumes, therefore, that the vmr of water vapour $[H_2O]$ increases at a rate

$$2k_1[CH_4] \tag{5.20}$$

or by using equation 5.19,

$$k_1(6.8 - [H_2O]) \tag{5.21}$$

which is expressed in ppmv and can also be written in terms of specific humidity, q, by simply dividing by 1.6×10^6 as

$$k_1(Q - q) \tag{5.22}$$

where $Q = 4.25 \times 10^{-6}$ (kg/kg). In addition, above approximately 60 km a term for the H_2O loss by photolysis has to be added, and so the complete ECMWF humidity parameterisation is

$$k_1(Q - q) - k_2\, q \tag{5.23}$$

The rate k_1 can be determined from a model with complete chemistry, such as was done in the past with the 2D-model of Edinburgh University (A. Simmons, personal communication, 2007). Nevertheless, a simpler option is used at present by the ECMWF, where analytical forms for k_1 and k_2 as a function of pressure are used (Dethof, 2003). Both k_1 and k_2 are defined using appropriate timescale factors τ_1 and τ_2:

$$k_1 = \frac{1}{86400 \cdot \tau_1} \tag{5.24}$$

$$k_2 = \frac{1}{86400 \cdot \tau_2} \tag{5.25}$$

where k_1 and k_2 are given in s^{-1}, and τ_1 and τ_2 in days. τ_1 and τ_2 are functions of pressure so that the photochemical lifetime of water vapour (Figure 5.5) follows that shown in Brasseur and Solomon (1984). The analytical function for the timescale factor τ_1 is

$$\tau_1 = \begin{cases} 100 & p \leq 50 \\ 100[1 + \alpha_1 \frac{ln(p/50)^4}{ln(10000/p)}] & 50 < p < 10000 \\ \infty & p \geq 10000 \end{cases} \tag{5.26}$$

where p has units of Pa and τ_1 is given in days. The factor α_1 is defined so that τ_1 is 2000 days at 1000 Pa. The corresponding function for τ_2

$$\tau_2 = \begin{cases} 3 & p \leq 0.1 \\ [exp\{\alpha_2 - 0.5(ln100 + \alpha_2)(1 + \cos \frac{\pi ln(p/20)}{ln0.005})\} - 0.01]^{-1} & 0.1 < p < 20 \\ \infty & p \geq 20 \end{cases} \tag{5.27}$$

in this case the factor α_2 has been empirically inferred as

$$\alpha_2 = \ln(\frac{1}{3} + 0.01) \tag{5.28}$$

5.5.2 H_2O scheme performance and need for improvement

The inclusion of the parameterisation described above in the IFS model significantly improved the distribution of H_2O in the ECMWF stratospheric analyses. Formerly, humidity values were too low in the tropical upper stratosphere and in most of the extratropical stratosphere (Simmons *et al.*, 1999). However, the current scheme still shows problems; Figure 5.6 shows the dry bias ERA-40 reanalysis presented compared to HALOE and MLS observations. ERA-40 values are about 10-15% drier than UARS in the upper stratosphere and lower mesosphere (Dethof, 2003). Lahoz *et al.* (2004) also showed that measurements from the Michelson Interferometer for

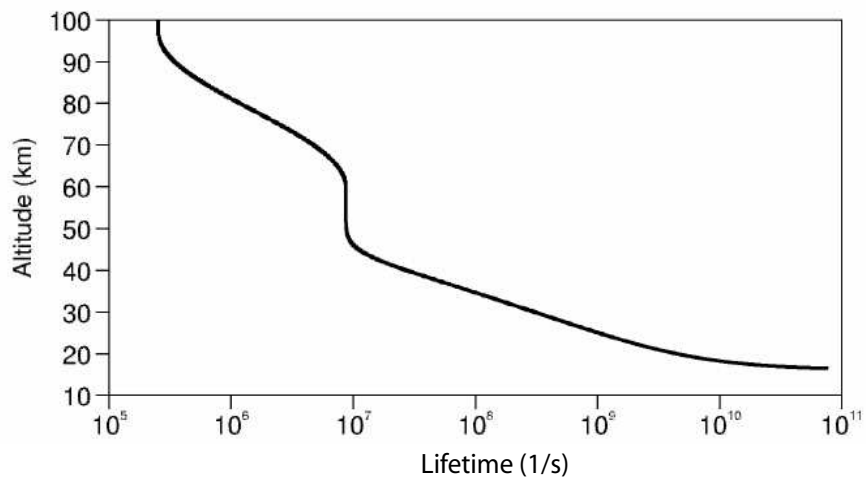

Figure 5.5: *H_2O photochemical lifetime (s^{-1}) used in current ECMWF stratospheric H_2O scheme. The lifetime corresponds to the combined CH_4 source and mesospheric loss terms $(k_1 + k_2)^{-1}$. Taken from the IFS Documentation - Cy31r1, available at http://www.ecmwf.int/research/ifsdocs/CY31r1/index.html*

Passive Atmospheric Sounding (MIPAS) are around 40% larger than ECMWF values in many areas, though some cloud contamination problems made MIPAS ozone and water vapour retrievals to be too large between 2002-2004. The reprocessed MIPAS data are similar to HALOE observations. The biases detected in ERA-40 led to the adoption of the 6.8 ppmv in equation (5.21), previously 6.0 ppmv, into the operational ECMWF system (Uppala *et al.*, 2005).

The too fast tropical upwelling transport in the ECMWF analyses make summers too moist and winters too dry in the tropical and subtropical LS region (*e.g.* Oikonomou and O'Neill 2006). Figure 5.7 from Simmons *et al.* (2007) shows the improvement in the annual cycle of the humidity field in the stratosphere (90-0.1 hPa) between ERA-40 and ERA-Interim tests, achieved by means of a more realistic transport (Chapters 3 and 4). The vertical propagation of the humidity annual cycle has been slowed down and the subtropical mixing reduced in the more recent ECMWF system.

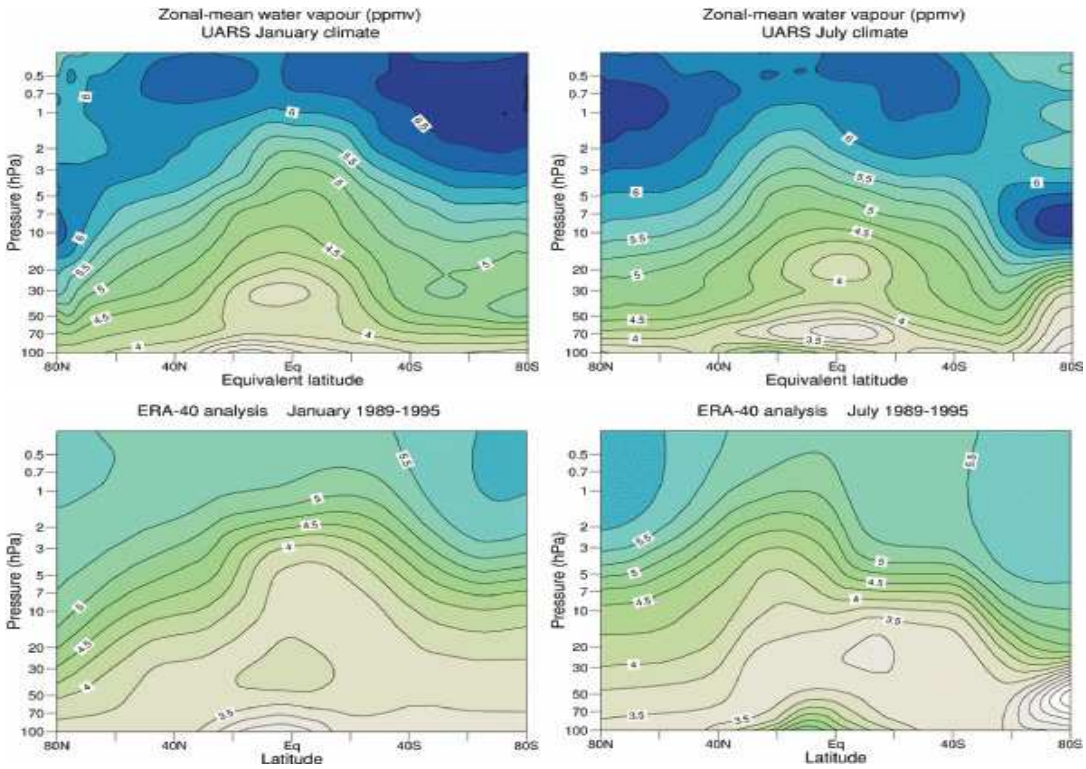

Figure 5.6: *Stratospheric zonal H_2O vmr (ppmv) for January (left) and July (right) from UARS measurements (upper panels) and from ERA-40 reanalyses (lower panels). Data have been averaged for the period 1989-1995. Taken from Dethof (2003).*

Need for improvement

In the current ECMWF scheme no latitudinal dependency is included in the parameters k_1 and k_2. Instead the scheme relies on the model transport for the correct distribution of water vapour after the entrance through the TTL. The deficiencies in the ECMWF model stratosphere highlighted in Chapters 3 and 4 can then feedback into the water vapour scheme and vice-versa. The too rapid stratospheric transport would then not allow for enough CH_4 oxidation to take place, causing the modelled stratosphere to be too dry. Deficiencies in H_2O distributions also affect transport, as stratospheric humidity interacts with radiation calculations affecting therefore the assimilation of satellite data.

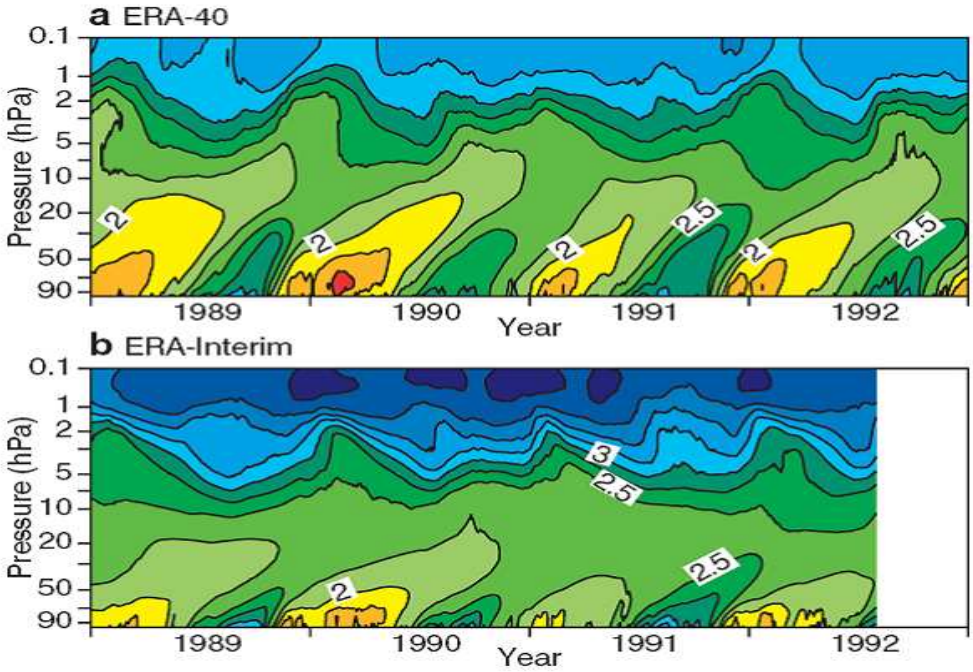

Figure 5.7: *Time series for the specific humidity (mg/kg) averaged from 10° N to 10° S from (a) ERA-40 and (b) ERA-Interim. Contour interval is 0.25 mg/kg. Taken from Simmons* et al. *(2007).*

On the other hand, CH_4 also enters into the radiative transfer scheme of the ECMWF model. In this radiation scheme a constant profile is adopted for CH_4, with no spatial variation, neither in latitude nor in altitude. Moreover, the value used is 1.7 ppmv, which corresponds to typical surface CH_4 concentrations and is a clear overestimation for stratospheric levels.

5.6 Summary and open issues

This chapter has presented an overview of present and past O_3 and H_2O parameterisations, and has discussed the current ECMWF stratospheric O_3 and H_2O schemes. The ECMWF ozone model performs well overall but still needs to be improved to allow it to be used interactively with radiation, in particular the polar regions are not well simulated. Other O_3 schemes have not yet been able to provide an accu-

rate simulation of the polar ozone loss either. Significant biases exist between the ECMWF stratospheric H_2O scheme and observations. Moreover, the current scheme is not flexible enough to allow any variability due to changes in the CH_4 oxidation source.

The ECMWF model ozone problems are due to deficiencies in both transport and in the chemistry parameterisation. These two aspects are linked through the assimilated radiances; the ECMWF O_3 scheme interacts with the dynamics via the radiance observation operators. Better assimilation of satellite radiances would contribute to better model stratospheric transport, and therefore to better O_3 distributions. Conversely, a better O_3 scheme would improve the assimilation of radiances, as well as contribute to the reduction of the model-observation departures. Lower departure values would be reflected in a lower impact on the model dynamics, and less spurious gravity waves enhancing the stratospheric circulation due to the insertion of observed radiances.

For a better assimilation of stratospheric radiances, and therefore more realistic transport, it is necessary to improve the O_3 and H_2O descriptions in the ECMWF model, as well as to include a new parameterisation for CH_4. Ideally, the chemical accuracy and experience of full-chemistry CTMs should be used to create sufficiently realistic chemical schemes for the NWP/DAS model. The main improvements that could be accomplished with the help of a state-of-the-art 3D CTM are:

a) For the O_3 scheme:

New linear ozone scheme coefficients should implicitly include heterogeneous chemistry, not only for a more realistic representation of polar ozone, but also for a more realistic description at mid and low latitudes. For an accurate evaluation of the scheme, the parameterisation should be tested within the full-chemistry model used to obtain the coefficients.

b) For H_2O /CH_4 schemes:

For a more efficient parameterisation of stratospheric H_2O a scheme for CH_4 should be included. The CH_4 scheme could follow a linear approach similar to the CD ozone scheme, obtaining coefficients from perturbation runs of a full-chemistry CTM. This CH_4 parameterisation linked to H_2O would provide a more realistic, and flexible, source of H_2O in the stratosphere than the current ECMWF water scheme.

The implementation of a linear CH_4 scheme in the ECMWF IFS model could have a considerable impact, particularly in the stratosphere, where the actual CH_4 concentrations differ significantly from the current value of $\sim$1.7 ppmv used for the radiative scheme calculations. In addition, the inclusion of this new CH_4 tracer could be used to diagnose stratospheric transport within the ECMWF model, which would provide a direct way to evaluate the effects that changes in the NWP/DAS model have on the BDC and mixing processes. Furthermore, this kind of methane scheme would also allow the assimilation of CH_4 concentrations to be used to constrain humidity analyses.

The remainder of this thesis describes the development of these improved schemes, explores their implementation and evaluates their effects. The improvements of the O_3 scheme are dealt with in Chapter 6, while Chapter 7 presents a new scheme to parameterise stratospheric CH_4 and water vapour.

Chapter 6

COPCAT: Ozone Scheme from TOMCAT/SLIMCAT Runs

6.1 Introduction

The aim of this chapter is the use of a detailed full-chemistry CTM to evaluate different aspects of the ECMWF ozone approach. The Global Earth Monitoring System (GEMS) project, coordinated by ECMWF, focuses on the eventual implementation of an operational full-chemistry model. However, while full-chemistry is too costly to be operational it is important to identify where, and how, the current ECMWF ozone scheme could be improved.

Here, a new set of coefficients for the Cariolle and Déqué (1986) ozone scheme (CD scheme) based on full-chemistry runs of the SLIMCAT 3D model has been calculated. In this version of the coefficients the effects of all forms of heterogeneous chemistry are included implicitly, which permits the use of the new scheme without any additional parameterised heterogeneous term.

SLIMCAT simulations have been run to test the new set of coefficients and a comparison with the operational ECMWF O_3 scheme is presented. Testing the coefficients within the same CTM used to obtain them provides an excellent framework

to assess the performance of the CD linear scheme and to identify where or when this scheme may be less suitable.

First, Section 6.2 compares the SLIMCAT full-chemistry ozone field against observations. Next the calculation of the new coefficients is presented in Section 6.3, and the parameterisation performance is shown in Section 6.4. A comparison against the ECMWF scheme is given in Section 6.5. Special attention is paid to the simulation of polar loss in Section 6.6 and the validity of the linear approximation is evaluated in Section 6.7. A summary of results is given in Section 6.8.

6.2 SLIMCAT full-chemistry runs against observations

The SLIMCAT CTM has been widely used in stratospheric studies and tested against observations. It has participated in numerous model and observation assessment campaigns such as the European Union TOPOZ III project (Kouker and Coauthors, 2005), the European SCOUT-O3 project (*e.g.* WMO 2006), the recent Scientific Assessment of Ozone Depletion 2006 (WMO, 2007) and the Chemistry-Climate Model Validation Activity (CCMVal) for SPARC (*e.g.* Eyring *et al.* 2007).

6.2.1 O_3 observations

Model results in this chapter are compared against Total Ozone Mapping Spectrometer (TOMS) column observations (McPeters *et al.*, 1998), and O_3 data from the Halogen Occultation Experiment (HALOE) (Brühl *et al.*, 1996).

TOMS data

TOMS provided near-continuous record of ozone measurements from 1978 to December 2005, with a high-density horizontal coverage of total ozone of about 200,000 observations per day (only daylight measurements). TOMS data have been widely used

for the validation of models and other observational sets. Monthly data of TOMS Earth Probe (EP) (McPeters *et al.*, 1998) for year 2000 have been used throughout this chapter. These data have been obtained from http://toms.gsfc.nasa.gov/. Zonal monthly means are available from 85°N-85°S with a 5° resolution.

HALOE O_3 data

HALOE O_3 monthly data have been provided by W. Randel and F. Wu (from NCAR, USA) and correspond to the version 19 of HALOE public data release. These HALOE data are zonally averaged and are available for 41 latitudes (80°N-80°S), and 49 pressure levels (from 100-0.01 hPa). HALOE data have very high vertical resolution (2 km), however, there are few observations for some individual months, so in this chapter only the annual averaged values have been used for 2000. O_3 HALOE data (Brühl *et al.*, 1996) have been used for numerous model results evaluation (*e.g.* Chipperfield *et al.* 2002; Steil *et al.* 2003; Eyring *et al.* 2006; Feng *et al.* 2007).

6.2.2 SLIMCAT versus observations

A SLIMCAT full-chemistry run (run 323) is compared against TOMS ozone column in Figure 6.1 for the period Jan-Dec 2000. SLIMCAT results are in good general agreement with TOMS, and the temporal and spatial evolution of ozone is well simulated, in particular the minimum in the southern hemisphere spring is accurately represented by SLIMCAT. However, model results are larger than observations at high latitudes and lower in the tropics (up to 30 DU lower for some periods); the tropical low values band is also narrower for the model. Overall at mid/high latitudes SLIMCAT values are larger than TOMS. These differences are partly due to SLIMCAT being forced by ERA-40 analyses, but also to the fact that the full-chemistry run used here is a low resolution run, with coarse vertical resolution in the LS region, the run uses 24 levels from 0 to 60 km.

Figure 6.2 compares the vertical profile averaged for January-December 2000,

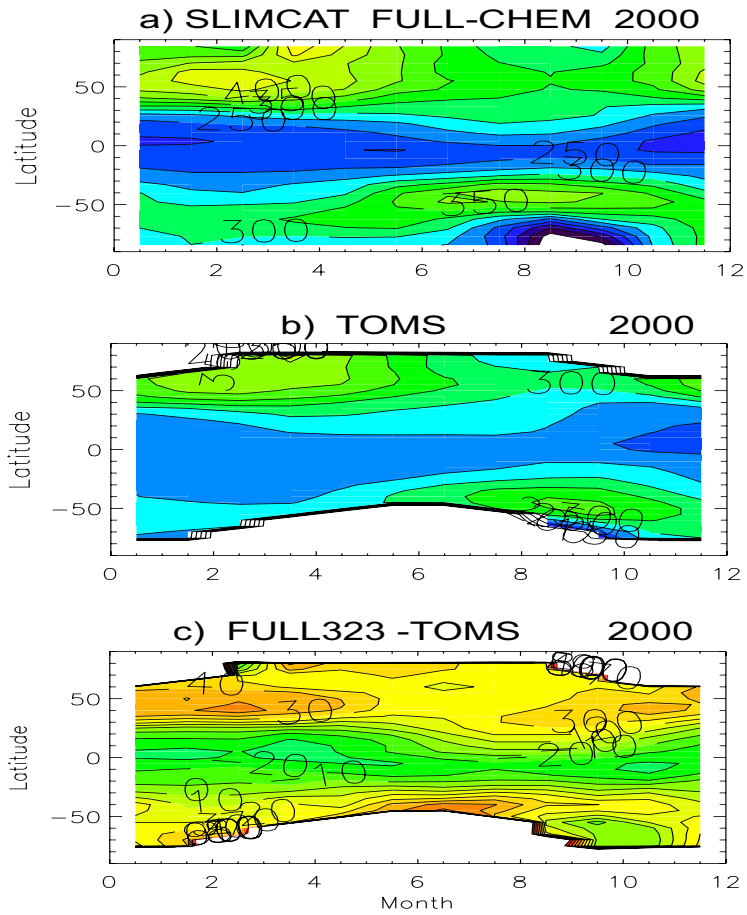

Figure 6.1: *Total ozone column (DU) from (a) the full-chemistry run 323 of SLIMCAT for year 2000, ERA-40 winds are used, (b) TOMS satellite and (c) differences between both. Contour intervals are 25 DU for (a) and (b), 10 DU for (c).*

averaged between 55°S-55°N, obtained from SLIMCAT and from HALOE observations. The agreement with the observed profile is good, although SLIMCAT run 323 O_3 is somewhat larger than HALOE around 100 hPa, and shows a ∼0.5 ppmv underestimation above 10 hPa. The underestimation of O_3 in the upper stratosphere was a general problem for models in the mid 1980s (*e.g.* Froidevaux *et al.* 1985, Eluszkiewicz and Allen 1993). In the mid 1990s Crutzen *et al.* (1995) showed that such an O_3 deficit disappeared when updated photochemical parameters were used. However, later studies showed that underestimations of 10-20% at around 40 km were still detected with more recent photochemical data (*e.g.* Khosravi *et al.*

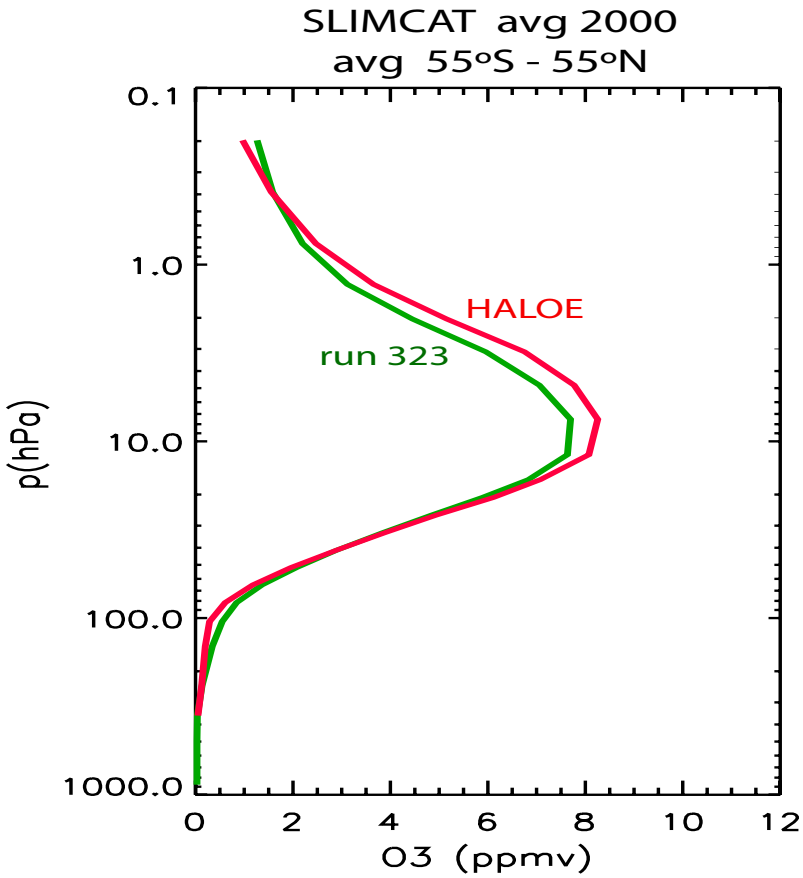

Figure 6.2: *O_3 profile (ppmv) averaged between 55°S-55°N for the period Jan-Dec 2000 obtained from SLIMCAT run 323 (green line) and from HALOE observations (red line).*

1998). As seen in Figure 6.2 an underestimation of up to 15% also exists for the SLIMCAT run 323 used in this chapter. Nevertheless, clarifying potential reasons for this upper stratospheric deficit is out of the scope of this thesis.

Here, the long experience of using SLIMCAT in stratospheric O_3 studies and the good overall agreement of SLIMCAT results with observations has encouraged the calculation of a new set of O_3 coefficients based on the SLIMCAT CTM.

6.3 COPCAT scheme: Calculation and coefficients

The SLIMCAT CTM has been used to obtain a new set of ozone coefficients to be used in 3D CTMs and GCMs. SLIMCAT stratospheric chemistry includes reactions occurring on liquid sulfate aerosols, and also on solid NAT and ice particles (see Section 2.6 in Chapter 2). This is, therefore, the first time that CD scheme coefficients are obtained from a 3D model that includes complete heterogeneous chemistry. One of the advantages is that no additional heterogeneous term is needed in the parameterisation, since the heterogeneous chemistry effect is already embedded in the calculation of the coefficients c_i $(i = 1, 2, 3)$ and the reference values ($\overline{f}$, $\overline{T}$ and $\overline{c}_{O_3}$). This is also a more realistic approach to simulate ozone loss processes over mid-latitudes, as discussed in Chapter 5. With the heterogeneous chemistry included in the other terms, the implemented parameterisation adopts a simpler form

$$\frac{\partial f}{\partial t} = c_0 + c_1(f - \bar{f}) + c_2(T - \bar{T}) + c_3(c_{O_3} - \bar{c}_{O_3}) \tag{6.1}$$

the difference with respect to equation (5.4) is that now equation (6.1) does include heterogeneous processes.

6.3.1 Calculation methodology

Several short runs of the CTM in box model mode were used to compute the ozone tendencies in the COPCAT (Coefficients for Ozone Parameterisation from a Chemistry And Transport model) scheme. The TOMCAT box model was initialised with the zonally averaged output of a full-chemistry simulation of the SLIMCAT 3D model (run 323), then seven 2-day runs of the box model were carried out from this initial state. The full chemistry run used to initialise the box model corresponds to January 2000 - December 2000, using ECMWF ERA-40 winds and temperatures. The resolution adopted is 24 latitudes, and 24 levels (from the surface up to $\sim$ 60km). Chemistry is computed every 20 minutes.

The coefficients corresponding to the climatological (reference) values in equation

(6.1), *i.e.* $\overline{f}$, $\overline{T}$ and $\overline{c}_{O_3}$, are directly provided by the zonal output of the 3D SLIMCAT initial state on the 15th of each month. For the four photochemical coefficients (c_i) box model runs are carried out and the corresponding linear tendencies for the net ozone production ($P - L$) calculated. Tendencies are calculated for odd oxygen O_x and then scaled by the factor $[O_3]/[O_x]$ to obtain the O_3 tendencies (coefficients).

One control run (using the unperturbed zonal initial values) is used to obtain the reference net production $c_0 = (P - L)_0$. For the three coefficients given by the partial derivatives, the initial values of f, T and c_{O_3} are perturbed, one at a time, to obtain the corresponding linear tendency in ($P - L$). The values used for the perturbations are $\pm 5\%$ for local ozone and column above, and ± 4 K for temperature, the same perturbation values as in McLinden *et al.* (2000).

The coefficients are based on the daily net production of O_3 averaged over the last day of the run (second day in this case). For the perturbed runs all radical species except O_3 are overwritten at every time step with their values at the end of the control run, for consistency with the definition of partial derivatives. For the ozone perturbed runs (local ozone and column), O_3 on the second day of the run is initialised with the average field over the first day of run.

The whole calculation procedure is applied to every month of the year. This methodology provides 7 coefficients for each month, on 24 latitudes and 24 vertical levels. The 12 files corresponding the monthly coefficients can then be read in by a CTM or GCM simulation in which ozone is treated as a tracer following the COPCAT approach in equation 6.1.

6.3.2 The new O_3 coefficients

Reference fields

COPCAT reference local ozone ($\overline{f}$) and column above ($\overline{c_{O_3}}$) fields are shown in Figures 6.3 and 6.4 respectively, for January, April, July and October. As seen in Section 6.2, SLIMCAT O_3 column is lower than observed over the tropics and higher over high latitudes; values of $\overline{f}$ are in good agreement with observations, although the value of the ozone maximum ($\sim$9 ppmv) is smaller than observed, *e.g.* compared to HALOE. The reference temperature ($\overline{T}$) is shown in Figure 6.5. This field comes from the analyses used to obtain the initial SLIMCAT state, ERA-40 in this case, interpolated onto the box model latitudes and levels. Therefore, $\overline{T}$ presents the same benefits and caveats as in the reanalyses (see Chapter 2).

Coefficients c_i

The COPCAT net O_3 production $(P-L)_0$ (coefficient c_0) zonal distribution for January, April, July and October (Figure 6.6) shows the stratospheric regions where O_3 is produced/destroyed. As expected, the tropical region is dominated by net photochemical production, as well as the upper stratosphere over winter mid-latitudes; everywhere else O_3 is net destroyed by chemistry.

As expressed in equation (5.6), the inverse of coefficient c_1 gives the relaxation times (τ) for the COPCAT scheme, which are represented (in days) in Figure 6.7. Values of τ are over 100 days in the whole LS region, with a maximum at the tropical tropopause region, and an infinite maximum in the polar night, indicating that O_3 in such regions can be considered as a passive tracer. Above 30 hPa τ decreases with altitude up to only several hours in the most upper levels, where O_3 concentrations are controlled by photochemistry. In these regions any deviation from the reference state will therefore be rapidly readjusted by the parameterisation.

Ozone destruction reactions in the stratosphere are generally strongly exother-

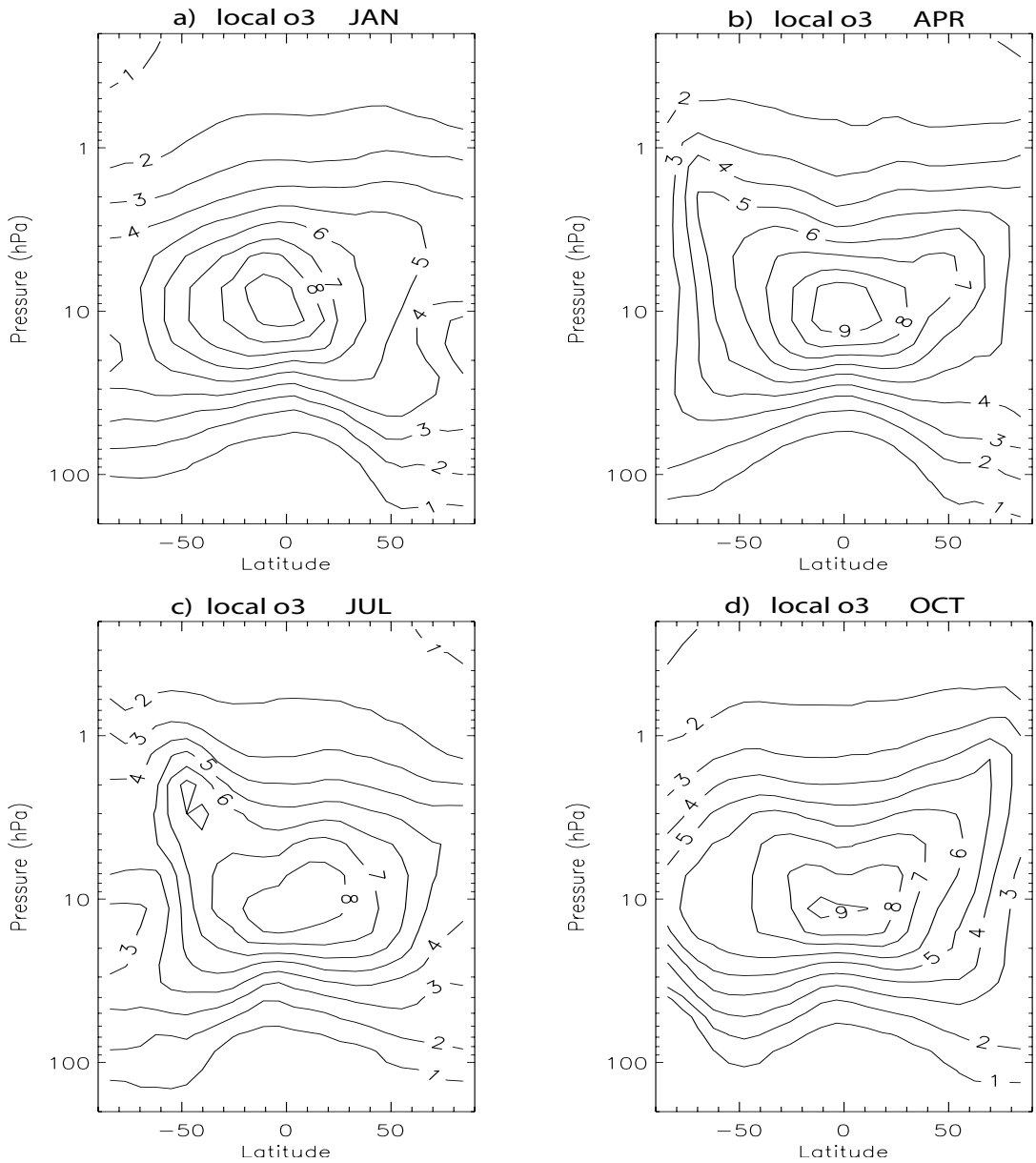

Figure 6.3: *Zonal mean of COPCAT local ozone* $\overline{f}$ *(ppmv) for (a) January, (b) April, (c) July and (d) October.*

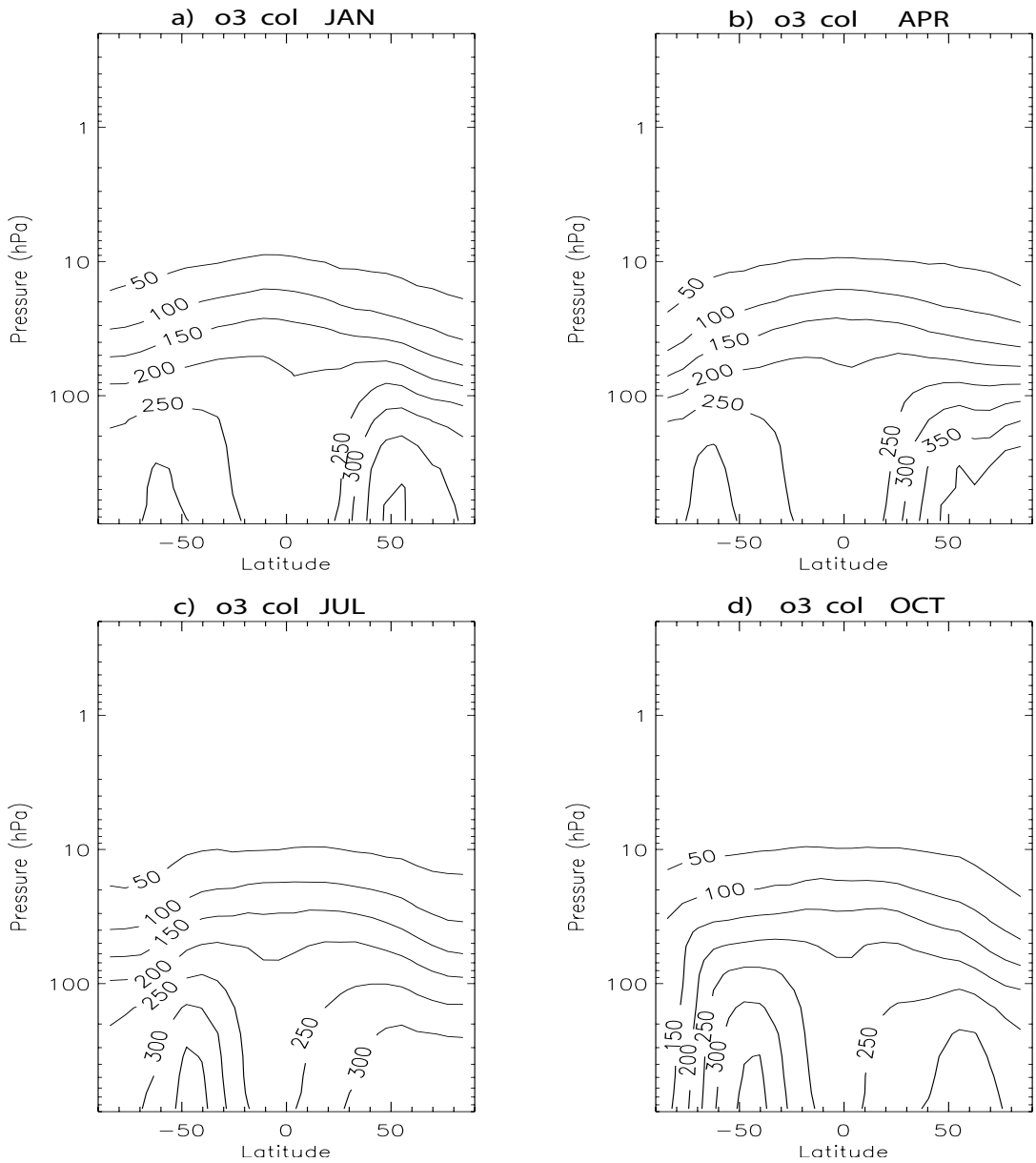

Figure 6.4: *Zonal mean of COPCAT ozone column* $\overline{c_{O_3}}$ *(DU) above a given pressure level for (a) January, (b) April, (c) July and (d) October.*

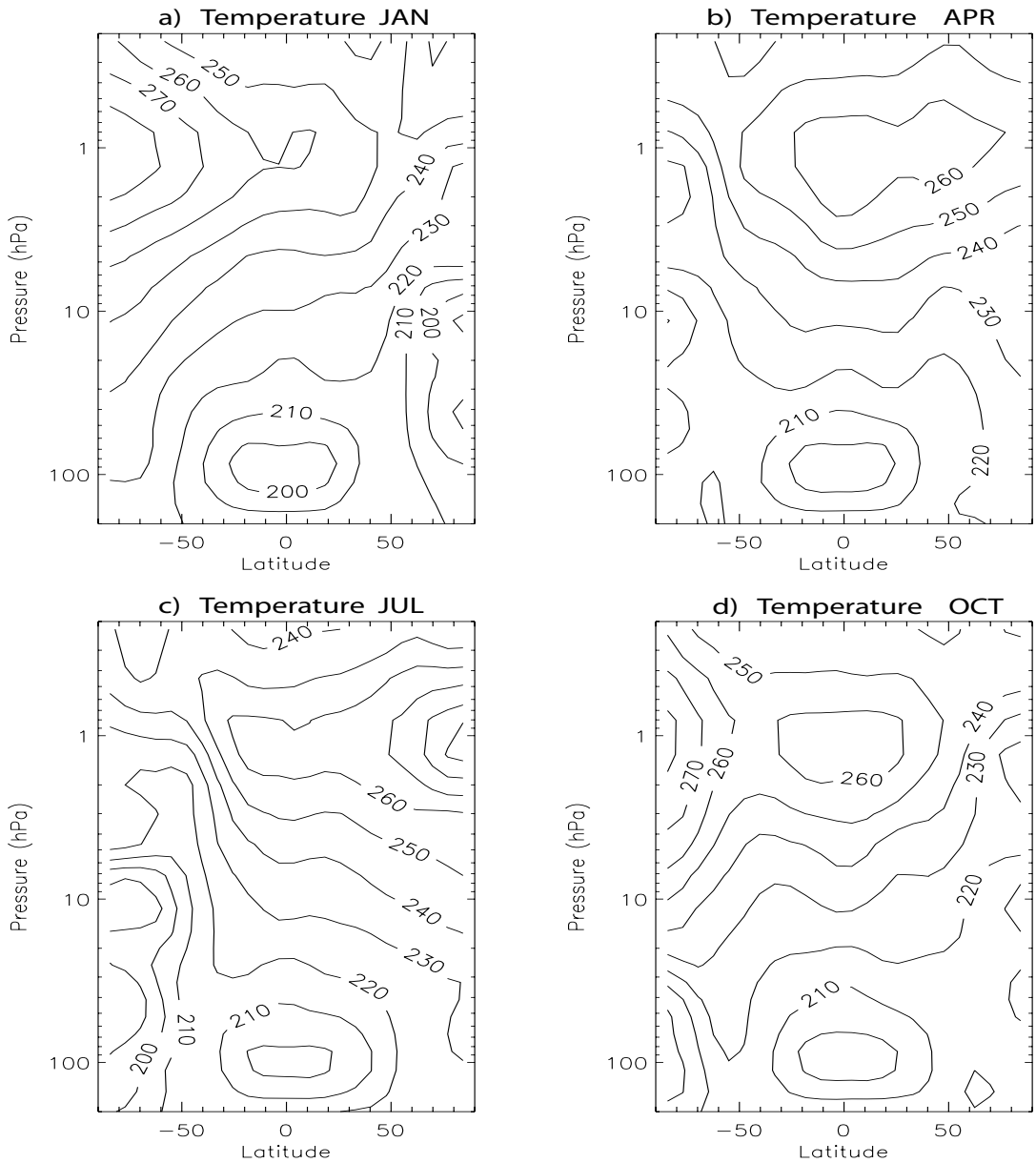

Figure 6.5: *Zonal mean of COPCAT* $\overline{T}$ *(K) for (a) January, (b) April, (c) July and (d) October.*

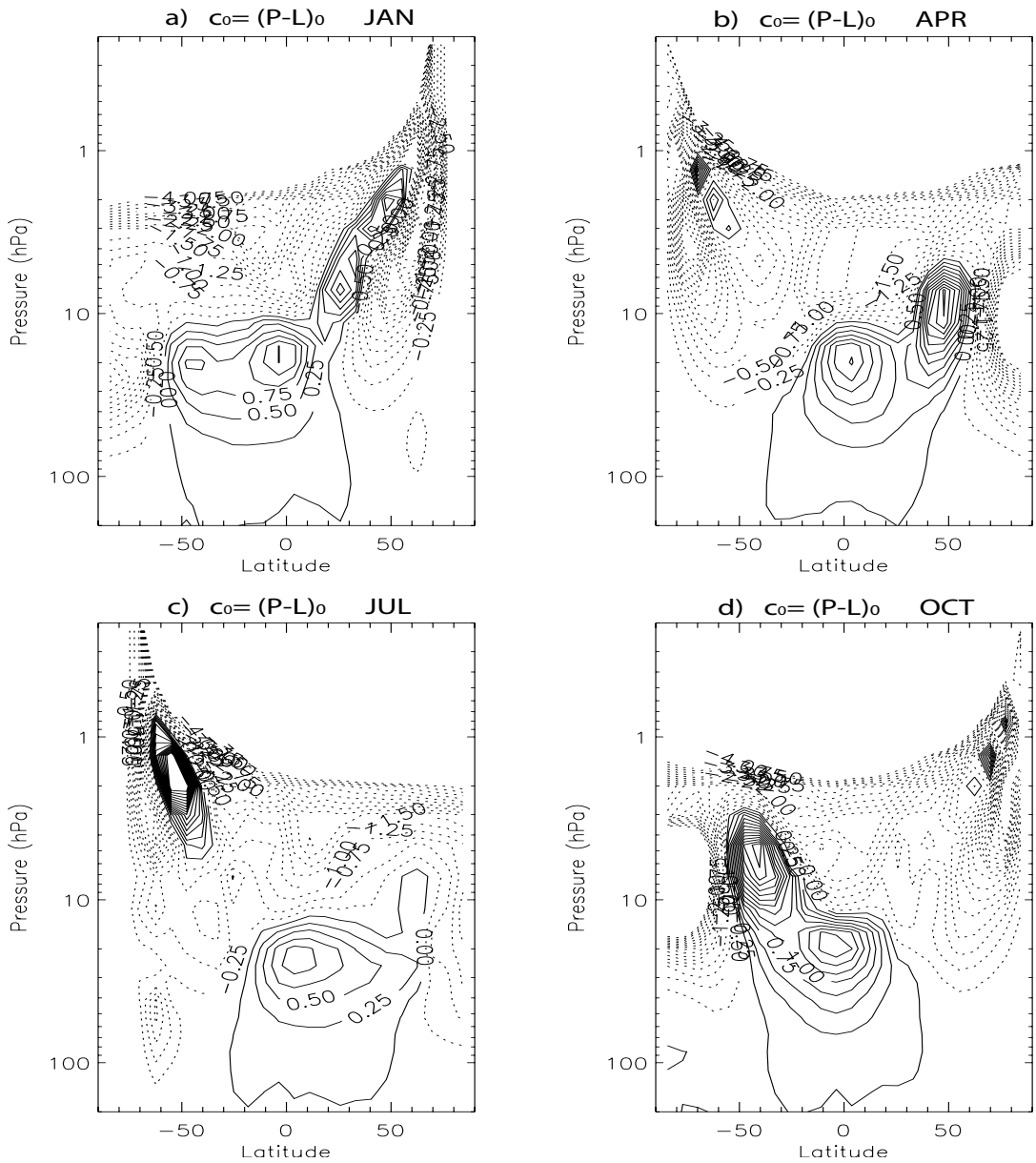

Figure 6.6: *Zonal mean of COPCAT net ozone production c_0 (ppmv/month) for (a) January, (b) April, (c) July and (d) October.*

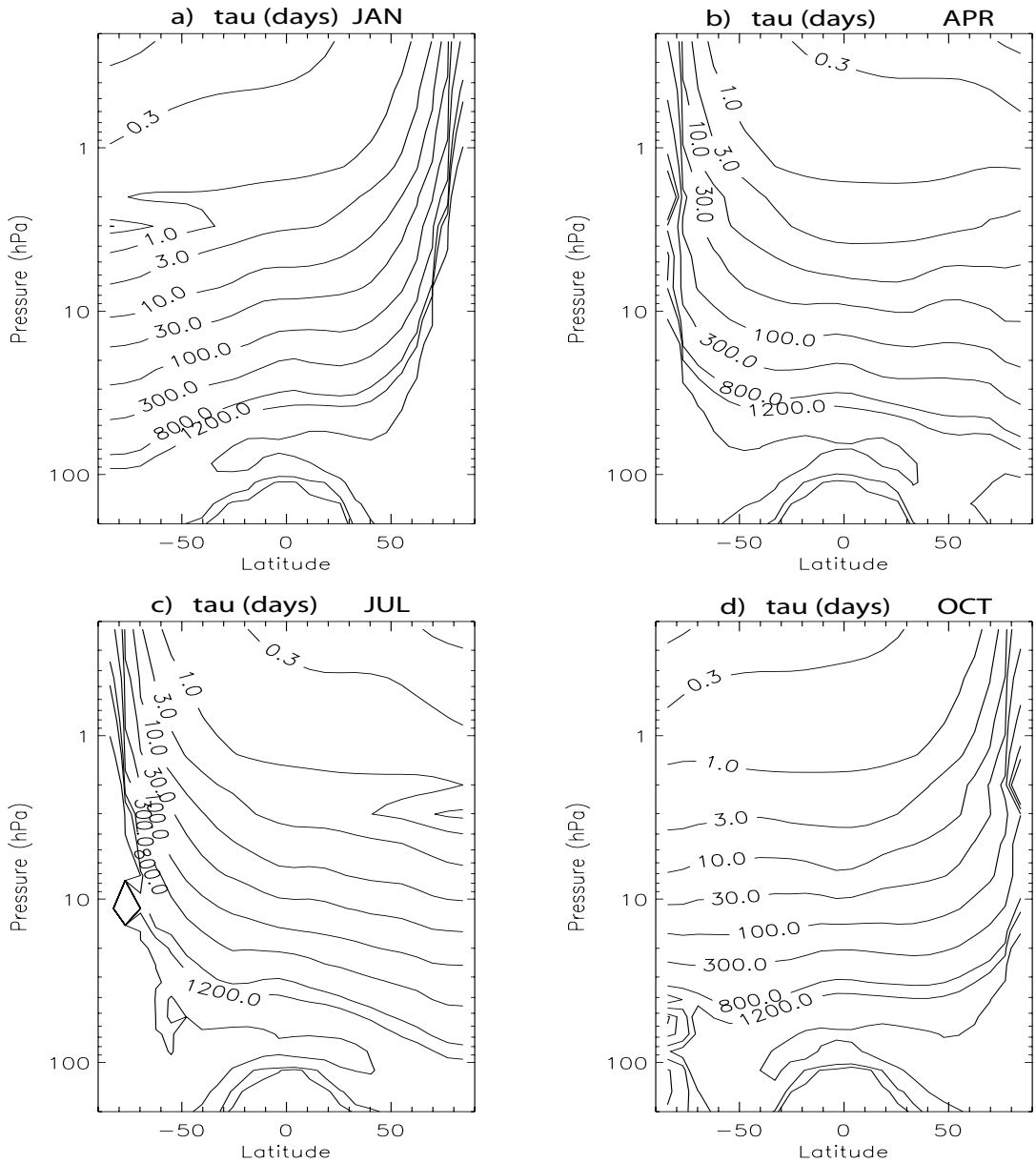

Figure 6.7: *Zonal mean of COPCAT relaxation times τ (days) for (a) January, (b) April, (c) July and (d) October.*

mic, thus a strong anticorrelation exists between O_3 and temperature (*e.g.* Barnett *et al.* 1975). This is reflected by the coefficient c_2 being negative throughout the stratosphere (Figure 6.8). The coefficient c_3 represents the O_3 self-healing effect. In the mid/low stratosphere it is always negative (Figure 6.9) meaning that a reduction in the ozone column above will have the opposite effect in the ozone concentrations below, which will increase by photolysis and compensate for some of the ozone column loss. In the upper stratosphere (above ∼5 hPa) c_3 is positive, hence a reduction in the above column will cause further O_3 destruction at these levels.

6.3.3 Implicit heterogeneous chemistry

A CTM (or 3D model) using COPCAT coefficients can successfully simulate polar and midlatitude O_3 depletion despite the fact that no additional heterogeneous term is included. This can be seen in Figure 6.10, where the total ozone (TO) column is represented for 2000 for three different SLIMCAT runs. The CTM has been driven by ERA-40 winds in all cases, but a different O_3 scheme has been used in each case: COPCAT, CHEM2D and Cariolle v2.3. Only the first three coefficients ($c_i, i = 1, 2, 3$) have been used. COPCAT is the only scheme able to simulate the ozone minimum over the Antarctic spring (Figure 6.10a), the others need an extra heterogeneous term.

By plotting the September reference net production $(P - L)_0$ (*i.e.* c_0) for the different schemes (Figure 6.11), it can be seen that COPCAT shows a depletion region centred at 50 hPa over the south pole. This represents the ozone destruction caused by PSCs and triggered by spring sunlight. None of the other schemes shows such a depletion region; only LINOZ shows a weak loss region at 100 hPa over southern high latitudes, but is not enough to produce spring ozone depletion over the Antarctic. Figure 6.12 shows the evolution of COPCAT c_0 coefficient in June-September. The loss region starts to develop at the edge of the vortex in June and July; in September values of -2.1 ppmv/month are reached around 40 hPa at high southern latitudes. Over the Arctic COPCAT gives lower column values than the

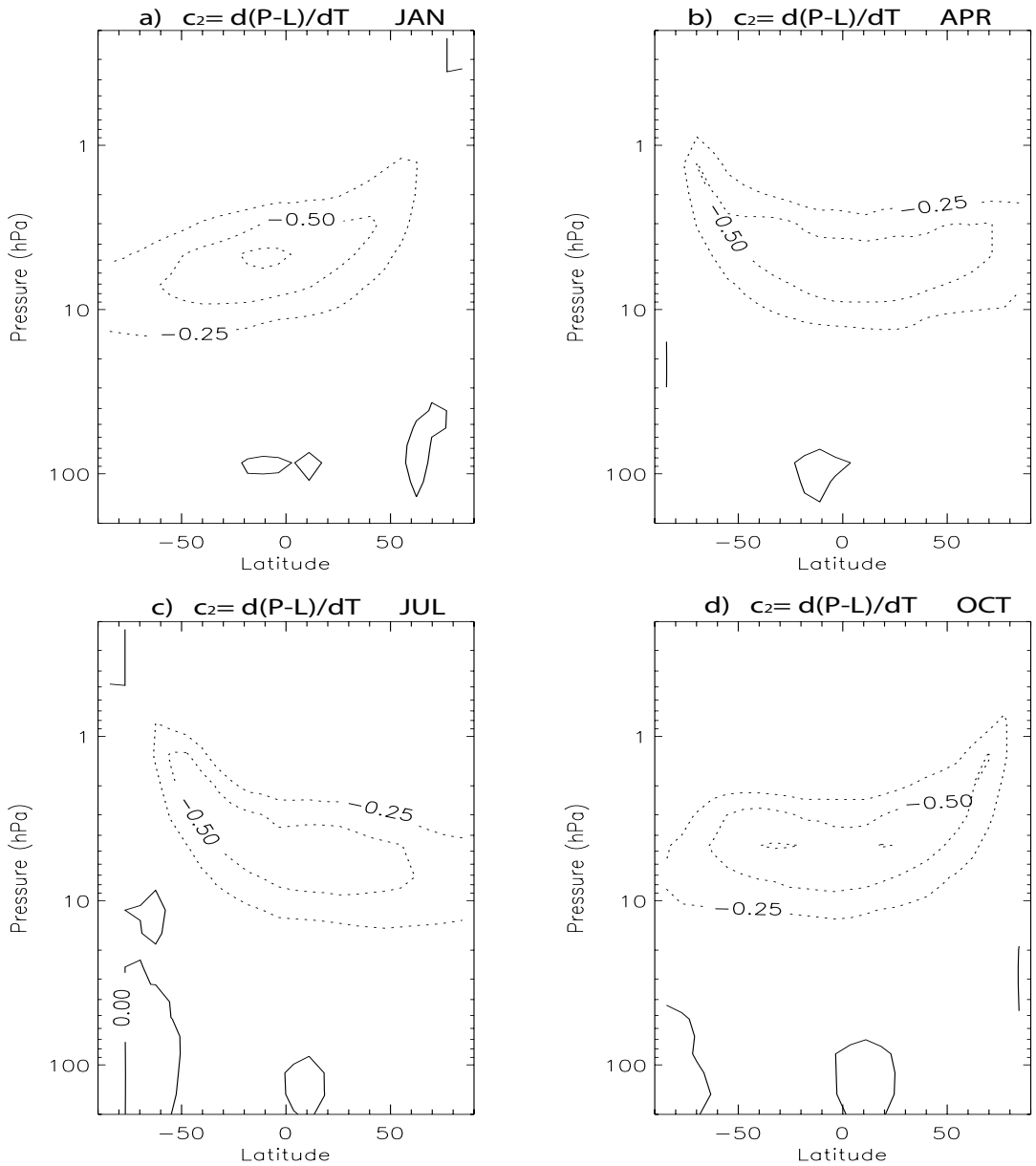

Figure 6.8: *Zonal mean of COPCAT coefficient c_2 (ppmv month^{-1} K^{-1}) for (a) January, (b) April, (c) July and (d) October.*

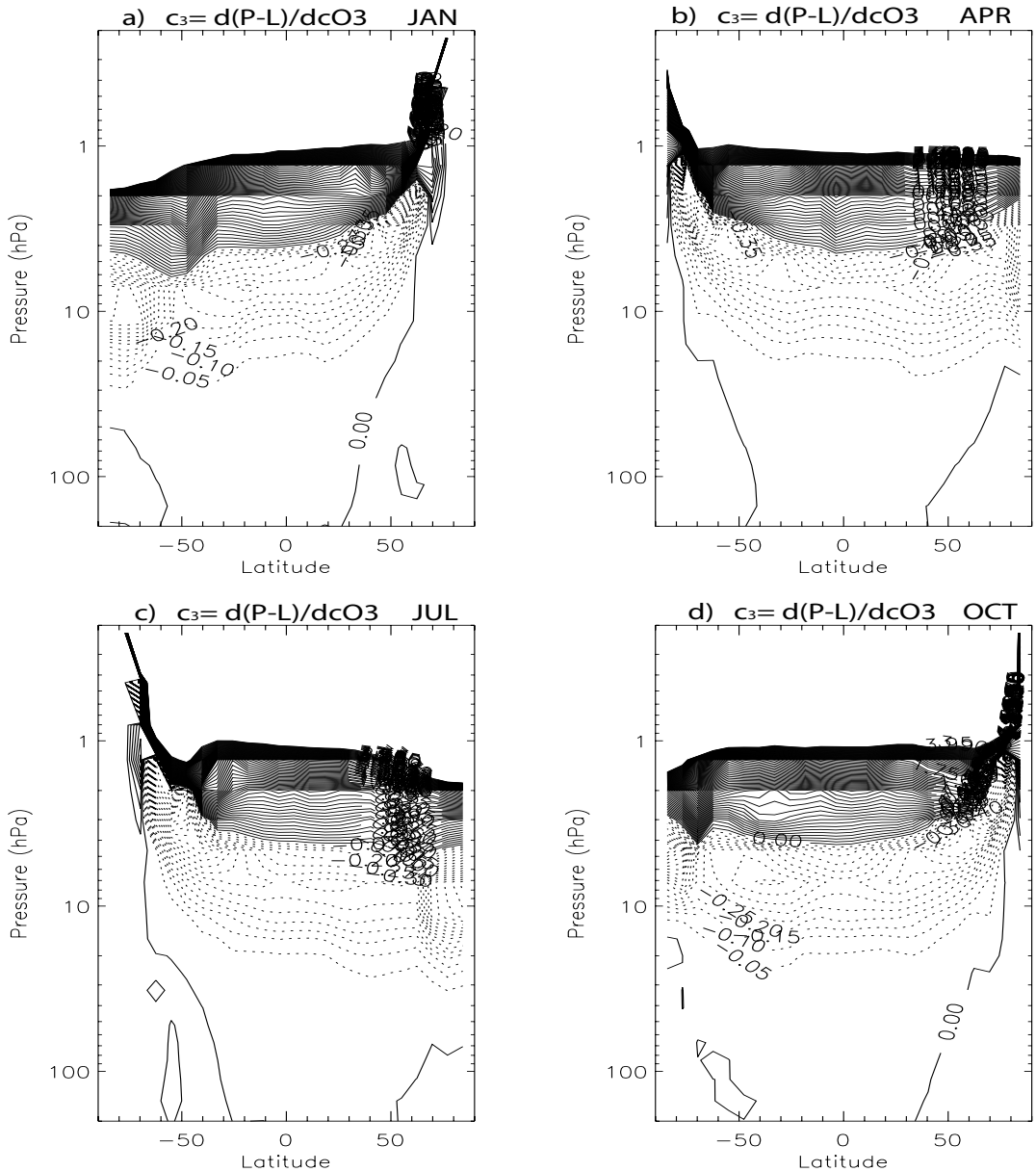

Figure 6.9: *Zonal mean of COPCAT coefficient c_3 (ppmv month^{-1} DU^{-1}) for (a) January, (b) April, (c) July and (d) October. Plotted values range is ±4 (ppmv month^{-1} DU^{-1}) with 0.05 contour intervals.*

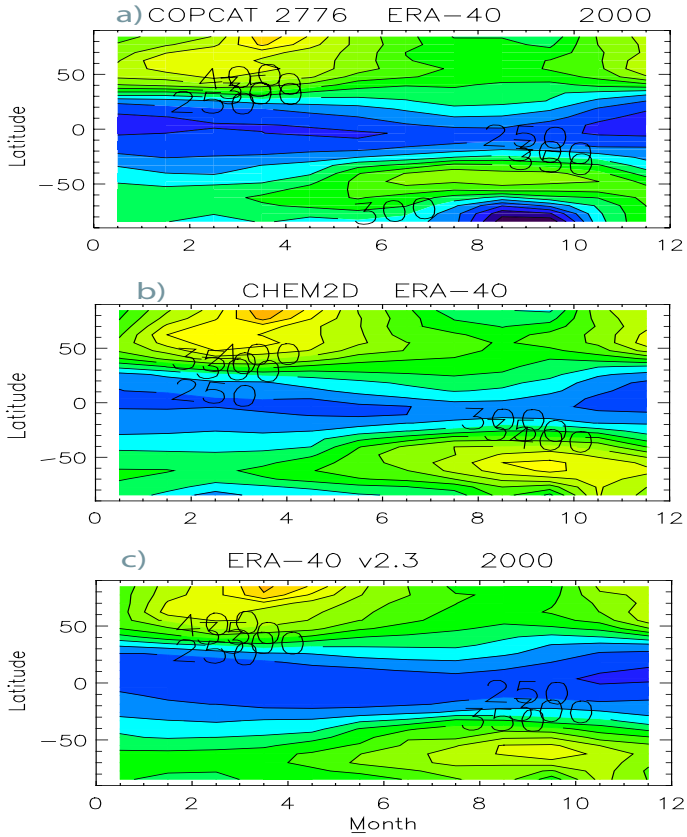

Figure 6.10: *Monthly evolution of zonal TO (DU) for year 2000 for (a) COPCAT, (b) CHEM2D and (c) Cariolle v2.3 used in SLIMCAT simulations. The CTM was driven by ERA-40 winds in all cases. No additional heterogeneous term has been used in the O_3 schemes, only the first 3 coefficients c_i ($i = 1, 2, 3$).*

gas-phase parameterisations (Figure 6.10b and Figure 6.10c). However, COPCAT column values are too large compared with observations, and larger than in the SLIMCAT full chemistry run (Section 6.4).

6.4 COPCAT scheme: Performance v. full-chemistry SLIMCAT

The way COPCAT coefficients have been calculated enables the comparison between the parameterisation and the CTM used to obtain it. In this way, the same

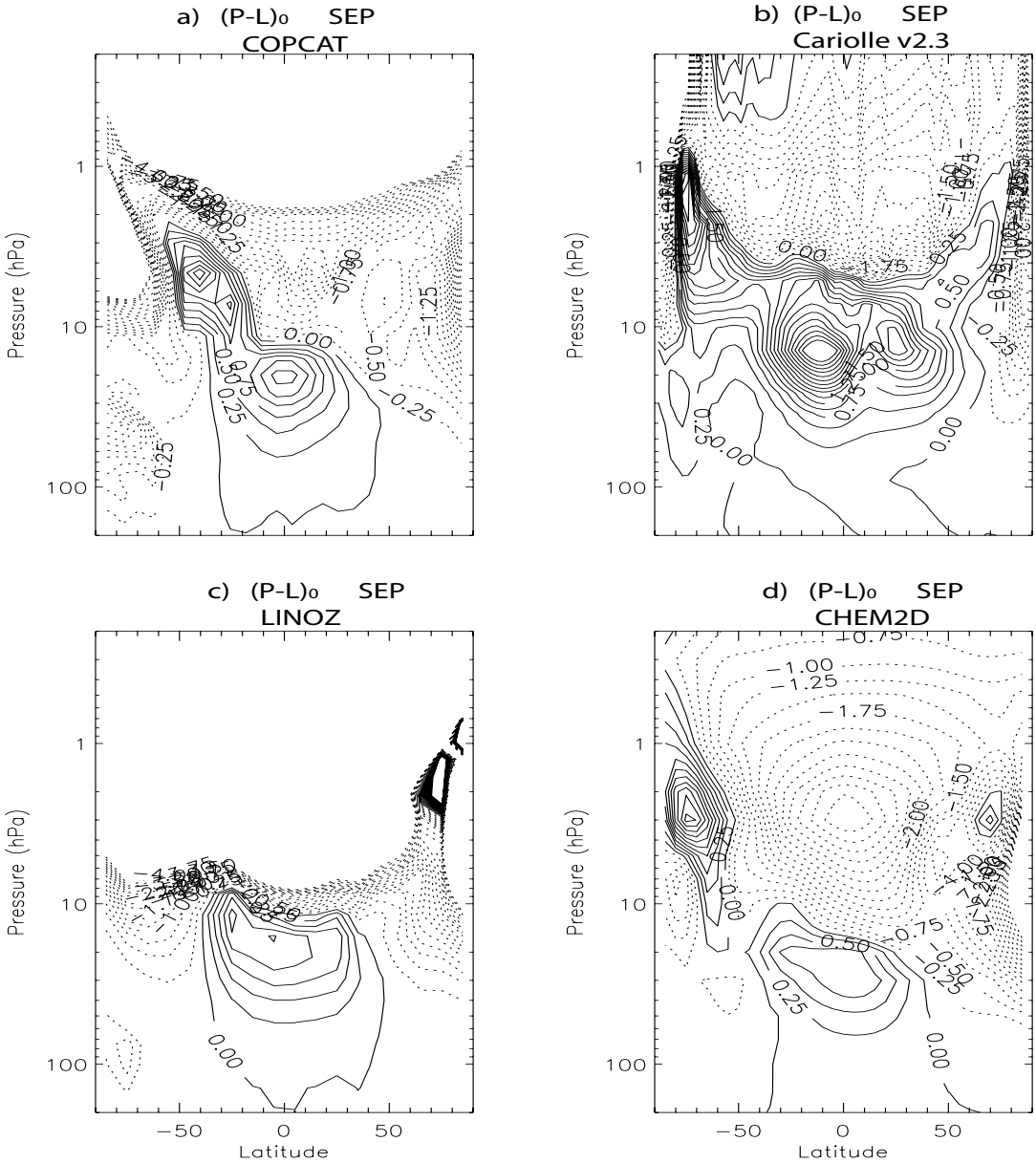

Figure 6.11: *Altitude/latitude distribution of c_0 (ppmv/month) for the month of September for (a) COPCAT, (b) Cariolle v2.3 (c) LINOZ and (d) CHEM2D.*

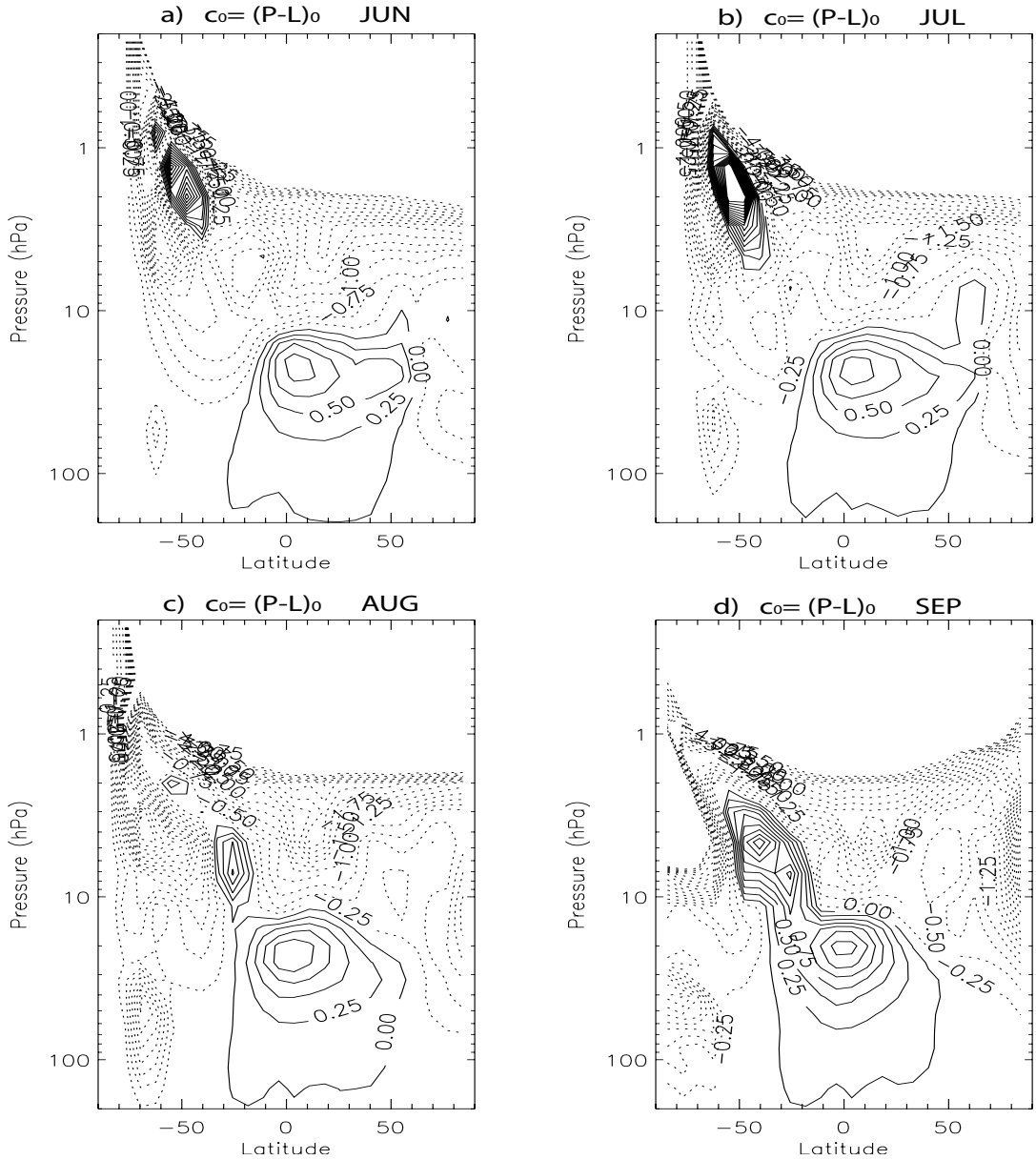

Figure 6.12: *Zonal mean of COPCAT net ozone production c_0 (ppmv/month) for (a) June, (b) July, (c) August and (d) September.*

numerics and dynamics are involved and differences can only be due to the use of the COPCAT scheme instead of the full-chemistry. This kind of evaluation was not possible for Cariolle v2.3 or CHEM2D coefficients, since they were computed by 2D photochemical models and then implemented within 3D GCMs or CTMs. LINOZ coefficients were calculated from a 3D box model (Prather *et al.*, 1990) but then implemented in a different 3D CTM (the University of California at Irvine CTM).

6.4.1 Total ozone column

Figure 6.13a shows the Jan-Dec 2000 total ozone (TO) column simulated by COPCAT. Differences with respect to the full-chemistry run 323 (Figure 6.1a) are also included in Figure 6.13b. The two CTM runs use ERA-40 winds, same resolution and advection schemes. The only difference between COPCAT and run 323 is in the chemistry. Results over the tropics and mid-latitudes are almost identical, although COPCAT column is ∼10 DU lower. The main differences are over high latitudes, where COPCAT values are larger than the full-chemistry. In the SH differences remain low (<20 DU) for all months except in late winter and early spring (ozone hole season), when COPCAT gives up to 40 DU higher values than the full-chemistry. The situation over the Arctic is very similar, differences are below 20 DU except in winter/spring. However, maximum differences over the Arctic are larger than in the Antarctic, reaching up to 60 DU in March.

6.4.2 Vertical structure

TO column is a good diagnostic for the global variability, both in time and space, achieved by the CTM. However, the vertical distribution of O_3 must also be accurate in order to get correct radiation amounts at the right levels. Figure 6.14 shows vertical monthly profiles, at 84°N and 84°S, obtained with the COPCAT parameterisation and full-chemistry in SLIMCAT runs driven by ERA-40 2000 winds. The O_3 destruction in spring between 30-100 hPa is successfully simulated by COPCAT. However, the ozone hole duration is much shorter in the parameterisation than in the

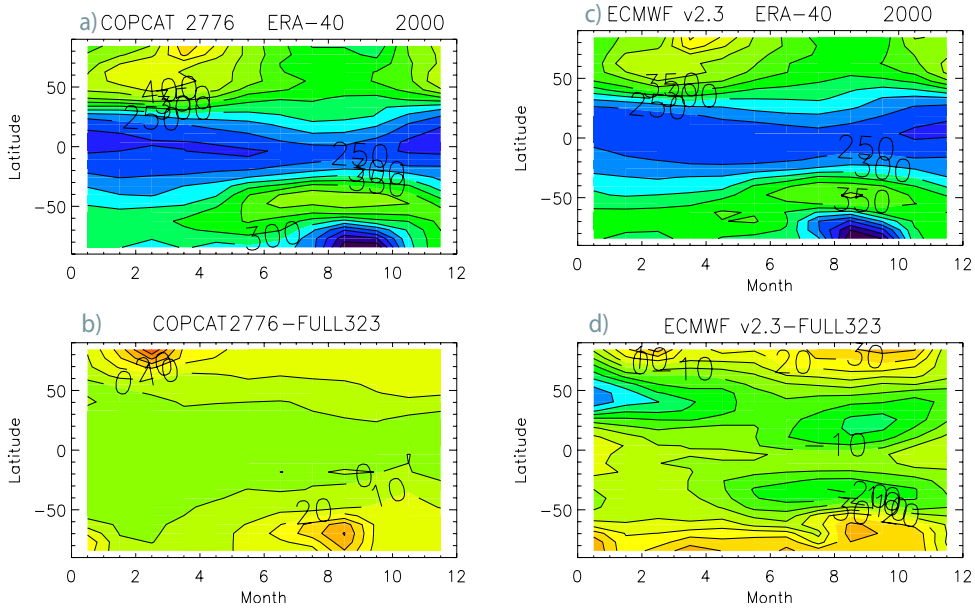

Figure 6.13: *TO column (DU) from (a) COPCAT scheme, (b) differences COPCAT-SLIMCAT full-chemistry, (c) ECMWF v2.3 scheme and (d) differences ECMWF-SLIMCAT full-chemistry. Both simulations use ERA-40 winds for year 2000. Contour interval for (a) and (c) is 25 DU and 10 DU for differences (b) and (d).*

full-chemistry. The parameterisation, both COPCAT and the operational ECMWF scheme, tend to overestimate O_3 in the mid/low stratosphere at high southern latitudes. The same occurs at 84°N during winter and spring. In the upper stratosphere, compared to full-chemistry, the parameterisations underestimate O_3 in spring and overestimate it in autumn.

Good agreement between COPCAT and the full-chemistry exists at 55°N (Figure 6.15); except for an underestimation/overestimation of ∼1 ppmv in the upper stratosphere in spring/autumn, and an underestimation (∼0.5 ppmv) around 10 hPa, the COPCAT run accurately reproduces the full-chemistry profiles. At 55°S (low panels in Figure 6.15) the discrepancies are larger, with differences also occurring between 10-100 hPa. At these levels COPCAT underestimates O_3 concentrations in autumn/winter and overestimates them in spring; the best agreement at this latitude

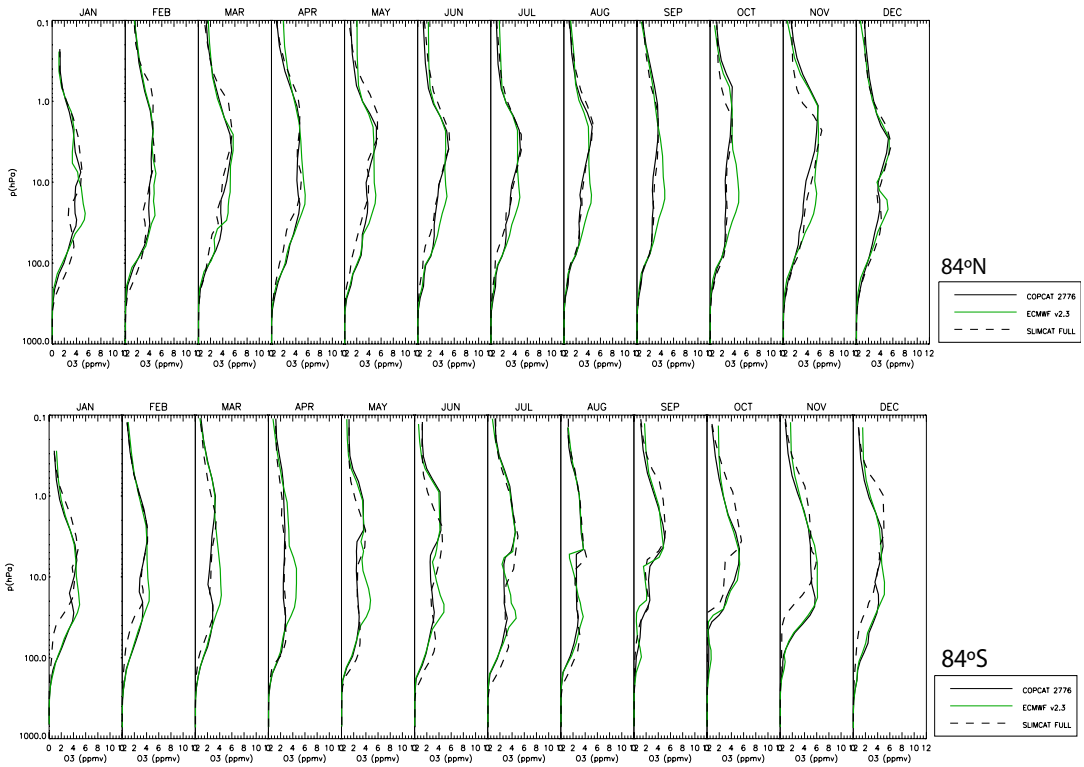

Figure 6.14: *January to December 2000 O_3 (ppmv) profiles, on the 15th of each month, from SLIMCAT runs using the COPCAT scheme (black solid line), full-chemistry (black dashed line) and ECWMF v2.3 scheme (green line), at 84°N (top) and 84°S (bottom).*

is found in summer. The agreement over the tropics (Figure 6.16) is very good except for the fact that the maximum value around 10 hPa is underestimated by the parameterisation.

The annual mean cross-sections from the COPCAT and ECMWF schemes as well as the SLIMCAT full-chemistry and HALOE observations for year 2000 can be seen in Figure 6.17. The general features are well reproduced, although all model simulations underestimate the tropical maximum compared to HALOE. COPCAT provides concentrations ∼1ppmv lower than the full-chemistry over the tropics and subtropics. The fact that the ECMWF scheme run in SLIMCAT gives higher maximum values than COPCAT (1 ppmv higher) suggests that the underestimation of

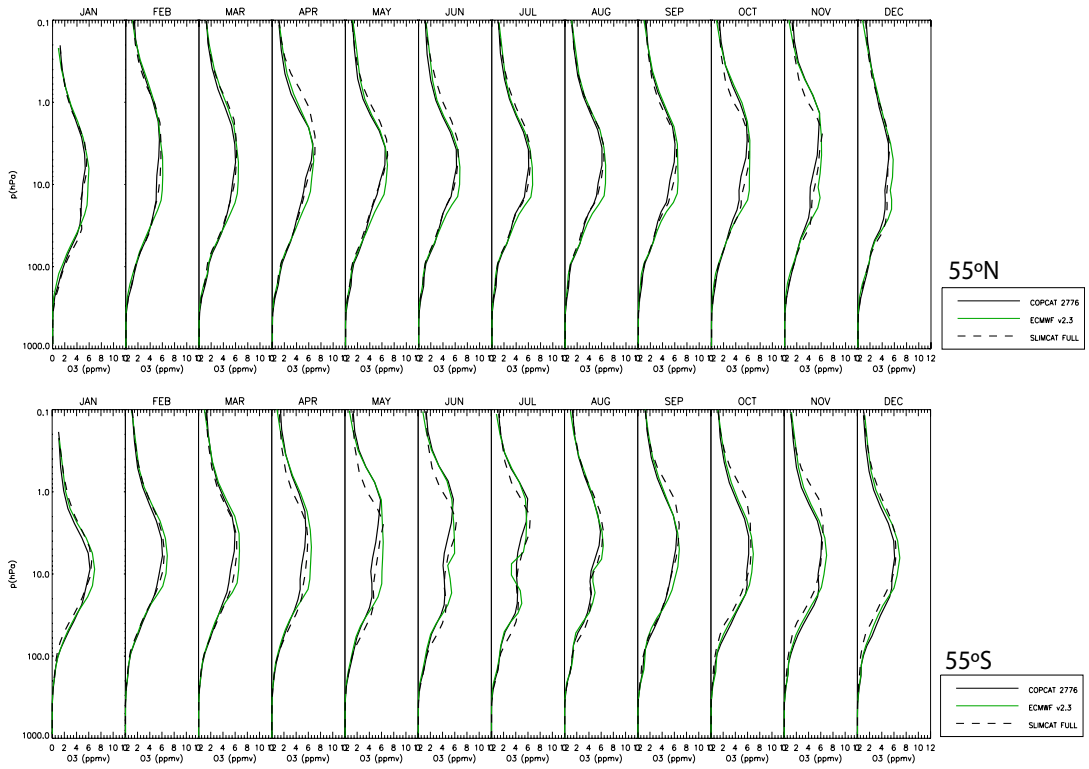

Figure 6.15: *As for Figure 6.14 but for 55°N (top) and 55°S (bottom).*

the tropical maximum may be related to the O_3 reference state ($\bar{f}$) used. In the case of COPCAT $\bar{f}$ comes from the full-chemistry run (Section 6.3), which is already lower than the observations. The second right-hand term in equation (6.1) establishes the upper limit to the contribution of this term to be the reference state $\bar{f}$; as c_1 is always negative, when the model O_3 (f) is over $\bar{f}$ this term starts to remove O_3.

Figure 6.18 is analogous to Figure 6.16 but in this case the COPCAT reference state has been replaced with that included in the CHEM2D scheme. The CHEM2D $\bar{f}$ field corresponds to the Fortuin and Kelder (1998) O_3 climatology. Results from Figure 6.18 show that using a different O_3 climatology does affect the maximum peak value over the tropics, and also adds ozone above 10 hPa, compared to the run using the default COPCAT $\bar{f}$ (Figure 6.16). With the CHEM2D climatology COPCAT results are closer to those with ECMWF scheme for levels above 10 hPa. Using the CHEM2D climatology improves results at low/mid latitudes and differences

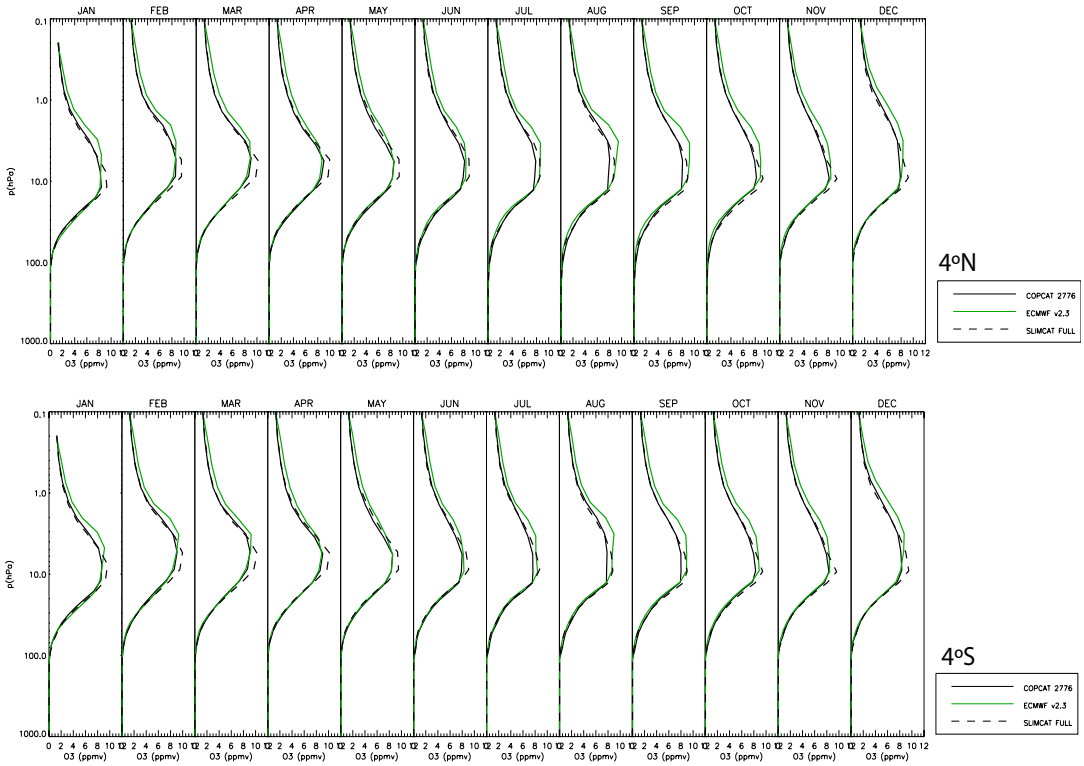

Figure 6.16: *January to December 2000 O_3 (ppmv) profiles from SLIMCAT runs using the COPCAT scheme (black solid line), full-chemistry (black dashed line) and ECWMF v2.3 scheme (green line), at 4°N (top) and 4°S (bottom).*

with TOMS are reduced (Figure 6.19c). However, the Antarctic ozone depletion is simulated worse with this climatology, the minimum in September-October is around 60 DU higher with the CHEM2D climatology. These results indicate the relevance of the climatology/reference state choice. With the appropriate reference state (*i.e.* based on observations or a better full-chemistry run) COPCAT would be able to provide more realistic O_3 distributions for all latitudes.

6.5 Comparison with ECMWF operational scheme

Although some comparisons have already been discussed above, the COPCAT scheme is compared here in more detail against the current ECMWF operational scheme (also denoted here v2.3 after the version of coefficients provided by Météo France).

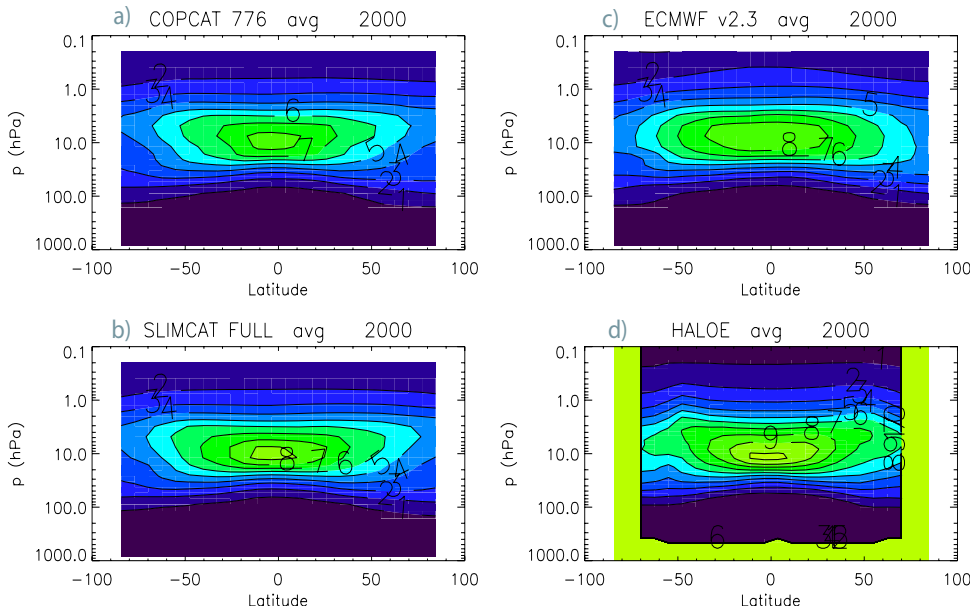

Figure 6.17: *Annual mean 2000 O_3 (ppmv) cross-section from (a) COPCAT, (b) SLIMCAT full-chemistry, (c) ECMWF v2.3 and (d) HALOE. Contour values are 1 ppmv.*

6.5.1 Total ozone column

The Jan-Dec evolution of the total O_3 column simulated by the ECMWF scheme in SLIMCAT is shown in Figure 6.13c; differences with the SLIMCAT full-chemistry run are plotted in Figure 6.13d. At low and mid latitudes, the ECMWF scheme produces larger underestimations with respect to the full-chemistry run than COPCAT. At high latitudes, the maximum differences are smaller than for COPCAT, however, the regions and times where such differences occur are much more widespread for the ECMWF scheme, another indication of the inaccuracy of the heterogeneous term in the ECMWF parameterisation.

Figure 6.19 shows total O_3 column differences between SLIMCAT runs using COPCAT and ECMWF ozone schemes and TOMS for year 2000. Over the tropics both schemes underestimate column values, simulating up to 30 DU less than observed. Over northern mid-latitudes the differences are smaller for the ECMWF

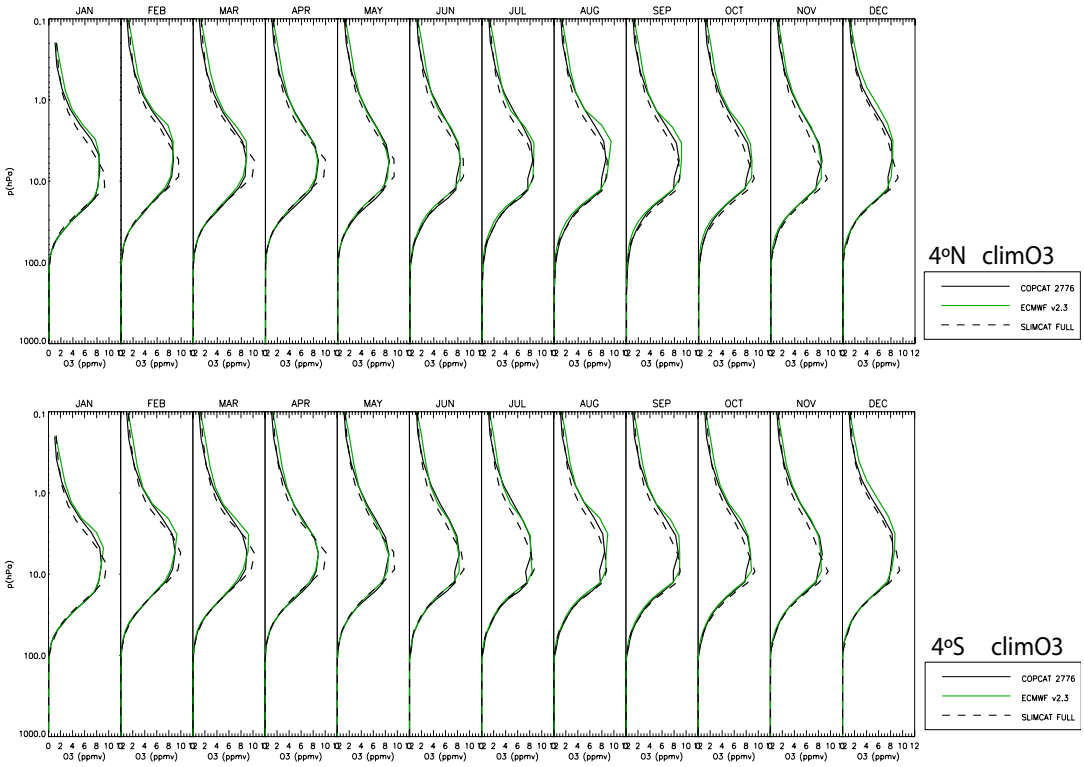

Figure 6.18: *As Figure 6.16 but in this case the climatology used in CHEM2D scheme (Fortuin and Kelder, 1998) has been used for* $\bar{f}$.

scheme, but over the Arctic COPCAT provides the distribution in better agreement with TOMS, although still overestimating column values. In the Antarctic, COPCAT gives better results for the first months of the year, for October-December, however, COPCAT underestimates column values. Further comparisons at polar latitudes, including the extent of the simulated ozone hole, can be found in Section 6.6.

6.5.2 Vertical structure

Like COPCAT, the ECMWF scheme underestimates the tropical maximum with respect to full chemistry (Figure 6.16). Nevertheless, ECMWF concentrations are ∼1ppmv higher than COPCAT at and above 10 hPa. The annual mean zonal mean ECMWF O_3 distribution (Figure 6.17c) also shows this; the ECMWF O_3 maximum centred at 10 hPa is larger than in the COPCAT simulation (Figure 6.17a) for all

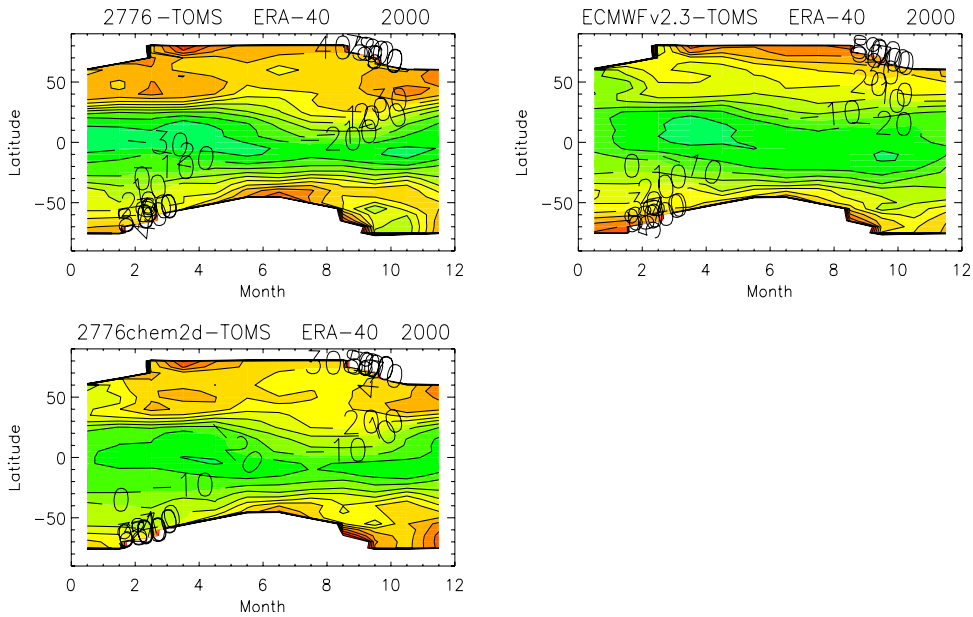

Figure 6.19: *Total O_3 column differences (DU) with respect to TOMS for SLIMCAT runs using (a) the COPCAT scheme, (b) the ECMWF v2.3 scheme and (c) the COPCAT scheme with the CHEM2D $\bar{f}$ climatology. Simulations use ERA-40 winds for year 2000. Contour interval is 10 DU.*

latitudes, although lower than the full-chemistry run (Figure 6.17b) over tropics and midlatitudes. All model simulations give lower maximum values than HALOE (Figure 6.17d), at all HALOE latitudes (70°N-70°S).

At midlatitudes, the ECMWF scheme shows similar features to COPCAT in the upper stratosphere (Figure 6.15), underestimating O_3 by ∼1 ppmv in spring and overestmating it in autumn, compared to full-chemistry. In the middle stratosphere, ECMWF produces more O_3 than COPCAT or the full-chemistry at 55°N and 55°S. In the NH mid-latitudes LS region both parameterisations behave in a similar way, in good agreement with full-chemistry. At 55°S, differences between the ECMWF scheme and COPCAT are larger than at 55°N between 2-50 hPa. At this altitude range the ECMWF scheme overestimates O_3 with respect to the full-chemistry (while COPCAT tends to underestimate it). The only exception to this

happens in July at 10 hPa, where the ECMWF schemes presents a very pronounced minimum, unlikely to correspond to a real feature.

At NH high latitudes (Figure 6.14) the ECMWF scheme simulates too high O_3 in the mid/lower stratosphere compared to both the full-chemistry and COPCAT, the differences are larger in autumn and winter (up to 2 ppmv higher in September, October and January), but are present for all months. At this altitude range ECMWF O_3 is also larger than HALOE (0.5-1.0 ppmv higher) at high/mid latitudes, while at the SH it is lower than HALOE (Figure 6.17). The differences in the mid/lower stratosphere between ECMWF ozone and COPCAT or full-chemistry are larger in the Antarctic region. From September to November the ECMWF scheme in the LS ($\sim$100 hPa) is higher than SLIMCAT full-chemistry or parameterisation. This explains that the ozone hole in Figure 6.13c shows higher values than using the COPCAT scheme (Figure 6.13b). Vertical features above 100 hPa also differ, with ECMWF O_3 being larger overall.

As discussed in Section 6.4, the use of a different O_3 climatology changed COPCAT tropical profiles above 10 hPa. Therefore, at low latitudes the different reference state $\bar{f}$ used in the ECMWF and COPCAT schemes might be playing the fundamental role in explaining the differences. At high latitudes, the heterogenous chemistry treatment is the most probable cause of discrepancy between both schemes. However, at mid-latitudes both factors play important roles and it is difficult to deduce why both schemes differ there.

6.6 Polar loss with COPCAT

This section compares COPCAT ability to simulate O_3 destruction at high latitudes with that of the full-chemistry and the ECMWF scheme. Since the treatment each of these models give to heterogenous chemistry is very different, a brief discussion on the heterogeneous chemistry approaches is also given below.

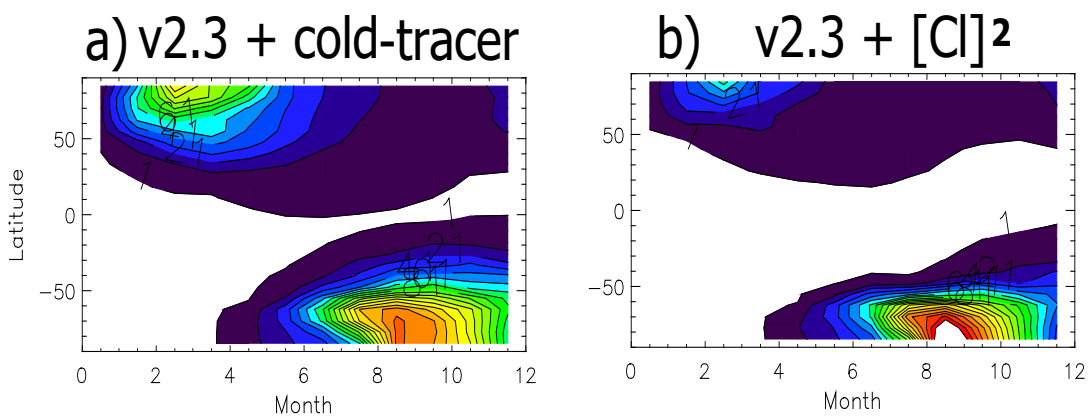

Figure 6.20: *January-December 2000 O_3 column loss (DU) produced by SLIMCAT runs using (a) the gas-phase ECMWF scheme with an additional cold-tracer and (b) the ECMWF scheme with its default heterogenous term. The CTM runs use ERA-40 winds and temperatures. Contour interval is 10 DU.*

6.6.1 Heterogeneous chemistry treatments

Local T term

The ECMWF operational scheme includes one extra term depending on temperature and chlorine content to simulate heterogeneous O_3 loss (Section 5.3 in Chapter 5). However, as already discussed in Chapter 5, this kind of approach is inaccurate in the quadratic dependence it includes, the assumption that all loss takes place within the low temperature region, and the neglect of any heterogeneous process outside the polar regions. Figure 6.20b shows the heterogeneous column loss produced by the ECMWF term in a SLIMCAT simulation. Not enough loss takes place in the Arctic, and compared to the performance of a cold-tracer (Figure 6.20a), the Antarctic region where loss occurs is too restricted.

Cold-tracer term

A cold-tracer approach (Section 5.3.3 in Chapter 5) is more realistic than the ECMWF term as it is also able to simulate loss occuring outside the low temperature region. This is particularly relevant for the Arctic, due to the lower stability

of the vortex. Figure 6.20a, shows the loss simulated by a cold-tracer added to the ECMWF scheme instead of its default heterogeneous term. The cold-tracer simulates over 80 DU more loss over the Arctic, and the areas where loss occurs are expanded in both the Arctic and the Antarctic. The Antarctic hole is, however, not deep enough in the cold-tracer run. This is due to the activation/deactivation parameters used not being able to simulate enough destruction for year 2000 Antarctic conditions. In the run shown in Figure 6.20a, the time that takes for the air to start being processed has been fixed to 8 hours and a deactivation constant of 10 days has also been used. The deactivation constant should probably be longer, in Cariolle and Teyssèdre (2007) the deactivation constant is considered equal to the HNO_3 lifetime, which at ∼20 km corresponds to nearly 20 days for SH subpolar latitudes in September.

A cold-tracer is therefore more realistic than the ECMWF heterogenous term, but this kind of tracer requires an accurate tuning in order to provide realistic O_3 destruction and, as meteorological and chemical conditions change, the same cold-tracer parameters would not be equally valid for every year.

Implicit heterogenous chemistry

The original Cariolle and Déqué (1986) scheme (CD scheme) did not include heterogeneous effects because their importance was still unknown at the time. Subsequent O_3 schemes based on the CD approach chose not to include heterogenous chemistry due to the non-linearity of the reactions involved (Cariolle and Teyssèdre, 2007) or to the lack of complete heterogenous chemistry in the photochemical model used to calculate the coefficients (McLinden *et al.*, 2000; McCormack *et al.*, 2006). The SLIMCAT CTM on which the COPCAT scheme is based includes complete heterogeneous chemistry and, as it is shown in Section 6.7, the linearity of the scheme is still a good approximation for a reasonable range of temperature and O_3 values. Therefore, the implicit treatment of heterogeneous chemistry in the coefficients calulation (Section 6.3) is considered as the most natural way of including heterogeneous

processes. As discussed in Chapter 5 heterogeneous chemistry reactions take place not only over the poles and not only during winter/spring. Thus, for the present atmospheric chemistry understanding, separating gas-phase chemistry and heterogeneous chemistry in a current full-chemistry model is not a realistic approach. The implicit heterogeneous treatment also ensures that all the revisions and improvements made to the full-chemistry model will be also reflected in subsequent versions of the COPCAT scheme.

6.6.2 Arctic loss

Figures 6.21a and 6.21b show TO column Jan-Dec 2000 at 85°N and 75°N, respectively. The SLIMCAT simulations plotted use the COPCAT scheme, the ECMWF scheme or the full-chemistry. The two parameterisations result in too large column values compared to the full-chemistry and TOMS. From January to May the COPCAT scheme values are higher than for the ECMWF scheme, while in summer and autumn COPCAT column is more realistic.

6.6.3 Antarctic ozone hole

In the Antarctic COPCAT column values are very close to full-chemistry (Figures 6.21c and 6.21d). The ozone hole in September-October is beter represented by COPCAT than by the ECMWF scheme and, based on the few TOMS observations available at 75°S, COPCAT is also closer to the satellite measurements. In particular, the ECMWF scheme produces too high column values during January-August. These results are a further proof of the suitability of the implicit heterogenous chemistry approach.

6.7 Validity of linear approximation

Despite the nonlinear interactions involved in O_3 chemistry (both homogeneous and heterogeneous), the validity of the linear approximation in the schemes based on the CD approach has been shown in the literature. For the original version (Cariolle

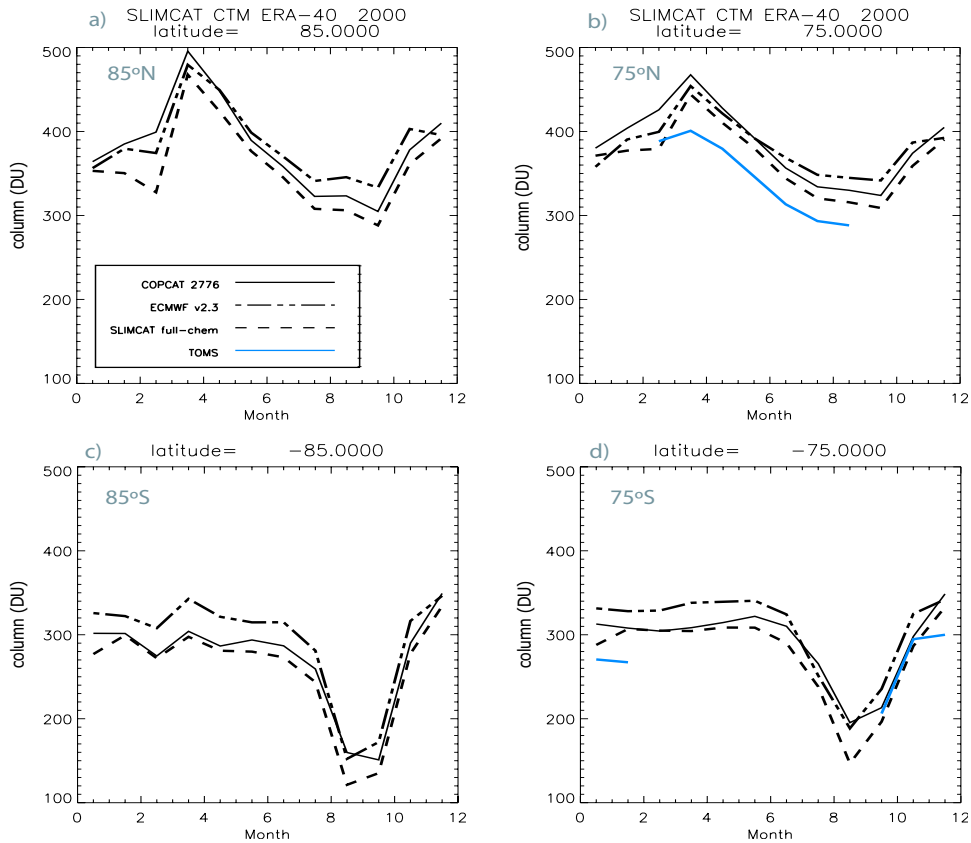

Figure 6.21: *Total ozone column (DU) time series Jan-Dec 2000 at (a) 85°N, (b) 75°N, (c) 85°S and (d) 75°S. Results are from SLIMCAT simulations using ERA-40 winds and O_3 from COPCAT (solid black line), ECMWF v2.3 (dot-dashed line) and full-chemistry (dashed line). TOMS data are also included at 75°N and 75°S from spring to autumn (blue line).*

and Déqué, 1986) the differences between the linear tendency in f and the real tendency were found to be less than 1% for variations of ±20% in the value of f. For LINOZ McLinden *et al.* (2000) showed the deviations $(P - L)$ presented from the linear tendencies with respect to f, c_{O_3} and T, such deviations were low enough to consider the linear approximation valid for the usual range of variability observed in GCMs. Also McCormack *et al.* (2006), showed the linearity in CHEM2D was valid for variations of ± 20 K in temperature and ±50% in ozone column. Analysing the linear approximation in the COPCAT scheme is also necessary, since the previous schemes did not include the polar heterogeneous chemistry implicitly, and only

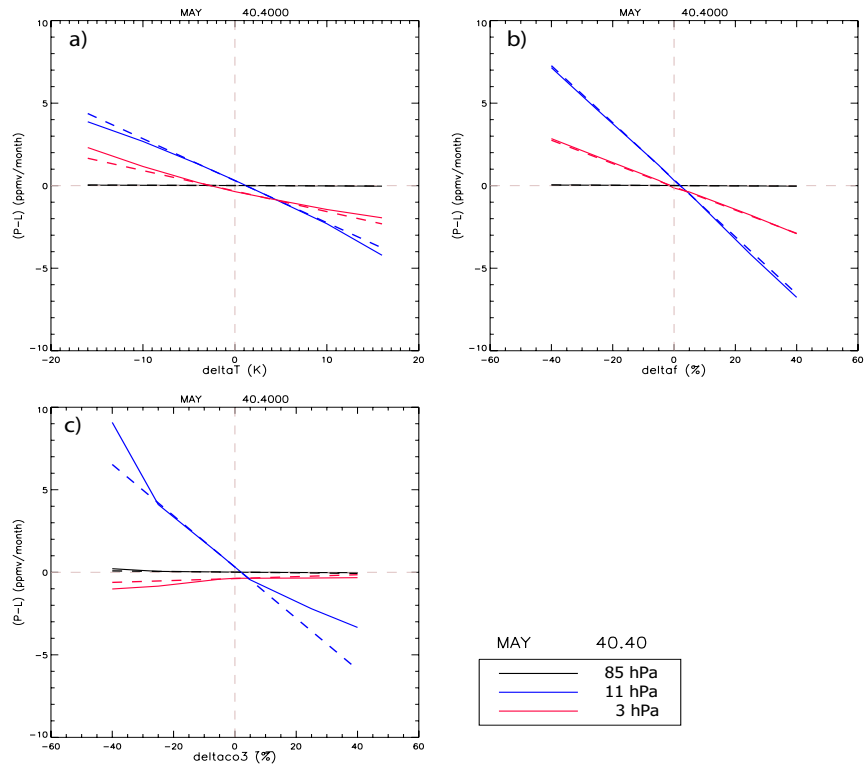

Figure 6.22: *COPCAT (P-L) values as a function of the perturbation in (a) temperature, (b) local ozone and (c) column above at 40°N in May. Pressure levels shown are 85 hPa (black), 11 hPa (blue) and 3 hPa (red). Solid lines correpond to the exact tendencies; dashed lines correspond to the least squares fit for the perturbation values used for COPCAT coefficients (Section 6.3). To show all results within the same vertical axis, those for the 3 hPa level have been scaled by 0.1, 0.25 and 0.1 for T, f and c_{O_3} respectively.*

LINOZ included processes on binary sulfate aerosols.

Figure 6.22 plots the COPCAT (P-L) values as a function of perturbation of local ozone f, temperature T and column above c_{O_3} for three vertical levels, at 40°N in May. The range of variation, with respect to the reference state, chosen for the three variables are ±40% in local ozone and column and ±16 K in temperature. The vertical levels represented correspond to 85 hPa, 11 hPa and 3 hPa. The exact tendency has been represented together with the linear squares fit to the

points used to obtain the COPCAT coefficients (Section 6.3). The linearisation is a good approximation for the three variables in the shown ranges and only the dependence with c_{O_3} shows some non-linearity for column variations larger than ±20%.

The level of agreement with the linear approximation shown in Figure 6.22 is similar for other months and latitudes, except for polar LS regions in spring. Figure 6.23 evaluates the linear approximation in the LS at 84°S in September. The linearity of the scheme is still good for the O_3 variables (local and column above), however, variations in temperature larger than 10 K take $(P - L)$ outside the linear COPCAT range. From Figure 6.23a it can be seen that the control run in the coefficients calculation ($\Delta T = 0$) is already under PSC conditions (negative $(P - L)$); further lowering T causes more loss, while increasing T reduces the amount of loss. This shows that the threshold for further PSC activation due to denitrification is actually a smooth threshold.

These results show that the linear approximation is also a good estimation for the scheme developed in this chapter. In spite of including heterogeneous chemistry implicitly COPCAT agrees with a linear approximation for local ozone variations of up to ±40%, column ozone c_{O_3} variations of ±20% and temperature variations of ±10 K for all latitudes and months; the range expands further for regions and times outside the maximum polar loss.

To ensure that the variations are within the range considered above, attention must also be paid when choosing the reference states (or climatologies). Also, perhaps the inclusion of higher order terms for the temperature dependency would be a better option to ensure the accuracy of the scheme in polar regions. This would not increase much the cost of the scheme, as it would only mean the coefficients files to be read-in would contain more data.

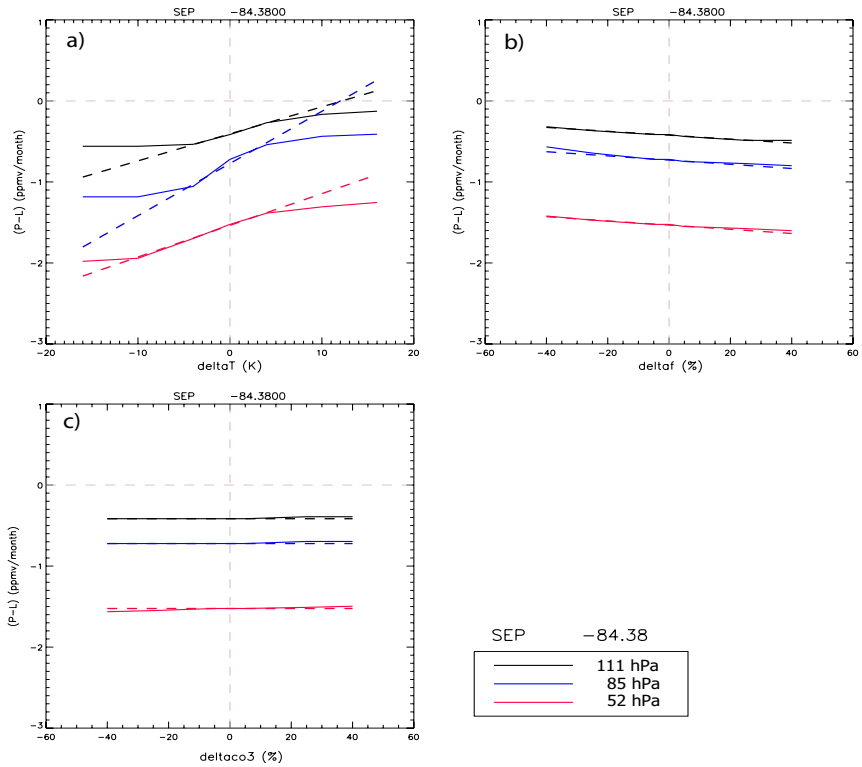

Figure 6.23: *Same as Figure 6.22 but for the LS at 84°S in September. Represented pressure levels are now 111 hPa (black), 85 hPa (blue) and 52 hPa (red).*

6.8 Conclusions

The scope of this chapter was testing the current ECMWF O_3 scheme, and suggesting improvements for the weaknesses such scheme presents. For this, a new O_3 parameterisation scheme (COPCAT) was developed with implicit heterogeneous chemistry. The inclusion of heterogenous processes has been presented as a suitable improvement for schemes based on the linear Cariolle and Déqué approach, such as the operational ECMWF scheme.

The new scheme has been obtained from SLIMCAT full-chemistry runs, and has been tested within the same CTM, which has allowed the isolation of chemistry differences from other factors, such as numerics, resolution or transport. COPCAT runs have also been compared to equivalent SLIMCAT runs using the operational

ECMWF scheme.

The quality of the SLIMCAT full-chemistry model has been widely shown in numerous stratospheric published studies. Obtaining a parameterisation based on a widely tested CTM is important to evaluate and understand differences with the full-chemistry. Moreover, the approach adopted here ensures that the parameterisation obtained is as close as possible to a state-of-the-art full-chemistry CTM.

COPCAT is in good overall agreement with SLIMCAT full-chemistry, although a significant reduction in the tropical maximum O_3 at 10 hPa occurs when using the parameterisation. A similar, although smaller, reduction takes place when using the ECMWF scheme in a SLIMCAT run, which identifies a drawback of this kind of scheme with respect to full-chemistry models. Results have also shown the relevance of the reference state (climatologies) choice; using the Fortuin and Kelder (1998) O_3 climatology the tropical differences against observations have been reduced for COPCAT runs.

The heterogenous treatment adopted by COPCAT avoids the inaccuracies of the ECMWF heterogenous term and the uncertainties of a cold-tracer, and has provided the scheme with a realistic polar loss simulation. The new scheme is able to reproduce a realistic Antarctic ozone hole, and also over northern high latitudes COPCAT is more realistic than the ECMWF scheme. Both treatments involve approximations, however, COPCAT has shown that heterogenous chemistry can be included in the parameterisation consistently with the rest of the chemistry, without any additional tunable parameter.

The inclusion of heterogenous chemistry in the scheme has not been detrimental for the linearity of the approach. Only at polar latitudes is the range of temperatures for which the linear approximation is a good estimation somewhat restricted. Such temperature range ($\pm$10K from the reference state) is still within the typical

variation range observed in global models, however, to ensure the accuracy of the scheme under all possible polar vortex conditions higher order terms could be included as a future improvement to the scheme.

The accuracy of COPCAT could also be improved by increasing vertical resolution and adding longitudinal variability to the coefficients calculation, and computing zonal means afterwards. This would help to capture features, *e.g.* at the edge of the polar vortex, that can be neglected when deriving the coefficients from zonal averaged runs. The increase in vertical resolution would help to better resolve the LS region, which is probably affecting column values in the run 323 used in this chapter. The coefficients could also be provided twice a month instead of monthly. This would increase the accuracy over spring polar regions; coefficients on the 15th March/September do not provide realistic loss rates for the sunlight levels found later in the month in the Arctic/Antarctic regions.

The good agreement COPCAT presents with SLIMCAT full-chemistry is encouraging and shows the scheme as a promising alternative to the use of parameterisations treating separately gas-phase and heterogeneous chemistry. Moreover, as the full chemistry SLIMCAT model is continuously subject to revisions and improvments, following versions of COPCAT would benefit from the same developments included in the CTM. The approach shown in this chapter would also be appropriate when full-chemistry models become operational, for a fully consistent way to obtain the O_3 parameterisation.

Chapter 7

CoMeCAT: Methane Scheme from TOMCAT/SLIMCAT Runs

7.1 Introduction

This chapter presents a new parameterisation for stratospheric CH_4 and explores its performance in a 3D CTM and a GCM. The CH_4 scheme is also used to parameterise a source of stratospheric water vapour. The impact of the coupled scheme on the GCM radiation and temperature fields is also evaluated.

The CoMeCAT CH_4 scheme is introduced in Section 7.2, details on the scheme calculation are given in Section 7.3, while the derived water scheme is described in Section 7.4. Information on the observations used to validate the model results is found in Section 7.5. Results obtained with the CoMeCAT scheme implemented in the CTM and in the GCM are discussed in Sections 7.6 and 7.7 respectively. Section 7.8 discusses the H_2O scheme performance within the GCM, and conclusions are presented in Section 7.9.

7.2 Linear approach for methane

Methane is produced at the Earth's surface through human and natural activities, and transported into the stratosphere mainly through the tropical tropopause. Unlike O_3, CH_4 in the stratosphere is only destroyed by oxidation with OH, O(^{1}D) and Cl. Therefore, the time tendency of stratospheric CH_4 due to chemistry corresponds to

$$\frac{\partial[CH_4]}{\partial t} = -L[CH_4] \tag{7.1}$$

where [ ] indicates concentrations (*e.g.* vmr) and L is the CH_4 loss rate (s^{-1}).

The three main reactions for the destruction of methane in the stratosphere are shown in equation (5.13). Based on such reactions, the oxidation rate of CH_4 can be written as

$$L = k_1[OH] + k_2[O(^1D)] + k_3[Cl] \tag{7.2}$$

The effective rate constants k_i (i=1, 2, 3), given in (cm^3 molecule$^{-1}s^{-1}$), can be expressed in the form

$$k_i = A \cdot exp(-E_a/RT) \tag{7.3}$$

where E_a is the activation energy of the reaction, T is temperature, R is the gas constant, and the factor A has units of (cm^3 molecule$^{-1}s^{-1}$). Values for A and E_a/R are tabulated for second order reactions; in this thesis the values in JPL2003 (Sander *et al.*, 2003) have been used.

Full chemistry models such as SLIMCAT calculate the oxidation rate in equation (7.2) analytically from the involved reactions. However, in order to provide NWP models with a simplified methane scheme, an alternative approach has been explored here. The new scheme parameterises the loss rate L instead of parameterising [CH_4] directly. Since the three reactions involved in CH_4 destruction depend on [CH_4]

and temperature (T), one can parameterise L following a scheme similar to the CD scheme for the ozone tendency:

$$L(CH_4, T) = c_0 + c_1([CH_4] - \overline{[CH_4]}) + c_2(T - \overline{T}) \tag{7.4}$$

In this case the coefficients c_i are

$$\begin{aligned} c_0 &= L_0 \\ c_1 &= \left.\frac{\partial L}{\partial [CH_4]}\right|_0 \\ c_2 &= \left.\frac{\partial L}{\partial T}\right|_0 \end{aligned} \tag{7.5}$$

L_0 is the loss rate for a given reference state (all subscripts 0 indicate values obtained at a reference state), c_1 represents how the loss rate adjusts with changes in the CH_4 concentration, while c_2 relates variations in temperature with changes in L. Unlike for the O_3 scheme (Chapter 6), the partial column above (c_{O_3}) term has not been included for the CH_4 loss parameterisation. Such a term considers the effects of changes in the amount of UV reaching the considered air parcel. The amount of UV light will only affect the photolysis reactions and, in the stratosphere, CH_4 loss is dominated by oxidation. This UV term will be of more importance in the mesosphere where the CH_4 destruction is led by photolysis. For this reason the weight of this term is expected to be much smaller than the other terms in the case of CH_4 and has not been included in equation (7.4). Ozone has an indirect effect on CH_4 destruction via OH. Ozone photodissociation produces $O(^1D)$ that recombines with H_2O to produce OH, which is one of the main sinks of stratospheric CH_4 as stated by equation (5.13). However, since it is the loss rate L, and not directly CH_4, that is parameterised, this effect is already taken into account in L (equation 7.2). The CH_4 scheme derived here has been called CoMeCAT (Coefficients for Methane from a Chemistry And Transport model).

7.3 CoMeCAT scheme: calculation and coefficients

The coefficients for the CH_4 scheme CoMeCAT can be obtained from a full-chemistry 3D CTM in a similar way as it was done for O_3. Here several runs of the SLIMCAT box model have been used to obtain the different coefficients in equation (7.5).

7.3.1 Calculation methodology

The box model was initialised from the zonal mean of the output of a 3D SLIMCAT full-chemistry run corresponding to the 15th of each month. The SLIMCAT 3D run used ECMWF operational winds for the year 2004. The model resolution is 24 latitudes and 24 levels (from the surface up to $\sim$ 60km), for both the 3D initial state and the box model. All the runs carried out with the box model are 2-day long, with a chemical time step of 20 minutes.

The reference loss rate L_0, is obtained from a control run in which the zonal 3D output is used without alteration to initialise the box model. The loss rate L is calulated from the three chemical reactions in equation (5.13) and the average over the second day is taken as the value of L_0 (coefficient c_0). For the reference state values of $\overline{[CH_4]}$ and $\overline{T}$ those from the SLIMCAT initial state are taken.

Then perturbed runs of the box model are carried out to obtain each of the coefficients c_1 and c_2 (two perturbed runs per coefficient). To obtain c_1 variations in $[CH_4]$ of $\pm$ 5% with respect to the reference state are introduced; and variations of $\pm$ 4 K to obtain c_2. Again, the values used to compute the tendencies are those averaged over the last day of the runs. For the runs aimed at obtaining c_1, all radical chemical species but CH_4 are overwritten at every time step with their values at the end of the control run; to obtain c_2 CH_4 is also overwritten. In this way a set of coefficients is obtained for each latitude, level and month of the year. The coefficients and climatologies are provided as 5 look-up tables (c_0, c_1, c_2, $\overline{[CH_4]}$ and $\overline{T}$) for every month.

7.3.2 The new CH_4 coefficients

Figure 7.1 plots the zonal mean of the reference values for $\overline{[CH_4]}$ and $\overline{T}$ for January and July. Stratospheric CH_4 in the full-chemistry SLIMCAT has been widely validated, for instance it compares very well with MIPAS observations (Kouker and Coauthors, 2005). The temperature field corresponds to OPER 2004 but interpolated onto the CTM latitudes and levels; it presents the same general features than ECMWF operational temperatures (Chapter 2).

The CoMeCAT lifetime, τ, zonal mean distribution is plotted in Figure 7.2 for January, April, July and October. The minimum lifetime values are reached at ∼1hPa and are almost 1 year over the summer pole, region where the maximum CH_4 loss rate takes place. Above 1hPa, CH_4 loss decreases (lifetime increases) due to the decrease in the abundance of OH. The lifetime values in Figure 7.2 are in overall agreement with those in Brasseur and Solomon (2005).

Methane time tendency is controlled by the first coefficient c_0 and the other terms add corrections due to changes in CH_4 and temperature. Figure 7.3 shows the impact that changes in CH_4 concentrations have on the loss rate for the months of January, April, July and October. Similarly, Figure 7.4 shows how temperature changes feedback on the loss rate. The minus sign in equation (7.1) has been included when calculating the coefficients c_i, so the scheme actually parameterises $L' = -L$. In the middle stratosphere, an increase in CH_4 concentration causes a decrease in loss rate L (Figure 7.3), a CH_4 increase implies a decrease of ClO at around 40 km and an overall decrease of HO_x, which leads to a decrease in CH_4 loss. The opposite effect occurs in the LS region and above the stratopause, where a CH_4 increase means an increased loss rate.

The values of c_2 are negative everywhere except in the equatorial LS (between 100-200 hPa) and in the Arctic summer LS (Figure 7.4). The negative sign agrees with the fact that by increasing temperature, k_i in equation (7.3) increases, which ac-

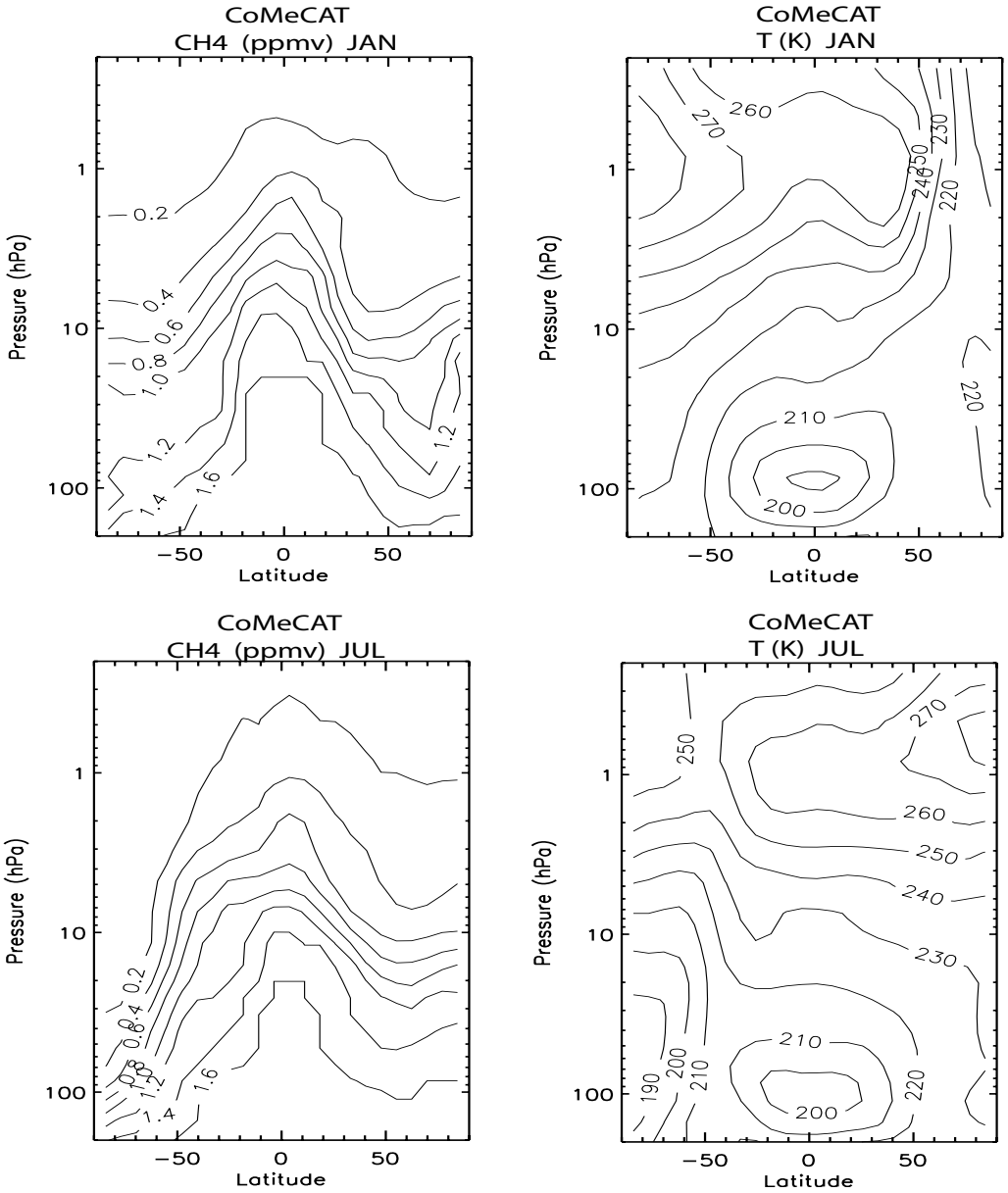

Figure 7.1: *Zonal mean of CoMeCAT (a)* $\overline{[CH_4]}$ *(ppmv) and (b) temperature (K) for January (top row) and July (bottom row).*

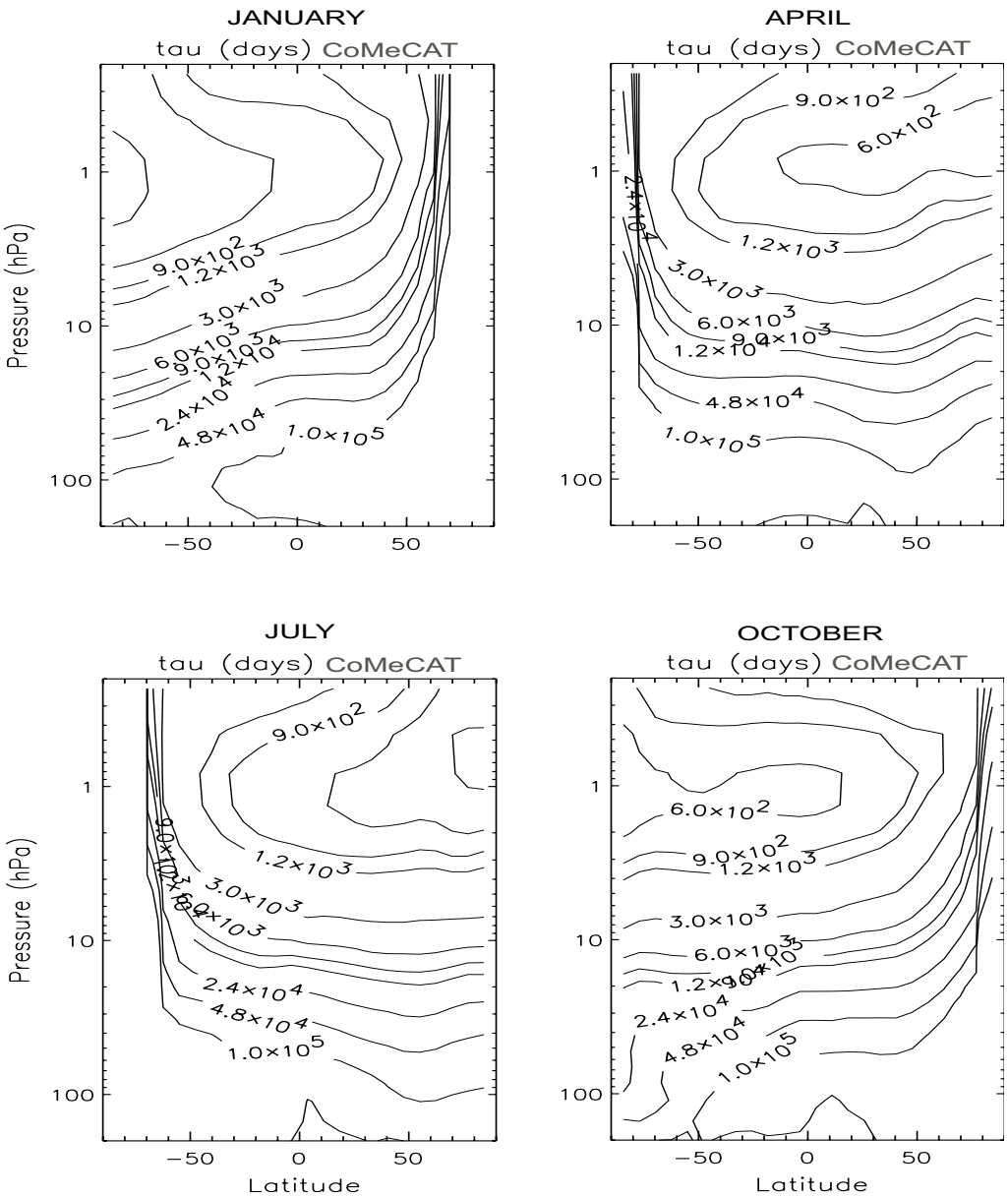

Figure 7.2: *Altitude/latitude distribution of CoMeCAT CH_4 lifetime values (in days) for January, April, July and October.*

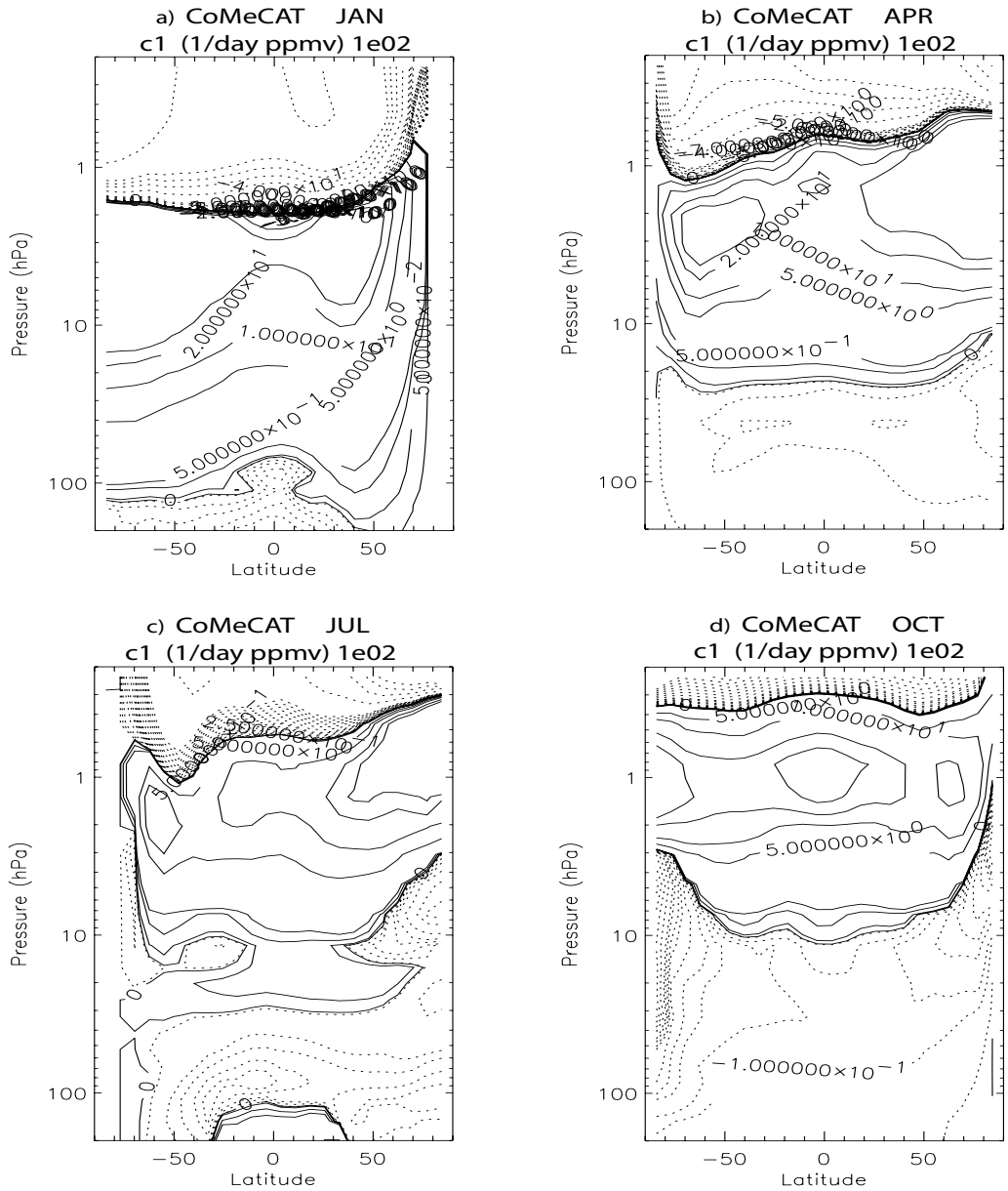

Figure 7.3: *Zonal distribution of the CoMeCAT loss tendency with [CH_4] (c_1) in units of (10 day^{-1}ppbv^{-1}) for (a) January, (b) April, (c) July and (d) October.*

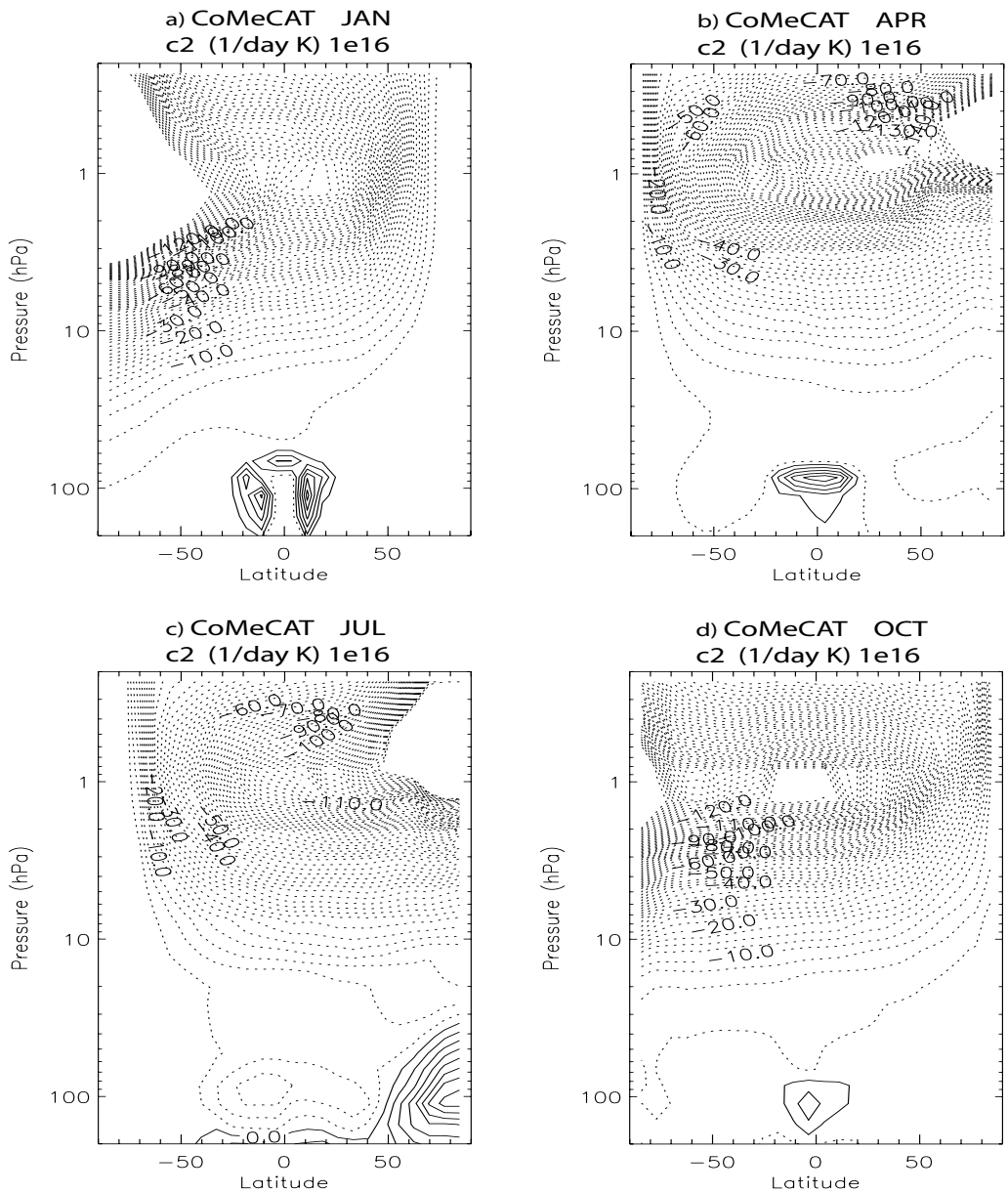

Figure 7.4: *Zonal distribution of the CoMeCAT loss tendency with temperature (c_2) in units of ($10^{16} day^{-1} K^{-1}$) for (a) January, (b) April, (c) July and (d) October. Contour value is 2.5 units.*

cording to equation (7.2) means more CH_4 loss. The decrease in loss over the Arctic summer (positive contours in Figure 7.4) might be explained by a secondary effect, coming from decreased OH concentrations, that outweighs the direct temperature effect in this region.

7.4 Scheme for water vapour

The final products of the CH_4 oxidation reactions in equation (5.13) are water vapour, molecular hydrogen and CO. As discussed in Chapter 5, the main source of stratospheric H_2O is the oxidation of methane (with an accuracy of 0.05 ppmv). Since CH_4 has no stratospheric source except entry through the tropopause, the CoMeCAT CH_4 scheme presented above can also be used to obtain H_2O tendencies in the stratosphere. Based on an approximation of equation (5.14) where the last two terms have been neglected, one can write

$$\frac{\partial[H_2O]}{\partial t} = -2\frac{\partial[CH_4]}{\partial t} \tag{7.6}$$

Such scheme has been implemented in SLIMCAT 3D runs, and ECMWF GCM runs, where CH_4 has been parameterised following the CoMeCAT approach and compared to H_2O observations (see Section 7.6.4).

7.5 HALOE observations of CH_4 and H_2O

The results of the model simulations have been validated against observations from the HALOE instrument on board the UARS satellite (Russell *et al.*, 1993) of CH_4 (Park *et al.*, 1996) and H_2O (Harries *et al.*, 1996). The observational data have been provided by W. Randel and F. Wu (from NCAR, USA), and correspond to the version 19 of HALOE public data release. These HALOE data are zonally averaged and are available for 41 latitudes (80°N-80°S), and 49 pressure levels (from 100-0.01 hPa); the monthly time series covers the period November 1991-November 2005. The accuracy for these CH_4 observations is better than 7% between 1-100

hPa (Park *et al.*, 1996) and 10 % for H_2O measurements at the same altitude range. Such HALOE data have been widely validated and have been used for several model results validation (*e.g.* Chipperfield *et al.* 2002; Bregman *et al.* 2006; Eyring *et al.* 2006; Feng *et al.* 2007).

7.6 CoMeCAT scheme performance in the SLIMCAT 3D CTM

In the 3D runs performed here the chemistry decks in the CTM have been switched off and replaced with the CoMeCAT scheme. Such runs include two tracers, one for CH_4 and one for H_2O, which follow the schemes described in equations (7.1) and (7.6), and are advected by the winds used to drive the model runs.

The CH_4 tracer in the 3D SLIMCAT runs was initialised with the concentrations from the reference climatology $[\overline{CH_4}]$. The same climatology was used to overwrite the tracer value at the surface at every time step, to prevent the surface values from drifting due to the lack of CH_4 sources in the model simulations. The initial values for the H_2O tracer were $7.0\times10^{-6} - 2[\overline{CH_4}]$. The results for H_2O are discussed in 7.6.4 at the end of this Section, first the CH_4 results are considered.

7.6.1 CoMeCAT against full-chemistry

Methane cross-sections

Methane distributions obtained with CoMeCAT for two different years (2000 and 2004) have been compared against the corresponding distributions from the SLIMCAT full-chemistry run 323. CoMeCAT and full-chemistry use the same ECMWF operational winds (ERA-40 2000 and OPER 2004). Figure 7.5 shows the annual means of the zonally averaged CH_4 concentrations from the parameterisation, the full-chemistry run and HALOE measurements above 100hPa. The CoMeCAT parameterisation is able to capture all general features and variability. The agreement

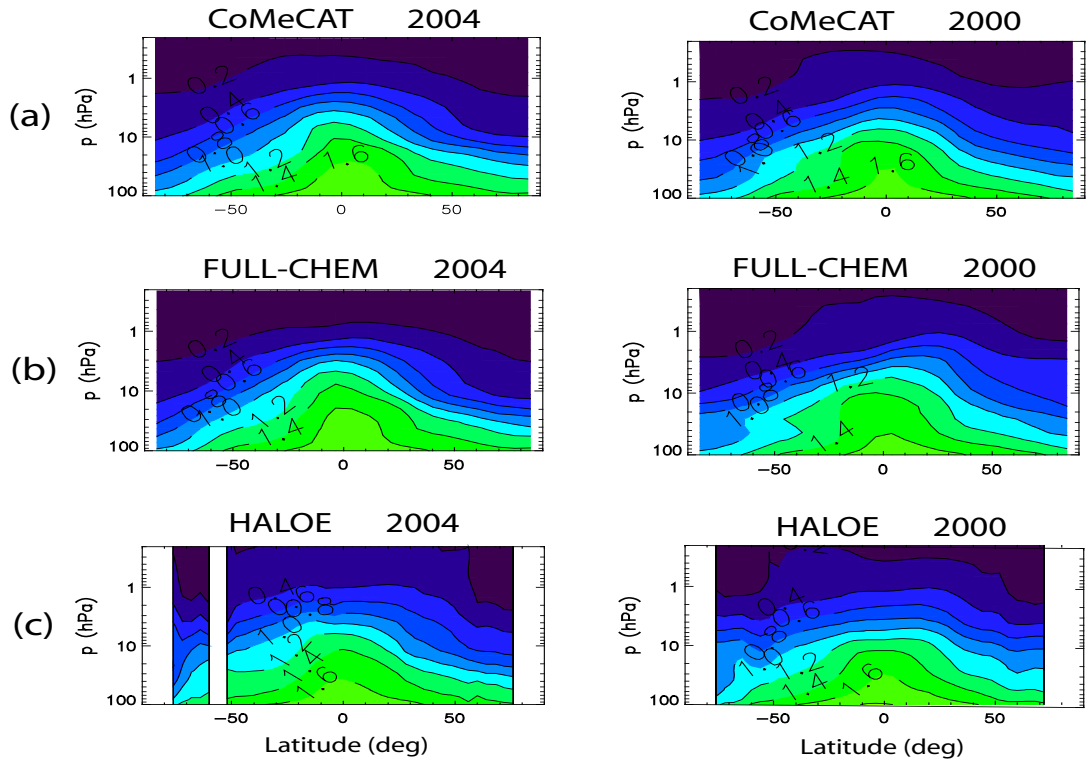

Figure 7.5: *Annual means for 2004 (left column) and 2000 (right column) of zonally averaged CH_4 distributions (ppmv) from (a) the CoMeCAT scheme, (b) a full-chemistry run of SLIMCAT (run323) and (c) HALOE observations. The model simulations use ERA-40 winds in 2000 and ECMWF operational winds in 2004.*

between CoMeCAT and full-chemistry is particularly good in 2004, explained by the fact that the parameterisation coefficients have been obtained from 2004 conditions (Section 7.2). To ensure the adaptability of the scheme its performance for a different year has also been checked. Also for 2000 the overall structure is very well simulated by CoMeCAT, although differences against the full-chemistry are now more obvious. There are differences over the tropics above 3 hPa, where the CoMeCAT CH_4 is slightly higher (<0.1ppmv), as well as in the NH high latiudes, where CoMeCAT simulates ∼0.2ppmv more than SLIMCAT full-chemistry between 5-10 hPa. The agreement with HALOE is good in both cases. In 2004 modelled concentrations, both CoMeCAT and full-chemistry, are ∼0.2 ppmv lower than HALOE in the upper most levels (above 1 hPa).

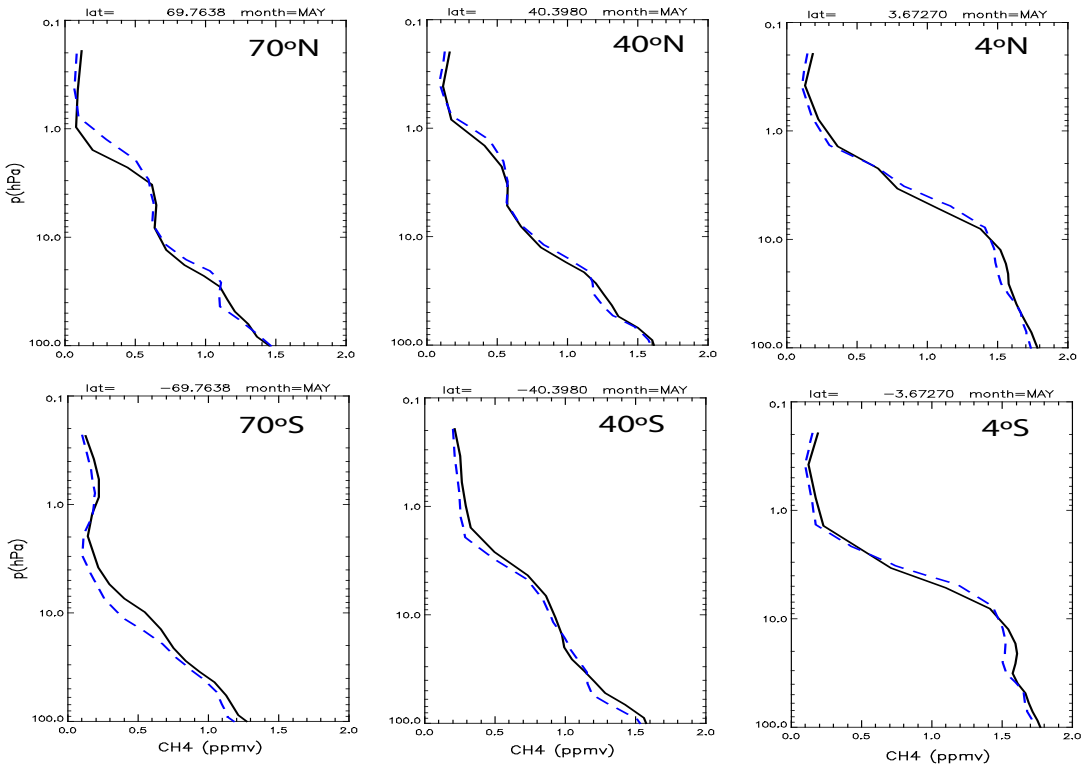

Figure 7.6: *Vertical profiles of CH_4 (ppmv) on the 15th May 2000 from the CoMeCAT scheme (black solid line) and the full-chemistry SLIMCAT run (blue dashed line). ERA-40 winds have been used for these simulations.*

Methane vertical profiles

To evaluate the ability of the CoMeCAT scheme to reproduce the vertical structure of CH_4, parameterisation profiles are validated against full-chemistry and HALOE observations. Vertical distributions from CoMeCAT and the full-chemistry run 323 between 100-0.2 hPa are shown in Figure 7.6 for the 15th May 2000. Both profiles are very close to each other, CoMeCAT reproduces the vertical gradients very well. The agreement is better over mid latitudes and the tropics, and overall better over the Northern Hemisphere. Larger differences are found over the SH high latitudes where the scheme produces a too linearly decreasing profile missing some of the full-chemistry features below 3hPa. The differences observed for May are representative of other months.

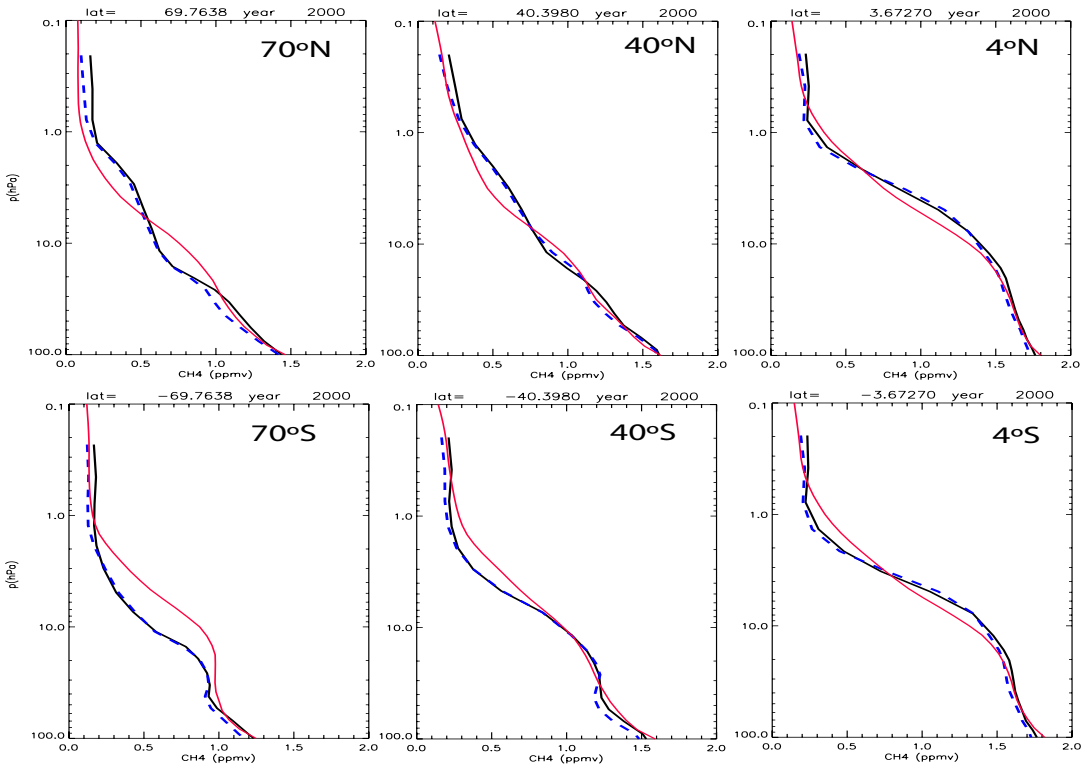

Figure 7.7: *Annual mean (year 2000) profiles of CH_4 (ppmv) from the CoMeCAT scheme (black solid line), the full-chemistry SLIMCAT run (blue dashed line) and HALOE (red line). The model simulations are driven by ERA-40 winds.*

The annual mean profiles for 2000 are shown in Figure 7.7, along with the HALOE CH_4 annual mean. CoMeCAT simulates more CH_4 than full-chemistry above 1hPa (∼0.1 ppmv more), and also in the troposphere CoMeCAT is ∼0.1 ppmv higher than SLIMCAT full-chemistry (not shown). Around 100 hPa, the parameterisation seems to be systematically higher than the full-chemistry, especially at high latitudes. The agreement with the observations is good, profiles of the differences CoMeCAT-HALOE are shown in Figure 7.8, the maximum differences are below 0.2 ppmv everywhere except over southern high latitudes, where differences reach 0.3 ppmv at 10 hPa.

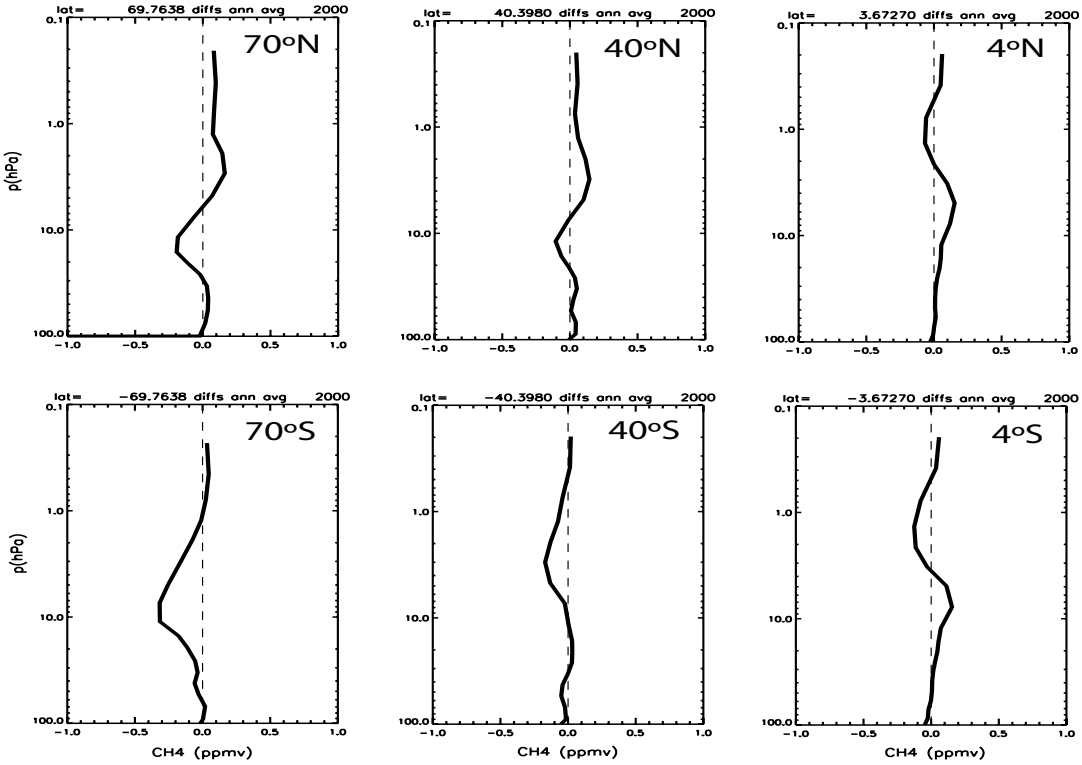

Figure 7.8: *Profiles of the differences (ppmv) between the annual mean (year 2000) profiles of CH_4 (ppmv) from the CoMeCAT run and the HALOE observations shown in Figure 7.7.*

7.6.2 Different terms

The CH_4 distributions shown above follow the parameterisation in equation (7.1). As shown in 7.3.2, the coefficients c_i have different order of magnitude, here the influence each term in equation (7.1) has on the resulting CH_4 distribution is investigated. Three different 3D runs have been performed using ERA-40 winds and the CoMeCAT scheme in SLIMCAT. The first run using only the first term in equation (7.1) (run11), the second run using the first two terms (run12) and a third run using the three terms (run13).

The vertical differences between such runs on the 15th July 2000 are shown in Figure 7.9 (run12-run11) and Figure 7.10 (run13-run12). The main contribution is made by the first term of the parameterisation, L_0, since, as the differences show,

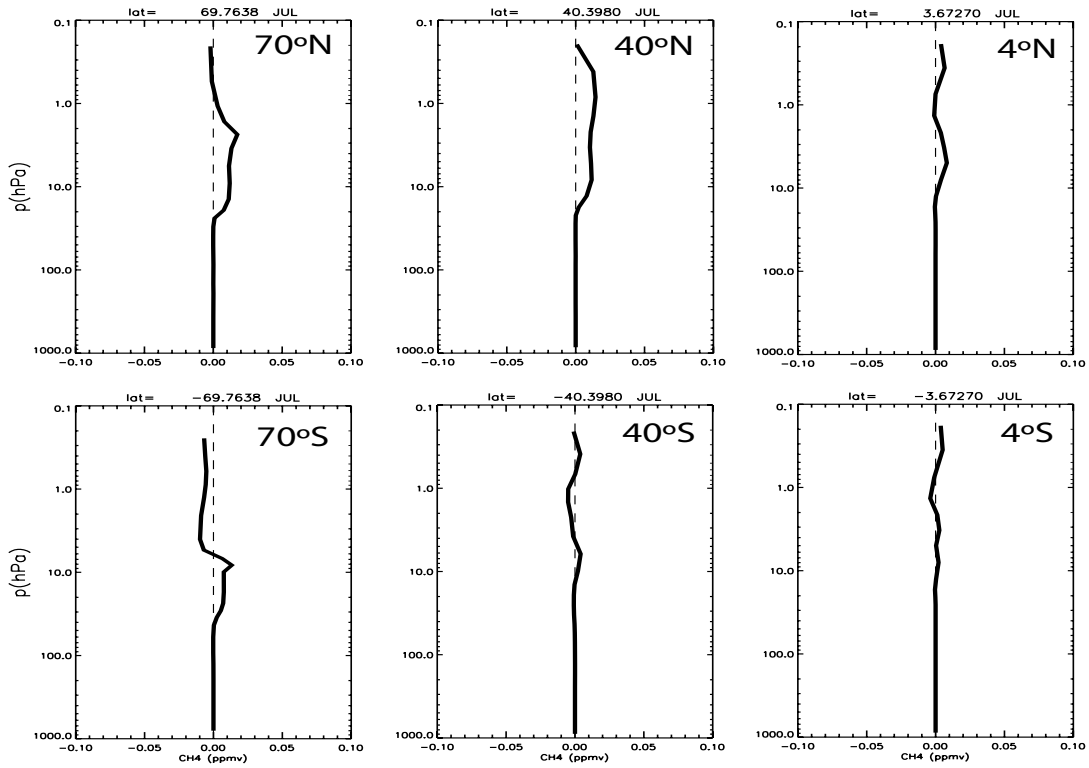

Figure 7.9: *Profiles of CH_4 differences (ppmv) on the 15th July 2000 between two runs from the CoMeCAT scheme, one using the c_0 term only and another using c_0 and c_1 terms. The two runs are driven by ERA-40 reanalyses.*

the next two terms only add corrections of up to ∼10% of the total parameterised concentration. It is in the middle stratosphere where c_1 and c_2 make their main contribution. Figure 7.9 (run12-run11) shows that the c_1 term contributes most in the summer hemisphere and over mid and high latitudes above 20 hPa. The contribution is positive in the summer hemisphere; while in the winter hemisphere it is positive up to ∼5hPa and negative above, with respect to run11. The c_2 term reduces the CH_4 values in the summer hemisphere, between 30-0.5 hPa, with respect to run12 (Figure 7.10). At low latitudes, in the upper most levels, the c_2 term increases the concentrations up to 0.01 ppmv, especially in the SH. The effect of this term in the winter high latitudes is a slight increase (<0.01 ppmv) with respect to the use of the first two terms only.

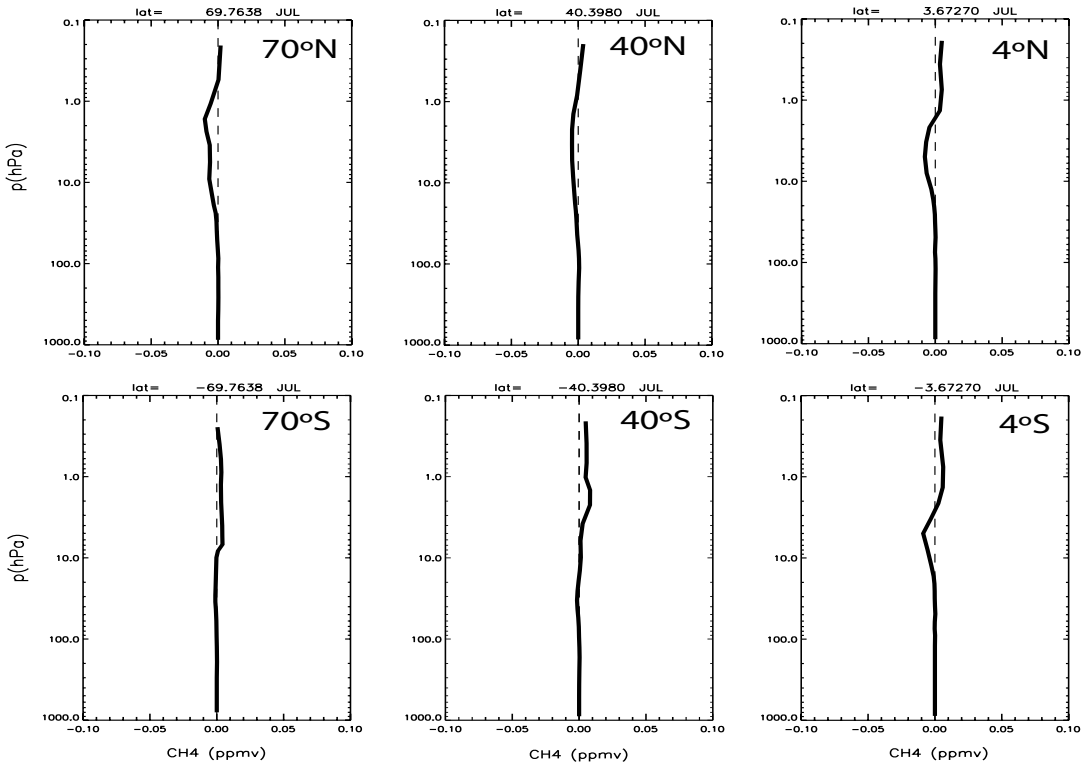

Figure 7.10: *CH_4 differences (ppmv) between run13-run12. Run12 uses the first two terms (c_0 and c_1) and run13 uses c_0, c_1 and c_2 terms in equation (7.1). Results are for the 15th July 2000. The two runs are driven by ERA-40 reanalyses.*

7.6.3 Different analysed winds

Results and discussions presented in Chapter 3 and Chapter 4 have shown how the use of different analysed winds leads to significantly different transport within a CTM. Figure 7.11 is a further example illustrating how different analyses affect the performance of the CoMeCAT scheme in a 3D simulation of SLIMCAT. It represents the annual mean (year 2000) of the vertical CoMeCAT CH_4 structure obtained using ERA-40 and EXP471 winds. The temperature term in the parameterisation (c_2) has not been used. Overall, with EXP471 winds CH_4 values are lower than with ERA-40 and at midlatitudes, and above 1 hPa for all latitudes, also closer to HALOE than the run with ERA-40. This agrees with findings in Chapter 3 on EXP471 producing a slower more realistic stratospheric transport than ERA-40. The largest differences between both winds are found in the range 5-50 hPa in the SH and between 1-

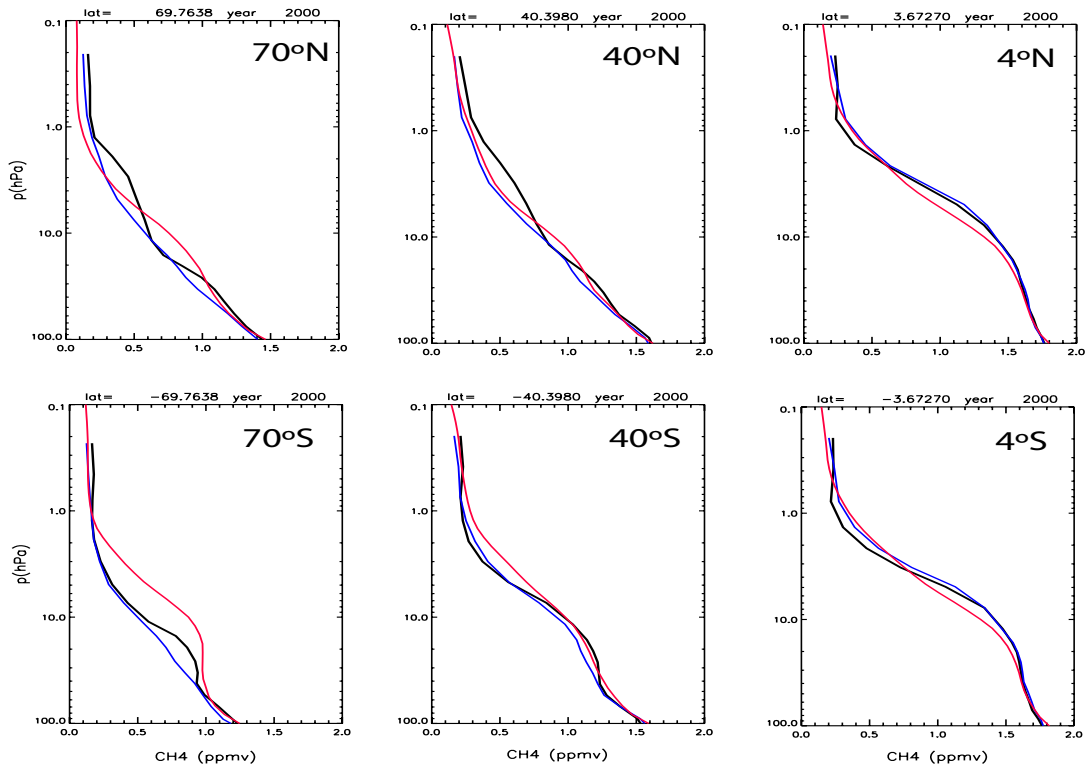

Figure 7.11: *Annual mean for 2000 of CH_4 profiles from the CoMeCAT scheme using ERA-40 (black line) and EXP471 (blue line) winds. HALOE annual mean (red line) is also included.*

10 hPa, and 20-50 hPa in the NH. The differences are small (∼0.1ppmv) over the tropics, and increase with latitude (up to 0.25 ppmv over the poles). The values at and below 100hPa are very similar for both sets of winds, the maximum difference is ∼0.05 ppmv and found at some subtropical latitudes in the SH.

7.6.4 CoMeCAT water distributions within the CTM

To obtain CoMeCAT water distributions with the SLIMCAT CTM, the humidity field from the analysis is used in the troposphere, while in the stratosphere the scheme described in Section 7.4 is used to obtain H_2O tendencies from CoMeCAT. The tropopause is defined differently in the tropics and outside the tropical region. In the tropics (15°S-15°N) it is defined as the level at which the minimum T is reached, while outside the tropics the stratospheric water scheme is used when the

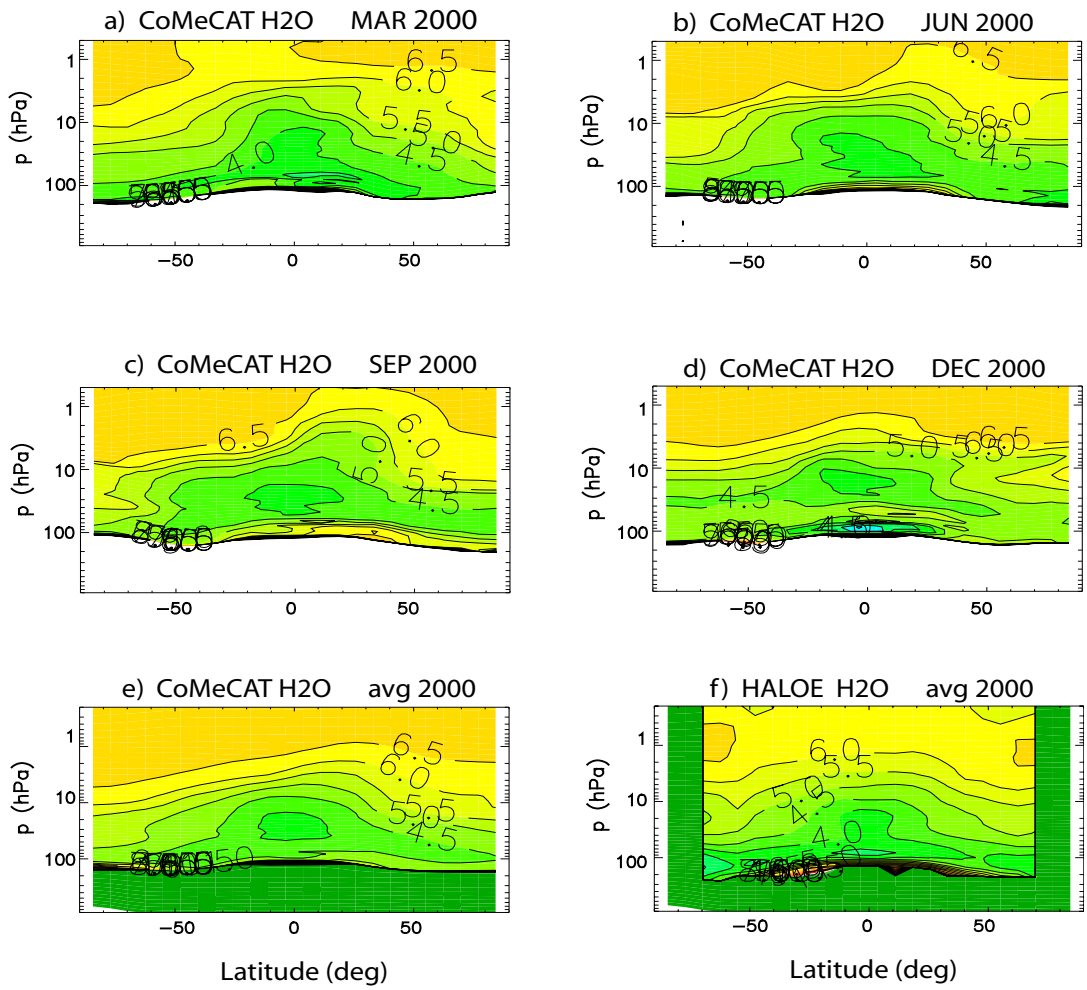

Figure 7.12: *Zonally averaged H_2O distributions (ppmv) from the CoMeCAT scheme for the 15th of (a) March, (b) June, (c) September and (d) December 2000. The annual mean for 2000 from CoMecAT is shown in panel (e) and HALOE H_2O annual mean in panel (f). CTM simulations are driven by ERA-40 fields.*

absolute potential vorticity (PV) is greater than 2 PVU and the potential temperature (θ) greater than 380 K, or if $\theta > 300$ K. The temperature term (c_2) in CoMeCAT has not been used here. The reasons for this are the small differences shown in Figure 7.10 and also the fact that this term has not been implemented in any of the ECMWF runs (Sections 7.7 and 7.8).

Zonally averaged water distributions obtained with the CoMeCAT scheme are

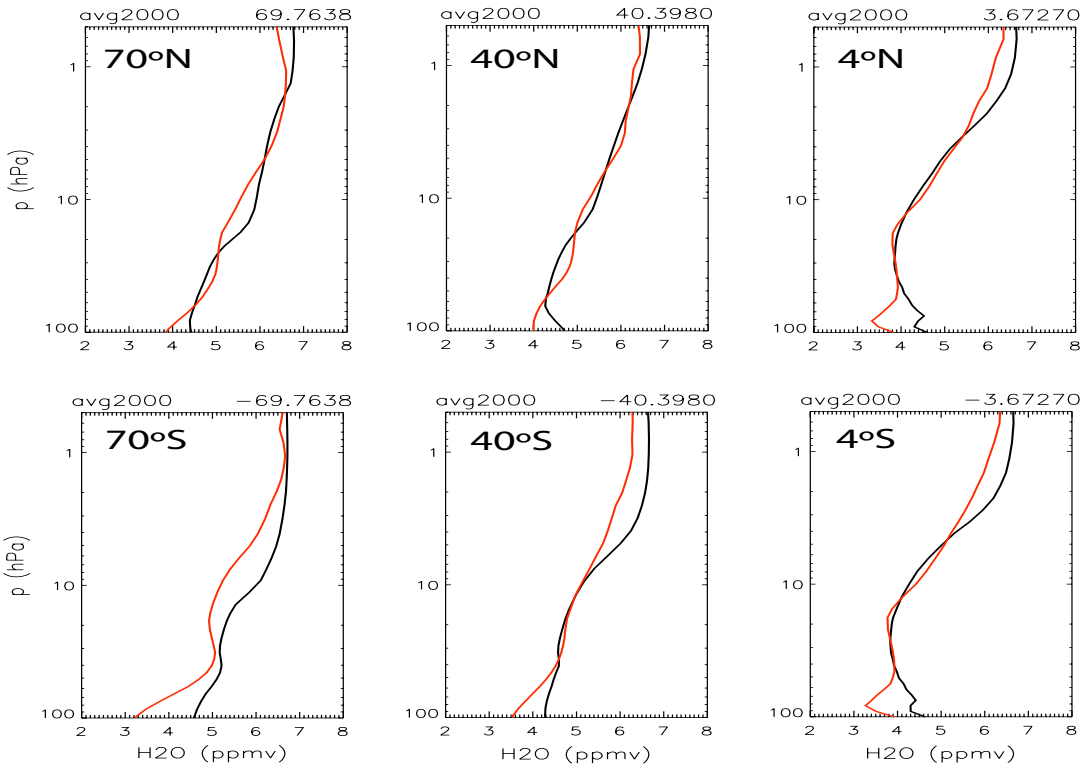

Figure 7.13: *Annually averaged H_2O distributions (ppmv) for year 2000 from the CoMeCAT scheme (black line) and HALOE (red line) for the latitudes 70°N, 40°N, 4°N, 70°S, 40°S and 4°S (as labeled).*

shown in Figure 7.12 for the 15th of March, June, September and December 2000. The variation with latitude and altitude follows that shown by the CoMeCAT CH_4 distributions. Also in Figure 7.12, the annual mean H_2O distribution from CoMeCAT and HALOE are represented for the year 2000. The CoMeCAT H_2O annual mean agrees well with HALOE, although in the LS CoMeCAT is ∼0.5 ppmv wetter. This wet bias is in agreement with findings in Oikonomou and O'Neill (2006), which shown that ERA-40 was wetter than HALOE in the LS region. In the CoMeCAT H_2O scheme this bias is accumulated in the stratosphere, reason why the parameterised H_2O concentrations are also ∼0.5 ppmv higher in the upper levels.

Water vertical profiles for the 2000 annual average from CoMeCAT are shown in Figure 7.13 along with HALOE observations. The overall variability is well cap-

tured by the CoMeCAT approach, the best agreement is found over NH high and mid latitudes. In CoMeCAT a wet bias in the LS is found between 100-50 hPa, then agreement in the middle stratosphere (50-3 hPa) is very good for all latitudes, except over southern high latitudes. Above 3 hPa, CoMeCAT produces again higher concentrations than observed (between 0.2-0.5 ppmv higher). Over southern high latitudes CoMeCAT produces up to 1.0 ppmv more H_2O than measured by HALOE in the LS, due to the lack of Antarctic dehydration in the CoMeCAT scheme.

7.7 CoMeCAT methane in the ECMWF GCM

A series of runs within the IFS model of ECMWF have been carried out by Agathe Untch and Jean-Jacques Morcrette (ECMWF) using the CoMeCAT scheme to parameterise stratospheric CH_4 and H_2O[1]. The runs have been performed with the Cy32r1 model version (operational in 2007) with a resolution of T159L60 and are 1 year long (initialised on 1st January 2000). The different ECMWF runs are described in Table 7.1 and Table 7.2. All these runs have used the same semi-implicit codification for CoMeCAT as those carried out with the CTM.

Table 7.1: *ECMWF runs with CoMeCAT CH_4 and H_2O schemes.*

ECMWF run	**GCM**	**CH_4 scheme**	**H_2O scheme**
f0uh	Free GCM	CoMeCAT	ECMWF default
f0wx	Free GCM	CoMeCAT	CoMeCAT
f0ww	Free GCM	none	none
f0x9	Nudged to ERA-40 every 6h	CoMeCAT	ECMWF default

In the ECMWF model the CoMeCAT scheme has been implemented using only the first two terms in equation (7.4), leaving out the temperature term. Runs

[1]For this part of the thesis, the author could decide what experiments to run at ECMWF but did not have personal access to the ECMWF system.

Table 7.2: *ECMWF runs performed to evaluate CoMeCAT CH_4 impact on the GCM radiation scheme.*

ECMWF run	GCM	CH_4 scheme	Interactive with radiation
f0yq	Free GCM	Global 1.72 ppmv	SW/LW
f0yt	Free GCM	CoMeCAT	SW/LW
f0yu	Free GCM	CoMeCAT	NO
f0yv	Free GCM	CoMeCAT	only LW
f0yw	Free GCM	CoMeCAT	only SW

included in Table 7.1 are used to examine the ability of CoMeCAT to reproduce CH_4 and H_2O in the ECMWF model, while the runs included in Table 7.2 are used to evaluate the impact of CoMeCAT on the ECMWF radiation scheme (Section 7.7.2).

7.7.1 ECMWF CoMeCAT CH_4 distributions

The ECMWF runs used here employ the same initial conditions as the CTM runs ([CH_4] CoMeCAT reference field). Figure 7.14 shows annually averaged CH_4 vertical distributions from the CoMeCAT scheme in the CTM and in the ECMWF GCM (run f0uh). Two different CTM runs have been included, the default SLIMCAT one ($\sigma - \theta$) and one TOMCAT run ($\sigma - p$) in order to have a more accurate comparison against the ECMWF runs, which use a $\sigma - p$ vertical coordinate. The scheme using only the first two terms in the parameterisation has also been used in the CTM, the CTM runs shown in Figure 7.14 are driven by ERA-40 winds.

The overall agreement in the LS (up to 10 hPa) is good between all runs and observations; in the troposphere the ECMWF run is 0.1 ppmv lower than the CTM runs, partly due to the lack of surface overwriting in the GCM run. Above 10 hPa there are larger differences between the three runs in Figure 7.14. In the highest

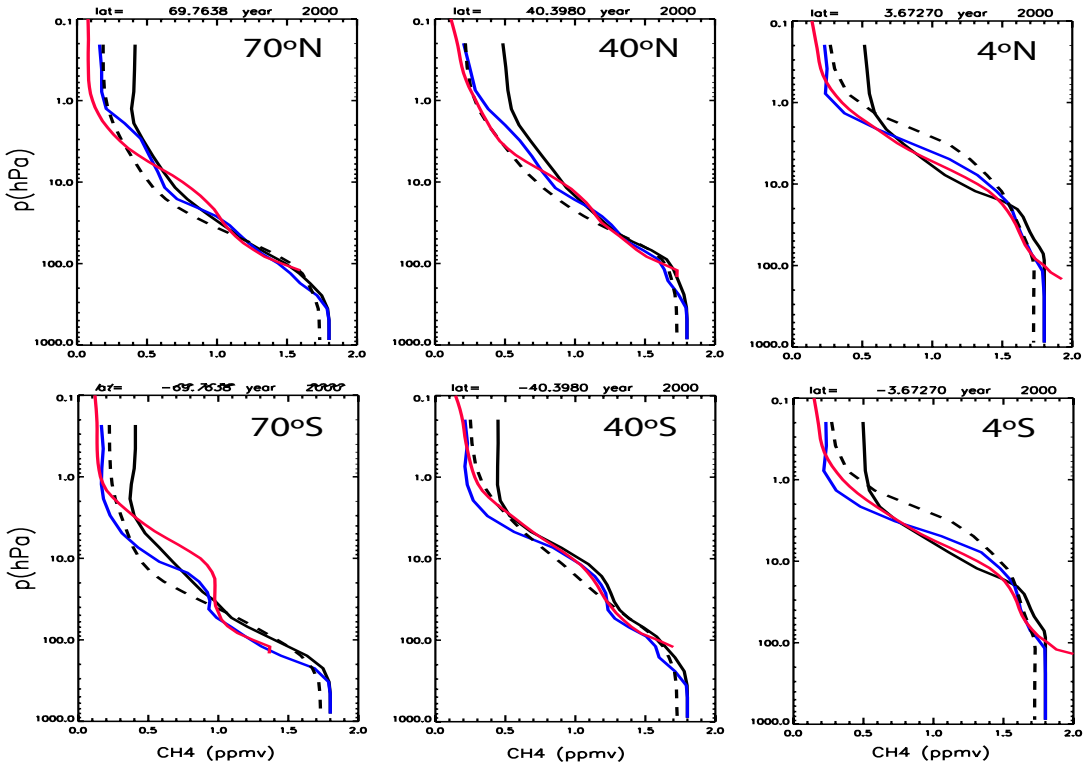

Figure 7.14: *Annually averaged CH_4 distributions (ppmv) for year 2000 from the CoMeCAT scheme in TOMCAT (solid black line), in SLIMCAT (blue line), in the ECMWF GCM (dashed black line) for the latitudes 70°N, 40°N, 4°N, 70°S, 40°S and 4°S (as labeled). HALOE observations have also been included (red line).*

levels the agreement with observations is good for f0uh and SLIMCAT but not for TOMCAT. The TOMCAT run produces more CH_4 than the SLIMCAT one, particularly above 1.0 hPa, where differences of up to 0.25 ppmv widely occur; the only exception is the tropics, where around 10 hPa the SLIMCAT run gives higher values than TOMCAT. The ECMWF f0uh run is overall closer to the SLIMCAT run, despite the different vertical coordinate. Between 1-50 hPa the ECMWF run is lower than the CTM runs at high and mid latitudes. However, the main differences appear at tropical latitudes, between 0.5-50 hPa where ECMWF f0uh presents higher concentrations than the CTM runs. These differences are due to transport, indicating an excess of vertical transport in the ECMWF model. The fact that f0uh is more realistic than TOMCAT in the upper levels shows the improvement in the

vertical dispersion achieved in the recent ECMWF model versions (the TOMCAT run uses ERA-40 winds). Nevertheless, definitive conclusions cannot be drawn on this issue since the vertical motion used is different: the CTM obtains it from the divergence of the horizontal winds, while the ECMWF runs use the vertical wind velocity w. The ECMWF w field has been reported to be too noisy (see Chapter 2) which might be causing the differences seen between the TOMCAT and f0uh runs.

7.7.2 Impact on the ECMWF stratospheric temperature

Methane is a strong greenhouse gas that contributes to cool the mesosphere/upper stratosphere and to warm the middle/lower stratosphere and troposphere. Despite this, most GCMs use only a fixed constant value for CH_4 concentrations (*e.g.* Collins *et al.* 2006), *i.e.* these models consider CH_4 as a well-mixed gas, which is unrealistic above the tropopause. Using a simpler parameterisation approach than CoMeCAT, Curry *et al.* (2006) already showed the impact that relaxing the well-mixed approximation for some greenhouse gases (GHGs) had in simulations obtained with a CCM. CoMeCAT concentrations in the stratosphere are, of course, notably lower than the global value currently used by ECMWF of 1.72 ppmv. Therefore, the implementation of CoMeCAT in the ECMWF model is expected to significantly impact the temperature field. Here, CoMeCAT has been made interactive with the ECMWF radiation scheme, and temperature differences in the GCM have been examined. The runs in Table 7.2 have been used for the comparisons. Because all such runs are only 1-year samples of a free-running GCM, only temperature differences in the mid-upper stratosphere in the summer hemisphere can be evaluated.

Figure 7.15a shows the JJA averaged differences in temperature in the ECMWF model using the default operational ECMWF CH_4 (control run f0yq) and using the CH_4 distributions from the CoMeCAT scheme (run f0yt). Absorption by CH_4 is considered both in the shortwave (SW) and the longwave (LW) in the two runs. With CoMeCAT T increases in the mid-upper stratosphere up to 1.8 K, due to having now less CH_4 at those levels. The cooling observed over the winter hemisphere

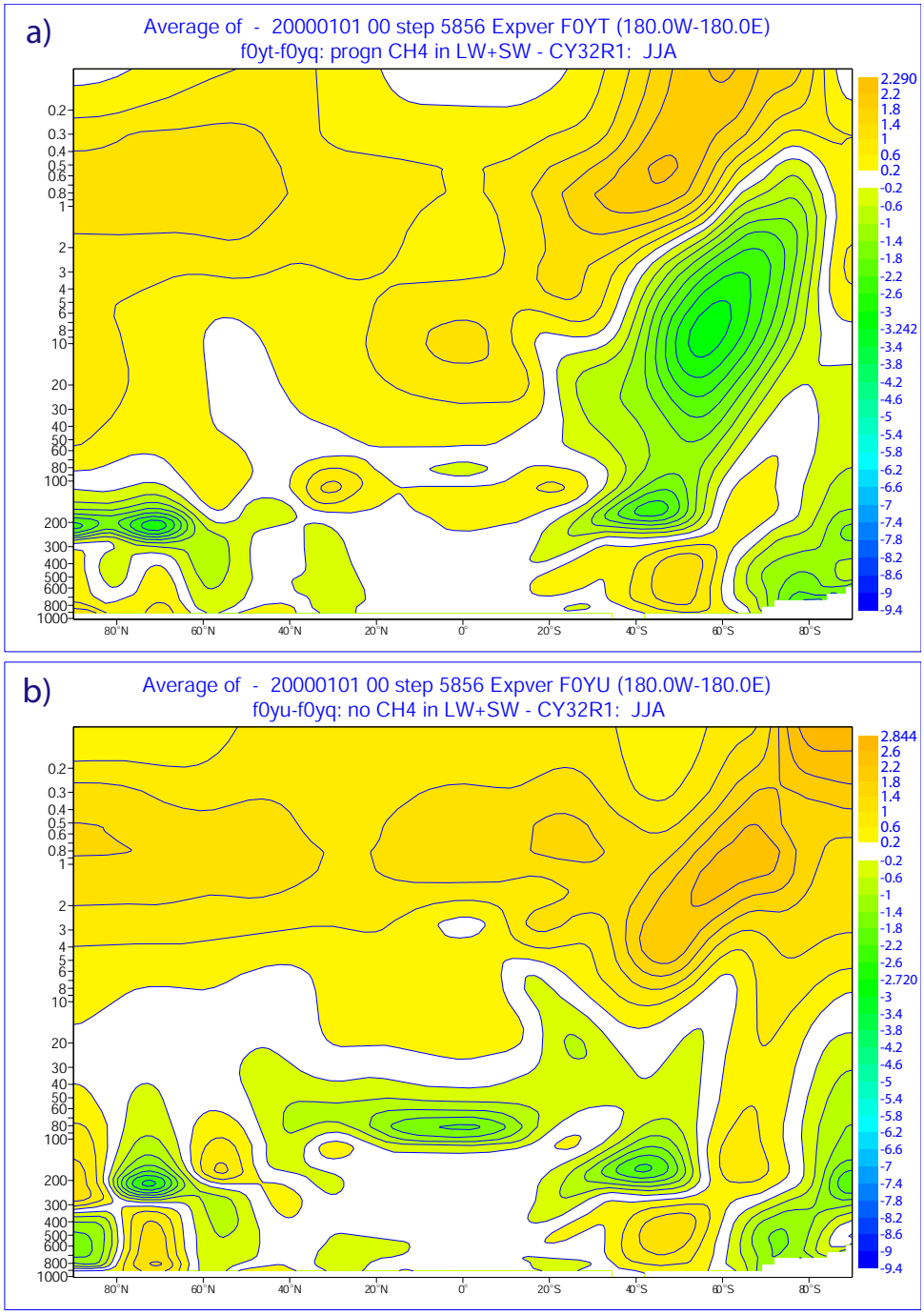

Figure 7.15: *Differences in T averaged over June-July-August (JJA) 2000 between the ECMWF runs (a) f0yt (CoMeCAT CH_4) and f0yq (default 1.72 ppm global value) and (b) f0yu (no CH_4) and f0yq. Courtesy of Jean-Jacques Morcrette (ECMWF).*

cannot be related to CH_4 as dynamical winter variability between the two compared runs can be larger than changes induced by different CH_4 distributions. Figure 7.15b shows temperature differences between a run with no CH_4 (f0yu) and the control run (f0yq). The same effects as in Figure 7.15a can be seen, although amplified by the fact that now the CH_4 reduction is even larger (from 1.72 to zero ppmv at all levels). In Figure 7.15b the cooling over the equator (-1.4 K at 80 hPa) is produced by a decrease of the "shielding" effect due to the reduction of CH_4 in the levels above.

Figure 7.16 shows the differences between the control run f0yq and two runs using CoMeCAT, one of them only in the LW (f0yv) and the other only in the SW (f0yw). Figure 7.16a shows that a warming (up to 1.4 K) takes place in the upper stratosphere and lower mesosphere, and the middle stratosphere is cooled (up to -1.4 K), due to having lower CH_4 values (CoMeCAT) in the LW radiation (and no CH_4 in the SW). Figure 7.16b, on the other hand, shows the effect of having CoMeCAT in the SW radiation (instead of constant 1.72 value) and no CH_4 in the LW.

Changes in stratospheric CH_4 affect radiation mostly in the LW, while only a minor contribution is expected to come from the SW (*e.g.* Curry *et al.* 2006). Comparing Figure 7.16a with Figure 7.15b gives the maximum possible contribution in the LW. In effect, having more CH_4 in the LW (run f0yv) cools the stratosphere above 10 hPa, and warms the LS. The maximum possible contribution in the SW is obtained by comparing Figure 7.16b and Figure 7.15b, both panels show very similar temperature differences, indicating that only a small effect is occurring in the SW.

Including the CoMeCAT scheme makes the ECMWF model more realistic, although the model itself suffers from a warm bias in the upper stratosphere (A. Untch, personal communication, 2007) and thus, the temperature field in this region presents an increased bias when implementing CoMeCAT. Recent experimental runs done including realistic climatologies for GHGs (CO_2, CH4, N_2O, CFC11 and CFC12) in the ECMWF model have shown that the model warm bias is significantly

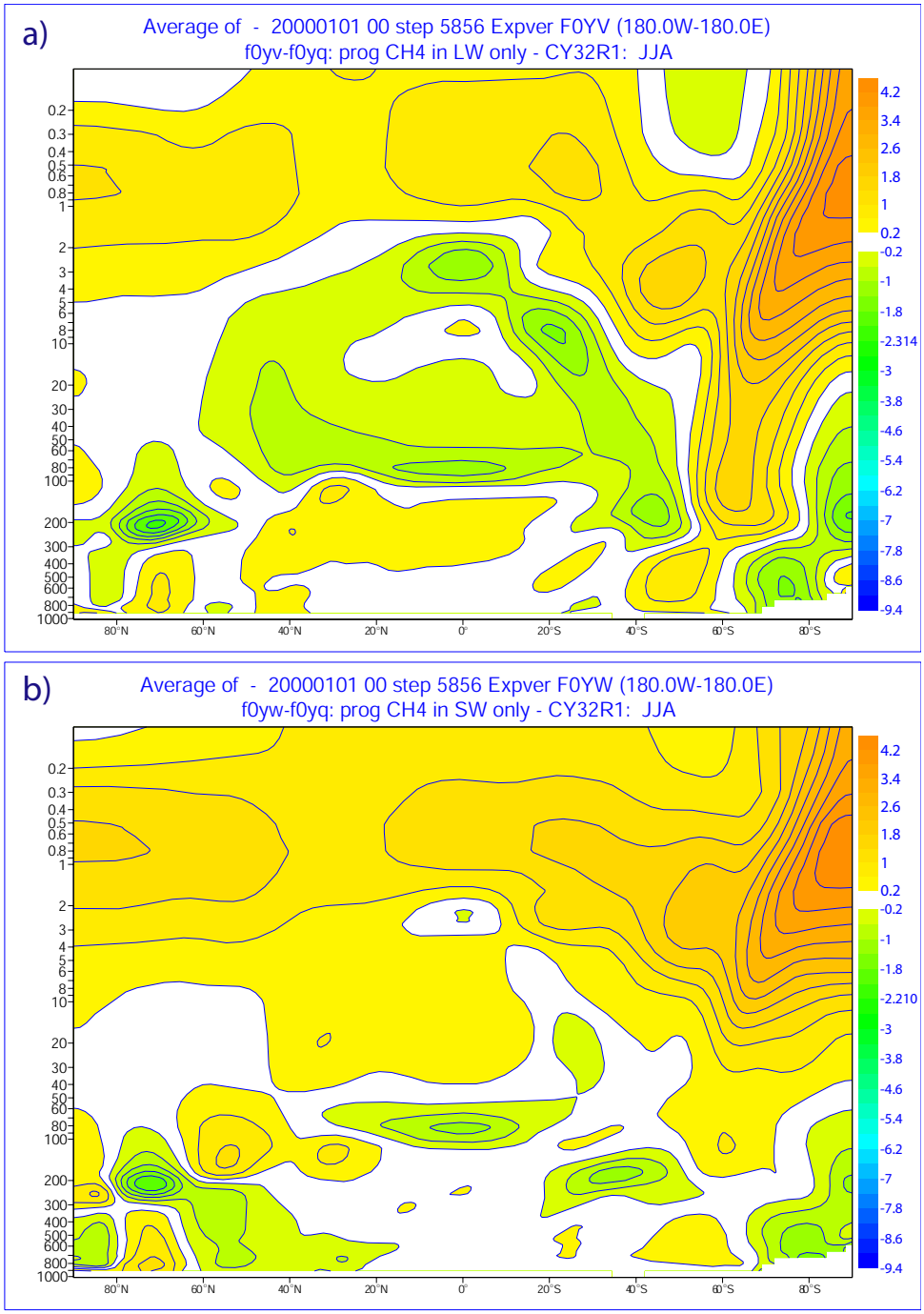

Figure 7.16: *Differences in T averaged over June-July-August (JJA) 2000 between the ECMWF runs (a) f0yv (CoMeCAT CH_4 in LW only) and default f0yq; and (b) f0yw (CoMeCAT CH_4 in SW only) and f0yq. Courtesy of Jean-Jacques Morcrette (ECMWF).*

reduced at the stratopause (J.-J. Morcrette, personal communication, 2008). The effect of using CoMeCAT and realistic distributions for the other GHGs should be investigated in the future.

7.7.3 Nudging effects: CTM v. GCM v. nudged GCM

The use of nudged GCMs is arising in the last years as a potential way to make these models closer to the real atmosphere (Telford *et al.*, 2008; Schmidt *et al.*, 2006; Jeuken *et al.*, 1996). Such an approach consists of relaxing, or nudging, the GCM dynamical fields towards meteorological (re)analyses, so that, if M is the model operator and G the nudging parameter, the evolution of a certain model variable $\vec{x}$ is given by

$$\frac{\partial \vec{x}}{\partial t} = M(\vec{x} + G(\vec{x_{an}} - \vec{x}) \tag{7.7}$$

For this thesis we have had the possibility to explore the effect that nudging the ECMWF GCM has for the transport of the CoMeCAT CH_4 tracer. The experiment f0x9 (Table 7.1) has been produced with the same GCM version and the same CoMeCAT parameterisation as the run f0uh, however, in f0x9 the dynamical variables are relaxed to ERA-40 values (year 2000). The relaxation is done instantaneously every 6 hours.

Figure 7.17 shows CoMeCAT CH_4 profiles for the free-running experiment f0uh, the nudged f0x9 and the CoMeCAT-SLIMCAT run, averaged for 2000. Compared to the the free-running f0uh, f0x9 results in higher CH_4 concentrations at almost all levels and latitudes. Only for the very LS (100-50 hPa) f0x9 is closer to the CTM and HALOE than f0uh. In the upper most levels (above 1 hPa) the nudged run produces between 0.2 ppmv (at high latitudes) and 0.3 ppmv (at the tropics) more than f0uh. This is similar to the effect observed when running CoMeCAT in TOMCAT ($\sigma - p$) as shown in Figure 7.14. In fact, by plotting the annually averaged cross-sections (Figure 7.18) it can be seen that the nudged f0x9 run is closer to the TOMCAT run than the free f0uh, with almost equivalent concentrations in the upper levels. This

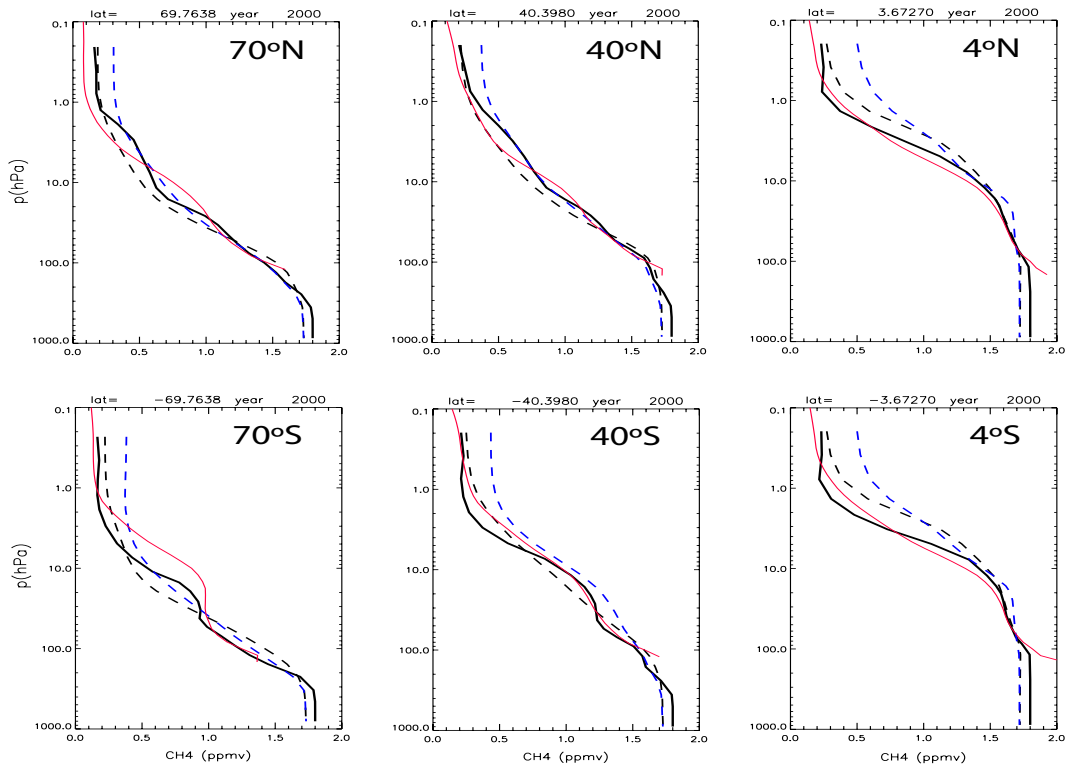

Figure 7.17: *Annually averaged CH_4 distributions (ppmv) for year 2000 from the CoMeCAT scheme in the free-running GCM f0uh (dashed black line), in the nudged GCM f0x9 (dashed blue line) and in the SLIMCAT CTM (solid black line). Latitudes shown are 70°N, 40°N, 4°N, 70°S, 40°S and 4°S (as labeled). HALOE observations have also been included (red line).*

too high CH_4 values in the upper stratosphere might be related to the excessive vertical diffusion exhibited by ERA-40 in TOMCAT simulations (see Lagrangian calculations in Chapter 3). These results suggest that nudging is bringing the GCM closer to the transport features in ERA-40, with the associated known problems. Thus, in a nudged GCM, an upper limit to the quality of the dynamical fields is set by the meteorological data used, ERA-40 in this case, causing the nudged GCM to show the same problems as an off-line CTM driven by the same ERA-40 winds.

In an instantaneous relaxation, as in the f0x9 run, the nudging parameter is very strong, G in equation (7.7) has the shape of a δ function. For this reason dynamical

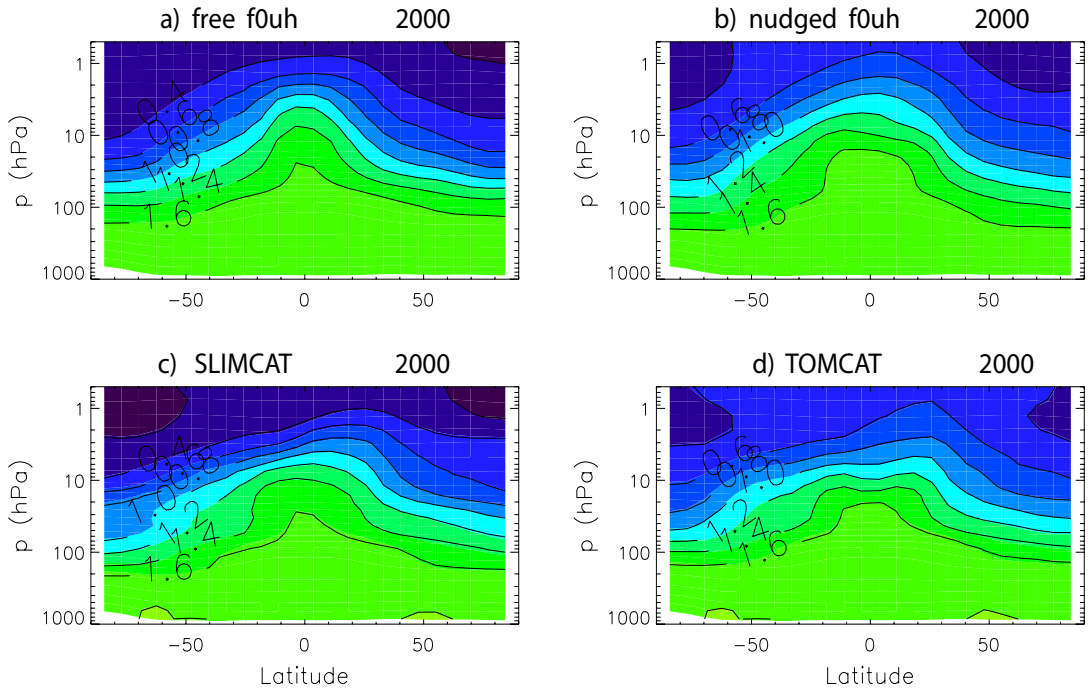

Figure 7.18: *Annually averaged CH_4 distributions (ppmv) for year 2000 from the CoMeCAT scheme in (a) the free-running GCM f0uh, (b) the nudged GCM f0x9, (c) the SLIMCAT CTM and (d) the TOMCAT CTM.*

imbalances in the (re)analyses could be artificially amplified (Jeuken *et al.*, 1996), making the GCM transport present, at least, the same problems as ERA-40 does. The use of a smoother relaxing parameter could produce more realistic results. This remains as a possible future research line, as for this thesis we did not have access to the ECMWF model.

7.8 CoMeCAT water distributions within the GCM

The ECMWF default (currently operational) stratospheric water scheme, as well as H_2O obtained from oxidation of the CoMeCAT CH_4 in the ECMWF runs, are here compared against HALOE and H_2O from CoMeCAT in the CTM. Figure 7.19 plots H_2O cross-sections averaged over 2000 obtained from CoMeCAT in the CTM and in the ECMWF model. Also shown in the same figure are H_2O from the default

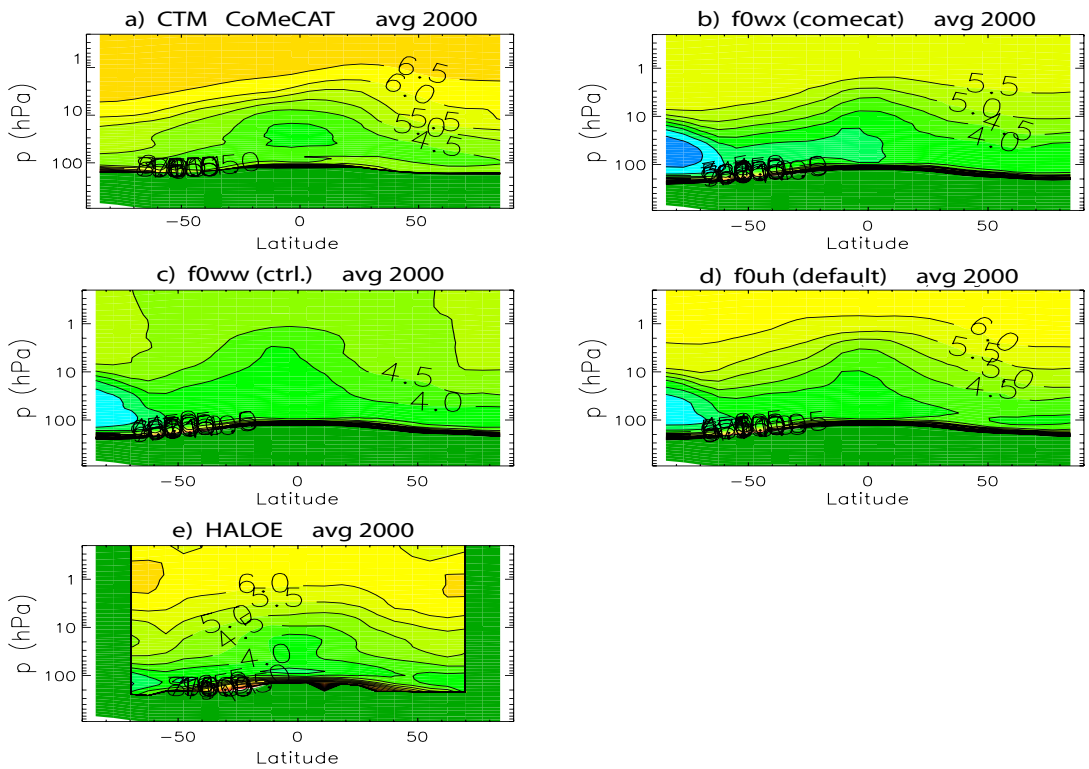

Figure 7.19: *H_2O (ppmv) cross-sections averaged over 2000 obtained from (a) CoMeCAT in a SLIMCAT run, (b) CoMeCAT in ECMWF run f0wx, (c) ECMWF control run f0ww, (d) ECMWF default scheme and (e) HALOE instrument. Contour interval is 0.5 ppmv.*

ECMWF scheme (run f0uh), as well as from an ECMWF control run (f0ww) in which no water source scheme is used in the stratosphere. The ECMWF run with the CoMeCAT H_2O source (f0wx) initialises the humidity field from ERA-40 data.

7.8.1 ECMWF default H_2O scheme

The ECMWF stratospheric water currently comes from a parameterisation based on a fixed profile based on water vapour observed lifetime (Section 5.5 in Chapter 5). This scheme does not include any latitudinal variation, relying on the accuracy of the Brewer-Dobson circulation to get the correct amounts of H_2O increase in the stratosphere due to CH_4 oxidation.

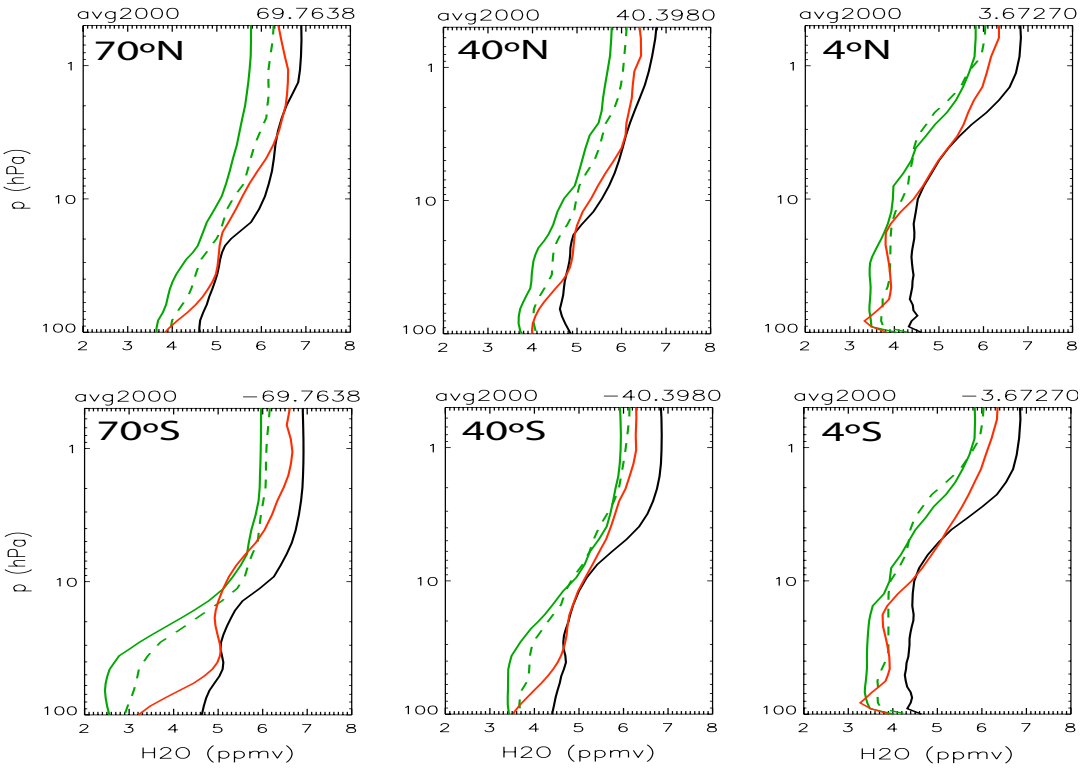

Figure 7.20: *H_2O (ppmv) profiles averaged over 2000 obtained from CoMeCAT in a SLIMCAT run (black line), ECMWF default run f0uh (dashed green line), CoMeCAT in ECMWF run f0wx (solid green line) and HALOE (red line).*

Figure 7.19d shows H_2O from an ECMWF run (f0uh) using their default stratospheric water scheme. In the upper levels (above 5 hPa) f0uh H_2O concentrations are around 0.5 ppmv lower than HALOE. The low water values at SH high latitudes come from the Antarctic dehydration scheme included in the ECMWF CH_4 oxidation model (Chapter 5). One control run has also been carried out (run f0ww) in which the source of water in the stratosphere has been switched off (Figure 7.19c). It can be seen that the H_2O field would be far too low in the stratosphere in the absence of a source parameterisation, up to 2.0 ppmv are added by the default ECMWF H_2O scheme which also makes the concentration gradients realistic.

7.8.2 ECMWF new H_2O scheme from CoMeCAT

The distribution of water from the CoMeCAT scheme implemented in the ECMWF model (run f0wx) is shown in Figure 7.19b. Compared to the performance of the same scheme in SLIMCAT (Figure 7.19a) the ECMWF run shows lower water values (up to 1 ppmv lower above 10 hPa). The SLIMCAT run is closer to the HALOE distribution(Figure 7.19e), also for mid-high latitudes in spite of not including Antarctic dehydration. In the ECMWF model, CoMeCAT produces similar but drier profiles than the default scheme (Figure 7.20), and it is still considerably drier than HALOE and CoMeCAT in the CTM. The differences between the SLIMCAT and the ECMWF distributions partly arise from the initial state being different and from the fact that f0wx comes from a free-running GCM while the SLIMCAT run is forced by 6-hourly ERA-40 analyses. The last factor is conditioning the concentrations entering through the tropopause, it is the analysed humidity field that is adopted for the troposphere in the CTM runs. ERA-40 presents a 10% wet bias with respect to HALOE in the LS (100 hPa) (Oikonomou and O'Neill, 2006). The too high water values that enter the CoMeCAT scheme from the tropopause are accumulated throughout the entire stratosphere causing the CoMeCAT CTM run to present higher concentrations than HALOE (Figure 7.19a). An additional problem for the comparison is that the ECMWF run is probably too short (1 year) to allow for the CoMeCAT scheme to have oxidised enough CH_4. Figure 7.21 shows the zonal distribution of H_2O+2CH_4 averaged over year 2000; compared to HALOE, ECMWF run f0wx shows a much less uniformly distributed field. This seems to indicate that 1 year is not long enough for the ECMWF model to correctly spin-up from the initial conditions used (ERA-40 H_2O). The initial condition for H_2O in the CTM run with CoMeCAT (Section 7.6) makes H_2O+2CH_4 to be equal to 7.0 ppmv everywhere above the tropopause, a realistic condition for the low/middle stratosphere as shown by Figures 7.21a and 7.21c. On the other hand, the problems presented by the ECMWF default H_2O scheme in previous analysis versions (*e.g.* ERA-40) might have been partially overcome due to a more realistic transport in the more recent ECMWF model versions (like the one used for run f0uh).

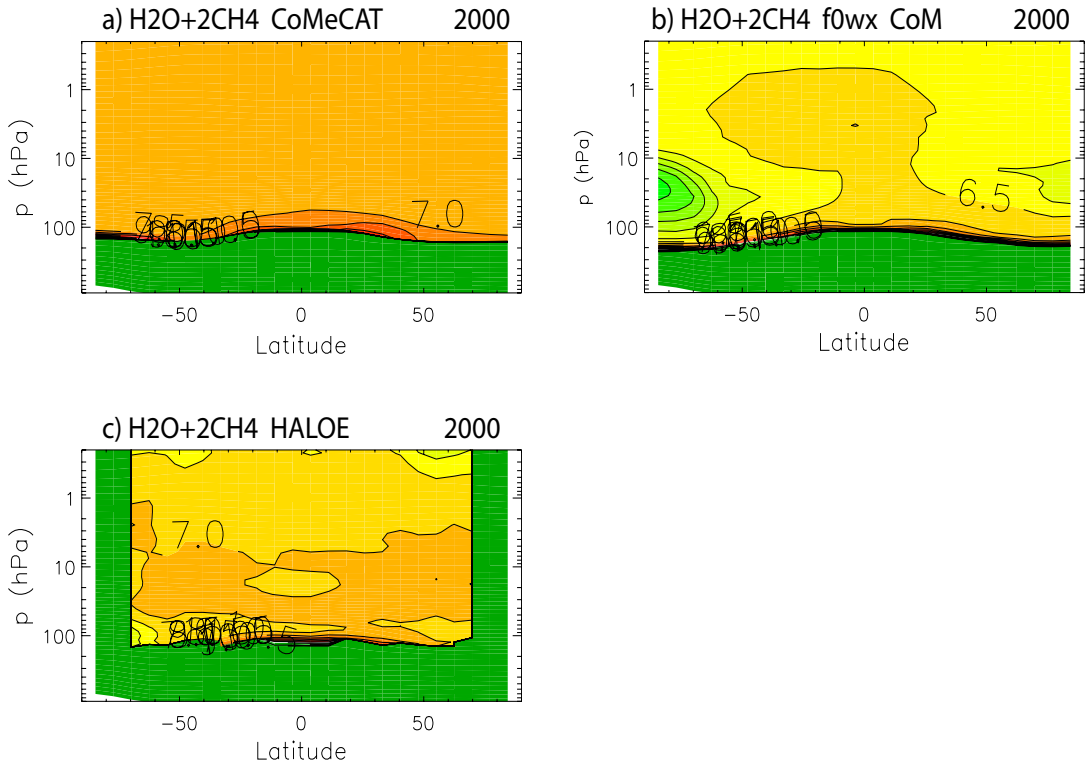

Figure 7.21: *H_2O+2CH_4 (ppmv) cross-sections averaged over 2000 obtained from (a) CoMeCAT in a SLIMCAT run, (b) CoMeCAT in ECMWF run f0wx, (c) HALOE.*

7.9 Conclusions

In this chapter a new CH_4 parameterisation scheme (CoMeCAT) has been developed for the stratosphere, and has been tested within a 3D CTM and a 3D GCM. The scheme has also been used to parameterise stratospheric water vapour in the two 3D models.

The CoMeCAT CH_4 performs well in the TOMCAT/SLIMCAT CTM, results are in very good agreement with observations from HALOE and with SLIMCAT full-chemistry runs. The largest differences with observations are found at high latitudes, especially in the SH, where CoMeCAT (and full-chemistry) runs with ERA-40 underestimate CH_4 compared to HALOE. The adaptability of the scheme to different conditions has been proved by showing results for atmospheric conditions differing

from those used to calculate the scheme coefficients (conditions for year 2004 were used to obtain the coefficients).

CoMeCAT also performs well in the ECMWF model, producing realistic CH_4 distributions, which also opens the possibility of exploring long-term transport features in the GCM. The impact of the new scheme in the ECMWF model is as expected, warming the upper stratosphere and cooling the UTLS region compared to the ECMWF global averaged used until now.

The differences observed between CoMeCAT CTM runs and CoMeCAT ECMWF runs are mainly due to transport issues, in particular the different variable used for vertical motion can be causing the discrepancies in the tropics; differences in resolution might also be affecting. Not having implemented the temperature term in the ECMWF runs might have been detrimental for the results obtained with the GCM, particularly in the middle/upper stratosphere, where the GCM presents the largest temperature biases with respect to observed climatologies.

The use of a nudged version of the GCM has also been explored. Nudging the GCM to ERA-40 analyses produced similar CH_4 distributions to those obtained with TOMCAT (σ-p) run by ERA-40. These results indicate that a nudged GCM incorporates the advantages and deficiencies of the analyses used, and nudging a recent version of the IFS model to ERA-40 is not recommended, at least for applications involving transport of stratospheric tracers.

The CH_4 time tendency obtained from CoMeCAT has been used in both models to parameterise the source of stratospheric water. The H_2O distributions obtained from CoMeCAT in the CTM runs are in good agreement with HALOE observations, except for a wet bias in the LS region. ECMWF CoMeCAT H_2O distributions show a realistic spatial variability although are more than 0.5 lower than HALOE observations and $\sim$1 ppmv lower than CoMeCAT in the CTM. Differences in the initial

states used in the CTM and the ECMWF are one of the reasons for the discrepancy, as well as the fact that the ECMWF run should be longer than 1 year for a realistic CH_4 oxidation to take place, which is in agreement with CoMeCAT CH_4 values being higher in the ECMWF model than in the CTM above 1 hPa.

Implementing schemes similar to CoMeCAT for other radiatively active gases like CO_2 and CFCs could also improve the representation of the stratosphere in the ECMWF GCM. In terms of potential applications, the CoMeCAT scheme also opens new possibilities for climate studies. In spite of being CH_4 the second most important greenhouse gas, most climate models use only a fixed value for CH_4 in the stratosphere. Including a realistic CH_4 profile, with latitude dependence and linked to other model variables (like temperature), is expected to produce different radiative forcing results in climate models.

If needed, a scheme following the CoMeCAT approach could be used to parameterise CH_4 directly, instead of the loss rate, however this would make the scheme less flexible. Coefficients of the form $\partial L/\partial X$ could also be derived from the CTM, X representing the main species involved in CH_4 stratospheric chemistry: Ideally OH, chlorine compounds and $O(^1D)$, but also O_3 and H_2O. Also one time depending entry term may be added to have into account the evolution of tropospheric CH_4 concentrations.

Chapter 8

General Conclusions

8.1 Summary of results

This thesis has explored two different aspects of stratospheric modelling. Chapters 2 to 4 have dealt with the representation of stratospheric transport achieved by different ECMWF (re)analyses and the implications for stratospheric CTM simulations. Chapters 5 to 7 explored new ways of parameterising stratospheric O_3, CH_4 and H_2O in a global 3D model. Findings obtained in each part are summarised below in Sections 8.1.1 and 8.1.2, respectively.

8.1.1 Stratospheric transport results

Chapter 2 presented the situation for stratospheric transport in CTMs when this PhD project started, highlighting areas that needed investigation. ERA-40 and other (re)analysis datasets, essential for the determination of atmospheric trends, had started to show some deficiencies for stratospheric CTM studies: The Brewer-Dobson circulation (BDC) and mixing processes were too strong in most existing (re)analyses. CTMs had implemented different correction strategies to minimise the impact of such deficiencies. However, such strategies are not exempt from problems and their effects depend on the particular model. For this reason it was necessary that future (re)analyses corrected these stratospheric circulation problems. The first

part of this thesis was motivated by the need to test new ECMWF stratospheric datasets prior to the production of the ERA-Interim reanalysis.

In Chapter 3, one experimental dataset (EXP471), produced with the new version of the ECMWF data assimilation system, was thoroughly tested within a CTM. EXP471 provided a realistic stratospheric age-of-air in the low/middle stratosphere, and trajectory calculations showed that vertical and horizontal dispersion with this dataset were also greatly reduced compared to previous datasets (ERA-40, ECMWF operational 2000 and UKMO). Tape recorder simulations also showed the superiority of the new ECMWF data. Contrary to previous literature statements (Schoeberl *et al.*, 2003; Stohl *et al.*, 2004; Rood, 2005), results from Chapter 3 showed that data assimilation products were indeed able to improve beyond their status in the early 2000's.

Possible causes for the improvements achieved by EXP471 were examined in Chapter 4. Available ECMWF experimental datasets allowed an assessment of the effect that aspects of the data assimilation procedure have on stratospheric transport. The use of the 4D-Var method was shown to be one main factor in reducing spurious dispersion, but also the length of the assimilation window and the treatment of errors played significant roles. More experimental assimilation runs would be necessary to extract further information on the causes for the improvements.

In Chapter 4 one set of GCM winds (EXP364) was also compared against the corresponding ECMWF DAS winds, showing that data assimilation increases horizontal mixing compared to free-running GCM winds. However, the frequency of the winds read-in by the CTM seems to determine the extent of vertical dispersion; with a 12h frequency GCM and DAS winds produced the same excessive vertical dispersion. Therefore, part of the problems attributed to data assimilation in the past is actually caused by the use of analysis frequencies of 12h or more to drive CTMs, producing too high vertical dispersion and unrealistic age-of-air distributions.

Results from Chapters 3 and 4 have shown the relevance the data assimilation method has for the quality of the (re)analysis, and how a CTM can be turned into a powerful tool for the evaluation of the stratospheric transport provided by the meteorological data. For the first time a CTM has been used to 'a priori' evaluate experimental assimilation runs and, subsequently, provide information for the final production decisions of a reanalysis series (ERA-Interim).

The use of satellite radiances in the data assimilation system is also essential for a DAS system to provide realistic datasets. For the correct assimilation of radiances stratospheric radiatively active gases need to be accurately represented in the NWP model. The CTM used in this thesis has also been used to develop improvements or new ways to parameterise O_3, CH_4 and H_2O in global models.

8.1.2 Stratospheric parameterisation results

The ECMWF currently operational schemes for O_3 and H_2O were discussed in Chapter 5, and aspects that needed improvement were identified. The main problem in the ECMWF operational O_3 scheme is the lack of realistic heterogenous chemistry. Only polar heterogeneous loss is simulated by the scheme and it is done by means of an inaccurate quadratic chlorine-dependent term. On the other hand, the stratospheric H_2O scheme implemented by the ECMWF model is not flexible enough to allow variability due to changes in the CH_4 oxidation source. Also the ECMWF radiation scheme uses a global value for CH_4 (1.72 ppmv) that is completely unrealistic for the stratospheric region. Chapters 6 and 7 have proposed and tested improvements for the existing ECMWF O_3 scheme and developed a new CH_4 and H_2O parameterisation.

In Chapter 6 the ECMWF O_3 approach was tested within a full-chemistry state-of-the-art CTM. Improvements to solve the ECMWF scheme weaknesses were suggested and results tested against the full-chemistry model and observations.

The ozone scheme developed (COPCAT scheme) successfully included heterogenous chemistry effects implicitly. COPCAT results obtained in the SLIMCAT CTM showed good overall agreement with SLIMCAT full-chemistry, TOMS and HALOE observations. The scheme simulates a realistic ozone hole and O_3 in the Arctic is also more realistic than with the ECMWF scheme. COPCAT produces too low tropical maximum O_3 compared to the full-chemistry, differences can be reduced with the use of an appropriate climatology, $\bar{f}$. However, this points to a shortcoming in the Cariolle and Déqué based schemes, related to the upper limit imposed in the O_3 term by $\bar{f}$. The inclusion of heterogenous chemistry has not damaged the linearity of the scheme, which is linear for deviations of $\pm 40\%$ in local O_3, of up to $\pm 20\%$ in O_3 column above and of up to ± 10 K deviations in temperature for all latitudes and months; the range for temperature expands further outside the polar regions. The approach adopted by COPCAT is proposed as an improved alternative to the operational ECMWF ozone approach.

In Chapter 7 a new linear parameterisation for stratospheric CH_4 (CoMeCAT) was developed. The parameterisation was tested in the SLIMCAT CTM, where it exhibited a good agreement with full-chemistry and HALOE observations. The scheme has also been implemented in the ECMWF GCM model, where it will replace their old global constant value. The SLIMCAT and the ECMWF simulations with CoMeCAT agreed well except in the tropical latitudes, where transport differences between the two models were most probably causing the discrepancies.

By using CoMeCAT CH_4 coupled to the ECMWF radiation scheme, temperature in the mid/upper stratosphere increased by 1.8 K, compared to ECMWF runs using their default CH_4 global value. This showed the necessity of including realistic distributions of radiatively active gases in NWP models. The inclusion of a realistic CH_4 tracer in the ECMWF model also allowed the evaluation of nudging effects in the GCM. One GCM run with dynamical fields nudged to ERA-40 values gave results similar to those obtained by TOMCAT ($\sigma - p$) driven by ERA-40. This

indicated that results obtained with a nudged GCM are limited by the quality of the analyses used for nudging. In the case shown in Chapter 7, the same transport problems exhibited by ERA-40 were present in simulations run with a recent version of the ECMWF GCM nudged to the reanalysis.

The CoMeCAT CH_4 scheme was used to derive a source of stratospheric H_2O. Results from the CTM using this approach agreed well with HALOE data, although model concentrations were 0.5 ppmv higher, at least partly due to the use of ERA-40 humidity entry values at the tropopause. GCM runs using the CoMeCAT H_2O source were 1.0 ppmv lower than in the CTM, differences in the initial state and simulations length are reasons for the underestimation obtained with the GCM run.

8.2 Concluding remarks

This thesis has revealed CTMs as powerful tools for evaluating meteorological datasets. The evaluation performed in this work has shown that ECMWF data assimilation products have significantly improved in recent years and, even if there is still room for future improvements, stratospheric transport problems detected for the ERA-40 data (Chapter 2) have been greatly overcome in the experimental data tested in Chapters 3 and 4. Results from this thesis have been used by ECMWF on taking their final decisions for the configuration of the ERA-Interim system. The new ECMWF reanalysis is considered to be a promising dataset for stratospheric CTM studies, as it will have significantly solved past stratospheric transport problems (Simmons *et al.*, 2007; Monge-Sanz *et al.*, 2007). Also, as shown in Chapter 3, with better quality reanalyses (EXP471 instead of ERA-40), the implementation of the correction techniques within the CTM makes much smaller difference, which means ERA-Interim will be on the right way towards the meteorological analysis that CTMs will be able to use directly.

The use of a CTM to evaluate reanalysis data 'a priori', *i.e.* previous to the

final production phase, has proved to be very fruitful for both CTM users and the involved data assimilation centre. Thus, this practice should be widely implemented in the future to obtain better products and increased knowledge on models. It is also recommended the use of analysis frequencies of 6h or less to drive CTM simulations, and DAS centres should consider archiving their products every 3h. Future efforts need to concentrate also on determining the causes for the improvements in the new data assimilation products, to achieve this the collaboration between CTM modellers and meteorological centres is essential (see Section 8.3).

Until data assimilation centres like ECMWF are able to operationally implement full-chemistry models, they rely on the accuracy of chemical parameterisations. Including heterogeneous ozone chemistry implicitly in the O_3 parameterisation is a more natural and realistic approach than that used operationally by ECMWF, or the use of a cold-tracer. Existing CTM models, such as SLIMCAT, include complete heterogeneous chemistry and are able to provide realistic O_3 parameterisations with implicit heterogeneous chemistry. This thesis has shown that, based on a widely tested full-chemistry model, it is possible to include heterogeneous chemistry in a CD-like O_3 parameterisation in a consistent way with the gas-phase chemistry, without needing any other additional tunable parameters.

A more realistic O_3 field in the NWP/DAS model will result in a more efficient use of satellite radiances. The impact stratospheric O_3 has on tropospheric pressure and winds has already been shown by *e.g.* Thompson and Solomon (2002), Shindell and Schmidt (2004) or Son *et al.* (2008). Thus, improving the O_3 field in NWP models will also have a positive effect on weather prediction, allowing more reliable long-term forecasts.

The use of a realistic CH_4 distribution (CoMeCAT) in the ECMWF GCM has a direct impact on the temperature field. Many GCMs are still using very simple representations for radiatively active gases in the stratosphere. The inclusion of

realistic schemes for these gases is thus also necessary for a more realistic use of satellite radiances and also for radiative forcing calculations.

Work carried out in this thesis contributes towards the improvement of stratospheric (re)analyses, and better reanalysis will improve the accuracy of CTM studies. Therefore, approaches adopted in this thesis have opened important research feedbacks that will help to increase present understanding of stratospheric processes and help to improve models.

8.3 Future research lines

Investigations carried out in this thesis have pointed towards new research lines, both concerning stratospheric transport and chemical parameterisations. Some of these lines make use of the improved (re)analysis data, while other lines are aimed at obtaining further improvements in the (re)analyses.

The quality of stratospheric transport achieved by EXP471 makes one expect similar, if not better, results with the final ERA-Interim product. Multiannual CTM runs with the ERA-Interim series will allow for stratospheric transport interannual variability studies. This, together with new global age-of-air observation-based distributions (Stiller *et al.*, 2008), will permit an assessment of possible changes in the BDC.

Transport studies in this thesis have shown how a CTM can be used to evaluate, not only the quality of different meteorological (re)analysis, but also how different aspects in the NWP/DAS model affect that quality. For a thorough evaluation of NWP/DAS model impacts on the stratospheric representation, longer customized datasets need to be produced by weather centres. Such datasets can then be evaluated by a CTM, so that NWP/DAS systems can invest research time more efficiently to get better (re)analysis products. This will also help to highlight aspects of the

NWP/DAS models that need to be improved, and how different feedbacks interact. At the same time CTM users will eventually obtain better products to drive their models, more accurate results will be obtained, and better understanding of stratospheric processes will be achieved. Some stratospheric research issues that remain open concern the UTLS region, where problems with existing (re)analyses cause uncertainties. Quantification of stratosphere-troposphere exchange (STE) and processes in the tropical tropopause layer (TTL) are key issues for understanding the distribution of many chemical species (*e.g.* O_3, H_2O, CH_4, VSLS) and, therefore, radiation and circulation in the stratosphere, as well as feedbacks with the troposphere. All these studies require accurate datasets to drive the CTMs. As noted by Shepherd (2007), with the help of more accurate stratospheric analyses, CTM studies will enter their 'golden age' in the next decade, and provide a better quantification of stratospheric processes.

Potential research lines deriving from the parameterisation work also include the development of linear schemes similar to CoMeCAT for other radiative active gases like CO_2 and CFCs, as well as further assessment of impacts in the NWP model when using the schemes interactively. Also, radiative forcing calculations could be performed with the new schemes and compared with results obtained with the simple global values included now in most climate models. The approach adopted to obtain COPCAT suggests an improvement for CD-like O_3 schemes that could be implemented by centres like ECMWF, while full-chemistry is not affordable for operational data assimilation and forecasting.

Appendix A

GRL paper

[BLANK PAGE]

[BLANK PAGE]

[BLANK PAGE]

[BLANK PAGE]

[BLANK PAGE]

Appendix B

ECMWF/GEO Workshop abstract

[BLANK PAGE]

[BLANK PAGE]

[BLANK PAGE]

[BLANK PAGE]

[BLANK PAGE]

[BLANK PAGE]

Bibliography

Anderson, J., Russell III, J. M., Solomon, S. and Deaver, L. (2000). Halogen Occultation Experiment confirmation of stratospheric chlorine decreases in accordance with the Montreal Protocol. *J. Geophys. Res.* **105**, 4483–4490.

Andrews, A. E., Boering, K. A., Daube, B. C., Wofsy, S. C., Loewenstein, M. and Jost, H. (2001). Mean ages of stratospheric air derived from in situ observations of CO_2, CH_4 and N_2O. *J. Geophys. Res.* **106**, 32295–32314.

Auligné, T., McNally, A. P. and Dee, D. P. (2007). Adaptive bias correction for satellite data in a numerical weather prediction system. *Q. J. R. Meteorol. Soc.* **133**, 631–642.

Austin, J., Shindell, D., Beagley, S. R., Brühl, C., Dameris, M., Manzini, E., Nagashima, T., Newman, P., Pawson, S., Pitari, G., Rozanov, E., Schnadt, C. and Shepherd, T. G. (2003). Uncertainties and assessments of chemistry-climate models of the stratosphere. *Atmos. Chem. Phys.* **3**, 1–27.

Austin, J., Wilson, J., Li, F. and Vömel, H. (2007). Evolution of water vapor concentrations and stratospheric age of air in coupled chemistry-climate model simulations. *J. Atmos. Sci.* **64**, 905–921, doi:10.1175/JAS3866.1.

Barnett, J. J., Houghton, J. T. and Pyle, J. A. (1975). The temperature dependence of the ozone concentration near the stratopause. *Q. J. R. Meteorol. Soc.* **101**, 245–257.

Bates, D. R. and Nicolet, M. (1950). The photochemistry of water vapour. *J. Geophys. Res.* **55**, 301–327.

Bengtsson, L. and Shukla, J. (1988). Integration of space and insitu observations to study global climate change. *Bull. Am. Meteorol. Soc.* **69**, 1130–1143.

Benito Garcia-Morales, M. and Dubus, L. (2007). Forecasting precipitation for hydroelectric power management: How to exploit GCMs seasonal ensemble forecasts. *Int. J. Climatol.* **27**, doi:10.1002/joc.1608.

Berthet, G., Huret, N., Lefèvre, F., Moreau, G., Robert, C., Chartier, M., Catoire, V., Barret, B., Pisso, I. and Pomathiod, L. (2006). On the ability of chemical transport models to simulate the vertical structure of the N_2O, NO_2 and HNO_3 species in the mid-latitude stratosphere. *Atmos. Chem. Phys.* **6**, 1599–1609.

Blake, D. and Lindzen, R. S. (1973). Effect of photochemical models on calculated equilibria and cooling rates in the stratosphere. *Mon. Wea. Rev.* **101**, 783–802.

Bloom, S., da Silva, A., Dee, D., Bosilovich, M., Chern, J.-D., Pawson, S., Schubert, S., Sienkiewicz, M., Stajner, I., Tan, W.-W. and Wu, M.-L. (2005). Documentation and validation of the Goddard Earth Observing System (GEOS) data assimilation system - Version 4. *Technical Report Series on Global Modeling and Data Assimilation 104606* **26**.

Boering, K. A., Wofsy, S. C., Daube, B. C., Schneider, H. R., Loewenstein, M., Podolske, J. R. and Conway, T. J. (1996). Stratospheric mean ages and transport rates from observations of carbon dioxide and nitrous oxide. *Science* **274**, 1340–1343.

Brasseur, G. and Solomon, S. (1984). *Aeronomy of the Middle Atmosphere.* D. Reidel Publishing, Co. Dordrecht.

Brasseur, G. and Solomon, S. (2005). *Aeronomy of the Middle Atmosphere.* Springer, Dordrecht.

Bregman, B., Meijer, E. and Scheele, R. (2006). Key aspects of stratospheric tracer modeling using assimilated winds. *Atmos. Chem. Phys.* **6**, 4529–4543.

Bregman, B., Segers, A., Krol, M., Meijer, E. and van Velthoven, P. (2003). On the use of mass-conserving wind fields in chemistry-transport models. *Atmos. Chem. Phys.* **3**, 447–457.

Brewer, A. W. (1949). Evidence for a world circulation provided by the measurements of helium and water vapour distribution in the stratosphere. *Q. J. R. Meteorol. Soc.* **75**, 351–363.

Briegleb, B. P. (1992). Delta-Eddington approximation for solar radiation in the NCAR community climate model. *J. Geophys. Res.* **97**, 7603–7612.

Brühl, C., Drayson, S. Roland, Russell III, James M., Crutzen, Paul J., Mclnerney, Joseph M., Purcell, Patrick N., Claude, Hans, Gernandt, Hartwig, McGee, Thomas J., McDermid, Iain S. and Gunson, Michael R. (1996). Halogen Occultation Experiment ozone channel validation. *J. Geophys. Res.* **101**, 10,217–10,240.

Butchart, N. and Remsberg, E. E. (1986). The area of the stratospheric polar vortex as a diagnostic for tracer transport on an isentropic surface. *J. Atmos. Sci.* **43**, 1319–1339.

Cardinali, C., Pezzulli, S. and Anderson, E. (2004). Influence-matrix diagnostic of a data assimilation system. *Q. J. R. Meteorol. Soc.* **130**, 2767–2786.

Cariolle, D. (1983). The ozone budget in the stratosphere: Results of a one-dimensional photochemical model. *Planet. Space Sci.* **31**, 1033–1052.

Cariolle, D. and Brard, B. (1984). The distribution of ozone and active stratospheric species: Result of a two-dimensional atmospheric model. In C. S. Zerefos and A. Ghazi (Eds.), *Atmospheric Ozone*, pp. 77–81. D. Reidel, Higham, Mass.

Cariolle, D. and Déqué, M. (1986). Southern hemisphere medium-scale waves and total ozone disturbances in a spectral general circulation model. *J. Geophys. Res.* **91**, 10825–10846.

Cariolle, D. and Teyssèdre, H. (2007). A revised linear ozone photochemistry parameterization for use in transport and general circulation models: Multi-annual simulations. *Atmos. Chem. Phys.* **7**, 2183–2196.

Carslaw, K. S., Luo, B. P., Clegg, S. L., Peter, T., Brimblecombe, P. and Crutzen, P. J. (1994). Stratospheric aerosol growth and HNO_3 gas phase depletion from coupled HNO_3 and water uptake by liquid particles. *Geophys. Res. Lett.* **21**, 2479–2482.

Challinor, A. J., Wheeler, T. R., Slingo, J. M., Craufurd, P. Q. and Grimes, D. I. F. (2005). Simulation of crop yields using ERA-40: Limits to skill and nonstationarity in weather-yield relationships. *J. Appl. Meteor.* **44**, 516–531.

Chapman, S. (1930). On ozone and atomic oxygen in the upper atmosphere. *Philosophical Magazine* **10**, 369–383.

Chipperfield, M. P. (1999). Multiannual simulations with a three-dimensional chemical transport model. *J. Geophys. Res.* **104**, 1781–1805.

Chipperfield, M. P. (2003). A three-dimensional model study of long-term mid-high latitude lower stratosphere ozone changes. *Atmos. Chem. Phys.* **3**, 1253–1265.

Chipperfield, M. P. (2006). New version of the TOMCAT/SLIMCAT off-line chemical transport model. *Q. J. R. Meteorol. Soc.* **132**, 1179–1203.

Chipperfield, M. P., Cariolle, D. and Simon, P. (1994). A 3-dimensional transport model study of PSC processing during EASOE. *Geophys. Res. Lett.* **21**, 1463–1466.

Chipperfield, M. P., Cariolle, D., Simon, P., Ramaroson, R. and Lary, D. J. (1993). A 3-dimensional modeling study of trace species in the Arctic lower stratosphere during winter 1989-1990. *J. Geophys. Res.* **98**, 7199–7218.

Chipperfield, M. P., Feng, W. and Rex, M. (2005). Arctic ozone loss and climate sensitivity: Updated three-dimensional model study. *Geophys. Res. Lett.* **32**, doi:10.1029/2005GL022674.

Chipperfield, M. P., Khattatov, B. V. and Lary, D. J. (2002). Sequential assimilation of stratospheric chemical observations in a three-dimensional model. *J. Geophys. Res.* **107**, doi:10.1029/2002JD002110.

Collins, W.D., Ramaswamy, V., Schwarzkopf, M.D., Sun, Y., Portmann, R.W., Fu, Q., Casanova, S.E.B., Dufresne, J.-L., Fillmore, D.W., Forster, P.M.D, Galin, V.Y., Gohar, L.K., Ingram, W.J., Kratz, D.P., Lefebvre, M.-P., Li, J., Marquet, P., Oinas, V., Tsushima, Y., Uchiyama, T. and Zhong, W.Y. (2006). Radiative forcing by well-mixed greenhouse gases: Estimates from climate models in the Intergovernmental Panel on Climate Change (IPCC) Fourth Assessment Report (AR4). *J. Geophys. Res.* **111**, doi:10.1029/2005JD006713.

Crutzen, P. J., Grooss, J. U., Brühl, C., Müller, R. and Russell III, J. M. (1995). A reevaluation of the ozone budget with HALOE UARS data: No evidence for the ozone deficit. *Science* **268**, 705–708.

Cunnold, D., Alyea, F., Phillips, N. and Prinn, R. (1975). 3-dimensional dynamical-chemical model of atmospheric ozone. *J. Atmos. Sci.* **32**, 170–194.

Curry, C. L., McFarlane, N. A. and Scinocca, J. F. (2006). Relaxing the well-mixed greenhouse gas approximation in climate simulations: Consequences for stratospheric climate. *J. Geophys. Res.* **111**, doi:10.1029/2005JD006670.

Derber, J.C. and Bouttier, F. (1999). Formulation of the background error covariances in the ECMWF global data assimilation system. *Tellus* **51A**, 195–221.

Dessler, A. (2000). *The chemistry and physics of stratospheric ozone*, Volume 74 of *International Geophysics Series*. Academic Press.

Dethof, A. (2003). Aspects of modelling and assimilation for the stratosphere at ECMWF. *SPARC Newsletter* (21).

Dethof, A. and Hólm, E. (2002). Ozone in ERA-40: 1991-1996, ERA-40 Proj. Rep. Ser. 4. Technical report, ECMWF, Reading, U.K.

Dethof, A. and Hólm, E. V. (2004). Ozone assimilation in the ERA-40 reanalysis project. *Q. J. R. Meteorol. Soc.* **130**, 2851–2872.

Dobson, G. M. B. (1956). Origin and distribution of the polyatomic molecules in the atmosphere. *Proceedings of the Royal Society of London* **A236**, 187–193.

Douglass, A. R., Schoeberl, M. R., Rood, R. B. and Pawson, S. (2003). Evaluation of transport in the lower tropical stratosphere in a global chemistry and transport model. *J. Geophys. Res.* **108**, doi:10.1029/2002JD002696.

Eckermann, S. D., McCormack, J. P., Coy, L., Allen, D., Hogan, T. and Kim, Y.-J. (2004). NOGAPS-ALPHA: A prototype high-altitude global NWP model, paper P2.6. In *Preprint Volume, Symposium on the 50th Anniversary of Operational Numerical Weather Prediction*, University of Maryland, College Park, MD, pp. 23. Am. Meteorol. Soc.

Elkins, J. W., Fahey, D. W., Gilligan, J. M., Dutton, G. S., Baring, T. J., Volk, C. M., Dunn, R. E., Myers, R. C., Montzka, S. A., Wamsley, P. R., Hayden, A. H., Butler, J. H., Thompson, T. M., Swanson, T. H., Dlugokencky, E. J., Novelli, P. C., Hurst, D. F., Lobert, J. M., Ciciora, S. J., McLaughlin, R. J., Thompson, T. L., Winkler, R. H., Fraser, P. J., Steele, L. P. and Lucarelli, M. P. (1996). Airborne gas chromatograph for in situ measurements of long-lived species in the upper troposphere and lower stratosphere. *Geophys. Res. Lett.* **23**, 347–350.

Eluszkiewicz, J. and Allen, M. (1993). A global analysis of the ozone deficit in the upper stratosphere and lower mesosphere. *J. Geophys. Res.* **98**, 1069–1082.

Eluszkiewicz, J., Hemler, R.S., Mahlman, J. D., Bruhwiler, L. and Tacks, L. L. (2000). Sensitivity of age-of-air calculation to the choice of the advection scheme. *J. Atmos. Sci.* **57**, 3185–3201.

Ertel, H. (1942). Ein Neuer hydrodynamischer Wirbelsatz. *Meteor. Z.* **59**, 277–281.

Eyring, V., Butchart, N., Waugh, D. W., Akiyoshi, H., Austin, J., Bekki, S., Bodeker, G. E., Boville, B. A., Brühl, C., Chipperfield, M. P., Cordero, E., Dameris, M., Deushi, M., Fioletov, V. E., Frith, S. M., Garcia, R. R., Gettelman, A., Giorgetta, M. A., Grewe, V., Jourdain, L., Kinnison, D. E., Mancini, E., Manzini, E., Marchand, M., Marsh, D. R., Nagashima, T., Newman, P. A., Nielsen, J. E., Pawson, S., Pitari, G., Plummer, D. A., Rozanov, E., Schraner, M., Shepherd, T. G., Shibata, K., Stolarski, R. S., Struthers, H., Tian, W. and Yoshiki, M. (2006). Assessment of temperature, trace species, and ozone in chemistry-climate model simulations of the recent past. *J. Geophys. Res.* **111**, doi:10.1029/2006JD007327.

Eyring, V., Harris, N. R. P., Rex, M., Shepherd, T. G., Fahey, D. W., Amanatidis, G. T., Austin, J., Chipperfield, M. P., Dameris, M., Forster, P. M. F., Gettelman, A., Graf, H. F., Nagashima, T., Newman, P. A., Pawson, S., Prather, M. J., Pyle, J. A., Salawitch, R. J., Santer, B. D. and Waugh, D. W. (2005). A strategy for process-oriented validation of coupled chemistry-climate models. *Bull. Am. Meteorol. Soc.* **86**, 1117–1133, doi:10.1175/BAMS–86–8–1117.

Eyring, V., Waugh, D. W., Bodeker, G. E., Cordero, E., Akiyoshi, H., Austin, J., Beagley, S. R., Boville, B. A., Braesicke, P., Brühl, C., Butchart, N., Chipperfield, M. P., Dameris, M., Deckert, R., Deushi, M., Frith, S. M., Garcia, R. R., Gettelman, A., Giorgetta, M. A., Kinnison, D. E., Mancini, E., Manzini, E., Marsh, D. R., Matthes, S., Nagashima, T., Newman, P. A., Nielsen, J. E., Pawson, S., Pitari, G., Plummer, D. A., Rozanov, E., Schraner, M., Scinocca, J. F., Semeniuk, K., Shepherd, T. G., Shibata, K., Steil, B., Stolarski, R. S., Tian, W. and Yoshiki, M. (2007). Multimodel projections of stratospheric ozone in the 21st century. *J. Geophys. Res.* **112**, doi:10.1029/2006JD008332.

Feng, W., Chipperfield, M. P., Dorf, M., Pfeilsticker, K. and Ricaud, P. (2007). Mid-latitude ozone changes: studies with a 3-D CTM forced by ERA-40 analyses. *Atmos. Chem. Phys.* **7**, 2357–2369.

Feng, W., Chipperfield, M. P., Roscoe, H. K., Remedios, J. J., Waterfall, A. M.,

Stiller, G. P., Glatthor, N., Hopfner, M. and Wang, D. Y. (2005). Three-dimensional model study of the Antarctic ozone hole in 2002 and comparison with 2000. *J. Atmos. Sci.* **62**, 822–837.

Fisher, M. (2003). Background error covariance modelling. In *Seminar on Recent developments in data assimilation for atmosphere and ocean, 8-12 September 2003*, pp. 45–64. ECMWF.

Fisher, M. (2006). "Wavelet" J_b - A new way to model the statistics of background errors. *ECMWF Newsletter No.* **106**, 23–28.

Fisher, M., O'Neill, A. and Sutton, R. (1993). Rapid descent of mesopheric air into the stratospheric polar vortex. *Geophys. Res. Lett.* **20**, 1267–1270.

Fleming, E. L., Chandra, S., Barnett, J. J. and Corney, M. (1990). Zonal mean temperature, pressure, zonal wind, and geopotential height as functions of latitude, COSPAR International Reference Atmosphere: 1986, Part II: Middle atmosphere models. *Adv. Space Res.* **10**, 11–59.

Fleming, E. L., Jackman, C. H ., Considine, D. B. and Stolarski, R. S. (2001). Sensitivity of tracers and a stratospheric aircraft perturbation to two-dimensional model transport. *J. Geophys. Res* **106**, 14245–14263.

Folkins, I. (2005). Temperatures, transport and chemistry in the TTL. *SPARC Newsletter* (25), 23–26.

Folkins, I. and Martin, R. V. (2005). The vertical structure of tropical convection and its impact on the budgets of water vapor and ozone. *J. Atmos. Sci.* **62**, 1560–1573.

Fortuin, J. P. F. and Kelder, H. (1998). An ozone climatology based on ozonesonde and satellite measurements. *J. Geophys. Res.* **103**, 31709–31734.

Fortuin, J. P. F. and Langematz, U. (1995). An update on the global ozone climatology and on concurrent ozone and temperature trends. In *Proceedings of SPIE Conference on Atmospheric Sensing and Modelling*, pp. 207–216.

Froidevaux, L., Allen, M. and Yung, Y. L. (1985). A critical analysis of ClO and O_3 in the mid-latitude stratosphere. *J. Geophys. Res.* **90**, 12999–13029.

Fueglistaler, S. and Fu, Q. (2006). Impact of clouds on radiative heating rates in the tropical lower stratosphere. *J. Geophys. Res.* **111**, doi:10.1029/2006JD007273.

Fueglistaler, S., Legras, B., Beljaars, A., Morcrette, J.-J., Simmons, A., Tompkins, A.M. and Uppala, S. (2008). The diabatic heat budget of the upper troposphere and lower/mid stratosphere in ECMWF reanalyses. *Q. J. R. Meteorol. Soc.*, submitted.

Fueglistaler, S., Wernli, H. and Peter, T. (2004). Tropical troposphere-to-stratosphere transport inferred from trajectory calculations. *J. Geophys. Res.* **109**, 16.

Gabriel, A. and Schmitz, G. (2002). Dynamical components of northern hemispheric zonal mean total ozone changes during 1979-93. *Geophys. Res. Lett.* **29**, doi:10.1029/2002GL015358.

Gauthier, P. and Thepaut, J. N. (2001). Impact of the digital filter as a weak constraint in the preoperational 4DVAR assimilation system of Météo-France. *Mon. Wea. Rev.* **129**, 2089–2102.

Geer, A. J., Lahoz, W. A., Bekki, S., Bormann, N., Errera, Q., Eskes, H. J., Fonteyn, D., Jackson, D. R., Juckes, M. N., Massart, S., Peuch, V. H., Rharmili, S. and Segers, A. (2006). The ASSET intercomparison of ozone analyses: Method and first results. *Atmos. Chem. Phys.* **6**, 5445–5474.

Geer, A. J., Lahoz, W. A., Jackson, D. R., Cariolle, D. and McCormack, J. P. (2007). Evaluation of linear ozone photochemistry parametrizations in a stratosphere-troposphere data assimilation system. *Atmos. Chem. Phys.* **7**, 939–959.

Gettelman, A., Holton, J. R. and Rosenlof, K. H. (1997). Mass fluxes of O_3, CH_4, N_2O and CF_2Cl_2 in the lower stratosphere calculated from observational data. *J. Geophys. Res.* **102**, 19149–19159.

Grant, W. B., Browell, E. V., Fishman, J., Brackett, V. G., Veiga, R. E., Nganga, D., Minga, A., Cros, B., Butler, C. F., Fenn, M. A., Long, C. S. and Stowe, L. L. (1994). Aerosol-associated changes in tropical stratospheric ozone following the eruption of Mount-Pinatubo. *J. Geophys. Res.* **99**, 8197–8211.

Gunson, M. R., Abbas, M. M., Abrams, M. C., Allen, M., Brown, L. R., Brown, T. L., Chang, A. Y., Goldman, A., Irion, F. W., Lowes, L. L., Mahieu, E., Manney, G. L., Michelsen, H. A., Newchurch, M. J., Rinsland, C. P., Salawitch, R. J., Stiller, G. P., Toon, G. C., Yung, Y. L. and Zander, R. (1996). The Atmospheric Trace Molecule Spectroscopy (ATMOS) experiment: Deployment on the ATLAS Space Shuttle missions. *Geophys. Res. Lett.* **23**, 2333–2336.

Hadjinicolaou, P., Pyle, J. A. and Harris, N. R. P. (2005). The recent turnaround in stratospheric ozone over northern middle latitudes: A dynamical modelling perspective. *Geophys. Res. Lett.* **32**, doi:10.1029/2005GL022476.

Haimberger, L. (2006). Bias correction of radiosonde observations. In *ECMWF/GEO Workshop on Atmospheric Reanalysis, 19-22 June 2006*, pp. 123–125. ECMWF.

Hall, T. M. and Plumb, R. A. (1994). Age as a diagnostic of stratospheric transport. *J. Geophys. Res.* **99**, 1059–1070.

Hall, T. M., Waugh, D. W., Boering, K. A. and Plumb, R. A. (1999). Evaluation of transport in stratospheric models. *J. Geophys. Res.* **104**, 18815–18839.

Hamilton, K., Wilson, R. J., Mahlman, J. D. and Umscheid, L. J. (1995). Climatology of the SKYHI troposphere stratosphere mesosphere general circulation model. *J. Atmos. Sci.* **52**, 5–43.

Hanson, D. and Mauersberger, K. (1988). Laboratory studies of the nitric acid trihydrate: Implications for the south polar stratosphere. *Geophys. Res. Lett.* **15**, 855–858.

Harnisch, J., Bischof, W., Borchers, R., Fabian, P. and Maiss, M. (1998). A stratospheric excess of CO2-due to tropical deep convection? *Geophys. Res. Lett.* **25**, 63–66.

Harnisch, J., Borchers, R., Fabian, P. and Maiss, M. (1996). Tropospheric trends for CF_4 and C_2F_6 since 1982 derived from SF_6 dated stratospheric air. *Geophys. Res. Lett.* **23**, 1099–1102.

Harries, J. E., Russell, J. M., Tuck, A. F., Gordley, L. L., Purcell, P., Stone, K., Bevilacqua, R. M., Gunson, M., Nedoluha, G. and Traub, W. A. (1996). Validation of measurements of water vapor from the Halogen Occultation Experiment (HALOE). *J. Geophys. Res.* **101**, 10205–10216.

Haynes, P. (2005). Stratospheric dynamics. *Annu. Rev. Fluid Mech.* **37**, 263–293, doi: 10.1146/annurev.fluid.37.061903.175710.

Hollingsworth, A. and Pfrang, C. (2005). A preliminary survey of ERA-40 users developing applications of relevance to GEO (Group on Earth Observations). *ECMWF Newsletter* (104), 5–9.

Holtslag, A. A. M. and Boville, B. A. (1993). Local versus nonlocal boundary-layer diffusion in a global climate model. *J. Climate* **6**, 1825–1842.

Hurst, D. F., Dutton, G. S., Romashkin, P. A., Wamsley, P. R., Moore, F. L. and Elkins, J. W. (1999). Closure of the total hydrogen budget of the northern extratropical lower stratosphere. *J. Geophys. Res.* **104**, 8191–8200.

Jeuken, A., Siegmund, P., Heijboer, L., Feichter, J. and Bengtsson, L. (1996). On the potential of assimilating meteorological analyses in a global climate model for the purposes of model validation. *J. Geophys. Res.* **101**, 16939–16950.

Jones, R. L. and Pyle, J. A. (1984). Observations of CH_4 and N_2O by the Nimbus 7 SAMA: A comparison with in situ data and two-dimensional numerical model calculations. *J. Geophys. Res.* **89**, 5263–5279.

Juckes, M.N. and McIntyre, M. E. (1987). A high resolution, one-layer model of breaking planetary waves in the stratosphere. *Nature* **328**, 590–596.

Kållberg, P (1997). Aspects of the re-analysed climate, ECMWF ERA-15 Proj. Rep. Ser. 2. Technical report, ECMWF, Reading, U.K.

Kalnay, E., Kanamitsu, M., Kistler, R., Collins, W., Deaven, D., Gandin, L., Iredell, M., Saha, S., White, G., Woollen, J., Zhu, Y., Chelliah, M., Ebisuzaki, W., Higgins, W., Janowiak, J., Mo, K. C., Ropelewski, C., Wang, J., Leetmaa, A., Reynolds, R., Jenne, R. and Joseph, D. (1996). The NCEP/NCAR 40-year reanalysis project. *Bull. Am. Meteorol.* **77**, 437–471.

Kanamitsu, M., Ebisuzaki, W., Woollen, J., Yang, S.-K., Hnilo, J. J., Fiorino, M. and Potter, G. L. (2002). NCEP-DOE AMIP-II reanalysis (R-2). *Bull. Am. Meteorol.* **83**, 1631–1643.

Khosravi, R., Brasseur, G. P., Smith, A., Rusch, D. W., Waters, J. W. and Russell III, J. M. (1998). Significant reduction in the ozone deficit: A 3-D model study using UARS data. *J. Geophys. Res.* **103**, 16203–16219.

Kida, H. (1983). General circulation of air parcels and transport characteristics derived from a hemispheric GCM, Part 2, Very long-term motions of air parcels in the troposphere and stratosphere. *J. Meteorol. Soc. Jpn.* **61**, 510–522.

King, J. C., Brune, W. H., Toohey, D. W., Rodriguez, J. M., Starr, W. L., and Vedder, J. F. (1991). Measurements of ClO and O_3 from 21°N to 61°N in the lower stratosphere during February 1988: Implications for heterogeneous chemistry. *Geophys. Res. Lett.* **18**, 2273–2276.

Kinnersley, J. S. and Harwood, R. S. (1993). An isentropic two-dimensional model with an interactive parameterization of dynamical and chemical planetary wave fluxes. *Q. J. R. Meteorol. Soc.* **119**, 1167–1193.

Kistler, R., Kalnay, E., Collins, W., Saha, S., White, G., Woollen, J., Chelliah, M., Ebisuzaki, W., Kanamitsu, M., Kousky, V., van den Dool, H., Jenne, R.

and Fiorino, M. (2001). The NCEP/NCAR 50-year reanalysis: Monthly means CD-Rom and documentation. *Bull. Am. Meteorol. Soc.* **82**, 247–267.

Knudsen, B. M. (1996). Accuracy of Arctic stratospheric temperature analyses and the implications for the prediction of polar stratospheric clouds. *Geophys. Res. Lett.* **23**, 3747–3750.

Knudsen, B. M. (2003). On the accuracy of analysed low temperatures in the stratosphere. *Atmos. Chem. Phys.* **3**, 1759–1768.

Kouker, W. and Coauthors (2005). Towards the Prediction of Stratospheric Ozone (TOPOZ III), Scientific Report. EC Contract EVK2-CT-2001-00102, European Commission, Brussels, Belgium.

Krüger, K., Tegtmeier, S. and Rex, M. (2008). Long-term climatology of air mass transport through the tropical tropopause layer (TTL) during NH winter. *Atmos. Chem. Phys.* **8**, 813–823.

Labitzke, K. and Coauthors (2002). *The Berlin Stratospheric Data Series.* Meteorological Institute, Free University of Berlin, CD-ROM.

Lahoz, W., Geer, A., Swinbank, R., Jackson, D., Thornton, H., Dethof, A. and D., Fonteyn (2004). Modelling and assimilation: Evaluation of MIPAS water vapour data. In *Proceedings of the Second Workshop on the Atmospheric Chemistry Validation of ENVISAT (ACVE-2), 3-7 May 2004*. ESA-ESRIN, Frascati, Italy.

Lait, L. R. (1994). An alternative form for potential vorticity. *J. Atmos. Sci.* **51**, 1754–1759.

Langematz, U. (2000). An estimate of the impact of observed ozone losses on stratospheric temperature. *Geophys. Res. Lett.* **27**, 2077–2080.

Le Texier, H., Solomon, S. and Garcia, R. R. (1988). The role of molecular hydrogen and methane oxidation in the water vapour budget of the stratosphere. *Q. J. R. Meteorol. Soc.* **114**, 281–295.

Lefèvre, F., Brasseur, G. P., Folkins, I., Smith, A. K. and Simon, P. (1994). Chemistry of the 1991-1992 stratospheric winter: Three-dimensional model simulations. *J. Geophys. Res.* **99**, 8183–8195.

Legras, B., Pisso, I., Berthet, G. and Lefèvre, F. (2005). Variability of the Lagrangian turbulent diffusivity in the lower stratosphere. *Atmos. Chem. Phys.* **5**, 1605–1622.

Lindzen, R. S. and Goody, R. (1965). Radiative and photochemical processes in mesospheric dynamics: Part I, models for radiative and photochemical processes. *J. Atmos. Sci.* **22**, 341–348.

Lorenc, A. C., Bell, R. S. and Macpherson, B. (1991). The Meteorological Office analysis correction data assimilation scheme. *Q. J. R. Meteorol. Soc.* **117**, 59–89.

Louis, J.-F. (1979). A parametric model of vertical eddy fluxes in the atmosphere. *Boundary Layer Meteorol.* **17**, 187–202.

MacKenzie, I. A. and Harwood, R. S. (2004). Middle atmospheric response to a future increase in humidity arising from increased methane abundance. *J. Geophys. Res.* **109**, doi:10.1029/2003JD003590.

Mahowald, N. M., Plumb, R. A., Rasch, P. J., del Corral, J., Sassi, F. and Heres, W. (2002). Stratospheric transport in a three-dimensional isentropic coordinate model. *J. Geophys. Res.* **107**, doi:10.1029/2001JD001313.

Manney, G. L., Sabutis, J. L., Allen, D. R., Lahoz, W. A., Scaife, A. A., Randall, C. E., Pawson, S., Naujokat, B. and Swinbank, R. (2005). Simulations of dynamics and transport during the September 2002 Antarctic major warming. *J. Atmos. Sci.* **62**, 690–707.

Manney, G. L., Sabutis, J. L., Pawson, S., Santee, M. L., Naujokat, B., Swinbank, R., Gelman, M. E. and Ebisuzaki, W. (2003). Lower stratospheric temperature differences between meteorological analyses in two cold Arctic win-

ters and their impact on polar processing studies. *J. Geophys. Res.* **108**, doi:10.1029/2001JD001149.

McCormack, J. P., Eckermann, S. D., Coy, L., Allen, D. R., Kim, Y. J., Hogan, T., Lawrence, B., Stephens, A., Browell, E. V., Burris, J., McGee, T. and Trepte, C. R. (2004). NOGAPS-ALPHA model simulations of stratospheric ozone during the SOLVE2 campaign. *Atmos. Chem. Phys.* **4**, 2401–2423.

McCormack, J. P., Eckermann, S. D., Siskind, D. E. and McGee, T. J. (2006). CHEM2D-OPP: A new linearized gas-phase ozone photochemistry parameterization for high-altitude NWP and climate models. *Atmos. Chem. Phys.* **6**, 4943–4972.

McLinden, C. A., Olsen, S. C., Hannegan, B., Wild, O. and Prather, M. J. (2000). Stratospheric ozone in 3-D models: A simple chemistry and the cross-tropopause flux. *J. Geophys. Res.* **105**, 14635–14665.

McPeters, R.D., Bhartia, P.K., Krueger, A.J., Herman, J. R., Wellemeyer, C.G., Seftor, C.J., Jaross, G., Torres, O., Moy, L., Labow, G., Byerly, W., Taylor, S.L., Swissler, T. and Cebula, R.P. (1998). Earth Probe Total Ozone Mapping Spectrometer (TOMS) data products user's guide. *NASA Ref. Publ. 206895*.

Meijer, E. W., Bregman, B., Segers, A. and van Velthoven, P.F.J. (2004). The influence of data assimilation on the age of air calculated with a global chemistry-transport model using ECMWF wind fields. *Geophys. Res. Lett.* **31**, doi:10.1029/2004GL021158.

Methven, J. (1997). Offline trajectories: Calculation and accuracy, Tech. Report 44, U.K. Univ. Global Atmos. Modelling Programme, Dept. of Meteorol., University of Reading, Reading, U.K.

Monge-Sanz, B. M. and Chipperfield, M. P. (2006). Chemical transport modelling. In *ECMWF/GEO Workshop on Atmospheric Reanalysis, 19-22 June 2006*, pp. 39–44. ECMWF.

Monge-Sanz, B. M., Chipperfield, M. P., Simmons, A. J. and Uppala, S. M. (2007). Mean age of air and transport in a CTM: Comparison of different ECMWF analyses. *Geophys. Res. Lett.* **34**, doi:10.1029/2006GL028515.

Morcrette, J.-J. (2003). Ozone-radiation interactions in the ECMWF forecast system, Tech. Mem. No. 375, ECMWF, Reading, U.K.

Mote, P. W., Dunkerton, T. J., McIntyre, M. E., Ray, E. A., Haynes, P. H. and Russell, J. M. (1998). Vertical velocity, vertical diffusion, and dilution by mid-latitude air in the tropical lower stratosphere. *J. Geophys. Res.* **103**, 8651–8666.

Mote, P. W., Rosenlof, K. H., McIntyre, M. E., Carr, E. S., Gille, J. C., Holton, J. R., Kinnersley, J. S., Pumphrey, H. C., Russell, J. M. and Waters, J. W. (1996). An atmospheric tape recorder: The imprint of tropical tropopause temperatures on stratospheric water vapor. *J. Geophys. Res.* **101**, 3989–4006.

Newman, P. A., Nash, E. R. and Rosenfield, J. E. (2001). What controls temperature of the Arctic stratosphere during spring? *J. Geophys. Res.* **106**, 19999–20010.

Oikonomou, E. K. and O'Neill, A. (2006). Evaluation of ozone and water vapor fields from the ECMWF reanalysis ERA-40 during 1991-1999 in comparison with UARS satellite and MOZAIC aircraft observations. *J. Geophys. Res.* **111**, doi:10.1029/2004JD005341.

Onogi, K., Tslttsui, J., Koide, H., Sakamoto, M., Kobayashi, S., Hatsushika, H., Matsumoto, T., Yamazaki, N., Kaalhori, H., Takahashi, K., Kadokura, S., Wada, K., Kato, K., Oyama, R., Ose, T., Mannoji, N. and Taira, R. (2007). The JRA-25 reanalysis. *J. Met. Soc. Japan* **85**, 369–432.

Park, J.H., Russell, J.M., L.Gordley, L., Drayson, S. R., Banner, D.C., McInerney, J.M., Gunson, M. R., Toon, G.C., Sen, B., Blavier, J.-F., Webster, C.R., Zipf, E.C., Erdman, P., Schmidt, U. and Schiller, C. (1996). Validation of Halogen Occultation Experiment CH_4 measurements from the UARS. *J. Geophys. Res.* **101**, 10217–10240.

Park, J. H., Ko, M. K. W., Jackman, C. H., Plumb, R. A., Kaye, J. A. and Sage, K. H., Editors (1999). Models and Measurements Intercomparison II. Technical Report 1999-209554, NASA.

Pawson, S., Stajner, I., Kawa, S. R., Hayashi, H., Tan, W.-W., Nielsen, J. E., Zhu, Z., Chang, L.-P. and Livesey, N. J. (2007). Stratospheric transport using 6-h-averaged winds from a data assimilation system. *J. Geophys. Res.* **112**, doi:10.1029/2006JD007673.

Plumb, R. A. and Ko, M. K. W. (1992). Interrelationships between mixing ratios of long lived stratospheric constituents. *J. Geophys. Res.* **97**, 10145–10156.

Prather, M.J. (1986). Numerical advection by conservation of second-order moments. *J. Geophys. Res.* **91**, 6671–6681.

Prather, M.J. (1992). Catastrophic loss of stratospheric ozone in dense volcanic clouds. *J. Geophys. Res.* **97**, 10187–10191.

Prather, M.J., Garcia, M. M. and Suozzo, R. (1990). Global impact of the Antarctic ozone hole: Dynamical dilution with a three-dimensional chemical transport model. *J. Geophys. Res.* **95**, 3449–3471.

Rabier, F., Järvinen, H., Klinker, E., Mahfouf, J.-F. and Simmons, A. (2000). The ECMWF operational implementation of four-dimensional variational assimilation. I: Experimental results with simplified physics. *Q. J. R. Meteorol. Soc.* **126**, 1143–1170.

Randel, W., Chanin, M.-L. and Michaut C., Editors (2002). SPARC intercomparison of middle atmosphere climatologies. Technical Report 3, SPARC.

Randel, W., Udelhofen, P., Fleming, E., Geller, M., Gelman, M., Hamilton, K., Karoly, D., Ortland, D., Pawson, S., Swinbank, R., Wu, F., Baldwin, M., Chanin, M. L., Keckhut, P., Labitzke, K., Remsberg, E., Simmons, A. and Wu, D. (2004a). The SPARC intercomparison of middle-atmosphere climatologies. *J. Climate* **17**, 986–1003.

Randel, W., Wu, F., Oltmans, S. J., Rosenlof, K. and Nedoluha, G. E. (2004b). Interannual changes of stratospheric water vapor and correlations with tropical tropopause temperatures. *J. Atmos. Sci.* **61**, 2133–2148.

Randel, W. J., Wu, F., Russell, J. M., Roche, A. and Waters, J. W. (1998). Seasonal cycles and QBO variations in stratospheric CH4 and H2O observed in UARS HALOE data. *J. Atmos. Sci.* **55**, 163–185.

Ray, E. A., Moore, F. L., Elkins, J. W., Dutton, G. S., Fahey, D. W., Vömel, H., Oltmans, S. J. and Rosenlof, K. H. (1999). Transport into the Northern Hemisphere lowermost stratosphere revealed by in situ tracer measurements. *J. Geophys. Res.* **104**, 26565–26580.

Reddman, T., Ruhnke, R. and Kouker, W. (2001). Three-dimensional model simulations of SF_6 with mesospheric chemistry. *J. Geophys. Res.* **106**, 14525–14537.

Remsberg, E. E., Russell, J. M., Gordley, L. L., Gille, J. C. and Bailey, P. L. (1984). Implications of stratospheric water vapour distribution as determined from the Nimbus 7 LIMS experiment. *J. Atmos. Sci.* **41**, 2934–2945.

Riishojgaard, L. P., Stajner, I. and Lou, G. P. (2000). The GEOS ozone data assimilation system. In *Remote Sensing and Applications: Earth, Atmosphere and Oceans*, Volume 25 of *Adv. Space Res.*, pp. 1063–1072.

Rodriguez, J. M., Ko, M. K. W. and Sze, N. D. (1991). Role of heterogeneous conversion of N_2O_5 on sulphate aerosols in global ozone losses. *Nature* **352**, 134–137.

Rogers, H. L., Norton, W. A., Lambert, A. and Grainger, R. G. (1999). Isentropic, diabatic, and sedimentary transport of Mount Pinatubo aerosol. *J. Geophys. Res.* **104**, 4051–4063.

Rood, R. B. (2005). Assimilation of stratospheric meteorological and constituent observations: A review. *SPARC Newsletter* (25), 31–37.

Russell, J. M., Gordley, L. L., Park, J. H., Drayson, S. R., Hesketh, W. D., Cicerone, R. J., Tuck, A. F., Frederick, J. E., Harries, J. E. and Crutzen, P. J. (1993). The Halogen Occultation Experiment. *J. Geophys. Res.* **98**, 10777–10797.

Sander, S. P., Friedl, R. R., Golden, D.M., Kurylo, M.J., Huie, R.E., Orkin, V.L., Moortgat, G.K., Ravishankara, A. R., Kolb, C.E., Molina, M.J. and Finlayson-Pitts, B.J. (2003). Chemical kinetics and photochemical data for use in atmospheric studies, Evaluation No. 14, JPL Publication No. 02-25. Technical report, Jet Propulsion Laboratory, Pasadena CA, USA.

Schär, C., Vidale, P. L., Lüthi, D., Frei, C., Häberli, C., Liniger, M. A. and Appenzeller, C. (2004). The role of increasing temperature variability in European summer heatwaves. *Nature* **427**, 332–336.

Scheele, M. P., Siegmund, P. C. and van Velthoven, P. F. J. (2005). Stratospheric age of air computed with trajectories based on various 3D-Var and 4D-Var data sets. *Atmos. Chem. Phys.* **5**, 1–7.

Schmidt, G., Ruedy, R., Hansen, J., Aleinov, I., Bell, N., Bauer, M., Bauer, S., Cairns, B., Canuto, V., Cheng, Y., Del Genio, A., Faluvegi, G., Friend, A., Hall, T., Hu, Y., Kelley, M., Kiang, N., Koch, D., Lacis, A., Lerner, J., Lo, K., Miller, R., Nazarenko, L., Oinas, V., Perlwitz, J., Perlwitz, J., Rind, D., Romanou, A., Russell, G., Sato, M., Shindell, D., Stone, P., Sun, S., Tausnev, N., Thresher, D. and Yao, M.-S. (2006). Present day atmospheric simulations using GISS Model: Comparison to in-situ, satellite and reanalysis data. *J. Climate* **19**, 153–192.

Schoeberl, M. R., Douglass, A., Zhu, Z. and Pawson, S. (2003). A comparison of the lower stratospheric age spectra derived from a general circulation model and two data assimilation systems. *J. Geophys. Res.* **108**, doi:10.1029/2002JD002652.

Schoeberl, M. R., Douglass, A. R., Polansky, B., Boone, C., Walker, K. A. and Bernath, P. (2005). Estimation of stratospheric age spectrum from chemical tracers. *J. Geophys. Res.* **110**, doi:10.1029/2005JD006125.

Schoeberl, M. R., Duncan, B. N., Douglass, A. R., Waters, J., Livesey, N., Read, W. and Filipiak, M. (2006). The carbon monoxide tape recorder. *Geophys. Res. Lett.* **33**, doi:10.1029/2006GL026178.

Searle, K. R., Chipperfield, M. P., Bekki, S. and Pyle, J. A. (1998). The impact of spatial averaging on calculated polar ozone loss 2. Theoretical analysis. *J. Geophys. Res.* **103**, 25409–25416.

Shepherd, T. G. (2007). Transport in the middle atmosphere. *J. Meteor. Soc. Japan* **85B**, 165–191.

Shindell, D. T. and Schmidt, G. A. (2004). Southern Hemisphere climate response to ozone changes and greenhouse gas increases. *Geophys. Res. Lett.* **31**, doi:10.1029/2004GL020724.

Shine, K. P. (1987). The middle atmosphere in the absence of dynamical heat fluxes. *Q. J. R. Meteorol. Soc.* **113**, 603–633.

Simmons, A., Uppala, S., Dee, D. and Kobayashi, S. (2007). ERA-Interim: New ECMWF reanalysis products from 1989 onwards. *ECMWF Newsletter* (110), 25–35.

Simmons, A. J., Hortal, M., Kelly, G., McNally, A., Untch, A. and Uppala, S. (2005). ECMWF analyses and forecasts of stratospheric winter polar vortex breakup: September 2002 in the Southern Hemisphere and related events. *J. Atmos. Sci.* **62**, 668–689.

Simmons, A. J., Untch, A., Jakob, C., Kallberg, P. and Unden, P. (1999). Stratospheric water vapour and tropical tropopause temperatures in ECMWF analyses and multi-year simulations. *Q. J. R. Meteorol. Soc.* **125**, 353–386.

Son, S.-W., Polvani, L.M., Waugh, D.W., Akiyoshi, H., Garcia, R., Kinnison, D., Pawson, S., Rozanov, E., Shepherd, T.G. and Shibata, K. (2008). The impact of stratospheric ozone recovery in the Southern Hemisphere westerly jet. *Science* **320**, 1486–1489.

Steil, B., Brühl, C., Manzini, E., Crutzen, P. J., Lelieveld, J., Rasch, P. J., Roeckner, E., and Krüger, K. (2003). A new interactive chemistry-climate model: 1. Present-day climatology and interannual variability of the middle atmosphere using the model and 9 years of HALOE/UARS data. *J. Geophys. Res.* **108**, doi:10.1029/2002JD002971.

Stiller, G. P., von Clarmann, T., Höpfner, M., Glatthor, N., Grabowski, U., Kellmann, S., Kleinert, A., Linden, A., Milz, M., Reddmann, T., Steck, T., Fischer, H., Funke, B., López-Puertas, M. and Engel, A. (2008). Global distribution of mean age of stratospheric air from MIPAS SF_6 measurements. *Atmos. Chem. Phys.* **8**, 677–695.

Stockwell, D. Z. and Chipperfield, M. P. (1999). A tropospheric chemical-transport model: Development and validation of the model transport schemes. *Q. J. R. Meteorol. Soc.* **125**, 1747–1783.

Stohl, A., Cooper, O. R. and James, P. (2004). A cautionary note on the use of meteorological analysis fields for quantifying atmospheric mixing. *J. Atmos. Sci.* **61**, 1446–1453.

Stolarski, R. S. and Douglass, A. R. (1985). Parameterization of the photochemistry of stratospheric ozone including catalytic loss processes. *J. Geophys. Res.* **90**, 10709–10718.

Strahan, S. E. and Polansky, B. C. (2006). Meteorological implementation issues in chemistry and transport models. *Atmos. Chem. Phys.* **6**, 2895–2910.

Swinbank, R. and O'Neill, A. (1994). A stratosphere troposphere data assimilation system. *Mon. Wea. Rev.* **122**, 686–702.

Tan, W. W., Geller, M. A., Pawson, S. and da Silva, A. (2004). A case study of excessive subtropical transport in the stratosphere of a data assimilation system. *J. Geophys. Res.* **109**, doi:10.1029/2003JD004057.

Taylor, C. P. and Bourqui, M. S. (2005). A new fast stratospheric ozone chemistry scheme in an intermediate general-circulation model, I: Description and evaluation. *Q. J. R. Meteorol. Soc.* **131**, 2225–2242, doi:10.1256/qj.04.18.

Tegtmeier, S. (2007). *Variationen der stratosphärischen Residualzirkulation und ihr Einfluss auf die Ozonverteilung.* Ph. D. thesis, Matematish-Naturwissenschaftliche Fakultät der Universität Potsdam.

Telford, P. J., Braesicke, P., Morgenstern, O. and Pyle, J. A. (2008). Technical Note: Description and assessment of a nudged version of the new dynamics Unified Model. *Atmos. Chem. Phys.* **8**, 1701–1712.

Thompson, D. W. J. and Solomon, S. (2002). Interpretation of recent Southern Hemisphere climate change. *Science* **296**, doi:10.1126/science.1069270.

Thomson, M. C., Doblas-Reyes, F. J., S. J. Mason, R. Hagedorn, Connor, S. J., Phindela, T., Morse, A. P. and Palmer, T. N. (2006). Malaria early warnings based on seasonal climate forecasts from multi-model ensembles. *Nature* **439**, 576–579.

Thuburn, J. (2003). Some issues in isentropic coordinate modelling and modelling the tropopause. In *ECMWF/SPARC Workshop on Modelling and Assimilation for the Stratosphere and Troposphere, 23-26 June*, pp. 235–242. ECMWF.

Tompkins, A. M., Bechtold, P., Beljaars, A. C. M., Benedetti, A., Cheinet, S., Janisková, M., Köhler, M., Lopez, P. and Morcrette, J.-J. (2004). Moist physical processes in the IFS: Progress and plans, Tech. Mem. No. 452, ECMWF, Reading, U.K.

Tompkins, A. M., Gierens, K. and Rädel, G. (2007). Ice supersaturation in the ECMWF integrated forecast system. *Q. J. R. Meteorol. Soc.* **133**, 53–63, doi:10.1002/qj.14.

Trenberth, K. E. and Olson, J. G. (1988). An evaluation and intercomparison of global analyses from the National Meteorological Center and the European

Centre for Medium-Range Weather Forecasts. *Bull. Am. Meteorol. Soc.* **69**, 1047–1057.

Untch, A., Simmons, A., Hortal, M., Jacob, C. and colleagues (1999). Increased stratospheric resolution in the ECMWF forecasting system. In *Proceedings of the SODA Workshop on Chemical Data Assimilation, 9-10 December 1998, De Bilt, The Netherlands*, pp. 45–52. KNMI.

Uppala, S. M., Kållberg, P. W., Simmons, A. J., Andrae, U., Bechtold, V. Da Costa, Fiorino, M., Gibson, J. K., Haseler, J., Hernandez, A., Kelly, G. A., Li, X., Onogi, K., Saarinen, S., Sokka, N., Allan, R. P., Andersson, E., Arpe, K., Balmaseda, M. A., Beljaars, A. C. M., Berg, L. Van De, Bidlot, J., Bormann, N., Caires, S., Chevallier, F., Dethof, A., Dragosavac, M., Fisher, M., Fuentes, M., Hagemann, S., Hólm, E., Hoskins, B. J., Isaksen, L., Janssen, P. A. E. M., Jenne, R., Mcnally, A. P., Mahfouf, J.-F., Morcrette, J.-J., Rayner, N. A., Saunders, R. W., Simon, P., Sterl, A., Trenberth, K. E., Untch, A., Vasiljevic, D., Viterbo, P. and Woollen, J. (2005). The ERA-40 Re-analysis. *Q. J. R. Meteorol. Soc.* **131**, 2961–3012, doi:10.1256/qj.04.176.

van Noije, T. P. C., Eskes, H. J., van Weele, M. and van Velthoven, P. F. J. (2004). Implications of the enhanced Brewer-Dobson circulation in European Centre for Medium-Range Weather Forecasts reanalysis ERA-40 for the stratosphere-troposphere exchange of ozone in global chemistry transport models. *J. Geophys. Res.* **109**, doi:10.1029/2004JD004586.

van Noije, T. P. C., Segers, A. J. and van Velthoven, P. F. J. (2006). Time series of the stratosphere-troposphere exchange of ozone simulated with reanalyzed and operational forecast data. *J. Geophys. Res.* **111**, doi:10.1029/2005JD006081.

Waugh, D. W. and Hall, T. M. (2002). Age of stratospheric air: Theory, observations and models. *Reviews of Geophysics* **40**, doi:10.1029/2000RG000101.

Waugh, D. W., Strahan, S. E. and Newman, P. A. (2007). Sensitivity of stratospheric inorganic chlorine to differences in transport. *Atmos. Chem. Phys.* **7**, 4935–4941.

Weaver, C.J., Douglass, A.R. and Rood, R.B. (2000). Lamination frequencies as a diagnostic for horizontal mixing in a 3D transport model. *J. Atmos. Sci.* **57**, 247–261.

WMO (1999). Scientific Assessment of Ozone Depletion: 1998, Global Ozone Research and Monitoring Project -Report No. 44, WMO (World Meteorological Organization), Geneva, Switzerland.

WMO (2006). Joint WMO/EC SCOUT-O3 Arctic ozone bulletin, winter/spring summary *Tech. Rep. 1* Global Atmosphere Watch Programme, available at http://www.wmo.int/pages/prog/arep/gaw/ozone/index.html.

WMO (2007). Scientific Assessment of Ozone Depletion: 2006, Global Ozone Research and Monitoring Project -Report No. 50, WMO (World Meteorological Organization), Geneva, Switzerland.

Wohltmann, I. and Rex, M. (2008). Improvement of vertical and residual velocities in pressure or hybrid sigma-pressure coordinates in analysis data in the stratosphere. *Atmos. Chem. Phys.* **8**, 265–272.